THE UNIVERSITY THOUGHT

PUBLICATION IN NATURAL SCIENCES

VOL. 8, Nº 2, 2018.

Aims and Scope

The University Thought - Publication in Natural Sciences (Univ. thought, Publ. nat. sci.) is a scientific journal founded in 1994. by the University of Priština, and was published semi annually until 1998.

Today, the University Thought - Publication in Natural Sciences is an international, peer reviewed, Open Access journal, published semi annually in the online and print version by the University of Priština, temporarily settled in Kosovska Mitrovica, Serbia. The Journal publishes articles on all aspects of research in Biology, Chemistry, Geography, Information technologies, Mathematics and Physics in the form of original papers, short communications and reviews (invited) by authors from the country and abroad.

The University Thought - Publication in Natural Sciences serves as an interdisciplinary forum covering a wide range of topics for a truly international audience. Journal is endeavor of the University of Priština to acquaint the scientific world with its achievements and wish to affirm the intellectual potential and natural resources of own region. Our aim is to put forward attitude of principle that science is universal and we invite all scientists to cooperate wherever their scope of research may be. We are convinced that shall contribute to do victory of science over barriers of all kinds erected throughout the Balkans.

UNIVERSITY THOUGHT-PUBLICATION IN NATURAL SCIENCES

Vol. 8, Nº 2, 2018.

CONTENTS

MATHEMATICS, COMPUTER SCIENCE AND MECHANICS

PHYSICS

CONTRIBUTION TO THE HERPETOFAUNA OF SERBIA - DISTRIBUTION OF REPTILES IN KOSOVO AND METOHIJA PROVINCE

LJILJANA TOMOVIĆ[1*], MAGDALENA TIMOTIJEVIĆ[2], RASTKO AJTIĆ[3], IMRE KRIZMANIĆ[1], NENAD LABUS[2]

[1]Institute of Zoology, Faculty of Biology, University of Belgrade, Belgrade, Serbia
[2]Faculty of Science and Mathematics, University of Priština, Kosovska Mitrovica, Serbia
[3]Institute for Nature Conservation of Serbia, Belgrade, Serbia

ABSTRACT

Kosovo and Metohija have already been recognized as regions with the highest diversity of reptiles in Serbia, where 92% (22 of 24) of existing reptile species can be found (Tomović et al., 2015a). First comprehensive contribution to herpetofauna of Kosovo and Metohija was provided by late Professor Gojko Pasuljević. In this study we present a complete dataset of distribution records for 13 most common reptile species in Kosovo and Metohija, including published and new distribution data compiled, and provide standardized 10 x 10 km UTM maps for these data. Results of this study include 1013 distribution records (278 new and 735 published data) for the following reptiles: *Testudo hermanni, Ablepharus kitaibelii, Anguis fragilis, Lacerta agilis, Lacerta viridis, Podarcis muralis, Podarcis tauricus, Coronella austriaca, Dolichophis caspius, Natrix natrix, Natrix tessellata, Zamenis longissimus* and *Vipera ammodytes*. The most widely distributed species, which occupy more than 50 UTM 10 x 10 km squares are: *Podarcis muralis* and *Vipera ammodytes*. Species with limited distribution which occupy less than 20 UTM 10 x 10 km are: *Dolichophis caspius* and *Lacerta agilis*. The largest numbers of new or confirmed literature data are recorded for: *Anguis fragilis, Testudo hermanni* and *Vipera ammodytes*. Having in mind that after 50 years, this is the first comprehensive study of the distribution of reptiles in Kosovo and Metohija exclusively, the presented faunistic data are far from being complete. Further systematic studies should provide a more complete insight into the distribution of herpetofauna of this province of Serbia.

Keywords: Herpetofauna, Faunistics, Serbia, Kosovo and Metohija.

INTRODUCTION

The first important step preceding the studies of systematics, ecology and biogeography is the comprehensive knowledge of biodiversity of a certain region. Therefore, systematic faunistic studies are of increasing significance, especially in the regions or countries with incomplete species distribution data (Margules et al., 2002; Jelić et al., 2013; Tomović et al., 2014). Detailed distribution data are essential for identification of biodiversity "hotspots" i.e. areas with exceptional species assemblages, high levels of endemicity and/or areas under significant threats (Gaston et al., 2002).

Concerning the herpetofauna, the Balkan Peninsula is recognized as one of the richest biodiversity hotspots in Europe (Džukić & Kalezić, 2004). Being situated in the central part of the Balkans, Serbia is a very important territory for diversity of reptiles, due to the occurrence of various biogeographical phenomena: presence of the Balkan endemic species and relicts, different faunal elements, marginality of certain species' ranges and presence of peripheral populations, as well as range fragmentation (Džukić, 1995; Džukić & Kalezić, 2004).

Province of Kosovo and Metohija has already been identified as one of the regions with the highest reptile's diversity in Serbia, with 22 species recorded (Tomović et al., 2015a). First comprehensive contribution to herpetofauna of Kosovo and Metohija was given by Pasuljević (1968). In the following decades, faunistic papers were primarily focused on several rare (or uncommon) species with peripheral or disjunct occurrence within the territory of ex-Yugoslavia or Serbia: *Algyroides nigropunctatus* (Džukić, 1970; Džukić & Pasuljević, 1979), *Darevskia praticola* (Džukić, 1974; Pasuljević & Džukić, 1979), *Cyrtodactylus kotschyi* (Ajtić & Tomović, 2001).

The most recent publication of complete herpetofauna of Serbia (including Kosovo and Metohija) presented only broad overview of confirmed or potential distribution of reptile species, but without precise distribution records (Tomović et al., 2014). Several species or group-oriented papers for the territory of Serbia provided complete distribution summary and filled up the gap concerning distribution of reptiles in Kosovo and Metohija: *Emys orbicularis* (Krizmanić et al., 2015; Golubović et al., 2017), *Testudo hermanni* (Ljubisavljević et al., 2014), *Testudo graeca* (Tomović et al., 2004; Ralev et al., 2013), *Ablepharus kitaibelii* (Ljubisavljević et al., 2015), Lacertids (Urošević et al., 2015), Colubrids (Tomović et al., 2015b) and Vipers (Jelić et al., 2013). However, data concerning the distribution of the most

---

* Corresponding author: lili@bio.bg.ac.rs

common, well-known and generally widespread species (e. g. *Lacerta agilis*, *Lacerta viridis*, *Podarcis muralis*, *Natrix natrix*, *Natrix tessellata*, *Coronella austriaca* and *Zamenis longissimus*) were relatively poor and scattered.

Therefore, with this study we aim to: (i) publish a complete dataset of distribution records of 13 most common reptile species in Kosovo and Metohija, summarizing already published and new distribution data, and (ii) provide standardized 10 x 10 km UTM maps of the summarized data.

MATERIAL AND METHODS

In this study, we presented a large dataset (1013 occurrence records) of distribution of the most common species of herpetofauna in Kosovo and Metohija.

This study is based on the species' occurrence records from authors' field observations (field data) which were kindly donated by our colleagues (see Acknowledgements). The species were identified using standard herpetological literature (Arnold & Ovenden, 2002), by visual inspection of specimens from the photographs, or directly in the field. Regarding taxonomy and current nomenclature, we followed Jablonski et al. (2016), Sillero et al. (2014) and Uetz et al. (2017). Due to several objective reasons, the entire territory of Kosovo and Metohija (Figure 1) was not covered by faunistic research. Our dataset is still incomplete; the lack of data from certain areas does not necessarily imply the absence of species. In addition to new (field) records, we used 735 published records from the available literature.

Figure 1. Map of Republic of Serbia with study area – Kosovo and Metohija province (grey).

The data were classified as: (i) new field data (red-white dots), (ii) literature data (red-black dots) and (iii) existing data confirmed by field work (red dots). All records were mapped in the 10 x 10 km UTM (Universal Transverse Mercator) grid.

We applied the threshold of occurrence in classifying the abundancy of the species: (i) most widely distributed species (more than 50 UTM 10 x 10 km squares), (ii) quite widely distributed species (43 – 47 UTM 10 x 10 km squares), (iii) relatively common species (27 – 34 UTM 10 x 10 km squares), (iv) species with limited distribution (less than 20 UTM 10 x 10 km squares).

RESULTS

Results of this study included 1013 distribution records (278 new and 735 published data) for 13 most common reptiles in Kosovo and Metohija province: *Testudo hermanni*, *Ablepharus kitaibelii*, *Anguis fragilis*, *Lacerta agilis*, *Lacerta viridis*, *Podarcis muralis*, *P. tauricus*, *Coronella austriaca*, *Dolichophis caspius*, *Natrix natrix*, *N. tessellata*, *Zamenis longissimus* and *Vipera ammodytes*. We excluded other nine reptile species which inhabit this part of Serbia (Tomović et al., 2015a), due to lack of new faunistic data. In Figures 2–5, detailed distribution records of 13 reptile species in Kosovo and Metohija province are provided.

For each species, new records in Kosovo and Metohija (with broad locations, exact localities, toponyms, UTM and names of persons who provided data) are given in Appendix 1. Data from the literature (with broad locations, exact localities, toponyms, UTM and literature sources) are presented in Appendix 2.

According to our dataset, the most widely distributed species in the entire territory of Kosovo and Metohija are: the wall lizard (*Podarcis muralis* – 55) and the nose-horned viper (*Vipera ammodytes* – 53). Four reptile species are quite widely distributed: the grass snake (*Natrix natrix* – 47), the green lizard (*Lacerta viridis* – 47), the Hermann's tortoise (*Testudo hermanni* – 44) and the Aesculapian snake (*Zamenis longissimus* – 43). Relatively common species are: the Balkan wall lizard (*Podarcis tauricus* – 34), the dice snake (*Natrix tessellata* – 31), the smooth snake (*Coronella austriaca* – 31), the snake-eyed skink (*Ablepharus kitaibelii* – 29) and the slow-worm (*Anguis fragilis* – 27). Species with limited distribution in Kosovo and Metohija are: the Caspian whip-snake (*Dolichophis caspius* – 15) and the sand lizard (*Lacerta agilis* – 13) (Figures 2–5). The largest numbers of new or confirmed literature data are recorded for the following species: *Anguis fragilis* (19 new and 6 confirmed literature data), *Testudo hermanni* (18 new and 11 confirmed literature data) and *Vipera ammodytes* (8 new and 32 confirmed literature data).
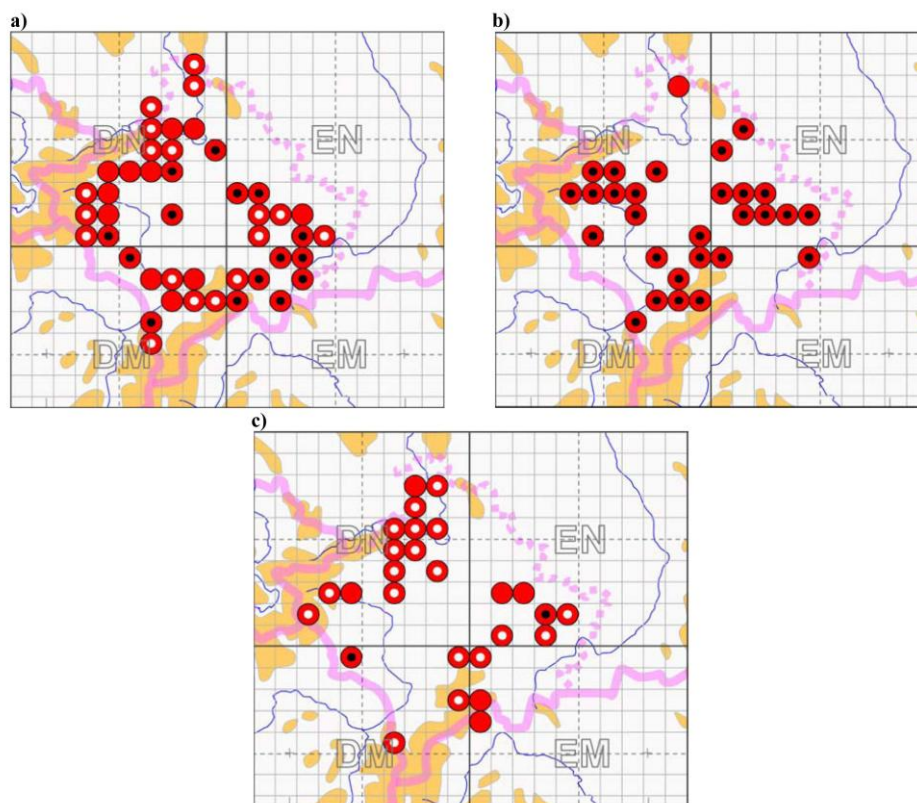
Figure 2. Records of a) *Testudo hermanni*, b) *Ablepharus kitaibelii*, c) *Anguis fragilis* in Kosovo and Metohija (National Grid UTM 10 x 10 km). Red-white dots – new records, Red-black dots – literature c records, Red dots – literature + new records.
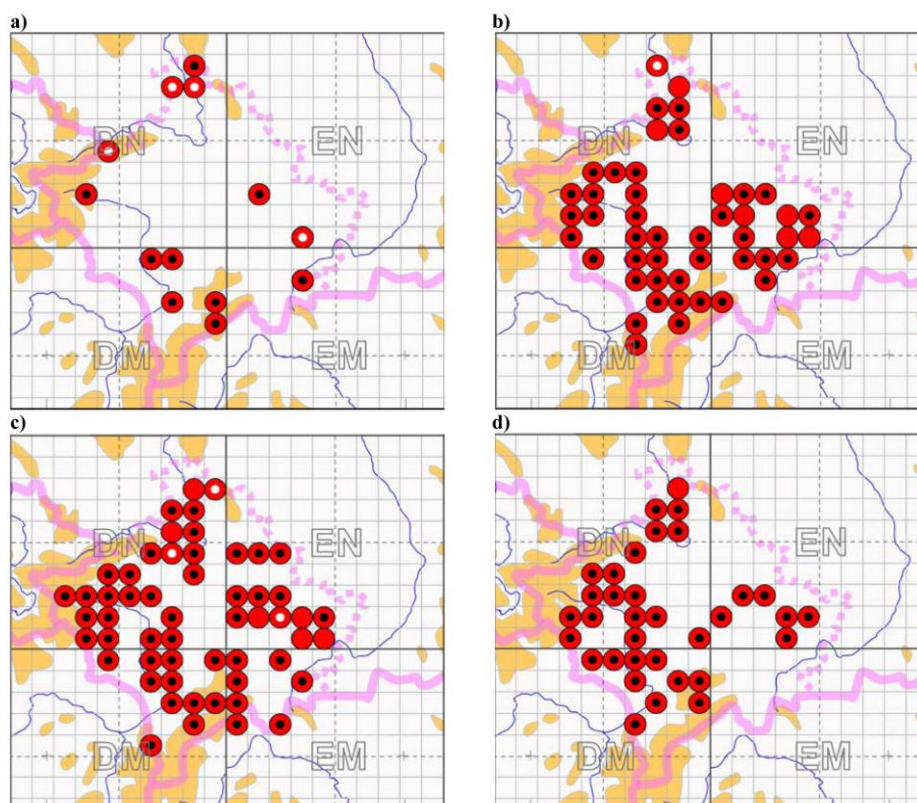
Figure 3. Records of a) *Lacerta agilis*, b) *Lacerta viridis*, c) *Podarcis muralis*, d) *Podarcis tauricus* in Kosovo and Metohija (National Grid UTM 10 x 10 km). Red-white dots – new records, Red-black dots – literature records, Red dots – literature + new records.

BIOLOGY
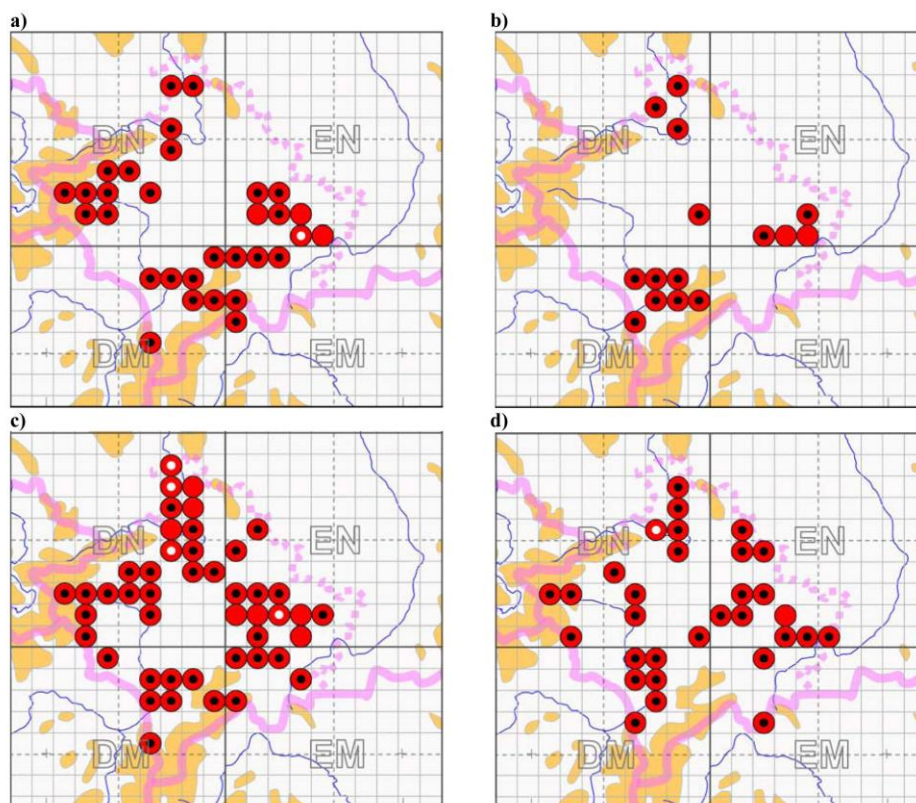
Figure 4. Records of a) *Coronella austriaca*, b) *Dolichophis caspius*, c) *Natrix natrix*, d) *Natrix tessellata* in Kosovo and Metohija (National Grid UTM 10 x 10 km). Red-white dots – new records, Red-black dots – literature records, Red dots – literature + new records.
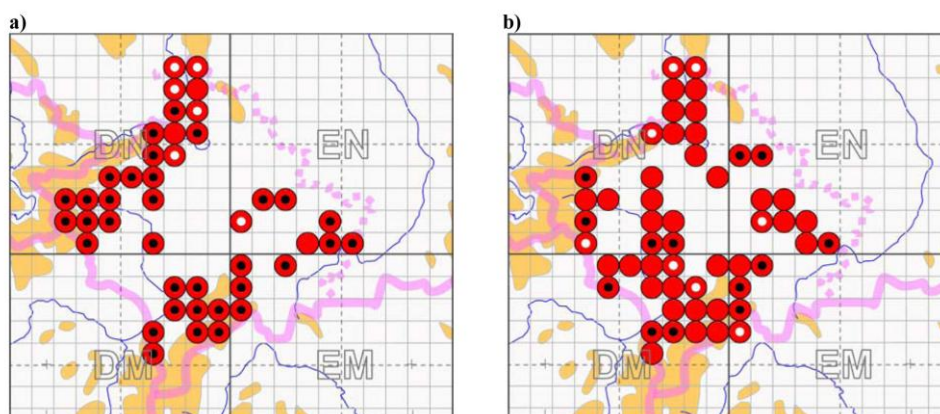
Figure 5. Records of a) *Zamenis longissimus*, b) *Vipera ammodytes* in Kosovo and Metohija (National Grid UTM 10 x 10 km). Red-white dots – new records, Red-black dots – literature records, Red dots – literature + new records.

DISCUSSION

Kosovo and Metohija have already been recognized as regions with the highest diversity of reptiles in Serbia, were 92% (22 of 24) of existing reptile species can be found (Tomović et al., 2015a). The only missing species are *Elaphe quatuorlineta* and *Platyceps najadum*, which occur in southern Serbia (Pčinja river valley) (Tomović et al., 2015a).

Comparison of distribution of reptiles in Kosovo and Metohija with the entire territory of Serbia reveals a similar

pattern: the most common species in Serbia are widely distributed in Kosovo and Metohija as well. All these species show uniform occurrence, determined by the presence of various adequate habitats, from lowlands to high mountains, as well as from aquatic to forest habitats. The new faunistic data expand their known distribution in Kosovo and Metohija. Presence of gaps in distribution reflects rather the lack of faunistic research in particular regions, than the actual absence of the species.

The largest number of new and literature records exist for three species which distribution in Serbia has not been published

yet (*Anguis fragilis*), or which distribution included the complete territory of ex Yugoslavia: *Testudo hermanni* (Ljubisavljević et al., 2014) and *Vipera ammodytes* (Jelić et al., 2013).

According to our dataset, two reptiles show limited and, to some extent, disjunct distribution in Kosovo and Metohija: *Lacerta agilis* and *Dolichophis caspius* (Figures 3 and 4). In Serbia, *Lacerta agilis* inhabits areas with continental and alpine climates, and avoids moderate-continental and sub-Mediterranean climates (Urošević et al., 2015); the same distribution pattern appears in Kosovo and Metohija. *Dolichophis caspius* has also a very fragmented and relatively restricted range in our country (Tomović et al., 2015b). The Caspian whip snake is associated with open steppe and forest-steppe habitats (Arnold & Ovenden, 2002). The most probable reason for its current distribution pattern is the lack of suitable habitats caused by alterations of original steppes and forest-steppes into agricultural fields. It should be noted that small number of distribution records for these two species could also be the consequence of insufficient faunistic research.

As previously mentioned (Tomović et al., 2015b), in addition to five Colubrid species recorded in Kosovo and Metohija until now, some other taxa can be expected: *Hierophis gemonensis*, *Malpolon insignitus, Telescopus fallax* and *Zamenis situla*. These species reach their distribution limits in Macedonia (Sterijovski et al., 2014) or in Albania (Haxhiu, 1998), very close to the Serbian border. Thus, we suppose that the presence of the abovementioned snakes in Kosovo and Metohija could be confirmed in the future studies. *Dinarolacerta montenegrina*, endemic lizard of the Prokletije mountain massif, is known from a small number of locations in Montenegro and Albania (Ljubisavljević et al., 2016; Mizsei et al., 2017). Parts of the Prokletije Massif lie in the bordering areas of the western Metohija, therefore, this species could also be expected in this area as well (Urošević et al., 2015).

Having in mind that after 50 years, this is the first comprehensive study of the distribution of reptiles in Kosovo and Metohija exclusively, the faunistic data presented herein are far from being complete; As it can be seen from this study, many areas (e.g. in Metohija) are still insufficiently studied. Further systematic studies of both rare and common reptile species, should provide a more comprehensive insight into the distribution and diversity of herpetofauna of this province of Republic of Serbia.

ACKNOWLEGMENTS

Appendix 1 and Appendix 2 are available at https://utnsjournal.pr.ac.rs

REFERENCES

Ajtić, R., & Tomović, Lj. 2001. First record of Kotschy's gecko Cyrtodactylus kotschyi (Steindachner, 1870) (Gekkonidae, Lacertilia) in FR Yugoslavia. Archives of Biological Sciences, 53, pp. 23P-24P.

Arnold, E., & Ovenden, D. 2002. A Filed Guide to the Reptiles and Amphibians of Britain and Europe.London: Harper Collins Publishers. 2nd edition.

Džukić, G. 1970. Beitrag zur kenntis der verbreitung der Algyroides nigropunctatus Dumeril et Bibron in Jugoslawien. Fragmenta Balcanica, 7, pp. 149-155.

Džukić, G. 1974. Prilog herpetofauni Srbije. Glasnik Prirodnjačkog Muzeja, Series B, 29, pp. 105-110.

Džukić, G. 1995. Diverzitet vodozemaca (Amphibia) i gmizavaca (Reptilia) Jugoslavije, sa pregledom vrsta od međunarodnog značaja. In V. Stevanović & V. Vasić Eds., Biodiverzitet Jugoslavije sa pregledom vrsta od međunarodnog značaja.Beograd: Biološki fakultet / Ecolibri. pp. 449-469.

Džukić, G., & Kalezić, M. L. 2004. The Biodiversity of Amphibians and Reptiles in the Balkan Peninsula. In H.I. Griffiths, B. Kryštufek, & J. M. Reed Eds., Balkan Biodiversity: Pattern and Process in the European Hotspot. Dordrecht: Springer Nature, pp. 167-192. doi:10.1007/978-1-4020-2854-0_10

Džukić, G., & Pasuljević, G. 1979. O rasprostranjenju ljuskavog guštera Algyroides nigropunctatus (Dumeril et Bibron, 1839) (Reptilia, Lacertidae). Biosistematika, 5, pp. 61-70.

Gaston, K. J., Pressey, R. L., & Margules, C. R. 2002. Persistence and vulnerability: Retaining biodiversity in the landscape and in protected areas. Journal of Biosciences, 27(4), pp. 361-384. doi:10.1007/bf02704966

Golubović, A., Grabovac, D., & Popović, M. 2017. Actual and potential distribution of the European Pond Turtle, Emys orbicularis (L. 1758) in Serbia, with conservation implications. Acta Zoologica Bulgarica, Supplementum, 10, pp. 49-56.

Haxhiu, I. 1998. The Reptilia of Albania: Species composition, distribution, habitats. Bonner zoologische Beiträge, 48, pp. 35-57.

Jablonski, D., Jandzik, D., Mikulíček, P., Džukić, G., Ljubisavljević, K., Tzankov, N., Jelić, D., Thanou, E., Moravec, J., & Gvoždík, V.. 2016. Contrasting evolutionary histories of the legless lizards slow worms (Anguis) shaped by the topography of the Balkan Peninsula. BMC Evolutionary Biology, 16(1).doi:10.1186/s12862-016-0669-1

Jelić, D., Ajtić, R., Sterijovski, B., Crnobrnja-Isailović, J., Lelo, S., & Tomović, Lj. 2013. Distribution of the genus Vipera in the western and central Balkans. Herpetozoa, 25, pp. 109-132.

Krizmanić, I., Urošević, A., Simović, A., Krstić, M., Jović, D., Ajtić, R., Anđelković, M., Slijepčević, M., Đorđević, S.,

Golubović, A., Žikić, V., & Džukić, G. 2015. Updated distribution of the European pond turtle Emys orbicularis (Linnaeus, 1758) and its conservation issues in Serbia. Arhiv za bioloske nauke, 67(3), pp. 1043-1053. doi:10.2298/abs150210067k

Ljubisavljević, K., Arribas, O., Džukić, G., & Carranza, S. 2007. Genetic and morphological differentiation of Mosor rock lizards, Dinarolacerta mosorensis (Kolombatovic, 1886), with the description of a new species from the Prokletije Mountain Massif (Montenegro) (Squamata: Lacertidae). Zootaxa, 1613, pp. 1-22.

Ljubisavljević, K., Džukić, G., Vukov, T. D., & Kalezić, M. L. 2014. Distribution patterns of Hermann's tortoise Testudo hermanni Gmelin, 1789, in the region of former Yugoslavia (Testudines: Testudinidae). Herpetozoa, 26, pp. 125-138.

Ljubisavljević, K., Polović, L., Vuksanović, S., & Iković, V. 2014. A new record of the Prokletije rock lizard, Dinarolacerta montenegrina (Squamata: Lacertidae) in Montenegro. Ecologica Montenegrina, 1, pp. 201-203.

Ljubisavljević, K., Tomović, Lj., Simović, A., Krizmanić, I., Ajtić, R., Jović, D., Urošević, A., Labus, N., Đorđević, S., Golubović, A., Anđelković, M., & Džukić, G. 2015. Distribution of the Snake-eyed skink Ablepharus kitaibelii Bibron and Bory, 1833 (Squamata: Scincidae) in Serbia. Ecologica Montenegrina, 2, pp. 247-254.

Margules, C. R., Pressey, R. L., & Williams, P. H. 2002. Representing biodiversity: Data and procedures for identifying priority areas for conservation. Journal of Biosciences, 27(4), pp. 309-326. doi:10.1007/bf02704962

Pasuljević, G. 1968. Prilog poznavanju herpetofaune Kosova i Metohije. Zbornik filozofskog fakulteta u Prištini, 1, pp. 61-74.

Pasuljević, G., & Džukić, G. 1979. Još jedna populacija šumskog guštera - Lacerta praticola pontica Lantz et Cyren (Reptilia: Lacertidae) na Balkanskom poluostrvu. Biosistematika, 5, pp. 181-186.

Podnar, M., Bruvo, M. B., & Mayer, W. 2013. Non-concordant phylogeographical patterns of three widely codistributed endemic Western Balkans lacertid lizards (Reptilia, Lacertidae) shaped by specific habitat requirements and different responses to Pleistocene climatic oscillations.

Journal of Zoological Systematics and Evolutionary Research, 52(2), pp. 119-129. doi:10.1111/jzs.12056

Ralev, A., Popović, M., Ružić, M., Shurulinkov, P., Daskalova, D., Spasov, L., & Crnobrnja-Isailović, J. 2013. new record of Testudo graeca ibera Pallas, 1814, in southern Serbia. Herpetozoa, 25, pp. 151-153.

Sillero, N., Campos, J., Bonardi, A., Corti, C., Creemers, R., Crochet, P.-A., Crnobrnja-Isailović, J., Denoël, M., Ficetola, G. F., Gonçalves, J., Kuzmin, S., Lymberakis, P., de Pous, P., Rodríguez, A., Sindaco, R., Speybroeck, J., Toxopeus, B., Vieites, D. R., & Vences, M. 2014. Updated distribution and biogeography of amphibians and reptiles of Europe. Amphibia-Reptilia, 35, pp. 1-31.

Sterijovski, B., Tomović, Lj., & Ajtić, R. 2014. Contribution to the knowledge of the Reptile fauna and diversity in FYR of Macedonia. North-Western Journal of Zoology, 10, pp. 83-92.

Tomović, Lj., Ajtić, R., Đoković, Đ., & Antić, S. 2004. Records of Testudo graeca ibera Pallas, 1814 in Serbia and Montenegro. Herpetozoa, 17, pp. 189-191.

Tomović, Lj., Ajtić, R., Ljubisavljević, K., Urošević, A., Jović, D., Krizmanić, I., Labus, N., Đorđević, S., Kalezić, M.L., Vukov, T., & Džukić, G. 2014. Reptiles in Serbia: Distribution and diversity patterns. Bulletin of the Natural History Museum, 7, pp. 129-158. doi:10.5937/bnhmb1407129t

Tomović, Lj., Kalezić, M., Džukić, G. (Eds.) 2015a. Gmizavci. In Crvena knjiga faune Srbije.Beograd: Univerzitet u Beogradu - Biološki fakultet / Zavod za zaštitu prirode Srbije. II.

Tomović, Lj., Urošević, A., Ajtić, R., Krizmanić, I., Simović, A., Labus, N., Jović, D., Krstić, M., Đorđević, S., Anđelković, M., Golubović, A., & Džukić, G. 2015b. Contribution to the knowledge of distribution of Colubrid snakes in Serbia. Ecologica Montenegrina, 2, pp. 162-186.

Uetz, P., Freed, P., Hošek, J. (Eds.) 2017. The Reptile Database. http://www.reptile-database.org. Accessed on 08.01.2018.

Urošević, A., Ljubisavljević, K., Tomović, Lj., Krizmanić, I., Ajtić, R., Simović, A., Labus, N., Jović, D., Golubović, A., Anđelković, M., & Džukić, G. 2015. Contribution to the knowledge of distribution and diversity of lacertid lizards in Serbia. Ecologica Montenegrina, 2, pp. 197-227.

ADDITIONAL DATA ON LEPIDOPTERA FROM SERBIA

PREDRAG JAKŠIĆ[1],[★]

[1]Faculty of Natural Sciences and Mathematics, University of Priština, Kosovska Mitrovica, Serbia

ABSTRACT

This work reports on results from occasional collections in many sites of Serbia in the period 2015-2018., as well as one earlier material from 1982. By more than 50 excursions, from March to October, by day and night and by light traps, a total amount of 45 selected species of Lepidoptera from 10 families were caught. A full list and description of the localities of collection, some colour plates and the comment about some species apart relevant are also included.

Keywords: Lepidoptera, Serbia

INTRODUCTION

During the few last decades our knowledge of the Lepidoptera fauna of Serbia has significantly increased. The most notable contributions are by Jakšić (2016b) for Serbian „Microlepidoptera",Vasić (2002) and Beshkov (2015) for Serbian Noctuidae, Tomić et al. (2002) and Dodok (2006) for Serbian Geometridae, as well as Stojanović (2012) and Vajgand (2012) for Vojvodina, also Beshkov (2015, 2017),Plant et al. (2017) and Jakšić (2017) for eastern Serbia. Still, a significant part of territory of Serbia remain with only few historical or recent publications. The researchers attention was focused on new species for Serbian fauna. On the other hand, data on "ordinary" species are insufficient.

The goal of this paper is to improve our knowledge about distribution of Lepidoptera species in Serbia. Besides, all available literature and collection data were taken into account.

MATERIALS AND METHODS

To gain an overview of the knowledge of the Lepidoptera fauna of Serbia all the available literature was consulted.

Specimens were collected with entomological net and light trap, using Mercury vapor bulb 125 W. The positions and coordinates at which the Lepidoptera were caught were determined using Garmin e-Trex 10 Vista GPS device. The following sites were investigated: **Beograd, Avala Mt.**, 320 m, 44°41' 45" N; 20° 31' 04" E; **Beograd, Zvezdara**, 187 m, 44° 47' 53" N; 20° 30' 18" E; 113–122, 8 figs, 80 m, 44° 48' 58" N; 20° 26' 02" E; **Zlatibor Mt., vic. Ljubiš village**, 1105 m, 43° 37' 42" N; 19° 45' 24" E; Kovin, vic. Dubovac village, 70 m, 44° 47' 36" N; 21° 12' 25" E; **Bela Palanka, Šljivovički Vis Mt.**, 926 m, 43° 08' 28" N; 22° 23' 09" E.; **Pirot, Crni Vrh Mt.**, 1123 m, 43° 10' 51" N; 22° 38' 52" E; **Svrljig, Tresibaba Mt.**, 700 m, , 43° 30' 14" N; 22° 12' 57" E; **Golubački grad,** 110 m, , 44° 38' 42" N; 21° 41' 15" E; **Novo Brdo, Bostane village**, 800 m, 46° 36' 02" N; 21° 25' 40" E; **Divčibare vic. Kaona**, 829 m, , 44° 06' 39" N; 19° 56' 17" E; **Sjenica, vic. Trijebine**, 1227 m, , 43° 13' 50" N; 19° 57' 19" E; **Niš, Jelašnička Klisura Gorge**, 442 m, , 43° 16' 05" N; 22° 04'

16" E; **Suva Planina Mt., Bojanine Vode**, 1000 m, 43° 13' 22" N; 22° 06' 54" E; **Gornje Kusce village, Gnjilane**, 580 m, 42° 29' 57" N; 21° 29' 00" E and **Zubin Potok, Velji Breg**, 600 m, 42° 55' 51" N; 20° 40' 38" E;

After preparing, we determined the specimens by the wing-patterns and in all cases the identification has been also carried out by an examination of the male genitalia. The preparations were carried out following the well known standard procedure: maceration by boiling in potash, dissecting and cleaning, clearing in xylolum and mounting in Canada balsam. The photos of genital parameters were taken using the "Nikon SMZ800N" microscope with compact PC-based camera.

Fieldwork on protected areas was done on the basis of permits provided by the Ministry of Environment, Mining and Spatial Planning, Republic of Serbia, No. 353-01-389/2016-17, dated from 8. 4. 2016. and No. 353-01-834/2017-17, dated from 11. 05. 2017.

All the material (specimens and genitalia slides) is deposited in the author's collection.

The taxonomic order and nomenclature follows Fibiger et al. (2011) for Noctuidae and Aarvik et al. (2017) for other Lepidoptera. ID number before the species follows Karsholt & Razowski (1996).

RESULTS AND DISCUSSION

Altogether 45 species were recorded. We present and discuss the results by taxonomic order.
Ordo Lepidoptera Linnaeus, 1758
Superfam. Tortricoidea Latreille, 1802
Fam. Tortricidae Latreille, 1803
Subfam. Olethreutinae Walsingham, 1895
4731 *Celypha lacunana* ([Denis & Schiffermüller], 1775)

Material examined: Beograd, Avala Mt., 320 m: 1 m, 28. V 2017. Observed and photo (Fig. 1.) by Jakšić P. The larva feeds on *Vaccinium myrtillus* and *Lycophotia porphyrea*. New species for Serbia.

[★] Corresponding author: jaksicpredrag@gmail.com

Figure 1. *Celypha lacunana* ([Denis & Schiffermüller], 1775). Photo Jakšić P.

Figure 2. *Plebejus argyrognomon* (Bergsträsser, 1779). Photo Jakšić P.

Superfam. Cossoidea Leach, 1815
Fam. Cosiidae Leach, 1815
4166 *Dyspessa ulula* (Borkhausen, 1790)

Material examined: Pirot, Crni Vrh,1123 m: 1 f, 20. V 2017., Bela Palanka, Šljivovički vis, 926 m: 2 m 2 f, 22. VI 2017.

Larval foodplants are *Allium* species, Marković (2014) reported eight species from this genus on Vidlič Mt.

Superfam. Gelechioidea Stainton, 1854
Fam. Lypusidae Herrich-Schäffer, 1857
Subfam. Chimabachinae Heinemann, 1870
2231 *Diurnea fagella* ([Denis & Schiffermüller], 1775)

Material examined: Beograd, Avala Mt., 320 m: 1 m, 2. IV 2017. Genitalia checked, slide SR-2936.; Gnjilane, Gornje Kusce, 550 m, 1 m, 24. III 2018., Janićijević T. leg., Jakšić P. coll.; Zubin Potok, Velji Breg, 630 m, 1 m, 14. IV 2018., Živković M. leg., Jakšić P. coll.

The larvae feed on various deciduous trees, such as *Quercus* and *Betula*.

Superfam. Papilionoidea Latreille, 1802
Fam. Lycaenidae Leach, 1815
7129 *Plebejus argyrognomon* (Bergsträsser, 1779)

Material examined: Niš, Jelašnička Klisura Gorge 450 m: 1 f, 12. V 2015. Photo Jakšić P.

This meso-xerophile species occur on calcareous habitat, such is Jelašnica gorge. Larval food plant is *Securigera varia.*

7171 *Polyommatus daphnis* ([Denis & Schiffermüller], 1775)

Material examined: Svrljig, Tresibaba Mt., 700 m: 1 f, 14. VI 2017. Observed and photo by Jakšić P. Monophage caterpillars feed on *Securigera varia*.

Fam. Nymphalidae Rafinesque, 1815
7312 *Lasiommata maera* (Linnaeus, 1758)

Material examined: Golubački Grad, 110 m: 1 m, 30. VII 2016. Genitalia checked, slide SR-2687 (Fig. 4).

The larva eats full-grown grasses, from the genus *Poa, Festuca, Glyceria, Calamagrostis, Deschampsia, Agrostis, Nardus, Dactylis, Lolium* and *Hordeum* species.

Superfam. Pyraloidea Latreille, 1809
Fam. Crambidae Latreille, 1809

Figure 3. *Polyommatus daphnis* ([Denis & Schiffermüller], 1775). Photo Jakšić P.

Figure 4. *Lasiommata maera* (Linnaeus, 1758), male genitalia.

6478 *Eurrhypis pollinalis* ([Denis & Schiffermüller], 1775)

A survey of the literature: Plant et al. (2017) has identified this species on Mt. Šljivovički Vis. Material examined: Svrljig, Tresibaba Mt., 700 m: 2 m 1 f, 14. VI 2017. Observed and photo (Fig. 5) by Jakšić P.

The caterpillars feed on *Genista, Glycirrhiza, Laburnum, Cytisus* and *Ononis* species.

Figure 5. *Eurrhypis pollinalis* ([Denis & Schiffermüller], 1775). Photo Jakšić P.

6604 *Pyrausta aurata* (Scopoli, 1763)

A survey of the literature: Common species, Rotschild (1912-1917) on Deliblato Sands; Plant et al. (2017) has identified this species on several localities: Pirot, Crni Vrh; Pčinja, Vražiji Kamen; Preševo, Trnava; and Bela Palanka, Šljivovički Vis. Material examined: Beograd, Avala Mt., 312 m: 1 m 1 f, 2. IV 2017, 1 m, 11. IV 2017.; 1 m, 26. IV 2017 (Fig. 6).
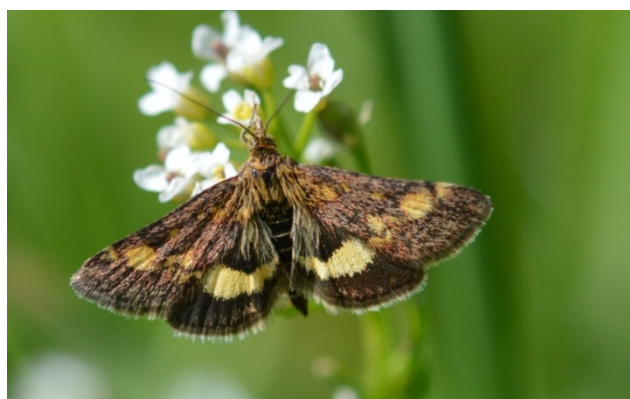
Figure 6. *Pyrausta aurata* (Scopoli, 1763). Avala Mt. Photo Jakšić P.

Superfam. Geometroidea Leach, 1815
Fam. Geometridae Leach, 1815
7527 *Lomaspilis marginata* (Linnaeus, 1758)

Material examined: Kovin, Dubovac, 75 m: 1 m, 8. VII 2016. Genitalia checked, slide SR-2933 (Fig. 7). The larvae feed on *Salix* and *Populus*, especially *P. tremula*.
7559 *Narraga tessularia* (Metzner, 1845)

A survey of the literature: Beshkov (2015) and Jakšić (2017). Both authors independently found this species in the same locality on Pirot, Crni Vrh Mt..

Material examined: Pirot, Crni Vrh Mt., 1123 m: common, 20-21. VI 2017.; Bela Palanka, Šljivovički vis, 926 m: common. Genitalia checked, slide SR-2918. Šljivovički Vis Mt. is the sec-
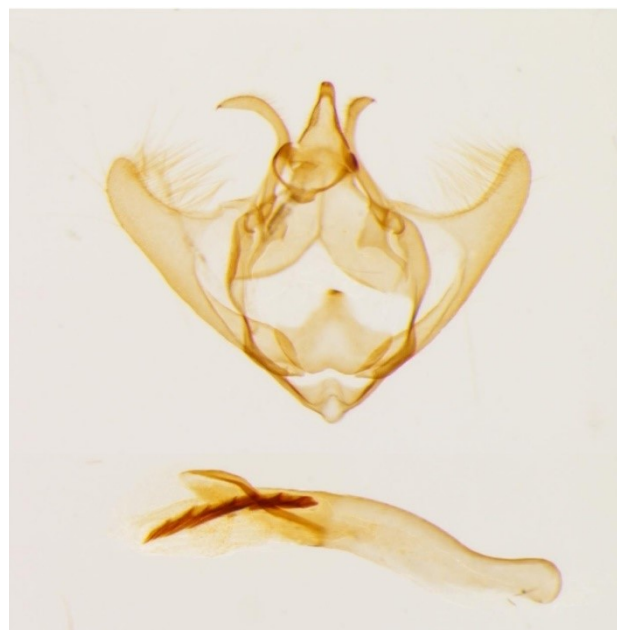
Figure 7. *Lomaspilis marginata* (Linnaeus, 1758), male genitalia, slide SR-2933.

ond locality on which this species has been established (Fig. 8). Ecologicaly, it is a specialist of salty steppes with *Artemisia maritima* as a larval food plant. In eastern Serbia it is locally distributed in the forest belt, up to 1000 m above sea level, occurring in forest margins. On so far known habitats in eastern Serbia *Artemisia alba* Turra were present. This means that the habitat shift has occurred. This is a taxon with a disjunct distribution. It is distributed in Iberian Peninsula (Granada), South-East Europe and central Asia (Russia, Kazakhstan). Agenjo (1956) described this species as a N. *isabel* Agenjo, 1956. Now, this name is synonym. Several subspecies are described: *N. t. tessularia* (Metzner, 1845); *N. t. illia* Wehrli, 1940; *N. t. kasyi* Moucha & Povolny, 1957 and *N. t. pannonica* Vojnits, 1977. According to Skou & Sihvonen (2015) populations from Serbia are related to nominal subspecies – N. tessularia tessularia (Metzner, 1845).
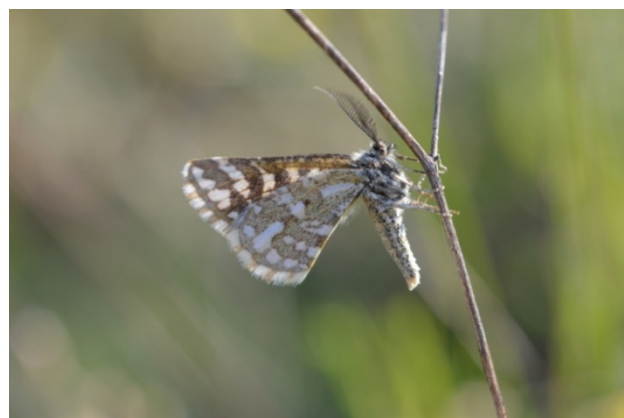
Figure 8. *Narraga tessularia* (Metzner, 1845), male, Bela Palanka, Šljivovički Vis. Photo Jakšić P.

7671 *Apocheima hispidaria* ([Denis & Schiffermüller], 1775)

Material examined: Beograd, Zvezdara, 187 m: 1 m, 14. III 2017.

The larvae feed on *Quercus, Salix, Carpinus, Prunus* and *Malus* species.

7676 *Lycia graecarius* (Staudinger, 1861)

Material examined: Zlatibor Mt., vic. Ljubiš, 1105 m: 1 m, 2. V 2017.

Polyphagous caterpillars feed on *Achillea, Laburnum, Rumex, Taraxacum, Trifolium* and *Centaurea* species. The presence of species of the genus *Lycia* in Serbia has not been completely resolved. This genus is present in Europe with eight species. In Serbia, four species are registered: *L. hirtaria* (Clerck, 1759), *L. graecarius* (Staudinger, 1861), *L. zonaria* (Denis und Schiffermüller, 1775) and *L. pomonaria* (Hübner, 1790) (Tomić et al., 2002; Stojanović et al., 2006; Jakšić, 2016a). However, the species of this genus due to insufficient morphological-anatomical distinction, as well as due to hybridization, are of particular interest (Harrison, 1919). Preliminary results of the current DNA barcoding method show that this method can solve complex taxonomic problems (Hausmann et al., 2011).

7699 *Erannis defoliaria* (Clerck, 1759)

A survey of the literature: Jovanović (1888). After Jovanović's first contributions there are another 35 literature data for presence of this species in Serbia (see distribution map on Fig. 9).

Material examined: Novo Brdo, Bostane, 800 m: common, 27. XI 1982.; Novi Beograd, vic. TC "Ušće", 1 f, 26. XI 2016. Jakšić P. photo (Fig. 10), observed and col.
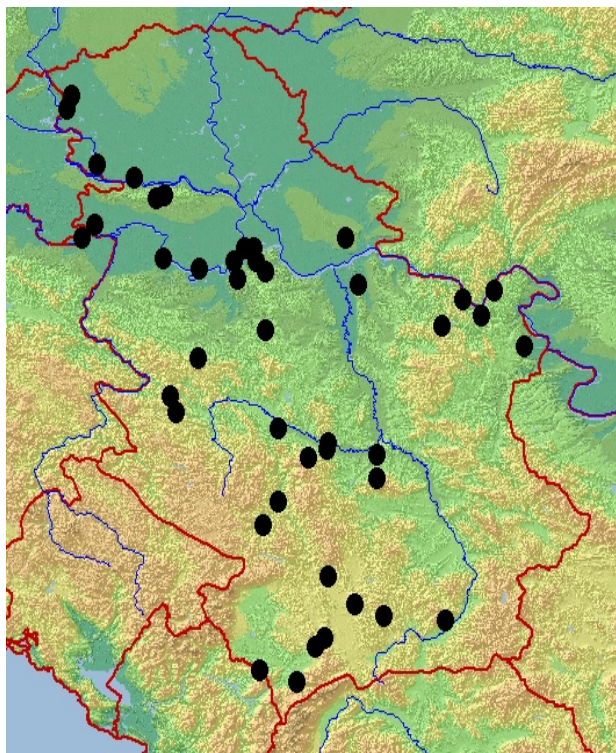
Figure 9. *Erannis defoliaria* (Clerck, 1759) distribution map in Serbia.

7822 *Bupalus piniarius* (Linnaeus, 1758)

Figure 10. *Erannis defoliaria* (Clerck, 1759), female. Photo Jakšić P.

A survey of the Literature: Species as pests in forestry were introduced early in professional literature (Todorović, 1900), but they were just Zečević & Radovanović (1974) gave the first faunistic data about it.

Material examined: Divčibare, vic. Kaona, 820 m: 14. VI 2017., 1 m, observed and photo (Fig. 11) by Jakšić P.

This species is an inhabitant of coniferous woodland, their caterpillar feed mainly on *Pinus* species.

Figure 11. *Bupalus piniarius* (Linnaeus, 1758), male. Photo Jakšić P.

8036 *Scopula immorata* (Linnaeus, 1758)

Material examined: Beograd, Zvezdara, 187 m: 1 m, 28. V 2017.

The caterpillar feeds on various low-growing plants, as *Thymus* and *Origanum*.

8102 *Idaea aureolaria* ([Denis & Schiffermüller], 1775)

Material examined: Svrljig, Tresibaba Mt., 700 m: 4 m, 19. VI 2017. Genitalia checked, slide SR-2919.

The caterpillars are polyphagous and have been recorded feeding on *Rumex, Onobrychis, Securigera* and *Vicia* species.

8184 *Idaea aversata* (Linnaeus, 1758)

Material examined: Beograd, Zvezdara, 187 m: 1 m, 4. IX 2017.

The larva feeds on a variety of plants, as *Galium, Stellaria, Taraxacum* and *Polygonum* species.

8240 *Scotopteryx mucronata* (Scopoli, 1763)

Material examined: Sjenica, Trijebine, 1227 m: 1 m, 5. VII 2017.

Ulex sp. and *Cytisus* sp. are food plants for caterpillars.

8255 *Xanthorhoe montanata* ([Denis & Schiffermüller], 1775)

Material examined: Sjenica, Trijebine, 1227 m: 1 f, 5. VII 2017.

Caterpillars on *Stachys, Geum* and *Rumex* species.

8274 *Epirrhoe tristata* (Linnaeus, 1758)

Material examined: Sjenica, Trijebine, 1227 m: 1 m, 5. VII 2017. Genitalia checked, slide SR-2934.

Caterpillars on *Galium* ssp.

8447 *Operophtera brumata* (Linnaeus, 1758)

Material examined: Beograd, Zvezdara, 187 m: 1 m, 17. XII 2017.

Larva feeds on *Cornus, Evonimus, Fraxinus, Ulmus, Acer, Quercus* ssp.

8513 *Eupithecia breviculata* (Donzel, 1837)

Beshkov (2017) for the first time reported this species for Serbia. Our finding is second. Material examined: Pirot, Crni Vrh, 1123 m: 1m, 20. VI 2017.

The larvae feed on *Peucedanum* and *Pimpinella* species.

Superfamily Noctuoidea Latreille, 1809

Fam. Notodontidae Stephens, 1829

8708 *Furcula furcula* (Clerck, 1759)

Material examined: Suva Planina Mt., Bojanine vode, 1000 m: 3 m, 19-20. VI 2017.

The host plants are *Salix* and *Populus* species.

8732 *Pterostoma palpina* (Clerck, 1759)

Material examined: Zlatibor Mt., vic. Ljubiš, 1105 m: 1 m, 2. V 2017.

The host plants are *Salix* and *Populus* species.

Fam. Erebidae Leach, [1815]

Subfam. Rivulinae Grote, 1895

9008 *Rivula sericealis* (Scopoli, 1763)

Material examined: Beograd, Avala, 320 m: 1 m, 28. V 2017.

The larvae feed on *Brachypodium* and *Molinia* species.

Subfam. Lymantriinae Hampson, [1893]

10414 *Leucoma salicis* (Linnaeus, 1758)

Material examined: Beograd, Zvezdara, 187 m: 1 m, 29. VII 2017.

The larvae feed on *Populus* and *Salix* species.

10387 *Calliteara pudibunda* (Linnaeus, 1758)

Material examined: Zlatibor Mt., vic. Ljubiš, 1105 m: 1 m, 2. V 2017.

The larvae feed on *Picea, Juniperus* and *Larix* species.

Subfam. Herminiinae Leach, 1815

8845 *Herminia tarsicrinalis* (Knoch, 1782)

Material examined: Kovin, Dubovac, 70 m, 1 m, 9. VII 2016. Genitalia checked, slide SR-2781.

Caterpillars on *Rubus fruticosus* and *Clematitis* ssp.

Subfam. Metoponinae Herrich-Schäffer, [1851]

8965 *Tyta luctuosa* (Denis & Schiffermüller, 1775)

Material examined: Beograd, Zvezdara, 187 m: 1 m, 28. V 2017.

Foodplant *Convolvulus arvensis*.

Subfam. Arctiinae Leach, [1815]

10583 *Diacrisia sannio* (Linnaeus, 1758)

Material examined: Beograd, Avala, 320 m: 1 m, 28. V 2017.; Sjenica, Trijebine, 1227 m, 1 f: 4. VII 2017.

The larvae feed on *Galium, Plantago, Taraxacum, Epilobium* and *Urticae* species.

10479 *Pelosia muscerda* (Hufnagel, 1766)

Material examined: Beograd, Avala Mt., 320 m, 15. VIII 2017., 1 male. Genitalia checked, slide SR-2914 (Fig. 12).

Larval food plants are algae, lichens and different plants, e. g. *Taraxacum*.

Figure 12. *Pelosia muscerda* (Hufnagel, 1766), male genitalia, slide SR-2914.

10499 *Eilema (Wittia) sororcula* (Hufnagel, 1766)

Material examined: Beograd, Zvezdara, 187 m: 1 m, 29. IV 2017. Genitalia checked, slide SR-2878.

Larval food plants different lichens.

10521 *Dysauxes ancilla* (Linnaeus, 1767)

Material examined: Kovin, Dubovac, 70 m: 1 m, 9. VII 2016. Genitalia checked, slide SR-2938 (Fig. 13).Caterpillars feed on *Taraxacum, Senetio, Plantago* and *Lactuca* species.

10526 *Spiris striata* (Linnaeus, 1758)

Material examined: Bela Palanka, Šljivovićki vis, 926 m: 1 f, 22. VI 2017.

Food plants of caterpillar: *Artemisia, Calluna, Festuca, Hieracium, Plantago*, and *Salvia* species.

Subfam. Boletobiinae Grote, 1895

8975 *Laspeyria flexula* (Denis & Schiffermüller, 1775)

Material examined: Beograd, Zvezdara, 187 m: 1 f, 29. V 2017.

Larval food plants different *Salix* and *Populus* species.

Figure 13. *Dysauxes ancilla* (Linnaeus, 1767), male genitalia, slide SR-2938.

Fam. Noctuidae Latreille, 1809
Subfam. Acontiinae Guenée, 1841
9097 *Emmelia trabealis* (Scopoli, 1763)
    Material examined: Beograd, Avala, 312 m: 1 m, 7. VII 2017.
Subfam. Oncocnemidinae Forbes Franclemont, 1954
9275 *Teinoptera olivina* (Herrich-Schäffer, [1852])

    A survey of the literature: the first data on this species was given by Rotschild (1911) who found it on Deliblato Sands, Flamunda. Then, for Serbia, Culot (1913) also quoted it, stating that it has material in its collection. But he does not say who collected the material. Gradojević (1963) and Vasić (1969) also state this species for Deliblato Sands. Recently, Ronkay & Ronkay (1995) describe subspecies deliblatica (G. Ronkay L. Ronkay, 1995) on material from Deliblato Sands. We can see from this review of literature that the species is known only from Deliblato Sands. Material examined: Bela Palanka, Šljivovički Vis, 926 m, 1f, 22. VI 2017.
    This is the second locality on which this species was found in Serbia.
    Larval food plants are *Dianthus* species.
Subfam. Heliothinae Boisduval, [1828]
9367 *Heliotis peltigera* ([Denis & Schiffermüller], 1775)
    Material examined: Beograd, Zvezdara, 187 m: 1f, 20. VIII 2017.
    The larvae feed on *Ononis, Senecio, Tagetes, Atropa* and other species.
Subfam. Bryophilinae Guenée, 1841
8801 *Cryphia algae* (Fabricius, 1775)
    Material examined: Beograd, Zvezdara, 187 m: 1 m, 15. VIII 2017. Genitalia checked, slide SR-2946 (Fig. 14).
    Caterpillars feed on lichen species.
8806 *Bryophila ereptricula* Treitschke, 1825
    Material examined: Beograd, Zvezdara, 187 m: 1 f, 29. VII 2017. Genitalia checked, slide SR-2917 (Fig. 15).

Figure 14. *Cryphia algae* (Fabricius, 1775), male genitalia, slide SR-2946.

    Caterpillars feed on lichen and algae species.

Figure 15. *Bryophila ereptricula* Treitschke, 1825, female genitalia, slide SR-2917.

Subfam. Xyleninae Guenée, 1841
9454 *Hoplodrina ambigua* ([Denis & Schiffermüller], 1775)
    Material examined: Beograd, Zvezdara, 187 m: 1 m, 24. V 2017., 1 f 4. IX 2017. Genitalia checked, slide SR-2947.
    The polyphagous larvae feed on *Betula, Medicago, Taraxacum* and other species.
9492 *Polyphaenis sericata* (Esper, [1787])
    Material examined: Kovin, Dubovac, 70 m, 1 m, 9. VII 2016. Genitalia checked, slide SR-2819.
    The larvae feed on *Ligustrum* vulgare.
9660 *Lithophane ornitopus* (Hufnagel, 1766)
    Material examined: Beograd, Zvezdara, 187 m: 1 m, 14. III 2017.
    The caterpillars on *Salix, Populus, Prunus, Ulmus, Quercus* species.
Subfam. Hadeninae Guenée, 1837
10039 *Orthosia cruda* ([Denis & Schiffermüller], 1775)

Material examined: Beograd, Zvezdara, 187 m: 1 f, 14. III 2017.

The larvae feed on a number of deciduous trees, mostly *Quercus* and *Salix*.

9895 *Calocestra trifolii* (Hufnagel, 1766)

Material examined: Beograd, Zvezdara, 187 m, 1 m: 4. IX 2017. Genitalia checked, slide SR-2948.

The larvae feed on *Atriplex* and *Chenopodium* species.

CONCLUSIONS

Species in Serbia are present on different types of habitats. Several species (7671, 7699, 8036, 8184, 8447, 10414, 8965, 10499, 8975, 9367, 8801, 8806, 9454, 9660, 10039 and 9895) were found in urban habitats of the city of Belgrade, with significant anthropogenic pressure, indicating ecological plasticity of these species. Some species (4743, 6604, 8845 and 10522) were found in suburban and rural habitats. These are synanthropic species, whose survival is dependent on man. The largest number of species (4166, 2231, 7129, 7171, 7312, 6478, 7527, 7676, 7822, 8102, 8240, 8255, 8274, 8513, 8708, 8732, 9008, 10388, 10583, 10479, 10526 and 9097) was found in typical habitats. Their occurrence is related to the presence of food for the caterpillars. In some species (7559) there was a change of habitat in relation to the typical ecological requirements of the species.

In unexplored areas, there are discovering new and rare species for Serbia's fauna. This speaks of insufficient exploration of this group of insects. Zečević (1996) summed up the knowledge for that time, quantitatively expressed by the number of 1334 species of Lepidoptera in Serbia. According to uncertificated data it is estimated that up to 2500 species have been found in Serbia so far. And that's about half the number of species known in Hungary or Romania. Our results show that, in addition to identifying new species, it is also important to identify already known species in new areas throughout Serbia.

ACKNOWLEDGEMENTS

REFERENCES

Aarvik, L., Bengtsson, B. , Elven, H., et al. 2017, Nordic Baltic Checklist of Lepidoptera. Norwegian Journal of Entomology, Supplement 3: 1-236.

Agenjo, R. 1956, Monografia del genero Narraga Wlk. (Lep. Geom.). Eos Revista española de entomologia, 32(1–4): pp. 7–56, pl. I–IV.

Beshkov, S. 2015, Eight new and some rare for Serbia nocturnal Lepidoptera species collected at light. Entomologist's Rec. Entomologist's Rec. J. Var., 127: pp. 212-227; 10.

Beshkov, S. 2017, Contribution to knowledge of the Lepidoptera fauna of the Balkan Peninsula. Entomologist's Rec. J. Var., 129(1); pp. 9-33; 54; 9.

Culot, J. 1913, Noctuelles et Géomètres d'Europe. In Première Partie Noctuelles.Genève. Volume II. 1–243, Pls. 1–81.

Dodok, I. 2006, The fauna of Geometridae (Lepidoptera) in the region of Užice in Western Serbia. Acta entomologica serbica: Beograd, 11(1/2); pp. 61-75.

Fibiger, M., Yela, J. L., Zilli, A., et al. 2011, Chesk list of the Quadrifid Noctuoidea of Europe. In T. Witt L. Ronkay Eds., Lymantriinae and Arctiinae including phylogeny and check list of the Quadrifid Noctuoidea of Europe. Noctuidae Europaeae.Sorø. 13: pp.23-44.

Gradojević, Z. 1963, Naselje Arthropoda travnih zajednica Deliblatske peščare i njhova sukcesija.[In Serbian]: Univerzitet u Beogradu. In Serbian; Doktorska disertacija.

Harrison, J. W. H. 1919, Studies in the hybrid bistoninae III. The stimulus of heterozygosis. Journal of Genetics, 8(4), pp. 259-265. doi:10.1007/bf02983267

Hausmann, A., Haszprunar, G., & Hebert, P. D. N. 2011, Barcoding the Geometrid Fauna of Bavaria (Lepidoptera): Successes, Surprises, and Questions. PLoS ONE, 6(2), p. 17134. doi:10.1371/journal.pone.0017134

Jakšić, P. 2016a, New contributions to the knowledge of Lepidortera fauna of Kosovo and Metohia (Republic of Serbia). The University Thought - Publication in Natural Sciences, 6(2), pp. 1-4. doi:10.5937/univtho6-12528

Jakšić, P. 2016b, Tentative check list of Serbian microlepidoptera. Ecologica Montenegrina, Podgorica, 7: pp. 33-258.

Jakšić, P. 2017, . A contribution to the knowledge of the Lepidoptera fauna of eastern Serbia. Biologica Nyssana, 8(1), pp.113–122, 8 figs.

Jovanović, D. 1888, Poljoprivredne štetočine i pomagači. Treće kolo: Štetni leptiri. Težak, XVIII(11): pp. 733–738; (12): 808–815, figs 8. Beograd. [In Serbian].

Karsholt, O. & Razowski, J. 1996, The Lepidoptera of Europe. A Distributional Checklist.Stenstrup: Apollo Book.

Marković, M. 2014, Uticaj požara na floru planine Vidlič.Niš: Prirodno-matematički fakultet. pp. 314, 8 graf., 14 tabs., 169 figs. [In Serbian].

Plant, W. C.and Beshkov, S., Jakšić, P., & Nahirnić, A. 2017, A contribution to knowledge of the Balkan Lepidoptera. Some Pyraloidea (Lepidoptera: Crambidae Pyralidae) encountered recently in southern Serbia, Montenegro, the Republic of Macedonia and Albania. The University Thought - Publication in Natural Sciences, 7(2), pp. 1-27. doi:10.5937/univtho7-15336

Ronkay, G. & Ronkay, L. 1995, Cuculliinae II. Noctuidae Europaea.Sorø: Entomological press. 7; 224, 4 pl.

Rotschild, C. 1912-1917, Adatok Magyarorszag lepkefaunajahoz / Beitrag zur Lepidopterenfauna Ungarns). Rovartani Lapok, Budapest, 1912-1917; XVI: 130-148; XVIII: 36-43; XIX: 21-29, 167-180; XX: 66-91, 170-175; XXI: 27-47, 72-77.

Rotschild, N. 1911, Adatok Magyarország lepkefaunájához. Rovartani Lapok, . XVIII(3): 36-43.

Skou, P. & Sihvonen, P. 2015, Ennominae. In A. Hausmann Ed., The Geometrid Moths of Europe. Vol. 5. – E. J. Brill Ed., 657 pages, 16 plates with 709 colour photos, 84 plates with 288 b/w photos; 145 b/w illustrations, b/w distribution maps.

Stojanović, D. 2012, Taksonomsko-faunistička studija leptira (Insecta: Lepidoptera) Fruške gore.Beograd: Biološki fakultet. pp. 1-621; Disertacija.

Stojanović, D. V., Poljaković-Pajnik, L., Drekić, M., & Vajgand, D. 2006, New findings of species zonaria (Denis und Schiffermüller, 1775) (Lepidoptera, Geometridae) for fauna of Serbia. In II International Symposium of Ecologists of Montenegro - The Book of Abstracts and Programme, Kotor. pp. 45-46.

Todorović, D. 1900, Osnovi šumarstva za niže poljoprivredne škole u Srbiji.Beograd: Državna štamparija Kraljevine Srbije. In Serbian.

Tomić, D., Zečević, M., Mihajlović, L., & Glavendekić, M. 2002, Fauna zemljomerki (Lepidoptera, Geometridae) Srbije. / Fauna of Geometrids (Lepidoptera, Geometridae) in Serbia.

In Zbornik radova o fauni Srbije.Beograd: SANU - Odeljenje hemijskih i bioloških nauka. VI: 73–164. [In Serbian, English summary].

Vajgand, D. 2012, Fauna sovica (Noctuidae, Lepidoptera) Vojvodine i parametri prognoze brojnosti / The Owlet Moths (Noctuidae, Lepidoptera) Fauna of Vojvodina and Parameters for Forecasting Abundance / Die Eulenfalterfauna (Noctuidae, Lepidoptera) der Vojvodina und die. . . .Univerzitet u Novom Sadu - Poljoprivredni fakultet. Disertacija, pp. 1–318, 2 maps, 2 figs., 180 grafs., 37 tabs. [In Serbian, English German summary].

Vasić, K. 1969, Prilog poznavanju faune sovica (Lep. Noctuidae) Deliblatskog peska. In Zbornik radova - "Deliblatski pesak" I.Beograd. 199-214.

Vasić, K. 2002, Fauna sovica (Lepidoptera, Noctuidae) Srbije / Fauna of Noctuids (Lepidoptera, Noctuidae) in Serbia. In Zbornik radova o fauni Srbije VI.Beograd: SANU - Odeljenje hemijskih i bioloških nauka. 165-293, [In Serbian, English summary].

Zečević, M. 1996, Pregled faune leptira Srbije.Beograd: Institut za istraživanja u poljoprivredi Srbija,; Beograd: IP "Nauka".

Zečević, M. & Radovanović, S. 1974, Leptiri Timočke Krajine (makrolepidoptera).Zaječar: Zavod za poljoprivredu Zaječar / Novinska ustanova "Timok"

ASSOCIATION BETWEEN FINGERPRINT PATTERNS AND MYOPIA

LJILJANA SRETIĆ[1]

[1]Faculty of Science and Mathematics, University of Priština, Kosovska Mitrovica, Serbia

ABSTRACT

Epidermal patterns are polygenically determined system of ridges on volar surface of fingers, palms and soles. Due to their mode of inheritance, and developmental time that coincide with the most critical period of embryogenesis, they are considered as a biological marker that may provide an insight in early fetal life. This study involved 102 participants, students from the University of Priština-Kosovska Mitrovica, 51 consisting myopic and 51 control group. Analysis of fingerprint patterns has showed significantly altered dermatoglyphic configuration of arch patterns in myopic group, which might be suggestive of developmental perturbances in embryogenesis of genetically vulnerable individuals prone to development of myopia.

Keywords: Epidermal patterns, Myopia, Arches.

INTRODUCTION

Fingerprint patterns, designated also as dermatoglyphics, are epidermal ridge configurations on fingers, palms, soles and toes. Although the other primates have ridges on the ventral surface of the palms and soles, the rich variety of dermal ridge patterns is unique for humans (Cummins & Midlo, 1976). Fingerprint development starts in the most sensitive period of fetal life, with the appearance of local temporary eminences-volar pads, as early as 6th gestational week. Once formed they remain permanent throughout lifetime.

Dermatoglyphic phenotype is considered to be a result of an interrelationship between genetic and environmental factors (Bouchard et al., 1990; Arrieta et al., 1992). Their high heritability has been demonstrated in the studies of monozygotic twins, reaching for some dermatoglyphic features, such as arch patterns or finger ridge count, heritability of 91%, i.e 95% or more (Holt, 1968; Bokhari et al., 2002; Reed et al., 2006; Machado et al., 2010). There is a wide agreement that inheritance of most dermatoglyphic features conforms to polygenic system (Holt, 1968; Chakraborty, 1991; Ismail et al., 2009; Karmakar & Kobyliansky, 2011). Since that dermatoglyphic patterns morphology depends on volar pads shape and size it is postulated that these genes affect epidermal ridge formation indirectly, through growth rate, timing events, skeletal factors, vascularization and innervation of dermis and other ontogenic factors (Wertheim & Maceo, 2002; Todd et al., 2006). In a study conducted by Nousbeck et al. *SMARCAD1* has been suggested as a possible genetic factor that might regulate dermatoglyphic morphogenesis. *SMARCAD1*, located at 4q22, is a gene that encodes a protein structurally related to SWI2/SNF2 superfamily of ATP dependant ATPases, which are catalytic subunits of chromatin remodeling complexes, considered as major regulators of transcriptional activity (Adra et al., 2000). A short isoform of *SMARCAD1* gene is exclusively expressed in the skin. A mutation, that likely exerts loss-of-function effect, disrupting conserved donor splice site adjacent to 3′ end of noncoding exon uniquely present in skin-specific short isoform of a gene, is found in condition known as adermoglyphia, thus indicating its possible role in friction ridge ontogenesis (Nousbeck et al., 2011). Genom wide association study of Ho et al. (2016), which tried to elucidate a genetic match with respect to the presence or absence of whorl patterns, found that the most of SNPs polymorphisms variants within *ADAMTS9-AS2* appear to be associated with whorl patterns incidence on all digits, at different levels of significance. Significant results were also found in an intergenic region on chromosome 12, near *TBX3* and *MED113L* genes and a variant within *OLA1* gene, but the finding for *ADAMTS9-AS2* were more concrete. *ADAMTS9-AS2* is tumor suppressor widely expressed in fetal tissues. Its product is an antisense RNA involved in chromatin remodeling and transcriptional/posttranscriptional regulation, but also serve as a precursor of siRNA, pointing to an epigenetic regulation in fingerprint formation.

Dermatoglyphics are phylogenetically more stable than other biological traits, and appear to be evolutionary conservative, which renders them more reliable for studies of the historical relationships of populations (Froehlich & Giles, 1981). Besides, mode of inheritance and morphogenesis in early fetal life make them a sensitive indicator of intrauterine disruptions of genetic and/or environmental origin (Martin et al., 2004). Deviant dermatoglyphic configurations have been found in numerous chromosomal and multifactorial disorders (Martin et al., 2004; Cam et al., 2008; Mital et al., 2012; Stošljević & Adamović, 2013; Gradiser et al., 2016).

Development of an eye is genetically determined process (Gehring, 2002). Structural changes in eye components are strongly associated with myopia, leading to blurred vision of distant objects. It is a complex disorder influenced by both genetic and environmental factors (Tang et al., 2008). Evidences

---

* Corresponding author: lsretic@gmail.com
BIOLOGY

of myopia heritability stem from the studies of familial clustering (Guggenheim et al., 2000), high reccurence risk in offspring (Farbrother et al., 2004) and heritability values in twins (Sanfilippo et al., 2010). Numerous genes that have been proposed as candidate genes in etiology of myopia are found to regulate neuronal development, neurotransmission, signaling, remodeling of extracellular matrix, retinoic acid metabolism and apoptosis (Li & Zhang, 2017).

Since that ocular components and skin share common ectodermal origin and developmental time, we hypothesized that deviant dermatoglyphic composition, due to the pleiotropic effect of the genes involved in oculogenesis, may indicate the dysmorphogenesis of the ectodermal tissue and its derivates. The aim of this study was to evaluate effect of myopic disorder on dermatoglyphic patterns, as a morphological biomarker that might provide a clue of genetic susceptibility to myopia, as well as a time window of intrauterine perturbancies.

MATERIAL AND METHODS

Research sample comprised 102 students of the University of Priština-Kosovska Mitrovica, 51 myopic individuals and 51 healthy controls. They were, according to sex and vision, split into four groups: control males (N=25), control females (N=26), myopic males (N=25) and myopic females (N=26). Fingerprints, provided by ink and paper method (Cummins & Midlo, 1976), were scanned (CannonScanLIDE 25) and processed by program for image editing (Adobe Photoshop CS3). Dermatoglyphic patterns were classified as arch (A), loops (L) and whorls (W) (Galton, 2004). They are differentiated according to landmark structures-triradius, a point from which three ridge systems course in three different directions at angles of about 120^0, and a core point referring to the center of the pattern. Arches are the simplest pattern with no triradius, formed by succession of more or less parallel ridges which traverse the pattern area and form a curve that is concave proximaly. Loops have one triradius and consist of series of ridges entering pattern area on one side, recurving and exiting from the same side. They are designated as radial, if the loop ridges open toward thumb (RL), and ulnar, if the ridges open toward little finger (UL). Whorl patterns, with two triradii, have ridges arranged as circles, ellipses or spirals around the core of the pattern. Comparisons of patterns distribution between groups were made using chi-square test,

with p value less than 0.05 considered as the minimum level of significance. The study provided written informed consent from each participant.

RESULTS

Table 1 presents patterns distribution, both hands pooled together, in males and females from control and myopic group. Significant sex differences have been noted for whorl and arch paterns in myopic group, being highly significant for arch patterns, but as for whorls significance was recorded in control group as well.

Table 1. Patterns distribution on both hands in control and myopic group.

		Pattern type N (%)			
Group	Sex	A	UL	RL	W
Control	Males	11(4.4)	123(49.2)	6(2.4)	110(44)
	Females	7(2.8)	152(60.8)	9(3.6)	82(32.8)
	χ^2	0.889	3.058	0.6	4.083
	p	0.346	0.08	0.439	0.043
Myopic	Males	2(0.80)	135(54.22)	10(4.02)	102(40.96)
	Females	20(7.69)	156(60.00)	10(3.85)	74(28.46)
	χ^2	14.727	1.515	0.000	4.455
	p	0.000	0.218	1.000	0.035

Comparison within the same sex also revealed significance for arch patterns, due to the low frequency in myopic males in relation to control males, and high frequency in myopic females in relation to control females (Table 2).

Table 2. Patterns distribution on both hands in males and females.

		Pattern type N (%)			
Group	Sex	A	UL	RL	W
Males	Control	11(4.4)	123(49.2)	6(2.4)	110(44)
	Myopic	2(0.80)	135(54.22)	10(4.02)	102(40.96)
	χ^2	6.231	0.558	1.000	0.302
	p	0.013	0.455	0.317	0.583
Females	Control	7(2.8)	152(60.8)	9(3.6)	82(32.8)
	Myopic	20(7.69)	156(60.00)	10(3.85)	74(28.46)
	χ^2	6.259	0.052	0.053	0.410
	p	0.012	0.820	0.819	0.522

Table 3. Patterns distribution on individual hands in males.

Hand	Control Pattern type N (%)				Myopia Pattern type N (%)			
	A	UL	RL	W	A	UL	RL	W
L	6(4.8)	64(51.2)	4(3.2)	51(40.8)	2(1.61)	82(66.13)	5(4.03)	35(28.23)
R	5(4.0)	59(47.2)	2(1.6)	59(47.2)	0(0.0)	53(42.4)	5(4.0)	67(53.6)
χ^2	0.0	0.25	0.17	0.79	0.51	13.18	0.09	15.54
p	1.0	0.61	0.67	0.37	0.47	0.001	0.75	0.001

Table 4. Patterns distribution on individual hands in females.

Hand	Control Pattern type N (%)				Myopia Pattern type N (%)			
	A	UL	RL	W	A	UL	RL	W
L	4(3.2)	77(61.6)	4(3.2)	40(32.0)	11(8.46)	72(55.38)	5(4.03)	39(30.0)
R	3(2.4)	75(60.0)	5(4.0)	42(33.6)	9(6.92)	84(64.62)	5(4.0)	35(26.92)
χ^2	0.0	0.01	0.0	0.01	0.05	1.93	2.60	0.17
p	1.0	0.89	1.0	0.89	0.81	0.16	0.10	0.68

Patterns distribution on the left and right hand of control and myopic males and females are displayed in Tables 3 and 4. The only significance was observed in myopic males who have more ulnar loops on the left and whorls on the right hand.

DISCUSSION

Myopia, or nearsightedness, is the most common human multifactorial eye disorder in the world, with a prevalence of an increasing tendency, so that there is a prediction that 49.8% of the world population will be with myopia and 9.8% with high myopia by 2050 (Holden et al., 2016).

The main limitation of this study was very sparse literature and reliable data referring dermatoglyphic characteristics in myopia, which considerably has reduced adequate comparison. The most striking finding of our study concerns arch patterns, significantly decreased in myopic males, which is in accordance with a previous work of Chaterjee (1991), and increased in myopic females. Morphogensesis of dermatoglyphic patterns depends on size and shape of volar pads that are genetically predetermined. Adverse intrauterine influences might disturb timing of volar pad regression and ridge differentiation. These abnormalities in growth process are liable to distort the alignment of dermal ridges (Ashbaugh, 1992; Babler, 1991; Wertheim & Maceo, 2002), leading to arch formation in the case of earlier volar pad regression (Meier, 1987). Since that difference in whorl patterns are found between males and females in both control and myopic group, it appears that it stems from sexual dimorphism found in general population. Sexual dimorphism may be under certain environmental influences, especially among males as a more sensitive during prenatal period (Kobyliansky & Micle, 1987). Differences in pattern distributions between hands were found to be significant only in myopic males. This might be due to the relatively unstable genetic control in myopic males during embryogenesis, since that, in general, one of the major indicator of developmental instability is presence of asymmetry between normally symmetric bilateral traits (Adams & Niswander, 1967; Naugler & Ludman, 1996).

CONCLUSION

The results of our studies confirmed altered dermatoglyphic configuration in myopic individuals, which might indicate developmental perturbances in early embryogenesis of genetically vulnerable individuals. Although suggestive they could not stand *per se* for dermatoglyphic marker of myopia. In order to establish more informative conclusion further investigation should incorporate quantitative parameters and a level of fluctuating asymmetry.

REFERENCES

Adams, M. S., & Niswander, J. D. 1967. Developmental 'Noise' and a congenital malformation. Genetical Research, 10(03), p. 313. doi:10.1017/s0016672300011071

Adra, C. N., Donato, J., Badovinac, R., Syed, F., Kheraj, R., Cai, H., . . . Drews, R. 2000. SMARCAD1, a Novel Human Helicase Family-Defining Member Associated with Genetic Instability: Cloning, Expression, and Mapping to 4q22–q23, a Band Rich in Breakpoints and Deletion Mutants Involved in Several Human Diseases. Genomics, 69(2), pp. 162-173. doi:10.1006/geno.2000.6281

Arrieta, M. I., Criado, B., Hauspie, R., Martinez, B., Lobato, N., & Lostao, C. M. 1992. Effects of genetic and environmental factors on the a-b, b-c and c-d interdigital ridge counts. Hereditas, 117(2), pp. 189-194. doi:10.1111/j.1601-5223.1992.tb00173.x

Ashbaugh, D. 1992. Defined pattern, overall pattern and unique pattern. Journal of Forensic Identification, 42 (6), pp. 503-512.

Babler, W. J. 1991. Embryologic development of epidermal ridges and their configurations. Birth Defects Original Article Series, 27(2), pp. 95-112.

Bokhari, A., Coull, B. A., & Holmes, L. B. 2002. Effect of prenatal exposure to anticonvulsant drugs on dermal ridge patterns of fingers. Teratology, 66(1), pp. 19-23. doi:10.1002/tera.10044

Bouchard, T., Lykken, D., McGue, M., Segal, N., & Tellegen, A. 1990. Sources of human psychological differences: the Minnesota Study of Twins Reared Apart. Science, 250(4978), pp. 223-228. doi:10.1126/science.2218526

Chakraborty, R. 1991. The role of heredity and environment on dermatoglyphic traits. Birth Defects Original Article Series, 27(2), pp. 151-191.

Chatterjee, S. K., & Mukherji, R. 1991. Genetics of epidermal ridges: a study in subjects with refractive errors. Journal of the Indian Medical Association, 89 (10), pp. 287-289.

Cummins, H., & Midlo, C. 1976. Fingerprints, palms and soles. New York: Dover Publications Inc.

Farbrother, J. E., Kirov, G., Owen, M. J., & Guggenheim, J. A. 2004. Family Aggregation of High Myopia: Estimation of the

Sibling Recurrence Risk Ratio. Investigative Opthalmology and Visual Science, 45(9), p. 2873. doi:10.1167/iovs.03-1155

Froehlich, J. W., & Giles, E. 1981. A multivariate approach to fingerprint variation in Papua New Guinea: Perspectives on the evolutionary stability of dermatoglyphic markers. American Journal of Physical Anthropology, 54(1), pp. 93-106. doi:10.1002/ajpa.1330540111

Galton, F. 2004. Finger prints: The classic 1892 Treatise. New York: Dover Publications Inc.

Gehring, W. J. 2002. The genetic control of eye development and its implications for the evolution of the various eye-types. The International Journal of Developmental Biology, 46, pp. 65-73.

Gradiser, M., Matovinovic, O. M., Dilber, D., & Bilic-Curcic, I. 2016. Assessment of Environmental and Hereditary Influence on Development of Pituitary Tumors Using Dermatoglyphic Traits and Their Potential as Screening Markers. International Journal of Environmental Research and Public Health, 13(3), p. 330. doi:10.3390/ijerph13030330

Guggenheim, J. A., Kirov, G., & Hodson, S. A. 2000. The heritability of high myopia: a reanalysis of Goldschmidt's data. Journal of Medical Genetics, 37(3), pp. 227-231. doi:10.1136/jmg.37.3.227

Ho, Y. Y. W., Evans, D. M., Montgomery, G. W., Henders, A. K., Kemp, J. P., Timpson, N. J., . . . Davey-Smith, G. 2016. Common Genetic Variants Influence Whorls in Fingerprint Patterns. Journal of Investigative Dermatology, 136(4), pp. 859-862. doi:10.1016/j.jid.2015.10.062

Holden, B. A., Fricke, T. R., Wilson, D. A., Jong, M., Naidoo, K. S., Sankaridurg, P., . . . Resnikoff, S. 2016. Global Prevalence of Myopia and High Myopia and Temporal Trends from 2000 through 2050. Ophthalmology, 123(5), pp. 1036-1042. doi:10.1016/j.ophtha.2016.01.006

Holt, S. B. 1968. The genetics of dermal ridges. Springfield, Illinois: C. C. Thomas.

Ismail, E., Shairah, A. R., Selamat, L., Gurusamy, R., Zariman, H., Shahrudin, M. S., . . . Mohamad, O. 2009. Dermatoglyphics: comparison between Negritos Orang Asii and the malays, Chinese and Indian. Sains Malaysiana, 38 (6), pp. 947-952.

Karmakar, B., & Kobyliansky, E. 2012. Finger and palmar dermatoglyphics in Muzeina Bedouins from South Sinai: qualitative traits. Papers on Anthropology, 20, p. 146. doi:10.12697/poa.2011.20.16

Kobyliansky, E., & Micle, S. 1987. Dermatoglyphic sexual dimorphism in middle eastern Jews. Bulletins et memoires de la Soc d'Anthropologie de Paris, 14(4), pp. 271-290.

Li, J., & Zhang, Q. 2017. Insight into the molecular genetics of myopia. Molecular Vision, 23, pp. 1048-1080.

Machado, J. F., Fernandes, P. R., Roquetti, R. W., & Filho, J. F. 2010. Digital Dermatoglyphic Heritability Differences as Evidenced by a Female Twin Study. Twin Research and Human Genetics, 13(05), pp. 482-489. doi:10.1375/twin.13.5.482

Martín, B., Fañanás, L., Gutiérrez, B., Chow, E. W. C., & Bassett, A. S. 2004. Dermatoglyphic profile in 22q deletion syndrome. American Journal of Medical Genetics Part B: Neuropsychiatric Genetics, 128B(1), pp. 46-49. doi:10.1002/ajmg.b.30034

Meier, R. J., Goodson, C. S., & Roche, E. M. 1987. Dermatoglyphic development and timing of maturation. Human Biology, 59 (2), pp. 367-373.

Mittal, V. A., Dean, D. J., & Pelletier, A. 2012. Dermatoglyphic asymmetries and fronto-striatal dysfunction in young adults reporting non-clinical psychosis. Acta Psychiatrica Scandinavica, 126(4), pp. 290-297. doi:10.1111/j.1600-0447.2012.01869.x

Naugler, C. T., & Ludman, M. D. 1996. A case-control study of fluctuating dermatoglyphic asymmetry as a risk marker for developmental delay. American Journal of Medical Genetics, 66(1), pp. 11-14. doi:10.1002/(sici)1096-8628(19961202)66:1<11::aid-ajmg3>3.0.co;2-z

Nousbeck, J., Burger, B., Fuchs-Telem, D., Pavlovsky, M., Fenig, S., Sarig, O., . . . Sprecher, E. 2011. A Mutation in a Skin-Specific Isoform of SMARCAD1 Causes Autosomal-Dominant Adermatoglyphia. The American Journal of Human Genetics, 89(2), pp. 302-307. doi:10.1016/j.ajhg.2011.07.004

Reed, T., Viken, R. J., & Rinehart, S. A. 2006. High heritability of fingertip arch patterns in twin-pairs. American Journal of Medical Genetics Part A, 140A(3), pp. 263-271. doi:10.1002/ajmg.a.31086

Sanfilippo, P. G., Hewitt, A. W., Hammond, C. J., & Mackey, D. A. 2010. The Heritability of Ocular Traits. Survey of Ophthalmology, 55(6), pp. 561-583. doi:10.1016/j.survophthal.2010.07.003

Sirri, C. F., Gul, D., Tunca, Y., Fistik, T., Ozdemir, E. M., Yildiz, H., . . . Solak, M. 2008. Analysis of the dermatoglyphics in Turkish patients with Klinefelter's syndrome. Hereditas, 145(4), pp. 163-166. doi:10.1111/j.0018-0661.2008.02049.x

Stošljević, M., & Adamović, M. 2013. Dermatoglyphic characteristics of digito-palmar complex in autistic boys in Serbia. Military Medical and Pharmaceutical Journal of Serbia, 70(4), pp. 386-390. doi:10.2298/vsp1304386s

Tang, W. C., Yap, M. K., & Yip, S. P. 2008. A review of current approaches to identifying human genes involved in myopia. Clinical and Experimental Optometry, 91(1), pp. 4-22. doi:10.1111/j.1444-0938.2007.00181.x

Todd, E. S., Scott, N. M., Weese-Mayer, D. E., Weinberg, S. M., Berry-Kravis, E. M., Silvestri, J. M., . . . Marazita, M. L. 2006. Characterization of dermatoglyphics in PHOX2B-confirmed central hypoventilation syndrome. Pediatrics, 118(2); e408-414.

Wertheim, K., & Maceo, A. 2002. The critical stage of friction ridge and pattern formation. Journal of Forensic Identification, 52(1), pp. 35-85.

SIMULATION OF CHEMICAL ACCIDENTS WITH ACETYLENE IN „MESSER TEHNOGAS" KRALJEVO PLANT BY „ALOHA" SOFTWARE PROGRAM

DANIJELA ILIĆ KOMATINA[1*], JOVANA GALJAK[1], SVETLANA BELOŠEVIĆ[1]

[1]Faculty of Technical Sciences, University of Priština, Kosovska Mitrovica, Serbia

ABSTRACT

Chemical plants are generally associated with potentially high risk of chemical accidents. During chemical accidents hazardous substances jeopardize human lives, destroy material assests and degrade natural environment. The release of flammable and explosive gases or liquids especially poses a significant threat to the environment. This paper introduces the simulation of a chemical accident caused by an uncontrolled acetylene cylinder release in the warehouse of Messer Tehnogas Kraljevo chemical plant. The simulation was performed by ALOHA program package which defines a possible accident development and determines threat and safety zones. The assessment of potential scenarios is based on physico-chemical properties of the substance causing the accident. This paper discusses accident situations occurring under the most unfavorable atmospheric conditions.

Keywords: Hazardous substances, Acetylene, Chemical accident, Simulations, Releaser, Messer Tehnogas Kraljevo, "ALOHA" software.

INTRODUCTION

Chemical industry is one of the major potential environmental pollutants. A great variety of its negative impacts affect both living organisms and material assets. This group of pollutants includes not only chemical factories, plants, warehouses of hazardous substances, and petrochemical industry, but all industrial complexes using dangerous substances in their production processes. Due to the high level of risk during its working performance, the activities of chemical industy have been frequently disputed.4 A large number of various hazards are reported especially with organic matters (Bogdanović, 2008).

THEORETICAL PART

Hazardous substances and chemical accidents

According to European Union Directive–*Seveso II*, a chemical accident is defined as a result of unplanned and unpredicted events in the course of industrial activity being manifested through emission of toxic substances in the environment or through fire or explosion. The accidents comprising one or more hazardous chemicals jeopardize humans and environment both immediately or with delay, inside or outside the installation. Chemical industrial processes using flammable and/or toxic substances under different pressures and temperatures are exceptionalaccident-prone sites (Abassi et al., 2013; Khan & Abassi, 1998a). It happens quite frequently that initial fires and explosions within the plant are initiators of new fires or explosions causing the so called "domino effect" enabling primary accident to be spread outside the building and

grown into widespread disaster (Khan, 1998b; Khan, 2001). These accidents kill a huge number of people and cause million euro losses.

According to International Labour Organization (ILO), chemical accidents occur during processing (40%), storage (25%) or transportation (35%) of hazardous substances. The major causes of chemical accidents appear to be human factor in 62% of cases and outdated technology in 20% of cases. Statistics show that, compared with all natural catastrophes, the highest number of casualties results from chemical accidents (Varma, 2005). As reported by International Labour Organization, around 6000 people per day or 2.2 million people per year die from workplace accidents or consequences of professional illnesses.

Depending upon the place of origin, chemical accidents can be classified as those occurring in fixed facilities (plants, warehouses, oil pipelines) and those occurring during the transport of chemicals. Figure 1 shows the fire in the acetylene warehouse in Dallas 2007. According to the area affected by them, chemical accidents can be categorized as local, regional, national, and global. The most significant factors affecting the spreading of chemical accidents in space and time include physico-chemical properties of hazardous substance and meteorological, hydrological, and geological conditions of the location. Negative consequences resulting form chemical accidents are:

Release of hazardous pollutants (toxic, flammable, corrosive substances) into air, water or soil.

Explosions of substances including both the formation of a strong impact wave and the emission of toxic substances into atmosphere.

Fires being followed by both the formation of toxic and flammable gas clouds and solid combustion products.

---

* Corresponding author: danijela.ilic@pr.ac.rs
CHEMISTRY

Numerous chemical accidents have been recorded both locally and worldwide (Bogdanovic, 2009). Some of major world chemical accidents should be mentioned: Flixborough (1974), Seveso (1976), Bhopal (1984), Basel (1986), Mexico (1988), Enschede (2000), AZF Toulose (2001) (Sengupta et al., 2016). Tragic consequences of these events initiated multiple efforts in order to increase chemical process safety. Regarding that, many articles and books have been written (Crowl & Louvar, 2001; Mannan, 2013; Sanders, 2015) as well as procedures concerning safety improvements while processing, using, and handling hazardous substances.

Figure 1. Fire in acetylene warehouse, Dalas, Texas, 2007. Source: http://canaryperch.com/evac9McLain.html

Acetylen – dangerous chemical

Acetylen (C_2H_2) is the simplest unsaturated hydrocarbon belonging to alkyne group. Its molecule is linear and built up from two carbon atoms bonded together in a triple bond. One hydrogen atom is bonded to every carbon atom.

At normal temperature and pressure, pure acetylene is colorless, odorless, and tasteless. It is lighter than air and highly flammable. It is one of the most dangerous gases regarding flammability and explosivity. It burns in air with a bright flame whereas in oxygen it burns with a very hot flame reaching 3100 ^{0}C. The physico-chemical characteristics of acetylene are shown in Table 1. Due to the presence of phosphine and hydrogen sulfide, technical acetylene has specific garlic-like odor. As a result of a high flame temperature, acetylene is widely used in welding and metal cutting. Acetylen is often used as an alternative fuel or as an additive in reducing NOx emission in internal combustion engines (Lakshmanan & Nagarajan, 2010a; Lakshmanan & Nagarajan, 2011b).

Handling with acetylene under the pressure being below atmospheric pressure appears to be quite safe. However, under higher pressures, due to the presence of unstable triple bond in its molecule, acetylene itself becomes highly unstable. Due to the

energy impact, this gas undergoes the process of decomposition the result of which flammable hydrogen and elementary carbon are obtained. Exothermic reactions release a great deal of energy with temperatures ranging from 2800 ^{0}C to 2900 ^{0}C. The acetylene decomposition can result in external and compressive heating, electric sparks, or a strong impact wave. Acetylene is known to be able to decompose even under the condition of complete lack of air. (Carver et al., 1972) Due to the energy impact or under the higher pressure, acetylene can decompose in the cylinder in the completely inert atmosphere. In the course of this process, 226.5 kJ of heat per mole is released so compressed acetylene can behave as a very strong explosive. Combined with air, acetylene under pressure is easily flammable even at low temperatures. Acetylene has a low ignition energy (minimal ignition energy is 0.019 mJ) and it possesses a high speed of chemical energy release making it a very hazardous gas.(Sarkar, 1990). The boundaries of its explosivity in the mixture with air range from 1.5-82 vol%, whereas with oxygen those intervals range from 2.3-93 vol%.

Table 1. Physico-chemical characteristics of acetylene.

Chemical formula	C_2H_2
Name	Acetylene, Ethyne (IUPAC)
The molar mass	26,04 g/mol
Appearance	Colorless gas
Odor	Odorless
Density	1,097 g/L
Melting point	-80,8 ^{0}C
Sublimation conditions	-84 ^{0}C
Vapor pressure	44 5,85 kPa (on 20 ^{0}C)
Acidity (pKa)	25
Self-ignition temperat.	305 ^{0}C
Limits of explosive mix	2,3-81 %

At higher temperatures and under higher pressures, acetylene decomposes spontaneously releasing a large quantity of energy and causing chain reactions which result in explosion. Uncontrolled acetylene release during production processes, transportation, or storaging can lead to explosions and detonations endangering safety of people and material assets.

Acetylene can also be associated with chemical explosions followed by detonation combustion characterized by a strong impact wave and deflagration combustion characterized by intense thermal radiation. Damaging effects of detonation and deflagration combustion in free space spread rapidly and can easily overcome the zero zone of regular fire impact. These conditions cause significant material devastations, human casualties, and ecological disasters.

Pure acetylene is not toxic but in high concentrations it has a narcotic and irritating effect on people. Strong impact waves during explosions can lead to blast injuries.

Handling acetylene conforms with special regulations strictly excluding sudden cylinder discharging, mechanical smashing, heating, and uncontrolled change of volume/pressure proportion. Acetylene that is stored or transported must be properly labeled as shown in Table 2.

High potential for explosive acetylene decomposition can be significantly decreased by mixing it with inert gases or dilluting it in suitable solvents. For this reason acetylene is stored in steel tanks, under pressure of 18 bar, dilluted in acetone. Various types of special porous materials are added into tanks in order to provide additional safety in acetylene handling.

Table 2. Acetylene labeling.

Package and storage labeling			
Class	F+		
NFPA 704 standard labeling			
Health hazards (1)– low risk	Fire hazards (4)–easy flammable	Reactivity (3)–risk of explosion	Not reacting with water
Transport labeling			
Hazardous substance class	2,1	Flammable gas	
Kemler code	239	Flammable gas, easy reactive	
UN number	1001		
CAS number	74-86-2		

Simulation of chemical accidents

Prior to the chemical accident, the estimate of its impact to the environment is performed whereas the further calculation of its imact is done only after the accident. Ecological risk of an accident can be estimated based on possible scenarios where modelling provides us with the insight into endangered zones in real space and time.

Cities hosting plants which process, remanufacture or storage hazardous substances, carry a higher risk of chemical accidents (Sanchez et al., 2018) Therefore, the simulation of hazardous substance release in industrial plants has become important in prevention and assessment of negative impacts of chemical accidents, in environment protection and workplace safety increase (Shao & Duan, 2012; Huang et al., 2015). Numerous mathematical models have been developed as useful tools for prediction of accidents in chemical processes (El

Harbawi et al., 2008). Each simulation of chemical accident represents a unique scenario.

This paper focuses on chemical accidents caused by acetylene cylinder release in the warehouse of Messer Tehnogas Kraljevo plant. The description of possible accident sdevelopment, threat zones and impact on the environment was done by software program ALOHA (*Areal Locations of Hazardous Atmospheres*). This program was developed by team efforts of *Environmental Protection Agency* (*EPA*) and *National Oceanic and Atmospheric Administration* (*NOAA*) of the USA. ALOHA is a part of CAMEO (*Computer Aided Managament of Emergency Operations*) software package. Not only does it function as an independent program, it also works with CAMEO *Chemicals* and MARPLOT programs. ALOHA is widely used to plan for and respond to chemical emergencies. ALOHA program's database contains over 1000 pure chemicals with ability to add new or modify the existing ones. ALOHA is a modelling program that estimates threat zones, including the clouds of toxic gas, fire and explosions. The threat zone is an area where a hazard i.e. a risk (such as toxicity, flammability, thermal radiation or damaging overpressure) has exceeded a user-specified Level of Interest, the Level of Risk or the Level of Concern – LOC (Jovanović, 2013). This program should be avoided in cases of chemical mixtures, indoor simulations, atmospheric fallouts, and in cases of distances farther than 10 km from the hazardous chemical release source. It is not suitable for simulations in urban areas with many tall buildings and where there is a probability for "canyon effect".

EXPERIMENTAL

Plant Messer Tehnogas Kraljevo

Messer Tehnogas company is the biggest producer and distributor of industrial, medical, and special gases in Serbia and in the Balkans. It supplies over 4000 buyers in Serbia and it delivers over 650 000 t of products per year. This company trades with gases produced in its own plant such as oxygen, hydrogen, helium, argon, carbon dioxide, acetylene. Beside the product distribution, the plant in Kraljevo also produces acytelene gas. It is located in the southern part of the city, in the urban area called Ribnica in Izletnička Street. As can be seen on the satellite picture of the plant (Figure 2), it is located in the urban part of the colony. The lowland terrain on which the plant was built lies at the altitude of 196m. The plant is located at latitude 43^0 42' 32" and longitude 20^0 41' 36". The total area of plant complex is around 5.0 ha. Since the plant is situated in the urban area, the population likely to be under the direct negative impact of the accident is estimated to be as high as 1000 people.

Primary school "Vuk Karadžić" being attended by 472 pupils is 100m northwest from the plant. Local Community Health Center is 100m north from the plant. Cultural Center "Ribnica" is also placed nearby the plant. Residential buildings

are situated around the plant facilities. The river Ribnica flows 50 m far from the eastern plant facility and at 500 m on the north it flows into the Ibar. The nursery of "Srbijašume" producing desiduous and coniferous tree seedlings lies in the southwest of the plant.
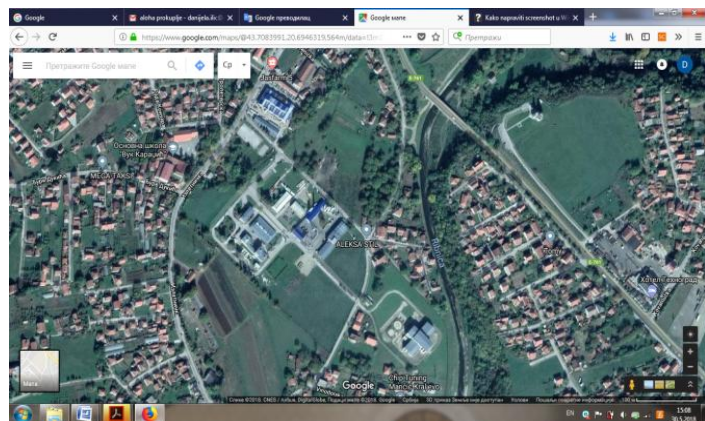
Figure 2. Satellite picture of the plant and surroundings.

The part of the plant where acetylene is stored was selected as the focus of the accident simulation, and fire and explosion risk analysis.

Simulations of acetylene release

This scenario implies a visualization of possible hazards by determining threat zones, accident extent, and consequences of immediate exposure to chemical impact on the selected area. In order to model an accident, quantitative and qualitative data are required: information on the chemical compound involved (quantity, state of matter, physico-chemical and ecotoxicology

properties), accident location data, and current meteorological conditions under which unpredicted events occur.

This paper investigates the scenario leading to the gas diffusion from acetylene cylinder in the warehouse caused by tank wall damage (cracking). Acetylene tank is cylider-shaped and has a 0.5m diameter and a length of 2m. It is filled to 90% of its volume. The dimensions of the cylinder wall damage made at the height of 0.1m from the ground, are 0.100 x 0.05 m.

The simulation of acetylene release was performed under the most unfavorable meteorological conditions. Starting from experiential data, these conditions include wind speed of 1.5 m/s, the highest daily temperature, the average humidity matching the location and the temperature, and atmospheric stability of F class (Cvetanović, 2015).

Atmospheric conditions, given in Table 3, representing input data in the software are retrieved from the internet site of Republic Hydrometeorological Service of Serbia (RHSS). These data show that western and eastern winds are the most frequent on the territory of the municipality of Kraljevo. Other wind types are not so present at this locality. Based on the geographical position of the warehouse in the plant complex, the eastern wind is deduced to make the most serious damage therefore it was taken as an atmospheric parameter for the simulation.

In the process of fire and explosion modelling, the boundaries of zones with damaging effect exposure should be determined (demolition, overpressure of impact wave, thermal energy effects) and the safety zone for people and objects should be defined.

Table 3. Meteorological data for Kraljevo, RHSS.

Month	T_{max} (^0C)	T_{min} (^0C)	Wind (E) speed (m/s)	Wind (W) speed (m/s)	Relative humidity (%)	Cloudiness (x/10)
January	17.1	15,6	2,2	2,1	84	7,2
February	24,8	-3,4	3,2	2,6	72	6,8
March	24,8	-2,0	1,0	1,9	75	6,7
Apryl	29,5	0,0	2,2	2,2	66	6,1
May	29,2	4,7	1,8	1,6	71	6,2
June	36	8,9	2,3	1,8	71	5,5
July	37,2	11.9	2,3	2,1	64	3,9
August	33,2	8,7	1,8	1,8	72	4,7
September	31,1	4,5	2,0	1,3	73	4,7
October	26,1	-0,5	3,0	1,8	81	7,6
November	21,7	-3,7	2,2	1,9	76	6,0
December	12,6	-9,5	1,1	2,5	78	5,8

Acetylene is stored in a cylinder where it is dissolved in acetone under 18 bar pressure so the damage on the cylinder causes a great deal of this gas to be released in the atmosphere in the aerosol form. Since acetylene is a highly flammable and explosive gas, there are various accident scenarios. Toxic effects of hazards were not considered since fire and explosion present

by far the greatest danger of acetylene release. The model of spreading of vapor clouds formed by gas release, the model of jet fires formed by ignition in the cylinder, and the model of liquid expanding vapor explosions were all examined. Our main objective was to estimate endangerment of people and objects in the plant and its vicinity.

As can be seen in Figure 3, the simulation in all these cases showed that acetylen was released from the cylinder in the form of aerosol at the speed of 1.57 kg/s. The total time of acetylene release was 60 seconds.
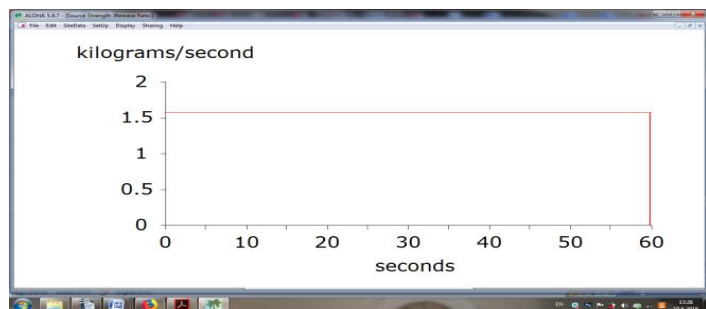
Figure 3. Chart of acetylene cylinder release speed.

The first scenario, given in Table 4, includes the release of non-burning acetylene forming a vapor cloud.

Table 4. Scenario 1.

Threatening danger	Weather		Releasing substance
Acetylene release without ignition with formation of flammable cloud	Temperature	37,2 ^{0}C	Dilluted acetylene
	Wind (E)	1,5 m/s	
	Cloud cover	4/10	
	Humidity	64%	
	Stability Class	F	

In this case the areas with gas vapor air concentration within the limits of flammability, which can easily result in fire, were defined.

The results of this simulation, shown in Figure 4, show that at 53 m distance from the hazard location spot in the wind direction, the gas concentration in the atmosphere is higher than 15000 ppm being 60% of lower flammability limit and can therefore cause forming pockets of fire and generating fire (red zone). In this zone workers caught at their workplaces and the part of the factory in the vicinity are most threatened.
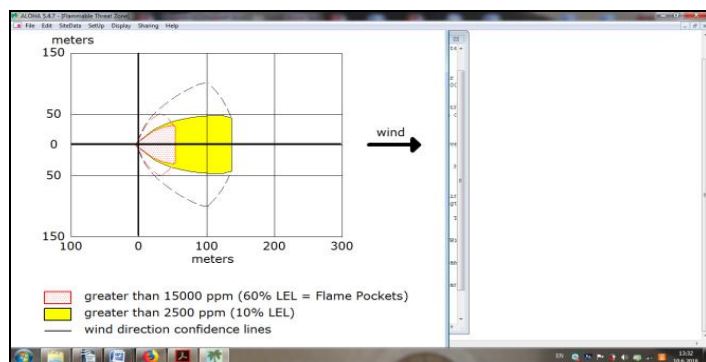
Figure 4. Characteristics of threat zones in Scenario 1.

The yellow zone occupies the area at 53 m to 138 m distance from the hazard source in the wind direction and it has a gas concentration of 2500 ppm being 10% of lower flammability limit. As can be seen in Figure 5 in this zone about 15 residential buildings and a part of local road leading through the urban area would be directly endangered.
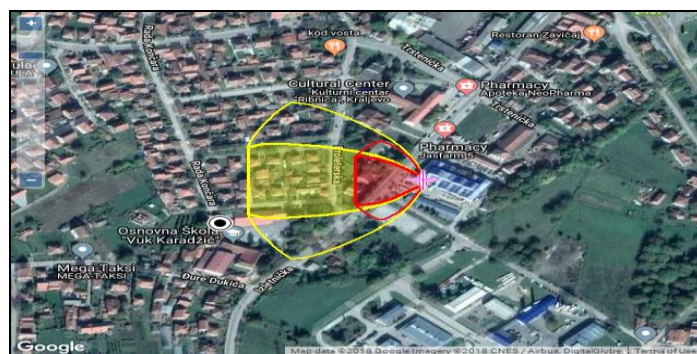
Figure 5. Zones of flammable acetylene cloud spreading in real space.

Although the second scenario, shown in Table 5, refers to the simulation of the accident under the same conditions, this simulation estimates the probability of forming an explosive zone caused by overpressure i.e. it defines the areas on which explosion of the formed acetylene cloud releasing into the atmosphere can occur.

Table 5. Scenario 2.

Threatening danger	Weather		Releasing substance
Acetylene release without ignition with formation of explosive cloud	Temperature	37,2 ^{0}C	Dilluted acetylene
	Wind (E)	1,5 m/s	
	Cloud cover	4/10	
	Humidity	64%	
	Stability Class	F	

The simulation was performed for the detonation ignition occurred in the time period of 60 seconds after the gas release.
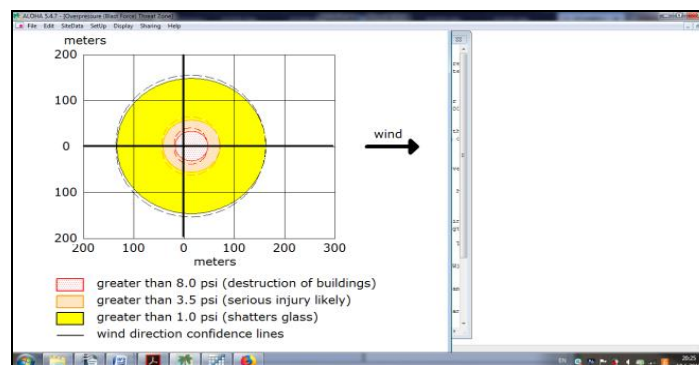
Figure 6. Characteristics of threat zones in Scenario 2.

As can be seen from Figure 6, in this case, the most endangered zone encloses the diameter of 48 m (red zone) whose center is slightly shifted in the wind direction. In this zone under the pressure higher than 55.16 kPa which has a destructive power, concrete buildings can be destroyed and human fatalities can be recorded. This scenario would include the warehouse of the plant and a part of the local road leading through the urban area. In the subsequent band placed at 48 to 72 m distance from the hazard source (orange zone), the pressure higher than 24.13 kPa can cause grave injuries and the destruction of light construction buildings. In the real space, shown in Figure 7, the orange zone includes a part of the plant, a part of the traffic road, sports facilities and a small number of residential buildings. The zone located at perimeter distance from 72 to 163 m (yellow zone) is the area under the pressure of 6.89 kPa. Minor injuries of people and slight building damages such as window cracking can be recorded in this zone. The yellow zone of this scenario would cover the Local Community Health Center, the Cultural Center, the primary school and about 20 residential buildings.

Figure 7. Zones of explosive acetylene cloud spreading in Scenario 2 in real space.

In the third scenario, given in Table 6, the release of dilluted acetylene in flame was predicted (fire in a tank, jet fire).

Table 6. Scenario 3.

Thretening danger	Weather		Releasing substance
Release of burning acetylene jet fire	Temperature	37,2 ^{0}C	Dilluted acetylene
	Wind (E)	1,5 m/s	
	Cloud cover	4/10	
	Humidity	64%	
	Stability Class	F	

Thermal radiation is the threatening danger signalled by the software. As can be seen in Figure 8, three dangerous zones are also defined in this scenario.

The software predicted a 32 m long jet flame lasting for 20 seconds. In the 10 m radius red zone, thermal radiation with energy over 10 kW/m^2 is expected. This zone is potentially

deadly and can cause severe burnings in only 60 seconds. The orange zone occupies the area at 10 to 23 m distance from the hazard source and is slightly shifted to the wind direction. Radiation energy in this zone reaches over 5 kW/m^2 causing second-degree burnings in only 60 s. The third band of danger lies at 23 to 45 m distance from the accident spot. Thermal radiation of 2 kW/m^2 in this zone can cause mild burnings in 60 s. Figure 9 shows the thermal radiation zones of acetylene in scenario 3 in the real space. This scenario would assume that the part of the plant in the vicinity of the hazard source belongs to the red zone. Beside the part of the plant, the orange zone would include a segment of local traffic road, whereas the majority of storage facilities of the plant, a part of the traffic road and one residential building would belong to the yellow zone.

Figure 8. Characteristics of threat zones in Scenario 3.

Figure 9. Zones of thermal radiation of acetylene in Scenario 3 in real space.

The fourth scenario, shown in Table 7, was modelled for the *Boiling Expanding Vapour Explosion* (BLEVE). Thermal radiation (surface heat flux of flame) of the burning tank is the danger predicted by the software.

Characteristics of threat zones in Scenario 4 are given in Figure 10. In the fourth scenario, the software predicted the fire diameter of 31 m in only 3 s. The red zone is the zone where the fire ball originates with energy flux higher than 10 kW/m^2 being potentially fatal to humans. The diameter of this zone reaches 74 m. The next zone is the orange one occupying the band from 74 to 104 m. This zone is characterized by thermal energy of 5

kW/m^2 which can cause fires in buildings and serios burnings with people. The yellow zone is situated in the subsequent band which lies at 104 to 163 m distance from the accident. Energy of thermal flux in this band reaches 2 kW/m^2 and can result in minor burnings.

Table 7. Scenario 4.

Threatening danger	Weather		Releasing substance
Boiling Expanding Vapour Explosion	Temperature	37,2 ^{0}C	Dilluted acetylene
	Wind (E)	1,5 m/s	
	Cloud cover	4/10	
	Humidity	64%	
	Stability Class	F	
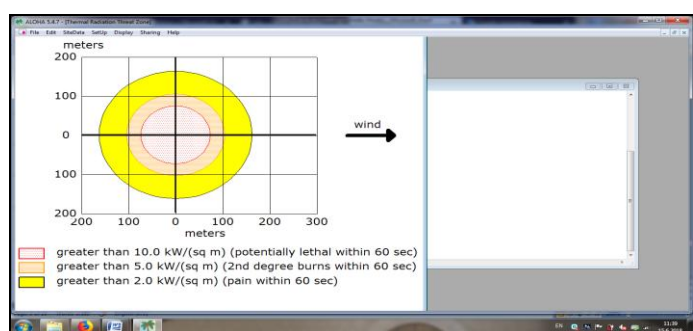
Figure 10. Characteristics of threat zones in Scenario 4.

Zones of thermal radiation of acetylene in Scenario 4 in real space are given in Figure 11. This scenario implies that the red zone would inlcude broader part of the plant complex area, a segment of the traffic road, playground, Health Center and 5-6 residential buildings. The orange zone would include a segment of the traffic road and 5 residential buildings. Cultural center, around 20 residential buildings and the acetylene production plant segment would belong to the yellow zone.
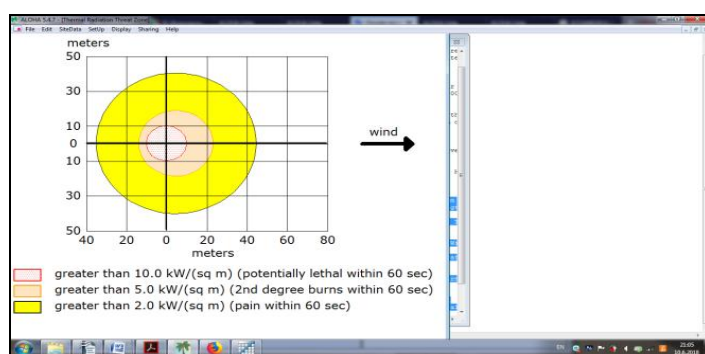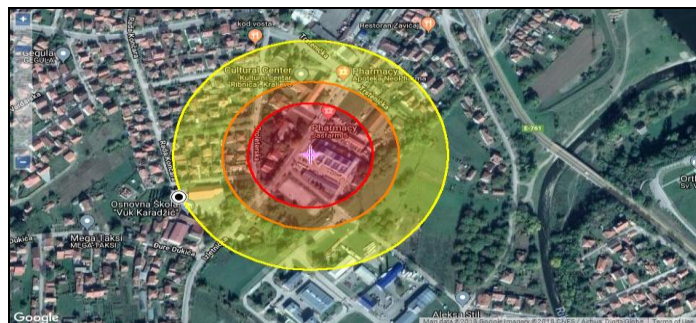

Figure 11. Zones of thermal radiation of acetylene in Scenario 4 in real space

CONCLUSION

The simulations of various acetylene cylinder release scenarios indicate the high risk of fire in explosion and significant endangerment of working and natural environment in Messer Tehnogas Kraljevo plant. The most endangered zone is the warehouse with different gases. Bearing in mind that acetylene is storaged in this zone, it can be logically deduced that fire or explosion of only one acetylene cylinder can trigger the avalanche of uncontrolled explosions and fires. This generates the so called "domino effect" whose consequences are far more serious than the described ones.

Together with assessment of safety and threat zones, ALOHA sotware program provides proper risk managament planning and improvement of people and object safety in the surroundings. According to damage risk estimates, this program contributes to taking adequate measures in order to prevent potential accidents in chemical plants. The simulation is substantially cheaper solution compared to *in vivo* experiments since it saves material, financial, and temporal resources.

REFERENCES

Abbasi, T., Ramasamy, E.V., Khan, F.I., & Abbasi, S.A. 2013. Regional EIA and Risk Assessment in a Fast Developing Country. New York: Nova Science. pp. x+433.

Bogdanović, M. 2008. Faze nastajanja akcidenata i mere zaštite od posledica hemijskih akcidenata. Facta universitatis - series: Working and Living Enviromental Protection; Niš, Vol. 5, No 1, pp. 89-95.

Bogdanović, M. 2009. Widely known chemical accidents. Facta universitatis -series: Working and Living Environmental Protection; Niš, Vol. 6, No 1, pp. 65-71.

Carver, F.W.S., Smith, C.M., & Webster, G.A. 1972. The explosive decomposition of acetylene in pipelines. In I.Chem.E. Symposium Instn chem. Engrs, London. Series No. 33.

Crowl, D.A., & Louvar, J.F. 2011. Chemical Process Safety: Fundamentals with Applications. Boston: Pearson Education.

Cvetanović, S. 2015. Integral model of systemic approach to risk management of chemical accidents at the local level. Niš: Faculty of Occupational Safety. Doctoral dissertation.

El, H.M., Mustapha, S., Choong, T.S.Y., Abdul, R.S., Kadir, S.A.S.A., & Abdul, R.Z. 2008. Rapid analysis of risk assessment using developed simulation of chemical industrial accidents software package. International Journal of Environmental Science & Technology, 5(1), pp. 53-64. doi:10.1007/bf03325997

Huang, D., Zhang, Q., Li, M., & Liu, M. 2015. Example application of risk assessment technology based on acute poisoning accident dispersion simulation. In 5th International Conference on Risk Analysis and Crisis Response, RACR; Tangier; Morocco. Pages 349-357.

Jovanović, T. 2013. The analysis and the simulation of fire risk in the facility for fruit treatment "Pobeda" in Prokuplje. Safety Engineering, pp. 183-187.

Khan, F.I., & Abbasi, S. 1998. Techniques and methodologies for risk analysis in chemical process industries. Journal of Loss Prevention in the Process Industries, 11(4), pp. 261-277. Discovery Publishing House, New Delhi. doi:10.1016/s0950-4230(97)00051-x

Khan F.I., & Abbasi S.A. 1998. Domiefect: (domino effect) a user-friendly software for domino effect-analysis. Environmental Modelling and Software, 13(2), pp. 163-177. doi:10.1016/s1364-8152(98)00018-8

Khan, F.I., & Abbasi, S. 2001. An assessment of the likelihood of occurrence, and the damage potential of domino effect (chain of accidents) in a typical cluster of industries. Journal of Loss Prevention in the Process Industries, 14(4), pp. 283-306. doi:10.1016/s0950-4230(00)00048-6

Lakshmanan, T., & Nagarajan, G. 2010. Experimental investigation of timed manifold injection of acetylene in direct injection diesel engine in dual fuel mode. Energy, 35(8), pp. 3172-3178. doi:10.1016/j.energy.2010.03.055

Lakshmanan, T., & Nagarajan, G. 2011. Study on using acetylene in dual fuel mode with exhaust gas recirculation. Energy, 36(5), pp. 3547-3553. doi:10.1016/j.energy.2011.03.061

Mannan, S. 2013. Lees' Process Safety Essentials: Hazard Identification, Assessment and Control. Butterworth-Heinemann. book.

Sanchez, E.Y., Represa, S., Mellado, D., Balbi, K.B., Acquesta, A.D., Colman, L.J.E., & Porta, A.A. 2018. Risk analysis of technological hazards: Simulation of scenarios and application of a local vulnerability index. Journal of Hazardous Materials, 352, pp. 101-110. doi:10.1016/j.jhazmat.2018.03.034

Sanders, R.E. 2015. Chemical Process Safety: Learning from Case Histories. Butterworth-Heinemann, book.

Sarkar, S. 1990. Fuels and combustion. Mumbai, India: Orient Longman Limited.

Sengupta, A., Bandyopadhyay, D., van Westen, C.J., & van der Veen, A. 2016. An evaluation of risk assessment framework for industrial accidents in India. Journal of Loss Prevention in the Process Industries, 41, pp. 295-302. doi:10.1016/j.jlp.2015.12.012

Shao, H., & Duan, G. 2012. Risk Quantitative Calculation and ALOHA Simulation on the Leakage Accident of Natural Gas Power Plant. Procedia Engineering, 45, pp. 352-359. doi:10.1016/j.proeng.2012.08.170

Varma, R., & Varma, D.R. 2005. The Bhopal Disaster of 1984. Bulletin of Science, Technology & Society, 25(1), pp. 37-45. doi:10.1177/0270467604273822

SYNTHESIS AND ANTIOXIDANT ACTIVITY OF A NEW 4-AMINOCOUMARIN DERIVATIVE

NOVICA RISTIĆ[1]*, NIKO RADULOVIĆ[2], BILJANA DEKIĆ[1], MILENKO RISTIĆ[1], VIDOSLAV DEKIĆ[1]

[1]Faculty of Science and Mathematics, University of Priština, Kosovska Mitrovica, Serbia
[2]Department of Chemistry, Faculty of Sciences and Mathematics, University of Niš, Niš, Serbia

ABSTRACT

Synthesis, spectral characterization, and evaluation of *in vitro* antioxidant activity of a new coumarin derivative, 4-((1,3,4-thiadiazol-2-yl)amino)-3-nitro-2*H*-chromene-2-one, are described. The synthesis of the new product was performed in three reaction steps, with a good overall yield (78%). The structure was corroborated by detailed spectral analysis, including the 1D and 2D NMR experiments (¹H- and ¹³C NMR; ¹H-¹H COSY, NOESY, HSQC, and HMBC). The *in vitro* antioxidant activity was evaluated using the DPPH test. The synthesized compound possesses a good free-radical scavenging activity, $IC_{50}=596.7\pm0.3$ µg/ml, and can serve as a model for the synthesis of similar compounds with promising antioxidant effects.

Keywords: Coumarin derivative, Spectral characterization, NMR spectroscopy, Antioxidant activity, DPPH.

INTRODUCTION

Coumarin (2*H*-chromen-2-one) belongs to the benzopyrones, a group of heterocyclic compounds which have a condensed benzene and α-pyrone ring. These naturally occurring secondary metabolites enumerate about 1300 derivatives isolated from a number of plant species and bacteria (Venugopala et al., 2013). Coumarins are deriving the shikimic acid biosynthetic pathway. Some coumarin derivatives of natural origin already have a medical application, for example, novobiocin, warfarin, acenocoumarin and umbelliferone (Stefanachi et al., 2018). For decades, more efforts have been made to make similar coumarin derivatives by organic synthesis. These derivatives possess an exceptionally wide spectrum of pharmacological properties such as: anticancer (Nofal et al., 2000; Ayati et al., 2018), anti-inflammatory (Bansal et al., 2013; Hadjipavlou-Litina et al., 2007), antibacterial (Naik et al., 2017; Zaki et al., 2012; Radulović et al., 2015) antiviral/anti-influenza (Kostova et al., 2006; Su et al., 2006; Yu et al., 2003; Yeh et al., 2010), antifungal (Pasqualotto et al., 2010; Al-Amiery et al., 2012), anti-Alzheimer (Anand et al., 2012; Piazzi et al., 2008), anticoagulant (Danis et al., 2010), and antioxidant (Kotaiah et al., 2014; Manojkumar et al., 2009; Fylaktakidou et al., 2004).

The interactions between the substituent and the coumarin core determined the biological activity of the molecule itself, which results in its selectivity. Differently substituted derivatives of nitrocoumarin have a remarkable range of selectivity and possess pronounced pharmacological effects like antibacterial (Vaso et al., 2010; Aiyelabola et al., 2017), cytotoxic (Aiyelabola et al., 2017), and antioxidant (Parfěnov & Smirnov, 1991). Some of them have significance in the treatment of kidney cancer cells (Finn et al., 2002) and in the study of enzyme kinetics.

In the light of the mentioned studies of biologically active coumarins, as well as our previous work (Dekić et al., 2010; Dekić et al., 2010), in this research we put emphasis on the synthesis, assignment of ¹H and ¹³C NMR spectral data from an interpretation of results of 2D (¹H-¹H COSY, NOESY, HSQC and HMBC) experiments and evaluation of the antioxidant activity of a new 4-amino substituted-3-nitrocumarin derivative.

EXPERIMENTAL

General chemistry

Reagents and solvents used in this research (A.R. grade) were of Sigma Aldrich (USA), Merck (Germany), Fluka (Germany) and Acros Organics (Belgium). Melting points were determined on MPM-HV2 (Germany) instrument. Recording of IR spectra was carried out on Thermo Nicolet model 6700 FTIR (USA) instrument and HR-MS(EI) spectra were recorded on a JEOL Mstation JMS 700 instrument (Germany). The reaction progress and purity of synthesized compounds checked by TLC, using silica gel plates (Kiesel 60 F_{254}, Merck). Visualization was performed by UV light or spraying the plates with 1:1 (v/v) aqueous sulfuric acid and then heating. The absorbance was measured using a UV-1800 Shimadzu spectrophotometer.

NMR measurement

¹H NMR (400 MHz) and ¹³C NMR (100.6 MHz) spectra were recorded on Bruker Avance III spectrometer (Switzerland) at 25°C in DMSO-d_6, using a TMS as an internal standard. Chemical shifts are reported in ppm (δ) values relative to TMS (δ_H 0 ppm) in ¹H or signals of residual solvents in ¹³C and heteronuclear 2D NMR spectra (residual DMSO-d_6 δ_H 2.54 ppm and ¹³CD₃SOCD₃ δ_C 40.45 ppm. The coupling constant (J) are reported in Hz. Multiplicities of proton resonance are designated as singlet (s), broad singlet (brs), a doublet of doublets (dd), a

---

* Corresponding author: risticnovica@gmail.com

CHEMISTRY

doublet of doublets of doublets (ddd) and a triplet of doublets (td). 2D spectra (^{1}H-^{1}H COSY, NOESY, HSQC, and HMBC) are performed on the same instrument with a standard pulse sequence.

Synthesis

Synthesis of 4-hydroxy-3-nitrocoumarin (2)

According to an already known procedure (Savel'ev et al., 1973), in suspension of 4-hydroxycoumarin (1) (5 g, 30.8 mmol) and glacial acetic acid (20 ml) the mixture of 72% NHO_3 (3 ml) and glacial acetic acid (2.6 ml) was added. The obtained suspension was heated on a water bath until all of 4-hydroxycoumarin are dissolved and does not show the brown vapors of nitrogen oxides. After cooled on ice bath yellow precipitate is obtained, then filtered and washed with saturated solution of sodium-bicarbonate and absolute ethanol. Recrystallization from absolute ethanol gives yellow crystals of 4-hydroxy-3-nitrocoumarin (2) (yield 84%, m.p. 171-172 °C).

Synthesis of 4-chloro-3-nitrocoumarin (3)

In *N,N*-dimethylformamide (2 ml, 26 mmol), cooled to 10°C, during the 15 min, with stirring, $POCl_3$ (4 g, 26 mmol) was added. The reaction then continued at room temperature for another 15 min. After the expiry of this period, 4-hydroxy-3-nitrocoumarin (2) (5.3 g, 26 mmol) dissolved in *N,N*-dimethylformamide (12.5 ml) was added dropwise. The addition of cold water (15 ml), after 15 min, stopped the reaction. The resulting yellow precipitate was filtered and washed with saturated sodium bicarbonate and water, to obtain the final product of 4-chloro-3-nitrocoumarin (3) (yield 87%, m.p. 162-163 °C) as a yellow crystals (Kaljaj et al., 1987), by recrystallization from the benzene:hexane mixture (1:1, v/v).

Synthesis of 4-((1,3,4-thiadiazol-2-yl)amino)-3-nitro-2H-chromen-2-one (5)

In the solution of 4-chloro-3-nitrocoumarin (3) (1 g, 4.4 mmol) in *N,N*-dimethylformamide (10 ml), 1,3,4-thiadiazol-2-amine (4) (0.45 g, 4.4 mmol) and sodium bicarbonate (0.75 g) was added. The mixture was stirred, and progress of the reaction was monitored by TLC. After 90 min, reaction was stopped by the addition of 20 ml of cold water. The formed light yellow solid precipitate was filtered and washed with water, to obtain 4-((1,3,4-thiadiazol-2-yl)amino)-3-nitro-2*H*-chromen-2-one (5) as yellow fine powder (yield 78%, m.p. 237-239 °C). IR (neat): 3262 (N-H), 3066 (Ar-H), 1745 (C=O), 1606 (C=C), 1543 and 1339 (NO_2), 1284, 1123, 867, 753 cm^{-1}. HR-MS(EI): M$^+$ ($C_{11}H_6N_4O_4S$) 290.0109, requires 290.0104 (Δ = + 0.4 mmu).

DPPH assay

Antioxidant activity of synthesized compound (5) was determined by DPPH (2,2-diphenyl-1-picrylhydrazyl) using the previously described method with slight modification (Braca et

al., 2001). In a test tube with 1 ml of a methanolic solution of tested compound (1.96-1000 μg/ml), 2 ml of 0.004% DPPH methanolic solution was added. Test tubes left to stand for 35 min. in the dark at room temperature. After the expiry of this period, absorbance was read at 517 nm. The control was constituted by methanol instead of tested compounds. The same procedure was repeated for the solutions of ascorbic acid (1.96-1000 μg/ml) which used as a standard. The percentage of inhibition of the DPPH radical was calculated using the equation (1):

$$\% \text{ of inhibition} = [(Ac–As)/Ac] \cdot 100 \qquad (1)$$

where *Ac* is the absorbance of control solution (2 ml of DPPH radical and 1 ml of methanol) and *As* is the absorbance of the methanolic solution of tested compound (2 ml DPPH and 1 ml of a methanolic solution of the tested compounds). Results were expressed as IC_{50} values in μg/ml (concentration of the tested compound required to decrease the initial DPPH concentration by 50%) and estimated from % inhibition versus the concentration sigmoidal curve, using a non-linear regression algorithm.

RESULTS AND DISCUSSION

Chemistry

The synthesis of the new coumarin derivative was performed in three steps to give 4-((1,3,4-thiadiazol-2-yl)amino)-3-nitro-2*H*-chromene-2-one (5) as the main product (Scheme 1). The structure of the obtained compound was confirmed by IR spectroscopy and HR-MS(EI), and also complete assignation of the ^{1}H and ^{13}C NMR spectra was performed, by combining the data obtained with 1D and 2D techniques NMR (^{1}H and ^{13}C NMR, ^{1}H-^{1}H COSY, NOESY, HSQC, and HMBC).

The IR spectrum of the synthesized compound showed the bands that confirm his structure. At 3262 and 3066 cm^{-1} appeared the bands of N-H and Ar-H bonds, respectively. The carbonyl group gives a strong vibration at 1745 cm^{-1}, while the band characteristic of the C=C bond occurs at 1606 cm^{-1}. The nitro group showed two strong bands at 1339 and 1543 cm^{-1}. The molecular weight based on HR-MS(EI) (290.0109) indicated the molecular formula of $C_{11}H_6N_4O_4S$, which additionally confirmed the structure of this compound.

In the ^{1}H NMR spectrum of the synthesized compound appeared six signals, two doublet of doublets with chemical shifts at 7.56 and 8.10 ppm, one triplet of doublets at 7.49 ppm, one doublet of doublets of doublets at 7.67 ppm, one wide singlet at 9.25 ppm and one singlet at 9.35 ppm (Fig. 1). The assignment of these signals can be determined based on the position of the hydrogen atoms in the assumed structure. The singlet corresponds to hydrogen atoms from the ring of the substituent and the secondary amino group. Based on the shape of the signal

(a wide singlet) can be concluded that the signal at 9.25 ppm corresponding to hydrogen bound to the nitrogen atom, so the signal at 9.34 ppm corresponds to the proton at the position H-5'.
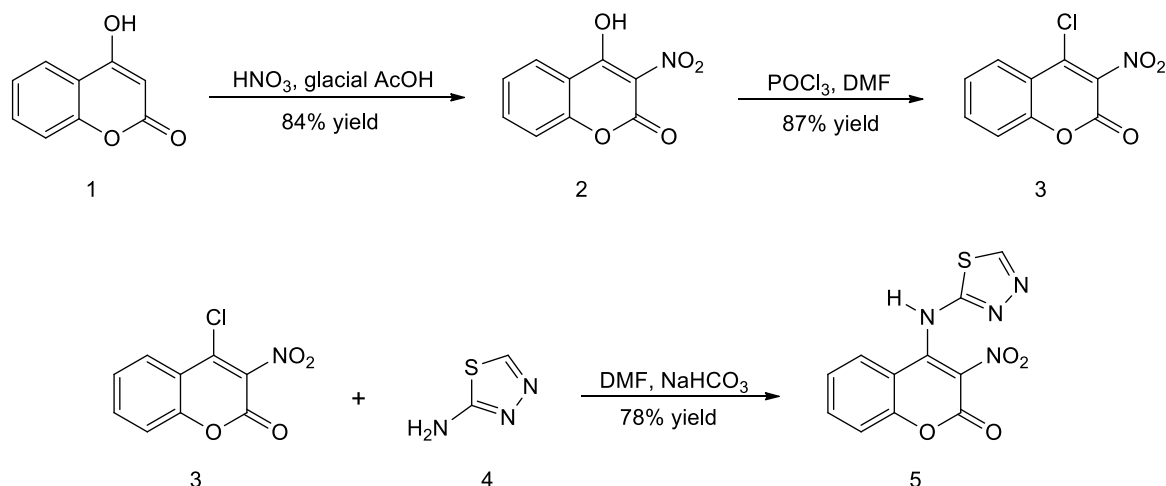
Scheme 1. Reaction steps in synthesis of 4-((1,3,4-thiadiazol-2-yl)amino)-3-nitro-2*H*-chromene-2-one.

This assumption is in accordance with the NOESY (Fig. 2) and the HSQC (Fig. 3) spectral data. The correlation in the NOESY spectrum showed only the singlet at 9.25 ppm. The cross peak of this signal with the doublet of doublets at 8.10 ppm, which corresponds to the proton bonded to the aromatic nucleus, confirms that it is near to the coumarin part of the molecule. On the other hand, the HSQC spectrum occurs interaction only for the signal at 9.35 ppm, which at the same time is assigned to C-5' at 151.1 ppm, while the interaction for proton at 9.25 ppm is absent, due to the fact that this proton is not bound to carbon, already for nitrogen.

Observing the structure of the compounds, it is easy to conclude that doublet of doublets at 7.56 and 8.10 ppm, respectively, and doublet of doublets of doublets at 7.67 ppm corresponding to protons bonded to the coumarin core.
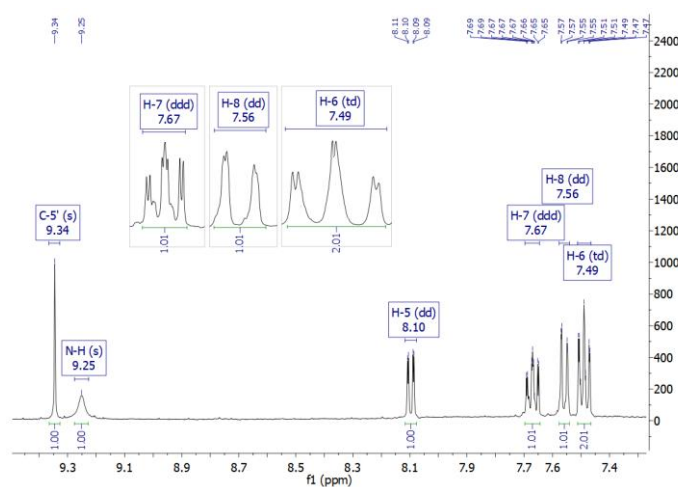
Figure 1. ¹H NMR (CDCl₃, 400 MHz) spectrum of compound (5).
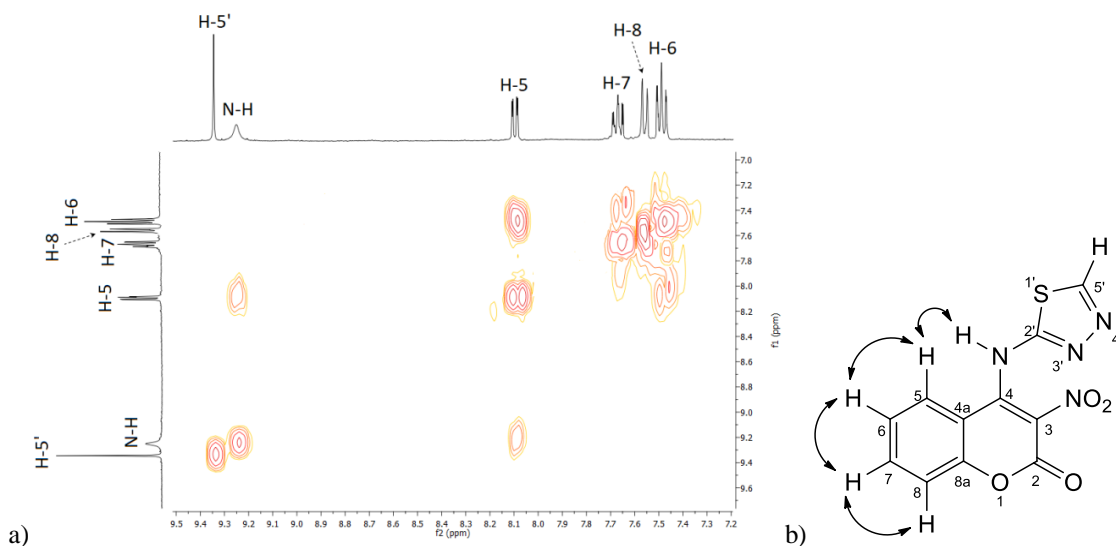
Figure 2. NOESY a) spectrum and b) correlations of compound (5).

Assignments can be performed starting from the signal which showed correlation with the hydrogen from an amino group (9.25 ppm) and doublet of doublets at 8.10 ppm. Based on the spatial disposition in the molecule, it is clear that this signal belongs to the proton H-5. The signal shape corresponding to the position of the proton in the molecule, since it is coupling with one vicinal (H-6, J = 8.0 Hz) and one distant (N-7, J = 1.6 Hz) proton. Signals of other protons, bound to the coumarin core are assigned based on their correlations in the NOESY spectrum, in a similar manner. Chemical shifts of the carbon atoms to which these protons are attached (C-5, δ 123.3; C-6, δ 125.7; C-7, δ 131.8; C-8, δ 118.0) were determined based on the HSQC spectrum. This assignation is in agreement with data obtained from the HMBC spectrum (correlation of hydrogen and carbon through three chemical bonds) (Fig. 4).

Based on interactions with the H-5 in the same spectrum, the chemical shifts of quaternary carbons, C-4a and C-8a, 113.2 and 153.0 ppm, respectively, were assigned. Proton H-5 in this spectrum showed a once more correlation, with the signal at 145.5 ppm, which assigned carbon at position C-4. The chemical shift of the only remaining quaternary carbon atom from the ring of the substituent, C-2' at 150.7 ppm (Table 1), was determined based on his HMBC correlation with the proton on position H-5'.

Table 1. NMR data of compound (5) recorded at 101 (^{13}C NMR) and 400 MHz (^{1}H NMR).

Position	δ_{H}, m (J, Hz)	δ_C	NOESY*	HMBC**
2		154.4		
3		116.5		
4		145.5		
4a		113.2		
5	8.10 dd (1.6, 8.0)	123.7	H-6	C-4, C-7, C-8a
6	7.49 td (0.8, 8.0)	125.7	H-5, H-7	C-4a, C-8a
7	7.67 ddd (1.6, 8.0, 8.4)	131.9	H-6, H-8	C-5, C-8a
8	7.56 dd (0.8, 8.4)	118.0	H-7	C-4a, C-6, C-8a
8a		153.0		
2'		150.7		
N-H	9.25 brs			
5'	9.34 s	151.1		C-2'

*NOESY interactions of the hydrogen from the column "Position" with the hydrogen from the column "NOESY"

**HMBC interactions of the hydrogen from the column "Position" with the carbons from the column "HMBC"

Figure 3. HSQC spectrum of compound (5).
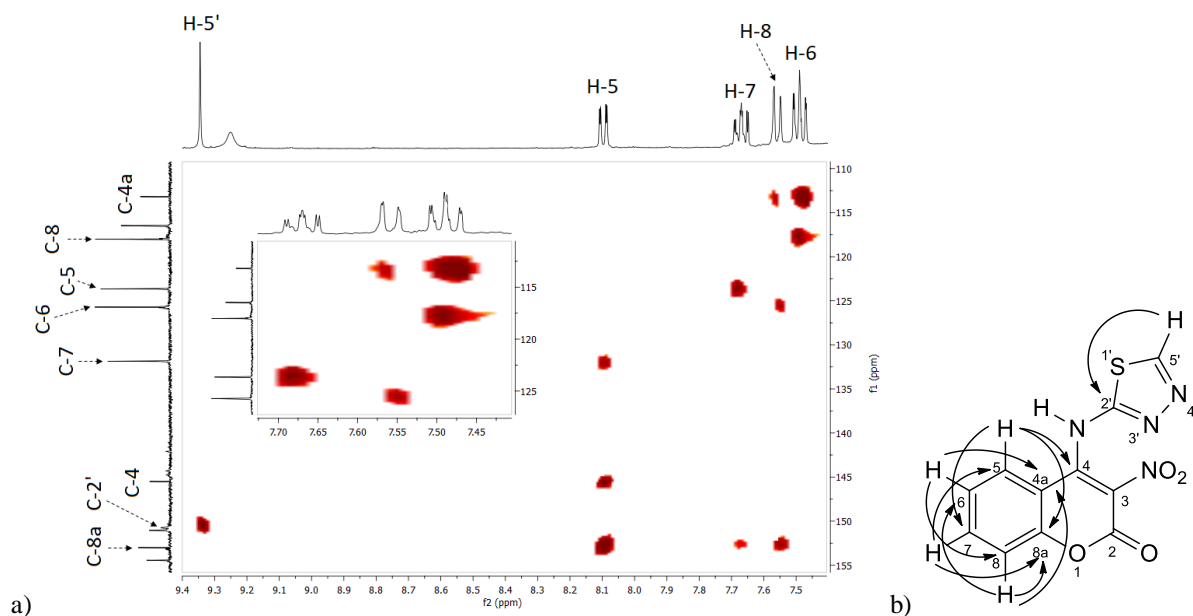
Figure 4. HMBC a) spectrum and b) correlations of compound (5).

In this way, the chemical shifts of all hydrogen and carbon atoms were determined, except for carbons at position C-2 and C-3, which showed no correlation in all of these two-dimensional NMR spectra. The two last unassigned signals in the ^{13}C NMR spectrum at 154.4 and 116.5 ppm (Fig. 5) were attributed to the C-2 and C-3, respectively, based on the expected values and compared with similar compounds of previous studies (Dekić et al, 2010; Dekić et al., 2016).
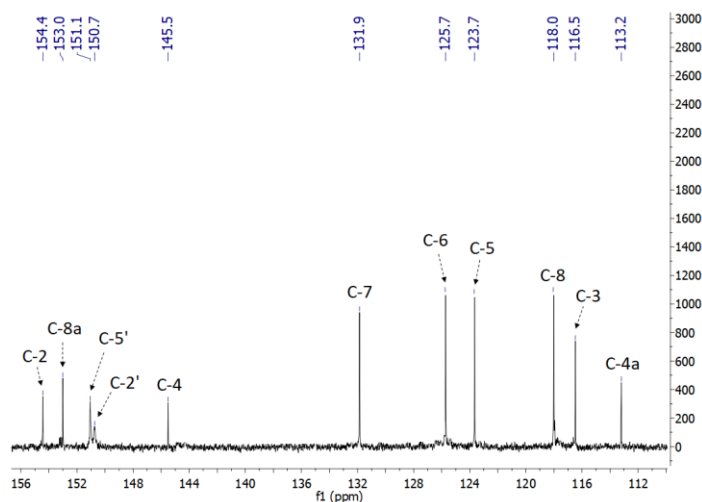
Figure 5. ^{13}C NMR (CDCl$_3$, 100.6 MHz) spectrum of compound (5).

DPPH assay

The DPPH assay is a simple, fast and reliable method for determining the antioxidant activity of the compounds. The percentage inhibition of DPPH radicals, depending on the concentration of the tested compound (5), is showed at Fig. 6. Also, the IC$_{50}$ value for the tested compound was determined, with the amount of 596.7±0.3 μg/ml.
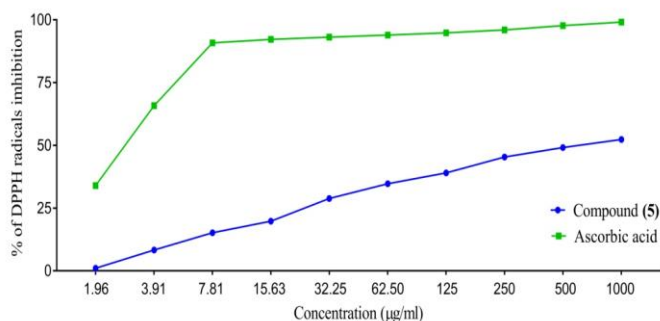
Figure 6. Percentage of inhibition (%) of DPPH radical depending on the concentration of the tested compound. Ascorbic acid was used as a positive control.

Ascorbic acid, known as an exceptional antioxidant, inhibits 50% of the DPPH radicals at a concentration of 3.0±0.1 μg/ml. By comparing the result obtained for the tested compound

with the result for ascorbic acid, it can be concluded that the tested compound showed a very good antioxidant potential.

CONCLUSION

Briefly, synthesis, spectral characterization and antioxidant activity of the new coumarin derivative 4-((1,3,4-thiadiazol-2-yl)amino)-3-nitro-2*H*-chromene-2-one, is described. The structure of the synthesized compound was confirmed by the complete assignment of ^{1}H and ^{13}C NMR spectra, based on data obtained by 1D and 2D NMR techniques. Determination of antioxidant activity was performed by DPPH assay. The tested compound showed a good antioxidant potential, which provides a strong basis for further research.

REFERENCES

Aiyelabola, T., Akinkunmi, E., Obuotor, E., Olawuni, I., Isabirye, D., & Jordaan, J. 2017. Synthesis Characterization and Biological Activities of Coordination Compounds of 4-Hydroxy-3-nitro-2 H -chromen-2-one and Its Aminoethanoic Acid and Pyrrolidine-2-carboxylic Acid Mixed Ligand Complexes. Bioinorganic Chemistry and Applications, pp. 1-9. doi:10.1155/2017/6426747

Al-Amiery, A.A., Kadhum, A.A.H., & Mohamad, A.B. 2012. Antifungal Activities of New Coumarins. Molecules, 17(5), pp. 5713-5723. doi:10.3390/molecules17055713

Anand, P., Singh, B., & Singh, N. 2012. A review on coumarins as acetylcholinesterase inhibitors for Alzheimer's disease. Bioorganic and Medicinal Chemistry, 20(3), pp. 1175-1180. doi:10.1016/j.bmc.2011.12.042

Ayati, A., Oghabi, B. T., Moghimi, S., Esmaeili, R., Majidzadeh-A, K., Safavi, M., Firoozpour, L., Emami, S., & Foroumadi, A. 2018. Synthesis and biological evaluation of new coumarins bearing 2,4-diaminothiazole-5-carbonyl moiety. European Journal of Medicinal Chemistry, 155, pp. 483-491. doi:10.1016/j.ejmech.2018.06.015

Bansal, Y., Sethi, P., & Bansal, G. 2013. Coumarin: a potential nucleus for anti-inflammatory molecules. Medicinal Chemistry Research, 22(7), pp. 3049-3060. doi:10.1007/s00044-012-0321-6

Braca, A., De Tommasi, N., Bari, L. D., Pizza, C., Politi, M., & Morelli, I. 2001. Antioxidant Principles from Bauhinia t arapotensis. Journal of Natural Products, 64(7), pp. 892-895. doi:10.1021/np0100845

Danis, O., Yuce-Dursun, B., Gunduz, C., Ogan, A., Sener, G., Bulut, M., & Yarat, A. 2011. Synthesis of 3-amino-4-hydroxy coumarin and dihydroxy-phenyl coumarins as novel anticoagulants. Arzneimittelforschung, 60(10), pp. 617-620. doi:10.1055/s-0031-1296335

Dekić, B., Dekić, V., Radulović, N., Vukićević, R., & Palić, R. 2010. Synthesis of new antimicrobial 4-aminosubstituted 3-

nitrocoumarins. Chemical Papers, 64(3). doi:10.2478/s11696-010-0004-z

Dekić, B., Radulović, N., Ristić, M., & Dekić, V. 2016. The synthesis and NMR spectral assignments of 3-nitro-4-((6-nitrobenzothiazol-2-yl)amino)-2H-chromen-2-one. The University Thought - Publication in Natural Sciences, 6(1), pp. 32-38. doi:10.5937/univtho6-10634

Dekić, V., Radulović, N., Vukićević, R., Dekić, B., Skropeta, D., & Palić, R. 2010. Complete assignment of the 1H and 13C NMR spectra of antimicrobial 4-arylamino- 3-nitrocoumarin derivatives. Magnetic Resonance in Chemistry, 48(11), pp. 896-902. doi:10.1002/mrc.2681

Fylaktakidou, K., Hadjipavlou-Litina, D., Litinas, K., & Nicolaides, D. 2004. Natural and Synthetic Coumarin Derivatives with Anti-Inflammatory / Antioxidant Activities. Current Pharmaceutical Design, 10(30), pp. 3813-3833. doi:10.2174/1381612043382710

Finn, G. J., Kenealy, E., Creaven, B. S., & Egan, D. A. 2002. In vitro cytotoxic potential and mechanism of action of selected coumarins, using human renal cell lines. Cancer Letters, 183(1), pp. 61-68. doi:10.1016/s0304-3835(02)00102-7

Hadjipavlou-Litina, D., Kontogiorgis, C., Pontiki, E., Dakanali, M., Akoumianaki, A., & Katerinopoulos, H. E. 2007. Anti-inflammatory and antioxidant activity of coumarins designed as potential fluorescent zinc sensors. Journal of Enzyme Inhibition and Medicinal Chemistry, 22(3), pp. 287-292. doi:10.1080/14756360601073914

Kaljaj, V., Trkovnik, M., & Stefanović-Kaljaj, L. 1987. Synthesis of new heterocyclocoumarins starting with 3-cyano-4-chlorocoumarin. Journal of the Serbian Chemical Society, 52(4), pp. 183-185.

Kostova, I., Raleva, S., Genova, P., & Argirova, R. 2006. Structure-Activity Relationships of Synthetic Coumarins as HIV-1 Inhibitors. Bioinorganic Chemistry and Applications, pp. 1-9. doi:10.1155/bca/2006/68274

Kotaiah, Y., Nagaraju, K., Harikrishna, N., Venkata, R. C., Yamini, L., & Vijjulatha, M. 2014. Synthesis, docking and evaluation of antioxidant and antimicrobial activities of novel 1,2,4-triazolo[3,4-b][1,3,4]thiadiazol-6-yl)selenopheno[2,3-d] pyrimidines. European Journal of Medicinal Chemistry, 75, pp. 195-202. doi:10.1016/j.ejmech.2014.01.006

Manojkumar, P., Ravi, T., & Subbuchettiar, G. 2009. Synthesis of coumarin heterocyclic derivatives with antioxidant activity and in vitro cytotoxic activity against tumour cells. Acta Pharmaceutica, 59(2), pp. 159-170. doi:10.2478/v10007-009-0018-7

Naik, N. S., Shastri, L. A., Joshi, S. D., Dixit, S. R., Chougala, B. M., Samundeeswari, S., Holiyachi, M., Shaikh, F., Madar, J., Kulkarni, R., & Sunagar, V. 2017. 3,4-Dihydropyrimidinone-coumarin analogues as a new class of selective agent against S. aureus: Synthesis, biological evaluation and molecular modelling study. Bioorganic and Medicinal Chemistry, 25(4), pp. 1413-1422. doi:10.1016/j.bmc.2017.01.001

Nofal, Z., El-Zahar, M., & Abd, E. S. 2000. Novel Coumarin Derivatives with Expected Biological Activity. Molecules, 5(12), pp. 99-113. doi:10.3390/50200099

Parfënov, É. A., & Smirnov, L. S. 1991. Heterocyclic bioantioxidants. 2. Interaction of 3-nitro-4-substituted coumarins with mercaptans. Chemistry of Heterocyclic Compounds, 27(11), pp. 1190-1192. doi:10.1007/bf00471742

Pasqualotto, A. C., Thiele, K. O., & Goldani, L. Z. 2010. Novel triazole antifungal drugs: focus on isavuconazole, ravuconazole and albaconazole. Current Opinion in Investigational Drugs, 11, pp. 165-174.

Piazzi, L., Cavalli, A., Colizzi, F., Belluti, F., Bartolini, M., Mancinni, F., Recanatini, M., Andrisana, V., & Rampa, A. 2008. Multi-target-directed coumarin derivatives: hAChE and BACE1 inhibitors as potential anti-Alzheimer compounds. Bioorganic and Medicinal Chemistry Letters, 18(1), pp. 423-426. doi:10.1016/j.bmcl.2007.09.100

Radulović, N., Stojanović-Radić, Z., Stojanović, P., Stojanović, N., Dekić, V., & Dekić, B. 2015. A small library of 4-(alkylamino)-3-nitrocoumarin derivatives with potent antimicrobial activity against gastrointestinal pathogens. Journal of the Serbian Chemical Society, 80(3), pp. 315-327. doi:10.2298/jsc140619085r

Savel'ev, V. L., Artamonova, O. S., Troitskaya, V. S., Vinokurov, V. G., & Zagorevskii, V. A. 1973. Investigations of pyrans and related compounds. Khimiya Geterotsiklicheskikh Soedinenii, 9(7), pp. 816-820. doi:10.1007/bf00471556

Stefanachi, A., Leonetti, F., Pisani, L., Catto, M., & Carotti, A. 2018. Coumarin: A Natural, Privileged and Versatile Scaffold for Bioactive Compounds. Molecules, 23(2), p. 250. doi:10.3390/molecules23020250

Su, C., Mouscadet, J., Chiang, C., Tsai, H., & Hsu, L. 2006. HIV-1 Integrase Inhibition of Biscoumarin Analogues. Chemical and pharmaceutical bulletin, 54(5), pp. 682-686. doi:10.1248/cpb.54.682

Vaso, K., Behrami, A., & Krasniqi, I. 2010. Antibacterial Activity of Compounds Synthesized From 4-Chloro-3-nitro-2H-[1]-benzopyran-2-one. Asian Journal of Chemistry, 22(9), pp. 7313-7317.

Venugopala, K. N., Rashmi, V., & Odhav, B. 2013. Review on Natural Coumarin Lead Compounds for Their Pharmacological Activity. BioMed Research International, pp. 1-14. doi:10.1155/2013/963248

Yeh, J. Y., Coumar, M. S., Horng, J. T., Shiao, H. Y., Kuo, F. M., Lee, H. L., Chen, I. C., Chang, C. W., Tang, W. F., Tseng, S. N., Chen, C. J., Shih, S. R., Hsu, J. T., Liao, C. C., Chao, Y. S., & Hsieh, H. P. 2010. Anti-Influenza Drug Discovery: Structure−Activity Relationship and Mechanistic Insight into Novel Angelicin Derivatives. Journal of Medicinal Chemistry, 53(4), pp. 1519-1533. doi:10.1021/jm901570x

Yu, D., Suzuki, M., Xie, L., Morris-Natschke, S. L., & Lee, K. 2003. Recent progress in the development of coumarin derivatives as potent anti-HIV agents. Medicinal Research Reviews, 23(3), pp. 322-345. doi:10.1002/med.10034

Zaki, R. M., Elossaily, Y. A., & Kamal, E. A. M. 2012. Synthesis and antimicrobial activity of novel benzo[f]coumarin compounds. Russian Journal of Bioorganic Chemistry, 38(6), pp. 639-646. doi:10.1134/s1068162012040152

SYNTHESIS AND STRUCTURE OF COBALT(II) COMPLEX WITH 2,6-DIACETYLPYRIDINE-BIS(PHENYLHYDRAZONE)

SVETLANA BELOŠEVIĆ[1], MARKO RODIĆ[2*], MIRJANA RADANOVIĆ[2], VUKADIN LEOVAC[2]

[1]Faculty of Technical Sciences, University of Priština, Kosovska Mitrovica, Serbia
[2]Faculty of Sciences, University of Novi Sad, Novi Sad, Serbia

ABSTRACT

The molecular and crystal structure of a newly synthesized Co(II) complex with 2,6-diacetylpyridine bis(phenylhydrazone) (L), of the formula [CoL$_2$]I$_2$ are described. The reaction of warm EtOH solutions of the ligand, 2,6-diacetylpyridine bis(phenylhydrazone) and CoI$_2$ in molar ratio 1:1 resulted in formation of black single crystals of the title complex. This is the first and so far, the only metal complex with this ligand that is characterized by single crystal X-ray crystallography. Co(II) is situated in a distorted *mer*-octahedral surrounding of two tridentate N$_3$ coordinated ligand molecules. Complex crystallizes in monoclinic crystal system in *C*2/*c* space group. Besides X-ray analysis, conductometric, spectroscopic and magnetic properties of the complex are investigated.

Keywords: Metal complex, Hydrazone, 2,6-diacetylpyridine derivative, Structure determination.

INTRODUCTION

Hydrazones represent a large and versatile group of organic compounds, characterized by $>C=N-N<$ atomic triade. They are usually prepared by the condensation of carbonyl compounds and hydrazine or its derivatives. Considering the variety of both carbonyl compounds and hydrazine derivatives, the large number of synthesized hydrazones is not surprising. This topic is very interesting for researchers, thus numerous review papers and monographs are published (Guimarães et al., 2017; Kitaev, 1977; Kitaev & Buzykin, 1974; Rollas et al., 2007; Shakdofa et al., 2014; Watanabe et al., 2018; Yang et al., 2016).

These compounds are important not only from theoretical, but also practical point of view (wide range of biological activity, catalytic activity, use as analytical reagents, etc.) (Guimarães et al., 2017; Rollas et al., 2007; Shakdofa et al., 2014; Watanabe et al., 2018; Yang et al., 2016).

Having different electron-donor atoms (N, O, S, etc.) to coordinate the metal ions, made this group of compounds very interesting topic for coordination chemists (Kogan et al., 1990; Shakdofa et al., 2014; Watanabe et al., 2018). Among these ligands, 2,6-diacetylpyridine bis(hydrazones) stand out. These ligands can have different denticity, depending on the hydrazine derivative, but the most common are tri- and pentadentate ones.

The simplest ligand of this group is 2,6-diacetylpyridine bis(hydrazone), which is obtained in the reaction of hydrazine hydate and 2,6-diacetylpyridine (Shee et al., 2013). This N$_3$ tridentate ligand coordinates the metal ion through pyridine and two imine nitrogen atoms, forming two 5-membered metallocycles. The only exception is a dimeric complex of Cd(II)

in which, besides the mentioned three ligators, the terminal nitrogen atom is involved in coordination as a bridge (Shee et al., 2013).

In (Curry et al., 1967) synthesis, spectroscopic and magnetic characterization of mono- and bis(ligand) complexes of Fe(II), Co(II), Ni(II) and Cu(II) with 2,6-diacetylpyridine bis(phenylhydrazone) (L), of the general formulas M(L)Cl$_2$, and [ML$_2$](ClO$_4$)$_2$, are described.

The survey of the Cambridge Structural Database (version 5.39, update May 2018) (Groom et al., 2016) revealed that there are no structurally characterized metal complexes with this ligand. Here we report molecular and crystal structure, as well as some physicochemical properties of a novel complex of CoI$_2$ with 2,6-diacetylpyridine bis(phenylhydrazone), of the formula [CoL$_2$]I$_2$. This is the first complex of any metal with this ligand, which is obtained in the form of single crystals, thus fully structurally characterized.

EXPERIMENTAL

Materials and methods

All chemicals used were commercial products of analytical reagent grade. Elemental analyses (C, H, N) of air-dried complexes were carried out by standard micromethods in the Center for Instrumental Analyses, ICTM in Belgrade. Molar conductivities of freshly prepared complexes solutions ($c = 1 \times 10^{-3}$ mol dm^{-3}) were measured on a Jenway 4010 conductivity meter. IR spectra were recorded using KBr pellets on a NEXUS 670 FTIR spectrophotometer (Thermo Nicolet) in the range of 4000–400 cm^{-1}. Melting points were measured on a Nagema melting point microscope Rapido. Magnetic susceptibility measurements were conducted at room temperature

---

* Corresponding author: marko.rodic@dh.uns.ac.rs
CHEMISTRY

on an MSB-MKI magnetic susceptibility balance, Sherwood Scientific Ltd. Cambridge.

Synthesis of ligand

The mixture of 0.80 g (5 mmol) 2,6-diacetylpyridine and 1.45 g (10 mmol) phenylhydrazine-hydrochloride was heated in 10 cm^3 EtOH. In the resulting red solution 2.00 g (20 mmol) LiOAc·2H$_2$O was added and this mixture was refluxed for 40 minutes, during which the solution became yellow. Cooling to the room temperature resulted in the formation of yellowish fibrous product, which was filtered and washed with EtOH and Et$_2$O. Yield: 1.28 g (75 %). Anal. Calcd. for C$_{21}$H$_{21}$N$_5$: C, 73.44; H, 6.16; N, 20.39. Found: C, 73.54; H, 6.05; N, 20.18. IR bands [$\tilde{\nu}$ /cm^{-1}]: 3432m, 3347m, 1601vs, 1563s, 1508m, 1452s, 1363w, 1291w, 1250vs, 1164vs, 1081w, 994w, 840w, 815w, 750m, 694m, 650w, 507w. M.p. = 216–218 °C.

Synthesis of complex

The mixture of 0.032 g CoI$_2$ (0.1 mmol) and 0.034 g (0.1 mmol) of L was heated in 10 cm^3 of MeOH until complete dissolution. The obtained dark solution was left at the room temperature and after two days black prismatic single crystals were filtered and washed with MeOH. Yield: 0.030 g (60 %). Anal. Calcd. for [C$_{42}$H$_{42}$CoN$_{10}$]I$_2$: C, 50.87; H, 4.11; N, 14.32. Found: C, 50.46; H, 4.23; N, 14.01. IR bands [$\tilde{\nu}$ /cm^{-1}]: 3545m, 3410m, 3160s, 3097m, 3050m, 2980m, 2938m, 1598vs, 1515s, 1494s, 1439m, 1380w, 1261vs, 1170m, 1090m, 1049m, 881w, 804w, 750s, 694s, 662w, 501w. M.p. > 250 °C. Molar conductivity, Λ_M (S cm^2 mol^{-1}): 150 (MeOH). μ_{eff} (BM): 4.58.

Crystal structure determination

Diffraction experiment was performed on an Oxford Diffraction Gemini S diffractometer, equipped with Sapphire3 detector. The measurements were performed at room temperature. Radiation from sealed tube with Mo-anode was used. Unit cell determination, data collection, and reduction was performed with the *CrysAlisPro* software (Rigaku Corporation, 2015). The crystal structure was solved by using *SHELXT* (Sheldrick, 2015a), and refined by full-matrix least squares method by using *SHELXL-2018* (Sheldrick, 2015b) and *ShelXle* (Hübschle et al., 2011). Software used for crystal structure analysis: *PLATON* (Spek, 2009), *Mercury CSD* (Macrae et al., 2008), and *CrystalExplorer* (Turner et al., 2017).

CCDC 1883840 contains the supplementary crystallographic data for this paper. These data can be obtained free of charge from The Cambridge Crystallographic Data Centre via www.ccdc.cam.ac.uk/structures.

A summary of the crystallographic data for crystal structures is given in Table 1.

Table 1. Crystallographic data and refinement statistics.

Crystal data	
Chemical formula	[C$_{42}$H$_{42}$CoN$_{10}$]I$_2$
M_r (g cm^{-3})	999.58
Crystal system	Monoclinic
Space group	*C*2/*c*
Temperature (K)	294
a (Å)	21.1576(4)
b (Å)	15.8949(3)
c (Å)	12.1287(2)
β (°)	92.247(2)
V (Å^3)	4075.72(13)
Z	4
Crystal size (mm)	$0.69 \times 0.42 \times 0.27$
Data collection	
Diffractometer	Gemini S (Oxford Diffraction)
Radiation type	Mo *Kα*
No. of measured reflections	17919
No. of independent reflections	4839
No. of observed [$I > 2\sigma(I)$] reflections	4092
R_{int}	0.020
$(\sin \theta/\lambda)_{max}$ (Å^{-1})	0.678
μ (mm^{-1})	1.98
Absorption correction	Analytical
T_{min}, T_{max}	0.168, 0.467
Refinement	
No. of reflections	4839
No. of parameters	257
No. of restraints	2
H-atom treatment	Mixed
$R[F^2 > 2\sigma(F^2)]$	0.032
$wR(F^2)$	0.079
S	1.05
$\Delta\rho_{max}$, $\Delta\rho_{min}$ (e Å^{-3})	0.74, −0.71

RESULTS AND DISCUSSION

Synthesis and physicochemical characterization of the compounds

Ligand, 2,6-diacetylpyridine bis(phenylhydrazone) is obtained in a good yield (75 %) in the reaction of warm EtOH solutions of stochiometric amounts of 2,6-diacetylpyridine and phenylhydrazine hydrochloride in the presence of the excess of LiOAc (scheme 1).

It should be mentioned that the same ligand was earlier obtained in the reaction of warm EtOH solutions of 2,6-diacetylpyridine and neutral phenylhydrazine (Curry et al., 1967).

The ligand is well soluble in acetone, partially soluble in MeOH and EtOH, and insoluble in Et$_2$O and H$_2$O. Hydrazone structure of the ligand, *i.e.* the condensation of both of keto-groups of the diketone, could be proven by the elemental

analysis, but also the absence of the characteristic very strong carbonyl band at 1707 cm^{-1} in the IR spectrum of the ligand.
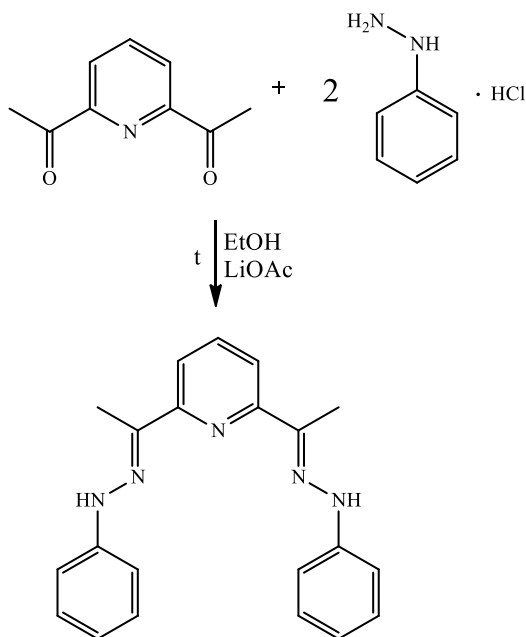
Scheme 1. Synthesis of the ligand.

Black single crystals of the complex are obtained in a good yield (60 %) in the reaction of warm EtOH solutions of the ligand and CoI$_2$. Despite the fact that metal–ligand molar ratio was 1:1, bis(ligand) complex was formed. Unlike this bis(ligand) complex, in (Curry et al., 1967) the synthesis of mono(ligand) complex of the formula Co(L)Cl$_2$ is reported. The obtained complex is stable in air and high temperatures (M.p. > 250 °C), partially soluble in EtOH and H$_2$O, while its solubility in MeOH

and DMF is better. Molar conductivity of MeOH solution of the complex has a value characteristic for 2:1 electrolyte type, thus is in concordance with the coordination formula (Geary, 1971). The value of the effective magnetic moment (μ_{eff} = 4.58 BM) is characteristic for high-spin octahedral Co(II) complexes.

In the IR spectrum of the complex, the band at 3155 cm^{-1} could be ascribed to ν(NH) vibrations. Other high-energy bands (3100 – 2940 cm^{-1}) correspond to the ν(CH) vibrations of CH$_3$-groups and aromatic rings (pyridine and benzene). Bands at 1599 and 1494 cm^{-1} could be assigned to ν(C$\cdots$C) and ν(C$\cdots$N) vibrations of pyridine and benzene rings, while the band at 1517 cm^{-1} corresponds to ν(C=N) vibrations of imine group. In free ligand, the latter is found at higher energy (1563 cm^{-1}), and due to coordination of nitrogen atom suffers a negative shift (Curry et al., 1967; Kazak et al., 2009).

Crystal structure of the complex

The compound crystallizes in monoclinic crystal system, space group *C*2/*c*. The content of the asymmetric unit, atom numeration, and molecular structure are depicted in Fig. 1. The complex cation exhibits a perfect *C*$_2$ symmetry imposed by the space-group symmetry since Co(II) atom occupies a special position. Thus, the asymmetric unit of the unit cell is comprised of a ligand molecule, half of a metal atom, and an iodide ion. The search for higher non-crystallographic symmetry of the complex cation by the method of Continuous Symmetry Measures (Zabrodsky et al., 1992) indicates that cation symmetry only slightly deviates from *D*$_2$ point group, as *CSM*(*D*$_2$) = 0.251. Apart from the crystallographic two-fold axis, the two additional non-crystallographic two-fold axes are positioned along N1–Co1–N1^i bonds and the bisector of N2A–N2B^i angle [symmetry code (i): −*x*+1, *y*, −*z*+1/2].
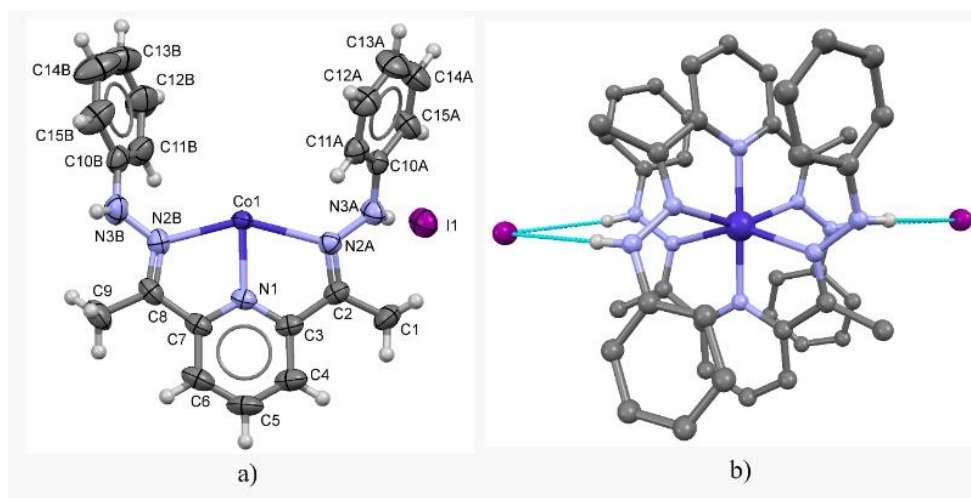
Figure 1. a) Asymmetric unit of [CoL$_2$]I$_2$ and atom labeling scheme. Displacement ellipsoids are drawn at the 50% probability level. Hydrogen atoms have been drawn as spheres of arbitrary radius. b) Perspective view of the molecular structure of [CoL$_2$]I$_2$.

The Co(II) atom is situated in a distorted octahedral environment, formed by two meridionally arranged tridentate N$_3$ chelate ligands. The octahedra is distorted, as two ligands are not

mutually perpendicular. The planes defined by N1, N2A and N2B donor atoms of the symmetry-related ligands enclose the dihedral angle of 75.65(6)°. The valence angles within the

coordination polyhedron deviate from ideal values (Table 2). The *trans*-valence angle N2A–Co1–N2A and *cis*-valence angles N1–Co1–N2A, N1–Co1–N2B with values of 150.69(7)°, 74.14(7)°, and 76.56(8)°, respectively, display the largest deviations. This is caused by geometry constraints imposed by the ligand structure and its chelate coordination.

Table 2. Selected bond lengths (Å), valence and torsion angles (°).

Bonds	Length (Å)	Bonds	Angle (°)
Co1–N1	2.0061(18)	N1–Co1–N1[i]	173.87(11)
Co1–N2B	2.1993(19)	N2A–Co1–N2B	150.69(7)
Co1–N2A	2.3057(19)	N1–Co1–N2A	74.14(7)
N1–C3	1.338(3)	N1–Co1–N2B	76.56(8)
N1–C7	1.346(3)		
C2–C3	1.467(3)	**Bonds**	**Torsion angle (°)**
C7–C8	1.465(4)	N1–C3–C2–N2A	16.1(3)
N2A–C2	1.298(3)	N1–C7–C8–N2B	4.3(3)
N2B–C8	1.302(3)	C2–N2A–N3A–C10A	−161.1(2)
N2A–N3A	1.374(3)	C8–N2B–N3B–C10B	−165.6(2)
N2B–N3B	1.366(3)		
N3A–C10A	1.390(3)		
N3B–C10B	1.400(4)		

Symmetry code: (i) −x+1, y, −z+1/2;

The two five-membered chelate rings are not planar and their conformational analysis is problematic due to large discrepancy between ring bond lengths. The method of Duax et al. (1976) reveals that conformations of these rings are intermediate between the envelope (E) and half-chair (T) forms. For the Co1–N1–C3–C2–N2A metallocycle, the lowest values of ΔC_s asymmetry parameters are $\Delta C_s(\text{Co1–N1}) = \Delta C_s(\text{C2}) = 6.9(2)°$ and $\Delta C_s(\text{N1–C3}) = \Delta C_s(\text{N2A}) = 9.1(2)°$, which point to ^4E and E_5 conformations, respectively. Also, the lowest ΔC_2 asymmetry parameter is $\Delta C_2(\text{C2–N2A}) = \Delta C_2(\text{N1}) = 2.3(2)°$, which suggests $^4T_5$ conformation. Similarly, for the Co1–N1–C7–C8–N2B ring, the lowest ΔC_s asymmetry parameters $\Delta C_s(\text{C7–C8}) = \Delta C_s(\text{Co1}) = 3.9(3)°$ and $\Delta C_s(\text{N1–C7}) = \Delta C_s(\text{N2B}) = 4.6(2)°$ hint to ^1E and E_5 conformations, respectively. Again, the lowest ΔC_2 asymmetry parameter is $\Delta C_2(\text{N2B–Co1}) = \Delta C_2(\text{C7}) = 2.3(2)°$ which signals $^1T_5$ conformation.

To resolve this ambiguity, a different approach by the method of Cremer & Pople (1975), followed by decomposition of puckering parameters into linear combinations of two basic forms (E and T) by the method of Evans & Boeyens (1989) was applied. The results are summarized in Table 3. The findings confirm that conformations of both rings are best described as a mixture of half-chair and envelope forms. For the ring Co1–N1–C3–C2–N2A, the conformation is described as 63% E_5 and 37% $^4T_5$, while the conformation of ring Co1–N1–C7–C8–N2B is expressed as 57% $^1T_5$ and 43% E_5.

Table 3. Cremer–Pople puckering parameters of five-membered rings.

Ring	Q_2 / Å	φ_2 / °	$a\varphi(E) + b\varphi(T)^*$
Co1–N1–C3–C2–N2A	0.169(2)	317.3(7)	62.7 (1.8) + 37.3 (1.7)
Co1–N1–C7–C8–N2B	0.1632(18)	349.7(9)	42.8 (2.0) + 57.2 (1.9)

* a and b are given as percentages. φ is expressed as a multiple of $\pi/2N$.

The ligand is coordinated in a neutral form through nitrogen atoms of the pyridine ring, and two azomethine nitrogen atoms. The same coordination mode is found in [ZnL$_2$](CF$_3$O$_3$S)$_2$, where L is structurally related ligand 2,6-diformylpyridine bis(phenylhydrazone) (Dumitru et al., 2009). Metal–ligand bond lengths are in the range of 2.0061(18)–2.3057(19) Å, with Co–N1 being the shortest one. The two phenylhydrazine moieties are asymmetrically coordinated, as indicated by different metal–ligand bond lengths (Table 2). Intra-ligand bond lengths are in the expected range. The bonds within pyridine and both phenyl rings have lengths indicative of electron delocalization along these moieties. The bonds C2–N2A and C8–N2B are the only two that have lengths characteristic of localized double bonds.

The ligand molecule significantly deviates from planarity. In order to avoid steric clashes with symmetry-related ligand within the coordination polyhedron, a twisting of phenylhydrazine moieties occurs. The magnitude or twisting along C3–C2 bond is greater when compared with that along C7–C8 bond, visualized through the values of torsion angles $\tau(\text{N1–C3–C2–N2A})=16.1(3)°$ and $\tau(\text{N1–C7–C8–N2B}) = 4.3(3)°$. The torsion along N2A–N3A and N2B–N3B bonds is similar in magnitude, yet in opposite sense relative to the chelate plane [$\tau(\text{C2–N2A–N3A–C10A}) = −161.1(2)°$, and $\tau(\text{C8–N2B–N3B–C10B}) = −165.6(2)°$]. The mentioned differences between twisting along these bonds lead to significant differences in the final positions of phenyl rings A and B with the respect to the position of the pyridine ring of the symmetry-related ligand

belonging to the same coordination sphere, as it is tabulated in Table 2.

The packing of structural units is dominated by the large complex cation. Cation's Hirshfeld surface (HS) decomposition into intermolecular atom–atom contacts (Fig. 2), reveals that 68.4% of the HS is dominated by cation–cation $H\cdots H$ contacts at distances around or beyond the sum of their Van der Waals radii.

The $C\cdots H$ and $H\cdots C$ contacts comprise 13.2% of the cation's HS. Due to the large discrepancy between cation and anion sizes, only 13.6% of the cation HS can be ascribed to the $H\cdots I$ contacts. However, these contacts correspond to the regions with the lowest d_{norm} values on the cation HS and match $NH\cdots I$ and $CH\cdots I$ hydrogen bonds (Table 4). The anion's HS is over 99% mapped with $I\cdots H$ contacts.
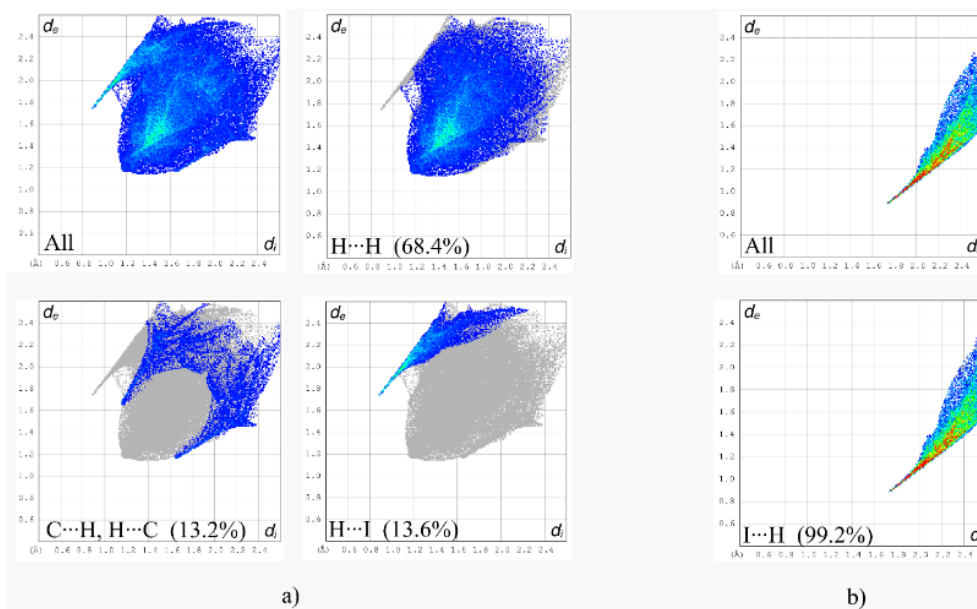
Figure 2. Fingerprint plot of intermolecular contacts, and its decomposition based on specific atom–atom contacts for cation $[CoL_2]^{2+}$ (a) and anion I^- (b).

Table 4. Selected hydrogen-bond parameters.

D–$H\cdots A$	D–H (Å)	$H\cdots A$ (Å)	$D\cdots A$ (Å)	D–$H\cdots A$ (°)
N3A–H3A$\cdots$I1	0.842 (17)	2.802 (18)	3.633 (2)	170 (3)
N3B–H3B$\cdots$I1^i	0.842 (17)	2.87 (2)	3.690 (2)	166 (3)
C1–H1C$\cdots$I1	0.96	3.16	3.947 (3)	140.3
C6–H6$\cdots$I1^{ii}	0.93	3.06	3.944 (3)	158.9
C9–H9C$\cdots$I1^i	0.96	3.18	3.927 (3)	136.1

Symmetry code(s): (i) $-x+1$, y, $-z+1/2$; (ii) $x-1/2$, $-y+1/2$, $z-1/2$.

CONCLUSION

By the reaction of warm methanolic solutions of CoI_2 and tridentate N_3 2,6-diacetylpyridine bis(phenylhydrazone), L, not only in molar ratio 1:2, but also in molar ratio 1:1, high-spin bis(ligand) complex of the formula $[CoL_2]I_2$ is obtained. Single crystal X-ray analysis has shown that the complex has a distorted *mer*-octahedral configuration. This is the first and so far, the only complex of any metal with the titled ligand, that is characterized by single crystal X-ray analysis.

ACKNOWLEGMENTS

REFERENCES

Cremer, D., & Pople, J. A. 1975. General definition of ring puckering coordinates. Journal of the American Chemical Society, 97(6), pp. 1354-1358. doi:10.1021/ja00839a011

Curry, J. D., Robinson, M. A., & Busch, D. H. 1967. Metal complexes derived from substituted hydrazones of 2,6-diacetylpyridine. Inorganic Chemistry, 6(8), pp. 1570-1574. doi:10.1021/ic50054a032

Duax, W. L., Weeks, C. M., & Rohrer, D. C. 1976. Crystal Structures of Steroids. In N. L. Allinger & E. L. Eliel Eds., Topics in Stereochemistry. Hoboken, NJ, USA: Wiley., pp. 271-383. doi:10.1002/9780470147184.ch5

Dumitru, F., Legrand, Y., Barboiu, M., Petit, E., & Lee, A.v. 2009. Metallosupramolecular Architectures of Pseudoterpyridine-Type Ligands and Zn II Metal Ions. Crystal Growth and Design, 9(6), pp. 2917-2921. doi:10.1021/cg9002466

Evans, D. G., & Boeyens, J. C. A. 1989. Conformational analysis of ring pucker. Acta Crystallographica Section B Structural Science, 45(6), pp. 581-590. doi:10.1107/s0108768189008190

Geary, W. J. 1971. The use of conductivity measurements in organic solvents for the characterisation of coordination compounds. Coordination Chemistry Reviews, 7(1), pp. 81-122. doi:10.1016/s0010-8545(00)80009-0

Guimarães, G. D., Rolim, A. L., de Gonsalves, A. A., & Araújo, M. C. R. 2017. Biological Potential of Synthetic Hydrazones in the Last Decade: A Systematic Review. Revista Virtual de Química, 9(6), pp. 2551-2592. doi:10.21577/1984-6835.20170151

Groom, C. R., Bruno, I. J., Lightfoot, M. P., & Ward, S. C. 2016. The Cambridge Structural Database. Acta Crystallographica Section B Structural Science, Crystal Engineering and Materials, 72(2), pp. 171-179. doi:10.1107/s2052520616003954

Hübschle, C. B., Sheldrick, G. M., & Dittrich, B. 2011. ShelXle: a Qt graphical user interface for SHELXL. Journal of Applied Crystallography, 44(6), pp. 1281-1284. doi:10.1107/s0021889811043202

Kazak, C., Arslan, N. B., Karabulut, S., Azaz, A. D., Namlı, H., & Kurtaran, R. 2009. Supramolecular lead(II) azide complex of 2,6-diacetylpyridine dihydrazone: synthesis, molecular structure, and biological activity. Journal of Coordination Chemistry, 62(18), pp. 2966-2973. doi:10.1080/00958970902980537

Kitaev, Y. P. 1977. Khimiya gidrazonov. Moscow: Nauka.

Kitaev, Y. P., & Buzykin, B. I. 1974. Gidrazony. Moscow: Nauka.

Kogan, V. A., Zelentsov, V. V., Larin, G. M., & Lukov, V. V. 1990. Kompleksy perekhodnykh metallov c gidrazomani. Moscow: Nauka.

Macrae, C. F., Bruno, I. J., Chisholm, J. A., Edgington, P. R., McCabe, P., Pidcock, E., Rodriguez-Monge, L., Taylor, R., van de Streek, J., Wood, P. A. 2008. Mercury CSD 2.0: New features for the visualization and investigation of crystal structures. Journal of Applied Crystallography, 41(2), pp. 466-470. doi:10.1107/s0021889807067908

-Rigaku Corporation. 2015. Rigaku Oxford Diffraction; CrysAlisPro Software system. Oxford, UK.

Rollas, S., & Küçükgüzel, S. 2007. Biological Activities of Hydrazone Derivatives. Molecules, 12(8), pp. 1910-1939. doi:10.3390/12081910

Shakdofa, M. M. E., Shtaiwi, M. H., Morsy, N., & Abdel-rassel, T. M. A. 2014. Metal complexes of hydrazones and their biological, analytical and catalytic applications: A review. Main Gr. Chem., 13, 187–218. https://doi.org/10.3233/MGC-140133

Shee, N. K., Dutta, S., Drew, M. G. B., & Datta, D. 2013. Bis complexes of zinc(II), cadmium(II) and mercury(II) with a potentially pentadentate N-donor ligand. Lewis acidity versus coordination tendency. Inorganica Chimica Acta, 398, pp. 132-135. doi:10.1016/j.ica.2012.12.024

Sheldrick, G. M. 2015a. SHELXT – Integrated space-group and crystal-structure determination. Acta Crystallographica Section A Foundations and Advances, 71(1), pp. 3-8. doi:10.1107/s2053273314026370

Sheldrick, G. M. 2015b. Crystal structure refinement with SHELXL. Acta Crystallographica Section C Structural Chemistry, 71(1), pp. 3-8. doi:10.1107/s2053229614024218

Spek, A. L. 2009. Structure validation in chemical crystallography. Acta Crystallographica Section D Biological Crystallography, 65(2), pp. 148-155. doi:10.1107/s090744490804362x

Turner, M. J., Mckinnon, J. J., Wolff, S. K., Grimwood, D. J., Spackman, P. R., Jayatilaka, D., & Spackman, M. A. 2017. CrystalExplorer. University of Western Australia. 17.

Watanabe, K., Mino, T., Yoshida, Y., & Sakamoto, M. 2018. Hydrazone-Palladium Catalyzed Reactions Using Allyl Compounds. Journal of Synthetic Organic Chemistry, Japan, 76(8), pp. 828-837. doi:10.5059/yukigoseikyokaishi.76.828

Yang, Y., Gao, C., Liu, J., & Dong, D. 2016. Recent developments in rhodamine salicylidene hydrazone chemosensors. Analytical Methods, 8(14), pp. 2863-2871. doi:10.1039/c6ay00135a

Zabrodsky, H., Peleg, S., & Avnir, D. 1992. Continuous symmetry measures. Journal of the American Chemical Society, 114(20), pp. 7843-7851. doi:10.1021/ja00046a033

TREND ASSESSING USING MANN-KENDALL'S TEST FOR PRIŠTINA METEOROLOGICAL STATION TEMPERATURE AND PRECIPITATION DATA, KOSOVO AND METOHIJA, SERBIA

NIKOLA R. BAČEVIĆ[1*], MILICA PAVLOVIĆ[1], ILHANA RASLJANIN[1]

[1]Faculty of Natural Sciences and Mathematics, University of Priština, Kosovska Mitrovica, Serbia.

ABSTRACT

The study includes statistical analysis of Priština meteorological station data on temperature and precipitation trends. The data are organized into four time series: average annual air temperatures (Ta), average maximal annual air temperatures (Tamax), average minimal annual air temperatures (Tamin), as well as annual precipitation sums (RRsum), all in the period 1949 – 1999. The Mann-Kendall′s (MK) trend test analysis of the corresponding hypotheses discloses that the H_0 hypothesis should be accepted. The general conclusion is that there is no trend neither in maximal, minimal, average temperatures, nor in average annual precipitation for the 1949 – 1999 period for the central Kosovo and Metohija (K&M).

Keywords: Air temperature trend, Mann-Kendall, Precipitation trend, Priština, Kosovo and Metohija, Serbia.

INTRODUCTION

According to the Intergovernmental Panel on Climate Change (IPCC 2007) report, the global average temperature have risen for 0.7°C within the last 100 years. However, the global temperature rise is not distributed uniformly over the all of the Earth surface.

The rise varies in different regions. Using data from 168 meteorological stations across European continent, Klein Tank (2002) presented tendency of the European average temperature rise. In general, an average temperature rise in Europe is recorded both on annual and seasonal levels (Brázdil et al., 1996; Brunetti, 2004; Feidas, 2004; Brunet, 2007).

In Serbia a trend of average temperature rise after 1975 is recorded too (Unkašević & Tošić, 2011). The results analysis of data on temperature extremes from 15 meteorological stations for the period 1949 – 2009 reveal that the climate in Serbia shows a worming tendency within last 61 years (Unkašević & Tošić, 2013). Similar results on climate in our country were published recently (Ducić & Radovanović, 2005; Unkašević & Tošić, 2009; Gavrilov et al., 2010, 2013a; Tošić et al., 2013; Hrnjak et al., 2013; Vukoičić et al., 2018; Milentijević et al., 2018). The climate in K&M was subject of several studies (Gavrilov et al., 2018; Ivanović et al., 2017; Bačević et al., 2017) and shows a mild temperature rise tendency for the 1949 – 1999 period. GIS analysis in combination with numerical methods are very powerful tool for calculating and climatological properties (Valjarević et al., 2018).

The focus of the study is the average annual and seasonal temperature and precipitation rise in Priština (central K&M) region for the 1949 – 1999 period.

MATERIAL AND METHODS

Data

The data from Priština meteorological station were organized into four time series: the average annual air temperatures (Ta), average maximal annual air temperatures (Tamax), average minimal annual air temperatures (Tamin), and annual precipitation sum (RRsum), all of them for the 1949 – 1999 period. While forming the time series, we noticed that the data for some of the years were incomplete. Therefore, the completion of the data was needed in order to form the time series (Douglas et al., 2000). For that reason *Random number generator function* was done for the missing data. As a result, we obtained comprehensive time series, and could start with the data processing using Microsoft Office Excel 2007. One column was used to input data for the 1949 – 1999 period, and another to input the time series. Both columns are marked and, using *Scatter* function, a graph showing the temperature values is obtained. The graph was transformed into 2-D histograms more convenient for the time series analysis. The resulting histogram consisted of 51 bars, the *x* axis was used to represent years, and the *y* axis was used to represent the measured values. In order to create the trend curve, a special function should be activated in Excel 2007. In the *Trendline options* check-box we check the linear trend function. The *Display Equation on Chart* option helps us in obtaining the formula. Here one can arrange the trend line, color, size and the value units. In this way we formed four graphs (figure 1 – the annual precipitation sum distribution, figure 2 – the average maximal annual temperatures, figure 3 – the average minimal annual temperatures, figure 4 – the average annual temperatures.

---

* Corresponding author: nikola.bacevic@pr.ac.rs
GEOGRAPHY, GEOSCIENCE AND ASTRONOMY

The temperature and precipitation trends were examined using three statistical analyses. The first data processing was used to calculate linear equations representing Priština meteorological station data trends. The trend was represented with a linear curve showing values of annual (maximal, minimal, average) temperatures and annual precipitation sums. The second statistical processing was done using XL-stat software that uses MK test on temperature and precipitation (Gilbert, 1987). The test is mostly used in environmental sciences that require meteorological data processing (e.g. Gavrilov *et al*., 2010, 2011, 2013a, 2018; Hrnjak *et al*., 2013). The MK trend test is very convenient because it could be used for different groups of data (Kendall, 1938, 1975). The minimal number of time series for a successful test is ten. After the trend processing, the XL-stat software tests two hypotheses: (1) H_a – there is a trend, and (2)

H_0 – there is no trend in time series. The trend probability is defined through the scientific reliability level (α-0.05). In the third data processing, differences between the first and the last values of temperatures/precipitation were calculated for the 1949 – 1999 period. These values represent the quantitative measure/value (Δy).

Study area

Priština, the capital of K&M province is located in the north part of Kosovo basin, on foothills of the Grmija Mountain. The urban core area covers 857 km², its altitude is 652 m above the sea level, and coordinates are: latitude 42° 65′ N and longitude 21° 15′ E. Priština meteorological station is located near the city airport, in Goleš. Its coordinates are: latitude 42° 67′ N and longitude 21° 17′ E, and its altitude is 573 m (Gavrilov et al., 2018).
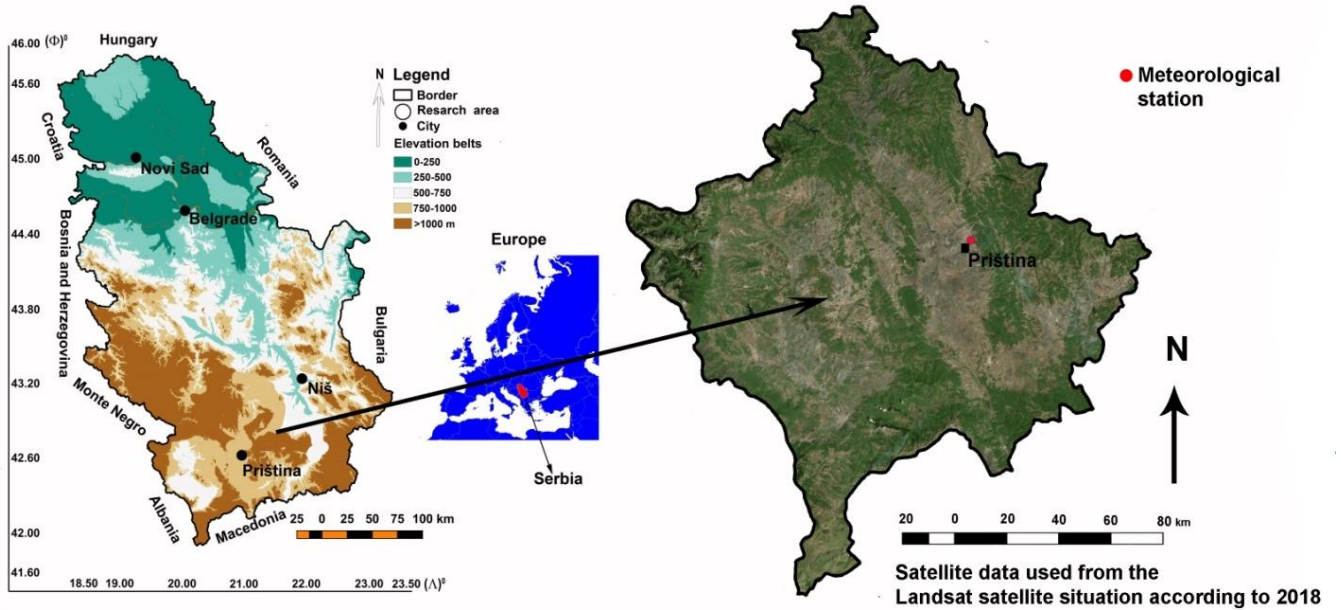
Figure 1. Physical-geographical map of the Republic of Serbia and Kosovo and Metohia in Europe, and the position of the meteorological station of Prishtina, which is especially marked with red circles.

NUMERICAL RESULTS

The four time series were subjected to three different ways of statistical data processing. The corresponding equations and relevant values for precipitation, maximal, minimal and average temperatures are as follows:

$(1 - RRsum)_{1,2,3,4.}$
$$y = -0.645x + 597.8, \tau = -0.073, p = 0.457, \Delta y_p = 39.96. \quad (1)$$

$(2 - Ta\max)_{1,2,3,4.}$
$$y = 0.013x + 23.1, \tau = 0.104, p = 0.292, \Delta y = -0.65. \quad (2)$$

$(3 - Ta\min)_{1,2,3,4.}$
$$y = 0.011x - 2.9, \tau = 0.137, p = 0.162, \Delta y = -0.58. \quad (3)$$

$(4 - Ta)_{1,2,3,4.}$
$$y = -0.005x + 10.2, \tau = -0.073, p = 0.471, \Delta y = 0.25. \quad (4)$$

The first equation $(1-Rrsum)_{1,2,3,4}$ represents the average precipitation sum in Priština for the 1949 – 1999 period, 1 – the linear equation, 2 – Kendall τ value (the range of values from + 1 to – 1), 3 – *p* - the trend probability, 4 – Δy_p is the difference in values at the beginning and the end of the period. The second equation $(2 - Ta\max)_{1,2,3,4}$ represents average maximal annual

temperatures in Priština for the 1949 – 1999 period, 1 – the linear equation, 2 – Kendall τ value (the range of values from + 1 to – 1), 3 – *p* - the trend probability, 4 – Δy_p is the difference in values at the beginning and the end of the period. The third equation $(Tamin)_{1,2,3,4}$ represents average minimal annual temperatures in Priština for the 1949 – 1999 period, 1 – the linear equation, 2 – Kendall τ value (the range of values from + 1 to – 1), 3 – *p* - the trend probability, 4 – Δy_p is the difference in values at the beginning and the end of the period. The fourth equation $(Ta)_{1,2,3,4}$ represents average annual temperatures in Priština for the 1949 – 1999 period, 1 – the linear equation, 2 – Kendall τ value (the range of values from + 1 to – 1), 3 – *p* - the trend probability, 4 – Δy_p is the difference in values at the beginning and the end of the period.

All four trends with their linear equations and magnitudes were obtained with the XL-stat software. There we dealt with (maximal, minimal, average) temperatures, as well as with precipitation sums. The conclusion is that the H_0 hypothesis should be accepted. It shows that there is no trend in the time series. Besides, in equations (1, 2, 3, 4) we calculated the Kendall τ correlation value, *p* value and the trend magnitude value (Δy).

Figures (2), (3), (4), (5) represent results of trend testing with the MK test with respective hypothesis assessment. Using these results we analyze trends for four time series.

Figure 2. Annual precipitation sum distribution, the trend line and the trend equation for Priština in the 1949 – 1999 period.

Figure 3. Average maximal annual temperatures, the trend line and the thrend equation for Priština in the 1949 – 1999 period.

Figure 4. Average minimal annual temperatures , the trend line and the trend equation for Priština in the 1949 – 1999 period.
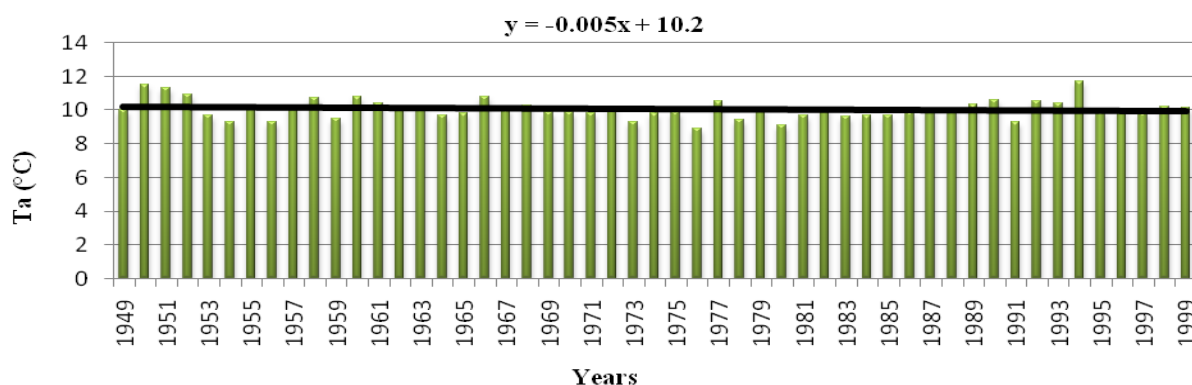
Figure 5. Average annual temperatures, the trend line, the trend equation for Priština in the 1949 – 1999 period.

Negative trend values in the time series can be seen in the Figure 2, as well as in the equation 1-(RRsum)$_{1,2,3,4}$. The hypothesis test will give us an answer whether this assertion is true or not. The calculated p value is higher than 0.05, which means that the null hypothesis should be accepted. The probability for its acceptance is 45.66 %. The precipitation difference Δy_p equals 39.96 mm.
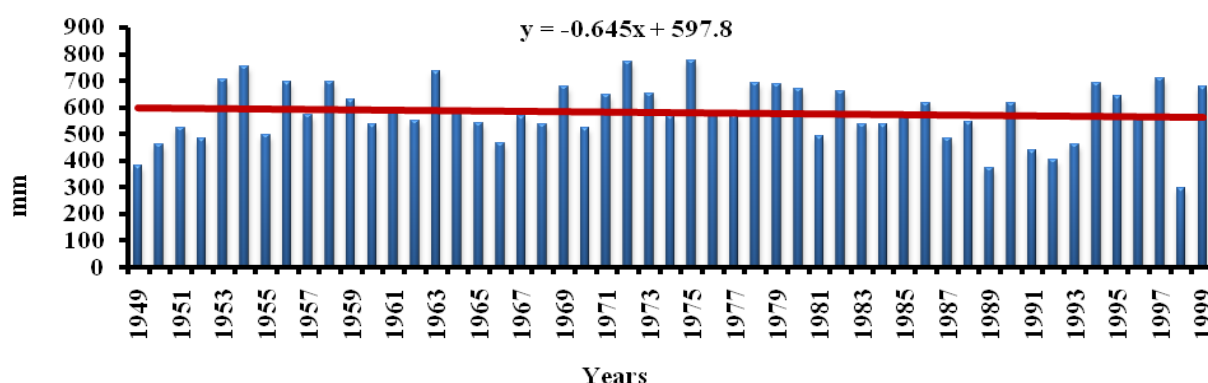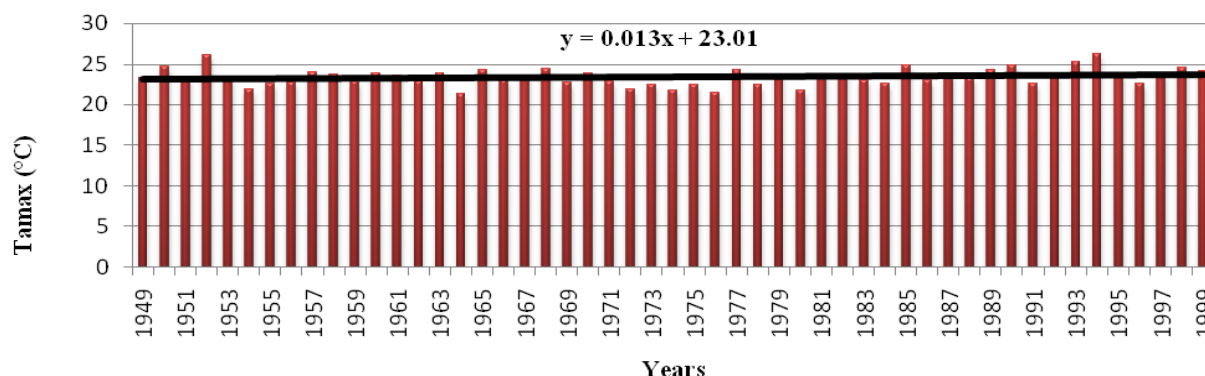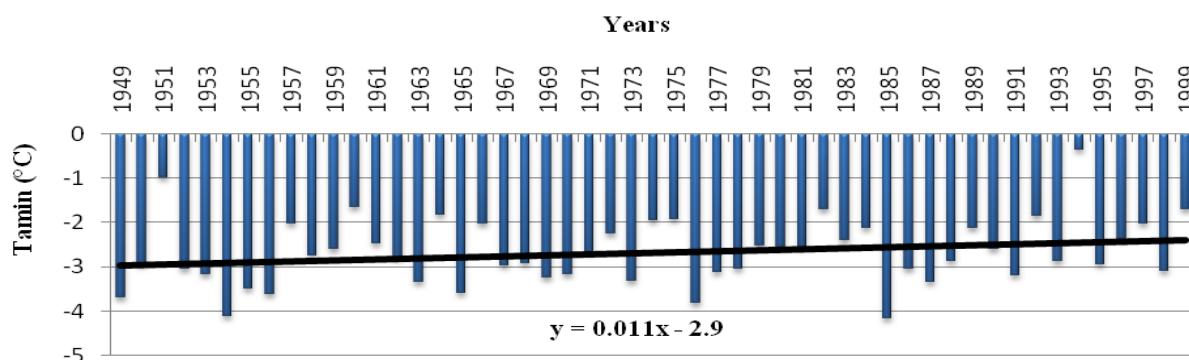
Positive trend values in the time series are seen in the Figure 3, as well as in the equation (2-Tamax)$_{1,2,3,4}$. The hypothesis test will give us an answer whether this assertion is true or not. The calculated p value is higher than 0.05, which means that the null hypothesis should be accepted. The probability for its acceptance is 29.19 %. The tempreature difference Δy equals – 0.65 °C.

Positive trend values in the time series are seen in the Figure 4, as well as in the equation (3-Tamin)$_{1,2,3,4}$. The hypothesis test will give us an answer whether this assertion is true or not. The calculated *p* value is higher than 0.05, which means that the null hypothesis should be accepted. The probability for its acceptance is 16.24 %. The tempreature difference Δy equals – 0.58 °C.

Negative trend values in the time series are seen in the Figure 5, as well as in the equation (4-Ta)$_{1,2,3,4}$. The hypothesis test will give us an answer whether this assertion is true or not. The calculated p value is higher than 0.05, which means that the null hypothesis should be accepted. The probability for its acceptance is 47.07 %. The tempreature difference Δy equals 0.25 °C.

CONCLUSION

Priština meteorological station was a part of Serbian meteorological system until 1999. It started with data collecting in 1949. Its significance is in its location – near the K&M province capital. The data used in this study was for the 1949 – 1999 period. The data processing was organized in two phases. In the first one a random data interpolation took place. In the second phase the XL-stat statistical software was chosen, and using it we came to assertions on data trends for (maximal, minimal, average) temperatures and precipitations. The Mann-Kendall′s trend test was used due to its suitability for meteorological data processing. For the purpose of obtaining long term climate assessments, three statistical trends for two time series were done and a conclusion about Priština trend was drawn. Having in mind results of the MK test, we come to a conclusion that the H_0 hypothesis should be accepted. The general conclusion is: there is no trend neither in maximal, minimal, average temperatures, nor in average precipitation sums for the 1949 – 1999 period.

REFERENCES

Bačević, R. N., Vukoičić, Z. D., Nikolić, M., Janc, N., Milentijević, N., & Gavrilov, B. M. 2017. Aridity in Kosovo and Metohija, Serbia. Carpathian Journal of Earth and Environmental Sciences, Vol. 12, No 2, 563-570.

Brázdil, R., Budíková, M., Auer, I., Böhm, R., Cegnar, T., Faško, P., . . . Weber, R.O. 1996. Trends of maximum and minimum daily temperatures in Central and Southeastern Europe. International Journal of Climatology, 16(7), pp. 765-782. doi:10.1002/(sici)1097-0088(199607)16:7<765::aid-joc46>3.0.co;2-o

Brunet, M., Jones, P.D., Sigró, J., Saladié, O., Aguilar, E., Moberg, A., . . . López, D. 2007. Temporal and spatial temperature variability and change over Spain during 1850–2005. Journal of Geophysical Research, 112(12). doi:10.1029/2006jd008249

Brunetti, M., Buffoni, L., Mangianti, F., Maugeri, M., & Nanni, T. 2004. Temperature, precipitation and extreme events during the last century in Italy. Global and Planetary Change, 40(1-2), pp. 141-149. doi:10.1016/s0921-8181(03)00104-8

Douglas, E.M., Vogel, R.M., & Kroll, C.N. 2000. Trends in floods and low flows in the United States: impact of spatial correlation. Journal of Hydrology, 240(1-2), pp. 90-105. doi:10.1016/s0022-1694(00)00336-x

Ducić, V., & Radovanović, M. 2005. Climate of Republic Serbia.Belgrade: Textbook Institute of Belgrade. in Serbian.

Feidas, H., Makrogiannis, T., & Bora-Senta, E. 2004. Trend analysis of air temperature time series in Greece and their relationship with circulation using surface and satellite data: 1955?2001. Theoretical and Applied Climatology, 79(3-4), pp. 185-208. doi:10.1007/s00704-004-0064-5

Gavrilov, M. B., Lazić, L., Pešic, A., Milutinović, M., Marković, D., Stanković, A., & Gavrilov, M. M. 2010. Influence of Hail Suppression on the Hail Trend in Serbia. Physical Geography, 31(5), pp. 441-454. doi:10.2747/0272-3646.31.5.441

Gavrilov, M., Lazic, L., Milutinovic, M., & Gavrilov, M. 2011. Influence of hail suppression on the hail trend in Vojvodina, Serbia. Geographica Pannonica, 15(2), pp. 36-41. doi:10.5937/geopan1102036g

Gavrilov, M.B., Marković, S.B., Zorn, M., Komac, B., Lukić, T., Milošević, M., & Janićević, S. 2013. Is hail suppression useful in Serbia? – General review and new results. Acta geographica Slovenica, 53(1), pp. 165-179. doi:10.3986/ags53302

Gavrilov, M. B., Marković, S. B., Janc, N., Nikolić, M., Valjarević, A., Komac, B., . . . Bačević, N. 2018. Assessing average annual air temperature trends using the Mann–Kendall test in Kosovo. Acta geographica Slovenica, 58(1). doi:10.3986/ags.1309

Gilbert, R.O. 1987. Statistical Methods for Environmental Pollution Monitoring.New York: Van Nostrand Reinhold.

Hrnjak, I., Lukić, T., Gavrilov, M. B., Marković, S. B., Unkašević, M., & Tošić, I. 2014. Aridity in Vojvodina, Serbia. Theoretical and Applied Climatology, 115(1-2), pp. 323-332. doi:10.1007/s00704-013-0893-1

-IPCC. 2007. Intergovenmental Panel Climate Change. The physical science basis. In S. Solomon, D. Qin, M. Manning, Z. Chen, M. Marquis, K. B. Averyt, . . . H. L. Miller Eds., Contribution of Working Group I to the Fourth Assessment Report of the Intergovernmental Panel on Climate Change.Cambridge: Cambridge University Press.

Ivanovic, R., Valjarevic, A., Vukoicic, D., & Radovanovic, D. 2016. Climatic regions of Kosovo and Metohija. The University Thought - Publication in Natural Sciences, 6(1), pp. 49-54. doi:10.5937/univtho6-10409

Kendall, M.G. 1938. A New Measure of Rank Correlation. Biometrika, 30(1/2), p. 81. doi:10.2307/2332226

Kendall, M.G. 1975. Rank correlation methods.London: Charles Griffin.

Klein, T.A.M.G., Wijngaard, J.B., Können, G.P., Böhm, R., Demarée, G., Gocheva, A., & et al., 2002. Daily dataset of 20th-century surface air temperature and precipitation series for the European Climate Assessment. International Journal of Climatology, 22(12), pp. 1441-1453. doi:10.1002/joc.773

Milentijevic, N., Dragojlovic, J., Cimbaljevic, M., Ristic, D., Kalkan, K., & Buric, D. 2018. Analysis of equivalent temperature - case of Kragujevac city. Bulletin of the Serbian Geographical Society, 98(1), pp. 61-77. doi:10.2298/gsgd180225003m

Tošić, I., Hrnjak, I., Gavrilov, M. B., Unkašević, M., Marković, S. B., & Lukić, T. 2014. Annual and seasonal variability of precipitation in Vojvodina, Serbia. Theoretical and Applied Climatology, 117(1-2), pp. 331-341. doi:10.1007/s00704-013-1007-9

Unkašević, M., & Tošić, I. 2009. Changes in extreme daily winter and summer temperatures in Belgrade. Theoretical and Applied Climatology, 95(1-2), pp. 27-38. doi:10.1007/s00704-007-0364-7

Unkašević, M., & Tošić, I. 2011. The maximum temperatures and heat waves in Serbia during the summer of 2007. Climatic Change, 108(1-2), pp. 207-223. doi:10.1007/s10584-010-0006-4

Unkašević, M., & Tošić, I. 2013. Trends in temperature indices over Serbia: relationships to large-scale circulation patterns. International Journal of Climatology, 33(15), pp. 3152-3161. doi:10.1002/joc.3652

Valjarević, A., Djekić, T., Stevanović, V., Ivanović, R., & Jandziković, B. 2018. GIS numerical and remote sensing analyses of forest changes in the Toplica region for the period of 1953–2013. Applied Geography, 92, pp. 131-139. doi:10.1016/j.apgeog.2018.01.016

Vukoičić, D., Milosavljević, S., Penjišević, I., Bačević, N., Nikolić, M., Ivanović, R., & Jandžiković, B. 2018. Spatial analysis of air temperature and its impact on the sustainable development of mountain tourism in Central and Western Serbia. Időjárás Quarterly Journal of the Hungarian Meteorological Service, 122(3), pp. 259-283. doi:10.28974/idojaras.2018.3.3

DIGITAL TOPOGRAPHIC MODELLING IN CASE WITH HIGHER FLOOD IN THE MUNICIPALITY OBRENOVAC

ALEKSANDAR VALJAREVIĆ[1*], DRAGICA ŽIVKOVIĆ [2]

[1]Faculty of Natural Science and Mathematics, University of Priština, Kosovska Mitrovica, Serbia
[2]Faculty of Geography, University of Belgrade, Belgrade, Serbia

ABSTRACT

The town of Obrenovac is situated near the banks of three rivers, the Sava River, the Kolubara River and the Tamnava River. It looks like a modern town, though it has often developed in an unplanned manner. This causes huge problems as it thrives in a rough terrain, without a plan, which the communal infrastructure cannot follow. Today's needs in terms of spatial planning, envisaging projects and keeping track of a different kind of information on space demand that new technologies be applied since they make it possible for procuring efficient and reliable information as well as connecting and interconnecting various sorts of data. Also with advanced numerical GIS data and relief analysis we were successfully calculated consequence of the last big flood in 2014.

Keywords: Rivers, Flood, Digital, Modelling, Preventive, GIS.

INTRODUCTION

The catastrophic floods in May 2014 was producing many damage consequences in the territory of the municipality of Obrenovac. The wild river Kolubara caused a flood to remember. The catastrophic floods which affected Obrenovac were not the first ones for the town to encounter through history. Built not too far away from the banks of the Sava, Kolubara and Tamnava River, Obrenovac seems destined to fight frequent floods. Once time in one-hundred year Obrenovac was hit by the catastrophe flood. Could we have learned a lesson from history and is the town council sufficiently technologically equipped and trained for managing modern technologies? Today's needs in the field of spatial planning, envisaging projects and keeping track of various information demand that new technologies be applied. They make way for efficient and precise information, including the possibility of connecting and interconnecting various sorts of data (www.gis.srbijavode.rs) bearing in mind the fact that the European Union offers a special support to digital society development. Obrenovac is located 28 km southwest of Belgrade capital of Serbia (Figure 1). It is rightly said to have a long past and a short history. The first settlement to have appeared in its backyard was in the Neolith, cut across by the Tamnava and the Kolubara River, while the rural settlement of Palez was first mentioned in 1717. The name originates from the subterranean swampy terrain that houses were built on. The settlement first developed near the Kolubara River (Radovanović, 1963). After the liberation from the Ottoman rule, it moved west and started being built near the Tamnava River. Because of the floods during high water levels, the town was separated from the river banks although it was near them. The town borders the rivers; the Sava River to the north, the Kolubara River to the west, the Tamnava

River to the south and the Velika Bara Canal to the east. The position of 77 metres above sea level, in the Sava and Kolubara alluvial plain, has had an impact on the town being shaped as an inverted letter T (Figure 1).
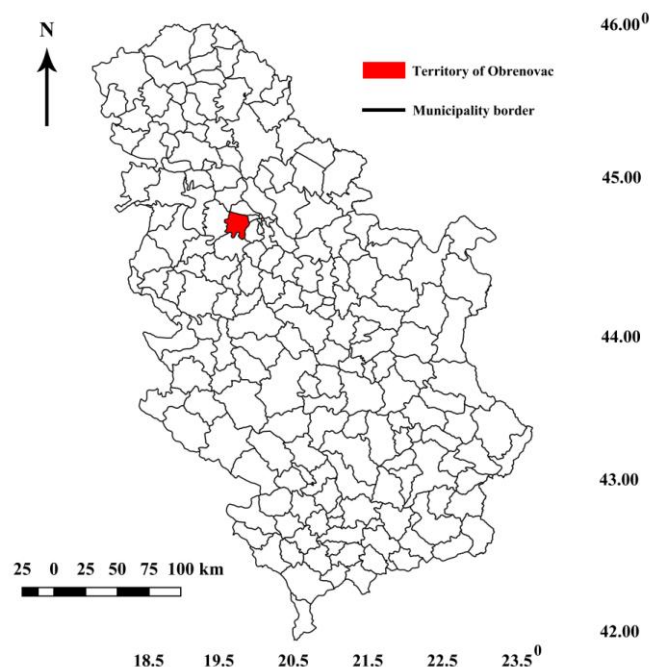
Figure 1. Position of the municipality of Obrenovac.

One leg moves north, near the Obrenovac- Zabrežje outline in the direction of the Sava River as the other gets through the town centre emerging south, at the Kolubara River, following the east-west direction (Živković, 1977). Obrenovačka Posavina is the macro flood area of the Kolubara River over which the Sava is pushed 10 kilometres north of its initial flow below the Posavina section (www.jp.zzs.org.rs.). Basically, all types of soil

---

* Corresponding author: aleksandar.varljarevic@pr.ac.rs
GEOGRAPHY, GEOSCIENCE AND ASTRONOMY

emerged from fluvial erosion or from accumulation. Near Oberenovac, the pronounced Posavina section stretches crosscut in the direction of the lower Kolubara valley. Its bottom fits into the Sava valley bottom and the one of the Srem Ditch. The Posavina section has its origin in a fissure but its appearance of today was created by the crosscut erosion of the Sava. The part of the Posavina Section between Obrenovac and Skela was cut across by wide valleys with terraces, with the bottom that most frequently continues as the Sava terrace with the serpentine and the elaborate Sava and Kolubara river beds. Because of the most recent lowering of the middle parts of the lower Kolubara basin, movement has been intensified, there has been intensified meandering, while the river flows have become dislocated, so that the elaborate Kolubara river beds create some kind of delta. The old Sava meanderings indicate the river's movement over the Sava terrace in the south-north direction (Jovanović, 1956). The process of erosion is ever so present in the territory of Obrenovac Municipality, especially east of the Kolubara River, including the process of eroded material accumulation in the lower flow of the Kolubara River, creating the ideal conditions for flood occurrence with every higher water level (Dragicević, 2002). 3D models make a more flexible view of topography possible while modern technologies account for simulating possible flood

scenarios, this way preventing devastating catastrophes one such is the one that hit Obrenovac.

OBTAINING FIELD EXPOSITIONS AND FLT OF OBRENOVAC MUNICIPALITY AREA FILE

At the beginning of DEM inserting, it is important that the projection to be converted onto the map be determined. The WGS 84 datum and Mercator Projection is taken as the projection file to be transferred onto the map. On determining the projection from the DEM area, the terrain Obrenovac zone borderlines are determined in the altitude range of 70-72, 72-74, 74-76, 76-78,78-80, >80 m (Table 1). Ttherefore, what is obtained among the contour lines in the areas later to be processed in the GIS software called QGIS and SAGA. The data processing is performed in the following way. DEM is inserted with the help of the software function Global Mapper 17. Then what is used is the function File Export Elevation from which the FLT grid format is derived. What is opened is the window in the software Export Slope Direction Values Instead of Evaluations, which is checked in order to determine the desirable altitudes and watershed properties (Figure 2). As FLT file is inserted, the window within DEM is activated (Clarke, 1988).
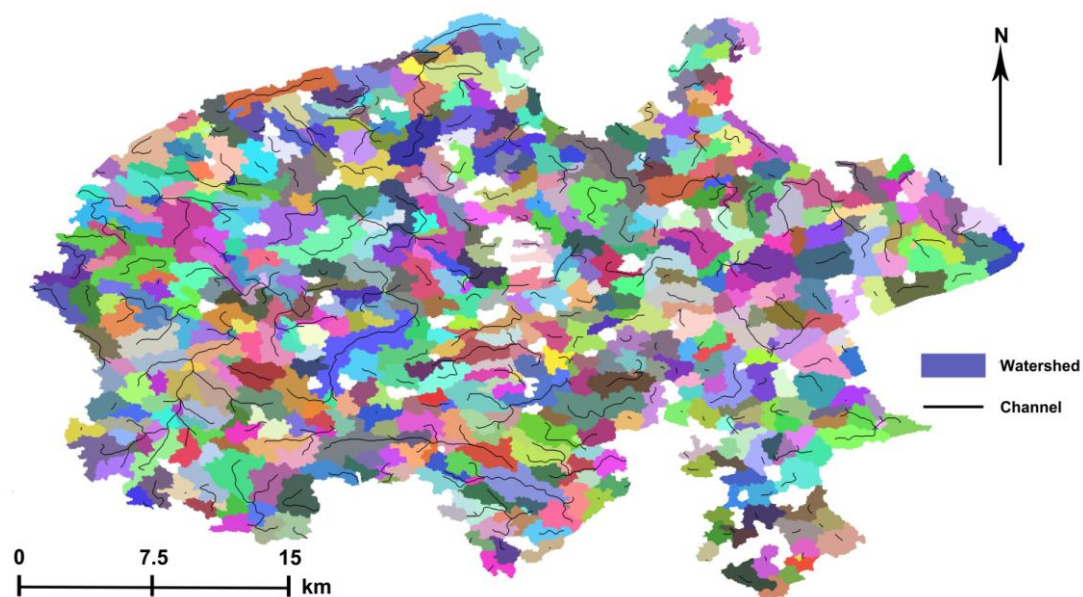
Figure 2. Watershed of the territory of Obrenovac.

DEM PREPARATION AND MAP CONVERSION

There are numerous ways and methods of data insertion in GIS. One of the methods of determining the contour lines on a particular digital map is the FLT file extrapolation, which is an extension of GRID file. FLT file is suitable as it belongs to a universal extension and as such, it can be read by major GIS software. Another big advantage of FLT is the small size of the outgoing file. The major trait, however, is that DEM can be made out of it, thus creating a 3D model. The example of Obrenovac involves the primary task of making a border on which the grid is

to be made. The border that has been taken is the one located on the geo portal http://www.geosrbija.rs/). The border is divided into cadastre sections. On determining the border, what is done next is making the GRID as an FLT format, which later determines the contour lines borders, and by using a special function in the software Global Mapper 17, the areas among these are determined too (Table 1). The scanning has been performed by obtaining altitudes and areas.

What appears to be a great problem of the town of Obrenovac lies in the fact that the Kolubara and Sava banks are at a greater altitude than certain parts of the town. What one can

see from the table is 10.20 km^2 or 24.2%, which is almost a quarter of the town's total area 72 metres high, 35.36 km^2 or 83.9% 74 metres high, as the Sava bank is 77 metres (the bank at Zabrezje); the Kolubara bank is 76 metres, that is near the Sava confluence and the altitude at the black point on the road to Sabacbetween Stocnjak and Rvat is 1 m. The lowest point of Obrenovac is at 73 metres above sea level, in the space called Plošće and inside the wide Sava meander, which changes its course near the vicinity of the village of Zabrezje and flooding level was 78 metres above absolute sea level. The digital visualization and simulation of events, for example, what area size would have been flooded if the Sava water level had risen for the altitude assumed, make it possible for envisaging and preventing unfortunate incidents.

Table 1. Area of contour belts of Obrenovac and its properties.

Altitude m	Area km^2	%
70-72	10.20	24.193
72-74	25.16	59.677
74-76	2.62	6.214
76-78	1.90	4.509
78-80	1.84	4.364
>80	0.44	1.043
∑	42.16	100.000

MULTI-CRITERIA GIS ANALYSIS

Geographic Information System and environmental modelling were applied in hazard investigation. All geospatial data can be used for mapping and modelling of the flood waves on the territory of the Municipality Obrenovac (Valjarević et al., 2018; Valjarević at al., 2017). In this research we used numerical and GIS methods. GIS software's used belongs to open-source software's this software's are QGIS and SAGA. GIS analysis in combination with numerical methods are very powerful tool for calculating flood effects. The process of DEM and basic relief analysis in an area provides letter manipulation in GIS software's. Although, there are a many other methods, but priority is given to 3D modelling and watershed analysis (Figure 2). These methods include numerical autocorrelation and statistical relationship between points into 3D space (Malczewski, 2004; Pew & Larsen, 2001: Patterson & Hoalst-Pullen, 2011; Valjarević, 2016). Both, GIS numerical analysis and spatial algorithms can be successfully can implemented in open-source GIS software QGIS. Using GIS software, we cropped territory of municipality Obrenovac after process of digitization. In this way we are manipulating with the vector data. Vector data after GIS total analysis we exported trough tool in one more software called Global Mapper 17. Global Mapper 17 has excellent advantages, especially in 3D analysing and representing (Figure 3). (Valjarević et al., 2015; Patterson &

Hoalst-Pullen, 2009). We monitored territory of Obrenovac for seven days.
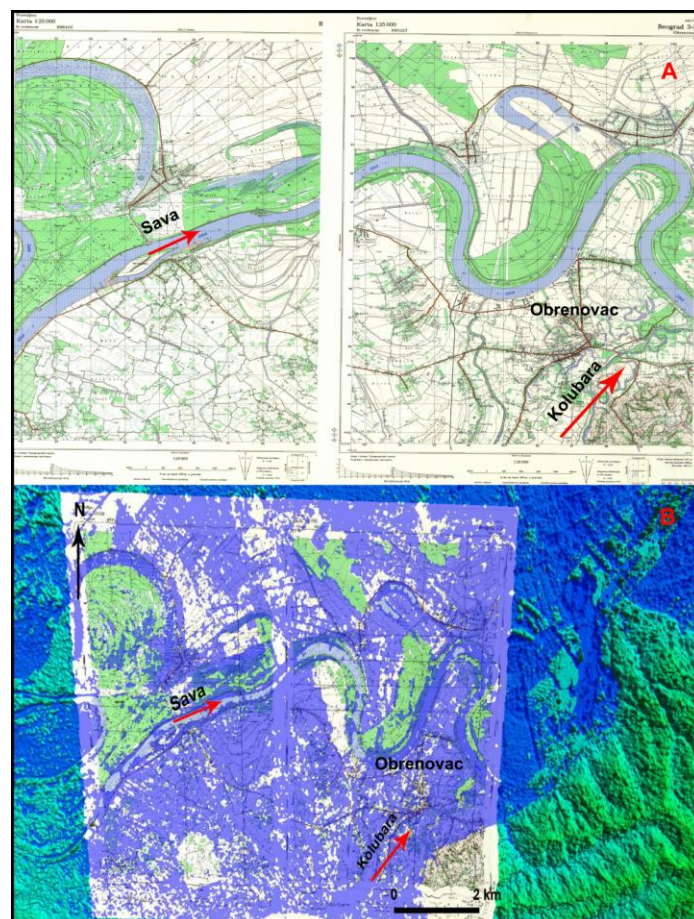
Figure 3. The high volume of wave on May 2014, with flooded areas. A- Situation before May 2014, B-situation in a day with highest wave. High point of Obrenovac is 76.2 m and after flood in May 2014 was 80.2 m.

ADVANCED GIS AND NUMERICAL METHODS

Advanced Geographical Information system in combination with remote sensing techniques gave satisfactory results. By applying advanced GIS methodology and numerical methods we analysed flood wave in the territory of Obrenovac. GIS analysis established belts into six values (see Table 1). The special algorithms which situated in the interface of Global Mapper software rendered and vectorised all data of volume of waves. The data of waves are downloaded from the official web page of the Meteorological service of the Republic of Serbia (http://www.hidmet.gov.rs/). But with the help of pairs of two sofwares Global Mapper and SAGA with techniques of Semi-automated and Full-automated kriging we were estimated volume of water in total. The process of vectorisation follows the process of pixelisation. The process of scattered pixels in an area provides later manipulation in GIS software Global Mapper and SAGA for obtaining density and the number of trees. Although there are a few other methods, priority is given to ordinary

kriging and global kriging methods. These methods include auto-correlation or the statistical relationship among the measured

points and are very flexible in the presentation of forest distribution and density (Jankowski et al., 2001).
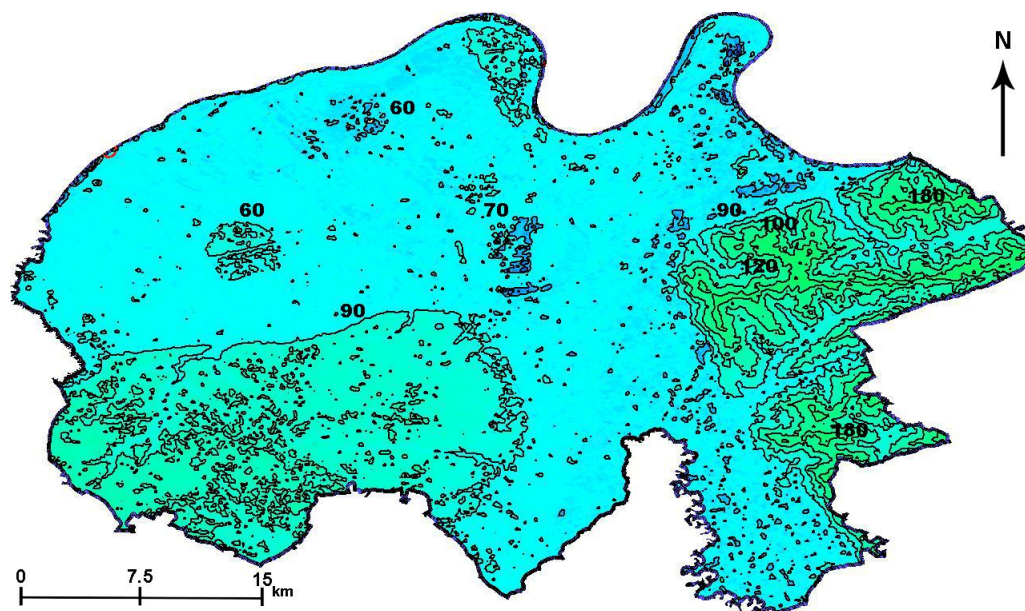
Figure 4. The elevation maps of the Municipality of Obrenovac with proposed contours lines.

RESULTS

By applying advanced GIS techniques and numerical data, we analyzed the condition of land belts in the municipality Obrenovac after the big flood in 2014 (Valjarević, 2016). With help of official meteorological and cadaster data, we found precise way to establish effects of the hazardous flood. According to GIS numerical and 3D analysis, we calculated area and volume of the flood in the territory of Obrenovac. The municipality of Obrenovac belong to the city of Belgrade and included such as city territory. The area of Obrenovac is 441 km^2 after big flood territory covered by water was 78%. But, a territory of a central core of Obrenovac were 99%, as well only 1% were without food. Reason for that is in the relief properties. West part of the municipality has higher altitudes for almost 10 m, and also distance from river Kolubara is 11 km. 12% of non-flooded areas situated in the north-west. When we talk about the volume of waves we have next results. First belt between 70-72 m was covered 12%, second belt 72-74 m was covered 20%, 74-76 m or third belt was covered 31%, third belt between 76-78 m was covered by 15% of water, fifth belt 78-80 m, was covered by 20%, finally sixth belt or altitudes higher than 80 m, was covered 2% of the territory. Also we calculated average and maximum wave of Kolubara and Sava rivers. Average wave of Kolubara river was 2.2 m, and maximum river was 3.7. On the river Sava average river was 3.1 and maximum wave was 4.5. Because terrain as well relief is lower near mouth of Kolubara river, north-east part of Obrenovac was destroyed more. The total volume of water was 17,856,345,455 m^3. Also, because of Obrenovac municipality terrain the central territory shows altitudes between 60 and 90 meters, as well west and central part

of the municipality lower than eastern and northern parts. After big floods the central part of the municipality is always at risk (see Figure 4; Table 1).

CONCLUSION

Today's needs in terms of spatial planning, envisaging projects and managing different sorts of information, result in obtaining efficient and reliable information, along with the possibility of connecting and interconnecting various sorts of data. New technology application demands concrete investment and a continual professional engagement, which would make it possible for experts to be used in critical situations and by which human lives would be saved along with the material welfare. By combining topographic and relief maps with 3D terrain models, it is possible to simulate events in space, envision their manifestations and in this light diminish the bad effects. Also with the help of advanced numerical methods results could be more effective. Next step must be in creation database of Obrenovac, in this database it would be necessary to input all vector and hazardous data for better management against future floods. The data updated would be used in the field of water management, agriculture, forestry, environment protection etc.

REFERENCES

Clarke, K. C. 1988. Scale-Based Simulation of Topographic Relief. The American Cartographer, 15(2), pp. 173-181. doi:10.1559/152304088783887107

Dragićević, S. 2002. Bilans nanosa u slivu Kolubare. Beograd: Univerzitet u Beogradu - Geografski fakultet, pp. 52-53.

Jovanović, B. 1956. Reljef sliva Kolubare, Prilog poznavanju razvitka polifaznog i poligenetskog reljefa sliva.Beograd: SANU. Poseba izdanja, knjiga CCLXIII.

Malczewski, J. 2004. GIS-based land-use suitability analysis: a critical overview. Progress in Planning, 62(1), pp. 3-65. doi:10.1016/j.progress.2003.09.002

Patterson, M. W., & Hoalst-Pullen, N. 2009. Local Government Use of GIS in Comprehensive Planning. In J. D. Gatrell & R. R. Jensen Eds., Planning and Socioeconomic Applications. Geotechnologies and the environment.Dordrecht: Springer Nature America, Inc., pp. 205-220. doi:10.1007/978-1-4020-9642-6_13

Patterson, M. W., & Hoalst-Pullen, N. 2011. Dynamic equifinality: The case of south-central Chile's evolving forest landscape. Applied Geography, 31(2), pp. 641-649. doi:10.1016/j.apgeog.2010.12.004

Pew, K., & Larsen, C. 2001. GIS analysis of spatial and temporal patterns of human-caused wildfires in the temperate rain forest of Vancouver Island, Canada. Forest Ecology and Management, 140(1), pp. 1-18. doi:10.1016/s0378-1127(00)00271-1

Radovanović, V. 1963. Obrenovac i okolina, Mografija mesta. Beograd: Opština Obrenovac.

Valjarević, A., Djekić, T., Stevanović, V., Ivanović, R., & Jandziković, B. 2018. GIS numerical and remote sensing analyses of forest changes in the Toplica region for the period of 1953–2013. Applied Geography, 92, pp. 131-139. doi:10.1016/j.apgeog.2018.01.016

Valjarević, A., Srećković-Batoćanin, D., Valjarević, D., & Matović, V. 2018. A GIS-based method for analysis of a better utilization of thermal-mineral springs in the municipality of Kursumlija (Serbia). Renewable and Sustainable Energy Reviews, 92, pp. 948-957. doi:10.1016/j.rser.2018.05.005

Valjarević, A., Srećković-Batoćanin, D., Živković, D., & Perić, M., 2015. GIS analysis of dissipation time of landscape in the Devil's city. Acta Montanistica Slovaca, 20(2), pp.148–155.

Valjarević, A., Živković, D. 2016. GIS & Sattelite detection of forest belt in Prokuplje municipality". Techical Gazette, 23(4), pp. 969-972 doi:10.17559/TV-20140222204458.

Valjarević, A. 2016. GIS modelling of solar potential in Toplica region. The University Thought - Publication in Natural Sciences, 6(1), pp. 44-48. doi:10.5937/univtho6-10739

Živković, D. 1977. Obrenovac-satelitsko naselje Beograda. Zbornik radova Geografskog instituta PMF, Beograd, sv. XXIV.

STATISTICAL CAUSALITY AND QUASIMARTINGALES

DRAGANA VALJAREVIĆ[1,*]**, LJILJANA PETROVIĆ**[2]

[1]Department of Mathematics, Faculty of Sciences and Mathematics, University of Priština, Kosovska Mitrovica, Serbia
[2]Department of Mathematics and Statistics, Faculty of Economics, University of Belgrade, Belgrade, Serbia

ABSTRACT

Concept of causality is very popular and applicable nowadays, especially when we consider the cases "what would happen if" and "what would have happened if". Here we consider the concept of causality based on the Granger's definition of causality, introduced in Mykland (1986). Many of the systems to which it is natural to apply tests of causality take place in continuous time, so we will consider the continuous time processes. Here we consider the connection between the concept of causality and the property of being a quasimartingale. Quasimartingales were investigated by Fisk (1965), Orey and specially Rao (1969). Namely, in this paper we prove an equivalence between the given concept of causality and preservation of quasimartingale property if the filtration is getting larger. We prove the same equivalence for the stopped quasimartingale with respect to the truncated filtrations.

Keywords: Causality, Filtration, Martingale, Quasimartingale.

INTRODUCTION

In this paper we consider a stochastic process X_t which have a decomposition into the sum of a martingale process and a process having almost every sample function of bounded variation on the interval $I(I \subseteq \mathbb{R})$. Such a process is called a quasimartingale.

After Introduction, in Section 2 we give definition of the causality concept, based on the Granger's definition of causality and some basic properties of that concept which will be used later.

One of the goals of science is to find causal relations. This cannot always be done by experiments and researchers are restricted to observe the system they want to describe. This is the case in, e.g., economics, demography, etc. In the papers of Florens & Mouchart (1982), Gill & Petrovic (1987), Mykland (1986), Petrović (1996) it is shown how the conditional independence can serve as a basis for a general probabilistic theory of causality for both processes and single events.

The paper introduces a statistical concept of causality which unifies the nonlinear Granger–causality with some related concepts.

The linear Granger–causality was introduced by Granger, 1969. We shall study a nonlinear version of the concept. Like the linear one, it defines that the process $\mathbf{Y} = \{Y_t, t \in I\}, (I \subseteq \mathbf{R})$ does not cause the process $\mathbf{X} = \{X_t, t \in I\}$ if, for all t, the orthogonal projection of the L^2-space representing $X_s, s > t$, on the space representing X_s and $Y_s, s \leq t$ is contained in the space representing $X_s, s \leq t$. However, the spaces representing stochastic variables are those over the σ-field generated by these variables, while in the linear case they are the smallest closed linear spaces containing the variables.

We give a generalization of a causality relationship "$\mathbf{G}$ entirely causes $\mathbf{H}$ within $\mathbf{F}$" which (in terms of σ-algebras) was introduced by Mykland (1986) and which is based on Granger's definition of causality (see Granger (1969)) and discuss the relationship to nonlinear Granger–causality.

In Section 3, we consider relations between the given causality concept and the quasimartingale properties. More precisely, we analyze connection between causality and the preservation of the quasimartingale property with respect to the enlarged filtration $\mathbf{F}$ ($\mathbf{F}$ is enlarged filtration of the natural filtration of quasimartingale $\mathbf{F}^X$).

The given concept of causality can be connected to the orthogonality of martingales (see Valjarević & Petrović (2012)) and the stable subspaces of H^p which contains the right continuous modifications of martingales (see Petrović & Valjarević (2013)). The preservation of the predictable representation property, in the case when the information σ-algebra increases, is strongly connected to the concept of causality (see Petrović & Valjarević (2014)). Also, the concept of statistical causality can be connected to the local weak solutions of stochastic differential equations driven with semimartingales (see Petrović & Valjarević (2015)).

NOTATIONS AND DEFINITIONS

Concept of causality

Following Granger's and Sims's pioneering papers (see Sims (1972)), the notion of causality in econometric is generally defined within framework of prediction theory. This notion refers to situations in which it is possible to reduce the size of the information set that is taken into account for predicting a given variable X_1 without affecting the precision level of the prediction.

More precisely, a set of economic variables, denoted by X_2, does not cause a set of variables X_1, if the information available about X_2 may be forgotten without any consequence regarding the prediction of future $X_1's$. Since the content of the "available in-

---

* Corresponding author: dragana.valjarevic@pr.ac.rs

formation" set is not precisely described, the definition remains ambiguous.

Modern financial econometrics is mainly devoted to the study of rapidly evolving stochastic processes. The recent development of continuous time modelling in finance is an important motivation for considering the concept of causality in continuous time.

In this part of the paper we give the definition of the concept of causality relationship (in continuous time) between the flow of information (represented by filtrations) and between the stochastic processes.

Let $(\Omega, \mathcal{F}, P)$ be an arbitrary probability space and let $\mathbf{F} = \{\mathcal{F}_t, \ t \in I(\subseteq \mathbf{R})\}$, be a family of sub-$\sigma$-algebras of $\mathcal{F}$. $\mathcal{F}_t$ can be interpreted as the set of events observed up to time t. Whether or not $\sup I = +\infty$ or $\inf I = -\infty$ we define $\mathcal{F}_\infty$ as the smallest σ-algebra containing all the $\mathcal{F}_t$ (even if $\sup I < +\infty$). So, we have $\mathcal{F}_\infty = \bigvee\limits_{t \in I} \mathcal{F}_t$ and $\mathcal{F}_{-\infty} = \bigcap\limits_{t \in I} \mathcal{F}_t$.

A filtration $\mathbf{F} = \{\mathcal{F}_t, \ t \in I\}$ is a nondecreasing family of sub-σ-algebras of $\mathcal{F}$, i.e. that is

$$\mathcal{F}_s \subseteq \mathcal{F}_t, s \le t.$$

A probabilistic model for a time-dependent system is described by $(\Omega, \mathcal{F}, \mathcal{F}_t, P)$, where $(\Omega, \mathcal{F}, P)$ is a probability space and $\{\mathcal{F}_t, \ t \in I\}$ is a "framework" filtration, i.e. $(\mathcal{F}_t)$ are all events in the model up to and including time t and $(\mathcal{F}_t)$ is a sub-σ-algebra of $(\mathcal{F})$. We suppose that the filtration $(\mathcal{F}_t)$ satisfy the "usual conditions", which means that $(\mathcal{F}_t)$ is right continuous and each $(\mathcal{F}_t)$ is complete.

Analogous notation will be used for filtrations $\mathbf{H} = \{\mathcal{H}_t\}$ and $\mathbf{G} = \{\mathcal{G}_t\}, \ t \in I$.

It will be said that the filtrations $\mathbf{G}$ and $\mathbf{F}$ are equivalent (and written as $\mathbf{G} = \mathbf{F}$) if $\mathbf{G} \subseteq \mathbf{F}$ and $\mathbf{F} \subseteq \mathbf{G}$, or equivalently, if $\mathcal{G}_t = \mathcal{F}_t$ for each t.

A family of σ-algebras induced by a stochastic process $\mathbf{X} = \{X_t, t \in I\}$ is given by $\mathbf{F}^X = \{\mathcal{F}_t^X, t \in I\}$, where

$$\mathcal{F}_t^X = \sigma\{X_u, u \in I, u \le t\},$$

being the smallest σ-algebra with respect to which the random variables $X_u, u \le t$ are measurable. The process X_t is $(\mathcal{F}_t)$-adapted (or adapted to the filtration $\mathbf{F} = \{\mathcal{F}_t\}$) if all $X_u, u \le t$ are $\mathbf{F}$-measurable, i.e. if

$$\mathcal{F}_t^X \subseteq \mathcal{F}_t \quad \text{for each } t.$$

The notation $(X_t, \mathcal{F}_t)$ means that X_t is $(\mathcal{F}_t)$-adapted.

A family of σ-algebras may be induced by several processes, e.g. $\mathbf{F}^{X,Y} = \{\mathcal{F}_t^{X,Y}, t \in I\}$, where

$$\mathcal{F}_t^{X,Y} = \mathcal{F}_t^X \bigvee \mathcal{F}_t^Y, t \in I.$$

On the probability space $(\Omega, \mathcal{F}, P)$ the process $\mathbf{Z} = \{Z_t, t \in I\}$ is a $(\mathcal{F}_t, P)$-martingale if Z_t is $(\mathcal{F}_t)$-adapted and $E(Z_t | \mathcal{F}_s) = Z_s$ for all $t \ge s$.

The intuitively plausible notion of causality formulated in terms of Hilbert spaces, is given in Petrović (1996). We shall use analogue notion of causality in terms of filtrations. Let $\mathbf{F}$, $\mathbf{G}$ and $\mathbf{H}$ be arbitrary filtrations. We can say that " $\mathbf{G}$ entirely causes $\mathbf{H}$ within $\mathbf{F}$ " if

$$\mathcal{H}_\infty \perp \mathcal{F}_t | \mathcal{G}_t \tag{1}$$

because the essence of (1) is that $(\mathcal{G}_t)$ contains all information from the $(\mathcal{F}_t)$ needed for predicting $\mathcal{H}_\infty$. Let us mention that the condition $\mathbf{G} \subseteq \mathbf{F}$ does not represent essential restriction. Thus, it is natural to introduce the following definition of causality between filtrations.

Definition 1. (see Petrović (1996)) It is said that $\mathbf{G}$ entirely causes (or just causes) $\mathbf{H}$ within $\mathbf{F}$ relative to P (and written as $\mathbf{H} \,|\!< \mathbf{G}; \mathbf{F}; P$) if $\mathcal{H}_\infty \subseteq \mathcal{F}_\infty$, $\mathbf{G} \subseteq \mathbf{F}$ and if $\mathcal{H}_\infty$ is conditionally independent of $(\mathcal{F}_t)$ given $(\mathcal{G}_t)$ for each t, i.e.

$$\mathcal{H}_\infty \perp \mathcal{F}_t | \mathcal{G}_t \text{ for each } t, \tag{2}$$

(i.e. $\mathcal{H}_u \perp \mathcal{F}_t | \mathcal{G}_t$ holds for each t and each u), or

$$(\forall A \in \mathcal{H}_\infty) \, P(A | \mathcal{F}_t) = P(A | \mathcal{G}_t).$$

If there is no doubt about P, we omit "relative to P".

The continuous time framework is fruitful, not only for the internal consistency of economic theories but also for the statistical approach to causality analysis between stochastic processes.

Intuitively, $\mathbf{H} \,|\!< \mathbf{G}; \mathbf{F}$ means that, for arbitrary t, information about $\mathcal{H}_\infty$ provided by $(\mathcal{F}_t)$ is not "bigger" than that provided by $(\mathcal{G}_t)$ or that it is possible to reduce available information from $(\mathcal{F}_t)$ to $(\mathcal{G}_t)$ in order to predict $\mathcal{H}_\infty$.

If $\mathbf{G}$ and $\mathbf{F}$ are such that $\mathbf{G} \,|\!< \mathbf{G}; \mathbf{F}$, we shall say that $\mathbf{G}$ is its own cause within $\mathbf{F}$ (compare with Mykland (1986)). It should be mentioned that the notion of subordination (as introduced in Rozanov (1974)) is equivalent to the notion of being one's own cause, as defined here. It should be noted that "$\mathbf{G}$ is its own cause" sometimes occurs as a useful assumption in the theory of martingales and stochastic integration (see Bremaud & Yor (1978), Revuz & Yor (2005)).

These definitions can be applied to stochastic processes if we are talking about the corresponding induced filtrations. For example, $(\mathcal{F}_t)$-adapted stochastic process X_t is its own cause if $(\mathcal{F}_t^X)$ is its own cause within $(\mathcal{F}_t)$, i.e. if

$$\mathbf{F}^X \,|\!< \mathbf{F}^X; \mathbf{F}; P, \quad \text{holds.}$$

Extensions of the definitions to vector processes are usually straightforward.

The process X which is its own cause is completely described by its behavior relative to its natural filtration $\mathbf{F}^X$. For example, process $X = \{X_t, t \in I\}$ is a Markov process relative to the filtration $\mathbf{F} = \{\mathcal{F}_t, t \in I\}$ on a filtered probability space $(\Omega, \mathcal{F}, \mathcal{F}_t, P)$ if and only if X is a Markov process relative to $\mathbf{F}^X$ and it is its own cause within $\mathbf{F}$ relative to P.

The concepts of causality in continuous time are truly relevant for economic reasons (see Comte & Renault (1996)).

In many situations we observe some system up to some random time, for example till the time when something happens for the first time. Definition 1 is extended from fixed times to stopping times in Petrović & Valjarević (2016).

The σ-field $(\mathcal{F}_T) = \{A \in \mathcal{F} : A \cap \{T \leq t\} \in \mathcal{F}_t\}$ is usually interpreted as the set of events that occurs before or at time T (see Elliot (1982)). For a process X, we set $X_T(\omega) = X_{T(\omega)}(\omega)$, whenever $T(\omega) < +\infty$. We define the stopped process $X^T = \{X_{t \wedge T}, t \in I\}$ with

$$X_t^T(\omega) = X_{t \wedge T(\omega)}(\omega) = X_t \chi_{\{t < T\}} + X_T \chi_{\{t \geq T\}}.$$

Note that if X is adapted and cadlag and if T is a stopping time, then the stopped process X^T is also adapted.

Let us mention that the truncated filtration $(\mathcal{F}_{t \wedge T})$ is defined as

$$\mathcal{F}_{t \wedge T} = \mathcal{F}_t \cap \mathcal{F}_T = \begin{cases} \mathcal{F}_t, & t < T, \\ \mathcal{F}_T, & t \geq T. \end{cases}$$

A martingale stopped at a stopping time is still a martingale. The natural filtration for the stopped martingale $X_{t \wedge T}$ is $\mathbf{F}^{X^T} = (\mathcal{F}_{t \wedge T}^X)$, with respect to which the process $X_{t \wedge T}$ is completely described. So, we have the definition of causality which involves the stopping times.

Definition 2. (Petrović & Valjarević (2016)) Let $\mathbf{H} = \{\mathcal{H}_t\}$, $\mathbf{G} = \{\mathcal{G}_t\}$ and $\mathbf{E} = \{\mathcal{E}_t\}, t \in I$, be given filtrations on the probability space $(\Omega, \mathcal{F}, P)$ and let T be a stopping time with respect to filtration $\mathbf{E}$. The filtration $\mathbf{G}^T$ entirely causes $\mathbf{E}^T$ within $\mathbf{H}^T$ relative to P (and written as $\mathbf{E}^T \Vdash \mathbf{G}^T; \mathbf{H}^T; P$) if $\mathbf{E}^T \subseteq \mathbf{H}^T$, $\mathbf{G}^T \subseteq \mathbf{H}^T$ and if $\mathcal{E}_T$ is conditionally independent of $\mathcal{H}_{t \wedge T}$ given $\mathcal{G}_{t \wedge T}$ for each t, i.e. $(\forall t)$ $\mathcal{E}_T \perp \mathcal{F}_{t \wedge \tau} \mid \mathcal{G}_{t \wedge \tau}$, or

$$(\forall t \in I)(\forall A \in \mathcal{E}_T) \quad P(A \mid \mathcal{H}_{t \wedge T}) = P(A \mid \mathcal{G}_{t \wedge T}). \tag{3}$$

The concept of causality given in Definition 2 includes the stopped filtrations. Namely, the causality relationship is defined up to a specified stopping time T.

Quasimartingales

The term quasimartingale is for the first time used by Fisk (1965). It is obvious that the sum and difference of two quasimartingales are again quasimartingales. The difference of two positive local martingales is necessarily a quasimartingale. Let us mention that there are some similarities between quasimartingales and supermartingales. Note that every finite set of random variables with expectations is trivially a quasimartingale. A mean right continuous quasimartingale always has a cadlag (right continuous with left limits) modification. Henceforth we will assume, unless otherwise stated, that all processes considered are cadlag at every time point.

Definition 3. (Protter, 2004) A finite tuple of points $\tau = (t_0, t_1, \ldots, t_{n+1})$ such that $0 = t_0 < t_1 < \cdots < t_{n+1} = \infty$ is a partition of $[0, \infty]$.

Definition 4. (Protter, 2004) Suppose that τ is a partition of $[0, \infty]$ and that $X_{t_i} \in L^1$, each $t_i \in \tau$. Define

$$C(X, \tau) = \sum_{i=0}^n |E(X_{t_i} - X_{t_{i+1}} \mid \mathcal{F}_{t_i})|.$$

The variation of X along τ is defined to be

$$Var_\tau(X) = E(C(X, \tau)).$$

The variation of X is defined to be

$$Var(X) = sup_\tau Var_\tau(X),$$

where supremum is taken over all such partitions.

Definition 5. (Protter, 2004) An adapted, cadlag process X is a quasimartingale on $[0, \infty]$ if $E(|X_t|) < \infty$, for each t, and if $Var(X) < \infty$.

Next Theorem defines a Doob decomposition of quasimartingale.

Theorem 6. (Rao, 1969) *A right continuous process X_t is a quasimartigale if and only if it has a generalised Doob decomposition*

$$X_t = Y_t + M_t - B_t,$$

where Y_t is a martingale, M_t is the difference of two non-negative local martingales, and B_t is the difference of two natural integrable increasing processes. This decomposition is unique.

The definition of natural integrable increasing process is given in Rao (1969).

CAUSALITY AND QUASIMARTINGALES

The certain results, not obvious from the definition of a quasimartingale or the fact that it is the difference of two supermartingales, follow from the decomposition from Theorem 6. The starting point in this section is the decomposition

$$X_t = M_t - B_t \tag{4}$$

of a quasimartingale X_t into a local martingale M_t and a natural process with finite expected total variation B_t. This decomposition is unique.

Let $(\mathcal{G}_t)$ be a subfiltration of the filtration $(\mathcal{F}_t)$, i.e. $(\mathcal{G}_t) \subseteq (\mathcal{F}_t)$. The next theorem holds.

Theorem 7. *Every quasimartingale X_t with respect to $(\mathcal{G}_t)$ is a quasimartingale with respect to $(\mathcal{F}_t)$ if and only if $\mathbf{G}$ is its own cause within $\mathbf{F}$, or equivalently if*

$$\mathbf{G} \Vdash \mathbf{G}; \mathbf{F}; P \ holds.$$

Proof. Let the process X_t be a $(\mathcal{G}_t)$ and $(\mathcal{F}_t)$ quasimartingale. From its unique decomposition (4) it follows that process M_t is a $(\mathcal{G}_t)$ and $(\mathcal{F}_t)$-local martingale. According to Theorem 3.3 in Valjarević (2012), the causality $\mathbf{G} \Vdash \mathbf{G}; \mathbf{F}; P$ holds.

Conversely, let $\mathbf{G} \nparallel \mathbf{G}; \mathbf{F}; P$ holds and let the process X_t be a $(\mathcal{G}_t)$-quasimartingale. Then, the process X_t has a unique decomposition $X_t = M_t - B_t$, where M_t is a $(\mathcal{G}_t)$-local martingale. From $\mathbf{G} \nparallel \mathbf{G}; \mathbf{F}; P$ and Theorem 3.3 in Valjarević (2012) it follows that the process M_t is $(\mathcal{F}_t)$-local martingale, too. Also, the process B_t is a natural process with finite expected total variation with respect to filtration $(\mathcal{F}_t)$, because $(\mathcal{G}_t) \subset (\mathcal{F}_t)$. Hence, the process X_t has a unique decomposition $X_t = M_t - B_t$ with respect to filtration $(\mathcal{F}_t)$, so it is a $(\mathcal{F}_t)$-quasimartingale.

Let $\mathbf{F}^X$ be a natural filtration of the quasimartingale X_t. Then the following theorem holds.

Theorem 8. *Process X_t is a $(\mathcal{F}_t)$-quasimartingale if and only if it is its own cause within $(\mathcal{F}_t)$, or equivalently if holds*

$$\mathbf{F}^X \nparallel \mathbf{F}^X; \mathbf{F}; P.$$

Proof. Follows directly by Theorem 7 (we set $\mathbf{G} = \mathbf{F}^X$). ∎

Theorem 9. *Let the process X be uniformly integrable quasimartingale with respect to $\mathbf{G}$, let T be a $(\mathcal{G}_t)$-stopping time and $\mathbf{G} \subset \mathbf{F}$. Then the stopped process $X^T = X_{t \wedge T}$ is quasimartingale with respect to $\mathbf{F}^T = \{\mathcal{F}_{t \wedge T}\}$ if and only if $\mathbf{G}^T$ is its own cause within $\mathbf{F}^T$, i.e. if*

$$\mathbf{G}^T \nparallel \mathbf{G}^T; \mathbf{F}^T; P \quad holds.$$

Proof. Let the process X be uniformly integrable quasimartingale with respect to $\mathbf{G}$, T be a $(\mathcal{G}_t)$-stopping time and

$$\mathbf{G}^T \nparallel \mathbf{G}^T; \mathbf{F}^T; P. \tag{5}$$

Due to Lemma I.1.8.12 in Skorohod & Gikhman (2005) we have that X_T is quasimartingale with respect to $\mathcal{G}_T$. According to the relation (5), from assumption of the theorem it follows that X^T is quasimartingale with respect to $\mathbf{G}^T = \{\mathcal{G}_{t \wedge T}\}$. By Definition 5, Theorem 6 and assumption on the beginning of the Section it follows that the process X^T can be represented as

$$X^T = M^T - B^T.$$

This decomposition is unique. Process M^T is martingale with respect to $\mathbf{G}^T$. According to Theorem 6 in Petrović & Valjarević (2016), from (5) it follows that the process M^T is martingale with respect to $\mathbf{F}^T$, too. Using the same technique as in the previous proof, we get that B^T is a process of bounded variation with respect to $\mathbf{G}^T$ and $\mathbf{F}^T$, too ($\mathbf{G}^T \subset \mathbf{F}^T$). So, process X^T can be presented as $X^T = M^T - B^T$ with respect to $\mathbf{F}^T$, where M^T is a local martingale and B^T is a process of bounded variation.

Conversely, suppose that X^T is quasimartingale with respect to $\mathbf{G}^T$ and $\mathbf{F}^T$, where T is a $(\mathcal{G}_t)$-stopping time. Due to decomposition of the quasimartingale and its uniqueness, follows that $X^T = M^T - B^T$ is unique decomposition with respect to $\mathbf{G}^T$ and $\mathbf{F}^T$. So, M^T is martingale with respect to filtrations $\mathbf{G}^T$ and $\mathbf{F}^T$. Due to Theorem 6 in Petrović & Valjarević (2016), it follows that $\mathbf{G}^T \nparallel \mathbf{G}^T; \mathbf{F}^T; P$ holds. ∎

REFERENCES

Bremaud, P. & Yor, M. 1978. Changes of filtrations and of probability measures. Zeitschrift fur Wahrscheinlichkeitstheorie und Verwandte Gebiete, 45(4), pp. 269-295. doi:10.1007/bf00537538.

Comte, F. & Renault, E. 1996. Noncausality in Continuous Time Models. Econometric Theory, 12(02). doi:10.1017/s0266466600006575.

Elliot, R. J. 1982. Stochastic Calculus and applications. New York: Springer-Verlag.

Fisk, D. L. 1965. Quasi-Martingales. Transactions of the American Mathematical Society, 120(3). doi:10.2307/1994531.

Florens, J. P. & Mouchart, M. 1982. Note on Noncausality. Econometrica, 50(3). doi:10.2307/1912602.

Gill, J. B. & Petrovic, L. 1987. Causality and Stochastic Dynamic Systems. SIAM Journal on Applied Mathematics, 47(6), pp. 1361-1366. doi:10.1137/0147089.

Granger, C. W. J. 1969. . Investigating Causal Relations by Econometric Models and Cross-spectral Methods. Econometrica, 37(3). doi:10.2307/1912791.

Mykland, P. A. 1986. Statistical Causality. Report, 2, pp. 1-21.

Petrović, L. 1996. Causality and Markovian representations. Statistics Probability Letters, 29(3), pp. 223-227. doi:10.1016/0167-7152(95)00176-x.

Petrović, L. & Valjarević, D. 2013. Statistical causality and stable subspaces of the australian mathematical society. Bulletin of the Australian Mathematical Society, 88(01), pp. 17-25. doi:10.1017/s0004972712000482.

Petrović, L. & Valjarević, D. 2014. Statistical causality and martingale representation property with application to stochastic differential equations. Bulletin of the Australian Mathematical Society, 90(02), pp. 327-338. doi:10.1017/s000497271400029x.

Petrović, L. & Valjarević, D. 2015. Lecture Notes in Computer Science: Statistical Causality and Local Solutions of the Stochastic Differential Equations Driven with Semimartingales. Cham: Springer Nature America, Inc., pp. 261-269. doi:10.1007/978-3-319-15765-8₁4.

Petrović, L. and Dimitrijević, S. & Valjarević, D. 2016. Granger causality and stopping times*. Lithuanian Mathematical Journal, 56(3), pp. 410-416. doi:10.1007/s10986-016-9325-0.

Protter, P. 2004. Stochastic Integration and Differential Equations. Berlin: Springer-Verlag.

Rao, K. M. 1969. Quasi-Martingales. Mathematica scandinavica, 24. doi:10.7146/math.scand.a-10921.

Revuz, D. & Yor, M. 2005. Continuous martingales and Brownian motion. New York: Springer.

Rozanov, Y. A. 1974. Theory of Innovation Processes. Monographs in Probability Theory and Mathematical Statistics. Moscow: Izdat Nauka.

Sims, C. A. 1972. Money, income and causality. American Economic Review, 62, pp. 540-552.

Skorohod, I. & Gikhman, L. 2005. Stochastic processes. New York: Springer. 1.

Valjarević, D. 2012. Theory of statistical causality, stochastic differential equations and martingale representation property. University thought, 82, pp. 1326-1330.

Valjarević, D. & Petrović, L. 2012. Statistical causality and orthogonality of local martingales. Statistics Probability Letters, 82(7), pp. 1326-1330. doi:10.1016/j.spl.2012.03.036.

SOME NEW RESULTS FOR REICH TYPE MAPPINGS ON CONE b-METRIC SPACES OVER BANACH ALGEBRAS

JELENA VUJAKOVIĆ[1*], ABBA AUWALU[2], VESNA ŠEŠUM-ČAVIĆ[3]

[1]Faculty of Sciences and Mathematics, University of Priština, Kosovska Mitrovica, Serbia
[2]Department of Mathematics, Faculty of Sciences and Arts, Near East University, Nicosia, Turkey
[3]Institute of Computer Languages, Vienna University of Technology, Austria

ABSTRACT

The main purpose of this paper is to present some fixed point results concerning the generalized Reich type α-admissible mappings in cone b-metric spaces over Banach algebras. Our results are significant extensions and generalizations of resent results of N. Hussain at al. (2017) and many well-known results in abundant literature. We also gave an example that confirmed our results.

Keywords: Cone b-metric space, Banach algebra, α-admissible mapping, α-regular, Fixed point, c-sequence.

INTRODUCTION

The concept of cone metric space was introduced by Huang and Zhang (2007). They supplanted the set of real numbers in metric space by a complete normed space and proved some fixed point results for different contractive conditions in such a space.

Recently, some scholars (see Du, 2010; Kadelburg et al., 2011) argued that extensions of fixed point results on metric space to cone metric space over complete normed spaces are redundand (not new results). In order to overcome this problem, Liu and Xu (2013) introduced the notion of a cone metric spaces over Banach algebras and proved that cone metric spaces over Banach algebras are not equivalent to metric spaces in terms of the existence of the fixed points of the generalized Lipschitz mappings. Very recently, Huang and Radenović (2016) introduced the notion of cone b-metric space over Banach algebras as a generalization of cone metric space over Banach algebra (see Xu & Radenović, 2014; Huang & Radenović, 2015b; Huang & Xu, 2013; Huang et al., 2017). On the other hand, Samet et al. (2012) introduced the notion of α-admissible mappings and proved some fixed point results that generalized several known results of metric spaces. Very recently, Malhottra et al. (2015; 2017) used the concept of α-admissibility of mappings defined on cone metric space over Banach algebras and proved Banach and Kannan fixed point results for Lipschitz contractions in such spaces. In 2017, Hussaini et al. (2017) used the concept of α-admissibility of mappings defined on cone b-metric spaces over Banach algebras and proved Banach fixed point results for Lipschitz contractions in such spaces. The Reich contraction was introduced by Reich (1971) as a generalization of the well-known Banach contraction principle and Kannan contraction. In this twork, we use the concept of α-admissibility of mappings defined on cone b-metric space over Banach algebras and proved Reich type fixed point theorems. We give an example to elucidate our results. Our results generalized the recent results of Malhotra et al. (2015; 2017), Hussain et al. (2017), Nieto and Rodríguez-López (2005).

PRELIMINARIES

It In this section we recall some known definitions and results which will be used.

A real Banach algebra $\mathcal{B}$ is a real Banach space in which an operation of multiplication is defined in the following way: for all $x, y, z \in \mathcal{B}, \alpha \in \mathbb{R}$

1) $(xy)z = x(yz)$,

2) $x(y + z) = xy + xz$ and $(x + y)z = xz + yz$,

3) $\alpha(xy) = (\alpha x)y = x(\alpha y)$,

4) $\|xy\| \leq \|x\|\|y\|$.

A subset $\mathcal{K}$ of Banach algebra $\mathcal{B}$ is called a cone if:

1) $\mathcal{K}$ is nonempty, closed and $\{\theta, e\} \subset \mathcal{K}$;

2) $\alpha\mathcal{K} + \beta\mathcal{K} \subset \mathcal{K}$, for all nonnegative $\alpha, \beta \in \mathbb{R}$;

3) $\mathcal{K}^2 = \mathcal{K}\mathcal{K} \subset \mathcal{K}$;

4) $\mathcal{K} \cap (-\mathcal{K}) = \{\theta\}$,

where θ and e denote the zero and unit elements of Banach algebra $\mathcal{B}$, respectively. For given cone $\mathcal{K} \subset \mathcal{B}$ we define a partial ordering $\preceq$ with respect to $\mathcal{K}$ on following way: $x \preceq y$ if and only if $y - x \in \mathcal{K}$. It is well known that $x \prec y$ stands for $x \preceq y$ and $x \neq y$, $x \ll y$ stands for $y - x \in \text{int}\,\mathcal{K}$ where $\text{int}\,\mathcal{K}$ means the interior of $\mathcal{K}$. We say that $\mathcal{K}$ is a solid cone if $\text{int}\,\mathcal{K} \neq \varnothing$.

In further work, we always assume that $\mathcal{B}$ is a Banach algebra with a unit e, $\mathcal{K}$ is a solid cone in $\mathcal{B}$ and $\preceq$ is the partial ordering with respect to $\mathcal{K}$.

Definition 2.1 (Huang & Zhang 2007; Liu & Xu, 2013) Let $\mathcal{Z}$ be a nonempty set. Suppose that the mapping $\rho: \mathcal{Z} \times \mathcal{Z} \to \mathcal{B}$ satisfies:

* Corresponding author: jelena.vujakovic@pr.ac.rs

MATHEMATICS, COMPUTER SCIENCE AND MECHANICS

(C1) $\theta \preceq \rho(x,y)$ for all $x,y \in \mathcal{Z}$ and $\rho(x,y) = \theta$ if and only if $x = y$;

(C2) $\rho(x,y) = \rho(y,x)$ for all $x,y \in \mathcal{Z}$;

(C3) $\rho(x,y) \preceq \rho(x,z) + \rho(z,y)$ for all $x,y,z \in \mathcal{Z}$.

Then ρ is called a cone metric on $\mathcal{Z}$ and $(\mathcal{Z},\rho)$ is called a cone metric space with a Banach algebra $\mathcal{B}$.

Definition 2.2 (Huang & Radenović, 2015a) Let $\mathcal{Z}$ be a nonempty set, $s \geq 1$ be a constant and $\mathcal{B}$ a Banach algebra. Suppose that the mapping $\rho : \mathcal{Z} \times \mathcal{Z} \to \mathcal{B}$ satisfies:

(C1) $\theta \preceq \rho(x,y)$ for all $x,y \in \mathcal{Z}$ and $\rho(x,y) = \theta$ if and only if $x = y$;

(C2) $\rho(x,y) = \rho(y,x)$ for all $x,y \in \mathcal{Z}$;

(C3) $\rho(x,y) \preceq s\left[\rho(x,z) + \rho(z,y)\right]$ for all $x,y,z \in \mathcal{Z}$.

Then ρ is called a cone b-metric on $\mathcal{Z}$ and $(\mathcal{Z},\rho)$ is called a cone b-metric space with a Banach algebra $\mathcal{B}$.

Note that if $s = 1$, a cone b-metric becomes a cone metric.

Definition 2.3 (Malhotra et al., 2015) Let $(\mathcal{Z},\rho)$ be a cone b-metric space over Banach algebra $\mathcal{B}$ with coefficient $s \geq 1$ and $\{z_i\}$ be a sequence in $(\mathcal{Z},\rho)$. Then,

1) $\{z_i\}$ converges to z whenever for each $c \in \mathcal{B}$ with $c \gg \theta$ there is a natural number N such that $\rho(z_i,z) \ll c$ for all $i \geq N$. We denote this by $z_i \to z$ $(i \to \infty)$ or $\lim_{i \to \infty} z_i = z$.

2) $\{z_i\}$ is Cauchy sequence whenever for each $c \in \mathcal{B}$ with $c \gg \theta$ there is a natural number N such that $\rho(z_i,z_j) \ll c$ for all $i,j \geq N$.

3) $(\mathcal{Z},\rho)$ is said to be complete if every Cauchy sequence in $\mathcal{Z}$ is convergent.

Definition 2.4 (Malhotra et al., 2015) A mapping $\mathcal{F} : \mathcal{Z} \to \mathcal{Z}$ is said to be continuous at $z \in \mathcal{Z}$, if for every sequence $\{z_i\}$ in $(\mathcal{Z},\rho)$ such that $z_i \to z$ $(i \to \infty)$, we have $\mathcal{F}z_i \to \mathcal{F}z$ $(i \to \infty)$.

Definition 2.5 (Kadelburg & Radenović, 2013) Let $\mathcal{K}$ be a solid cone in a Banach algebra $\mathcal{B}$. A sequence $\{z_i\} \subset \mathcal{K}$ is said to be a c-sequence if for each $c \gg \theta$ there exists $N \in \mathbb{N}$ such that $z_i \ll c$ for all $i > N$.

Lemma 2.6 (Huang & Radenović, 2015b) *If E is a real Banach space with a solid cone $\mathcal{K}$ and $\{z_i\} \subset \mathcal{K}$ be a sequence with $\|z_i\| \to 0$ $(i \to \infty)$, then for each $c \gg \theta$ there exists $N \in \mathbb{N}$ such that for any $i > N$ we have $z_i \ll c$.*

Lemma 2.7 (Xu & Radenović, 2015) *Let $(\mathcal{Z},\rho)$ be a complete cone b-metric space over Banach algebra $\mathcal{B}$ with coefficients $s \geq 1$ and $\mathcal{K}$ be the underlying solid cone. Let $\{z_i\}$ be a sequence in $(\mathcal{Z},\rho)$. If $\{z_i\}$ converges to $z \in \mathcal{Z}$, then:*

1) $\{\rho(z_i,z)\}$ is a c-seqauence;

2) for any $j \in \mathbb{N}$, $\{\rho(z_i,z_{i+j})\}$ is a c-sequence.

Lemma 2.8 (Kadelburg & Radenović, 2013) *Let $\mathcal{B}$ be a real Banach algebra with a solid cone $\mathcal{K}$ and let $\{\alpha_n\}$ and $\{\beta_n\}$ are sequences in $\mathcal{K}$. If $\{\alpha_n\}$ and $\{\beta_n\}$ are c-sequences and $k_1,k_2 \in \mathcal{K}$ then $\{k_1\alpha_n + k_2\beta_n\}$ is a c-sequence.*

Lemma 2.9 (Rudin, 1991; Huang & Radenović, 2015a) *Let $\mathcal{B}$ be a Banach algebra with a unit e and $k \in \mathcal{B}$. Then $\lim_{n \to \infty} \|k^n\|^{\frac{1}{n}}$ exists and the spectral radijus $\delta(k)$ satisfies*

$$\delta(k) = \lim_{n \to \infty} \|k^n\|^{\frac{1}{n}} = \inf \|k^n\|^{\frac{1}{n}} .$$

If $\delta(k) < |\lambda|$, then $\lambda e - k$ is invertible in $\mathcal{B}$. Moreover, for complex constant λ are $(\lambda e - k)^{-1} = \sum_{j=0}^{\infty} \dfrac{k^j}{\lambda^{j+1}}$ and

$$\delta\left[(\lambda e - k)^{-1}\right] \leq \frac{1}{|\lambda| - \delta(k)} .$$

Remark 2.10. (Xu & Radenović, 2015) If $\delta(k) < 1$ then $\|k^i\| \to 0$ $(i \to \infty)$.

Lemma 2.11 (Rudin, 1991) *Let $\mathcal{B}$ be a Banach algebra with a unit e and $k_1,k_2 \in \mathcal{B}$. If k_1 commutes with k_2 , then*

$\delta(k_1 + k_2) \leq \delta(k_1) + \delta(k_2)$ and $\delta(k_1 k_2) \leq \delta(k_1)\delta(k_2)$.

Lemma 2.12 (Kadelburg & Radenović, 2013) *Let E is a real Banach space with a solid cone $\mathcal{K}$.*

1) *If $a,b,c \in E$ and $a \preceq b \ll c$, then $a \ll c$.*

2) *If $a \in \mathcal{K}$ and $a \ll c$ for each $c \gg \theta$, then $a = \theta$.*

3) *If $a \preceq ka$, where $a,k \in \mathcal{K}$ and $\delta(k) < 1$, then $a = \theta$.*

MAIN RESULTS

First we introduce the notion of α-admissible mapping and α-regularity in the setting of cone b-metric space over Banach algebra $\mathcal{B}$.

Definition 3.1 Let $(\mathcal{Z},\rho)$ be a cone b-metric space over Banach algebra $\mathcal{B}$ with coefficients $s \geq 1$, $\mathcal{K}$ be the underlying solid cone, $\mathcal{F} : \mathcal{Z} \to \mathcal{Z}$ and $\alpha : \mathcal{Z} \times \mathcal{Z} \to \mathcal{B}$ be mappings. Then:

1) $\mathcal{F}$ is α-admissible mapping if $\alpha(z,y) \succeq s$ implies $\alpha(\mathcal{F}z,\mathcal{F}y) \succeq s$, for all $z,y \in \mathcal{Z}$;

2) $(\mathcal{Z}, \rho)$ is α-regular if for any sequence $\{z_i\}$ in $(\mathcal{Z}, \rho)$, with $\alpha(z_i, z_{i+1}) \succeq s$ for all $i \in \mathbb{N}$ and $z_i \to z_* \in \mathcal{Z}$ $(i \to \infty)$, follows $\alpha(z_i, z_*) \succeq s$, for all $i \in \mathbb{N}$.

Now we are able to define generalized Reich type contraction in cone b-metric spaces over Banach algebra $\mathcal{B}$.

Definition 3.2 Let $(\mathcal{Z}, \rho)$ be a cone b-metric space over Banach algebra $\mathcal{B}$ with coefficient $s \geq 1$, let $\mathcal{K}$ be the underlying solid cone and $\alpha : \mathcal{Z} \times \mathcal{Z} \to \mathcal{B}$ be a function. The mapping $\mathcal{F} : \mathcal{Z} \to \mathcal{Z}$ is called generalized Reich type contraction if there exist vectors $v_k \in \mathcal{K}$ $(k = 1, 2, 3)$ such that $2s\delta(v_1) + (s+1)\delta(v_2 + v_3) < 2$ and

$$\rho(\mathcal{F}z, \mathcal{F}y) \preceq v_1\rho(z, y) + v_2\rho(z, \mathcal{F}z) + v_3\rho(y, \mathcal{F}y), \quad (1)$$

for all $z, y \in \mathcal{Z}$ with $\alpha(z, y) \succeq s$.

Now, we shall show that generalized Reich type α-admissible contraction mappings on cone b-metric spaces over Banach algebra $\mathcal{B}$ has a fixed points.

Theorem 3.3 *Let* $(\mathcal{Z}, \rho)$ *be a complete cone b-metric spaces over Banach algebra $\mathcal{B}$ with coefficient $s \geq 1$, $\mathcal{K}$ be the underlying solid cone and let $\alpha : \mathcal{Z} \times \mathcal{Z} \to \mathcal{B}$ be a function. Suppose the mapping $\mathcal{F} : \mathcal{Z} \to \mathcal{Z}$ is a generalized Reich type contraction with vectors $v_k \in \mathcal{K}$ $(k = 1, 2, 3)$ such that v_1 commutes with $v_2 + v_3$. Suppose that*:

1) *$\mathcal{F}$ is a α-admissible mapping*;
2) *there exists z_0 in $\mathcal{Z}$ with $\alpha(z, \mathcal{F}z_0) \succeq s$* ;
3) *$\mathcal{F}$ is continuous or $(\mathcal{Z}, \rho)$ is α-regular*,

then $\mathcal{F}$ has a fixed point z_* in $\mathcal{Z}$.

PROOF. Let z_0 be an arbitrary point in $\mathcal{Z}$ such that $\alpha(z_0, \mathcal{F}z_0) \succeq s$. Define a sequence $\{z_i\}$ in $(\mathcal{Z}, \rho)$ by

$$z_{i+1} = \mathcal{F}z_i = \mathcal{F}^{i+1}z_0 \text{ for all } i \in \mathbb{N}. \quad (2)$$

If $z_{i+1} = z_i$ for some $i \in \mathbb{N}$, then $z_* = z_i$ is a fixed point of $\mathcal{F}$ and the result is proved. Suppose now that $z_{i+1} \neq z_i$ for all $i \in \mathbb{N}$. Since $\mathcal{F}$ is α-admissible mapping, we have

$$\alpha(z_0, z_1) = \alpha(z_0, \mathcal{F}z_0) \succeq s .$$

Hence,

$$\alpha(\mathcal{F}z_0, \mathcal{F}^2 z_0) = \alpha(z_1, z_2) \succeq s$$

and by induction we get

$$\alpha(z_i, z_{i+1}) \succeq s , \text{ for all } i \in \mathbb{N}. \quad (3)$$

Now, according to (1), (2) and (3), we have

$$\rho(z_i, z_{i+1}) = \rho(\mathcal{F}z_{i-1}, \mathcal{F}z_i)$$
$$\preceq v_1\rho(z_{i-1}, z_i) + v_2\rho(z_{i-1}, \mathcal{F}z_{i-1}) + v_3\rho(z_i, \mathcal{F}z_i)$$
$$= (v_1 + v_2)\rho(z_{i-1}, z_i) + v_3\rho(z_i, z_{i+1}), \text{ i.e.}$$
$$(e - v_3)\rho(z_i, z_{i+1}) \preceq (v_1 + v_2)\rho(z_{i-1}, z_i). \quad (4)$$

Similarly,

$$\rho(z_{i+1}, z_i) = \rho(\mathcal{F}z_i, \mathcal{F}z_{i-1})$$
$$\preceq v_1\rho(z_i, z_{i-1}) + v_2\rho(z_i, \mathcal{F}z_i) + v_3\rho(z_{i-1}, \mathcal{F}z_{i-1})$$
$$= (v_1 + v_3)\rho(z_{i-1}, z_i) + v_2\rho(z_i, z_{i+1}), \text{ i.e.}$$
$$(e - v_2)\rho(z_i, z_{i+1}) \preceq (v_1 + v_3)\rho(z_{i-1}, z_i). \quad (5)$$

Adding up (4) and (5), we have

$$(e - v_2 - v_3)\rho(z_i, z_{i+1}) \preceq (2v_1 + v_2 + v_3)\rho(z_{i-1}, z_i), \text{ i.e.}$$
$$(e - v)\rho(z_i, z_{i+1}) \preceq (2v_1 + v)\rho(z_{i-1}, z_i), \quad (6)$$

where $v = v_2 + v_3$.

Note that, $2\delta(v) \leq (s+1)\delta(v) \leq 2\delta(v_1) + (s+1)\delta(v) < 2$, i.e. $\delta(v) < 1 < 2$. From Lemma 2.9 we conclude that $2e - v$ is invertible. Moreover, $(2e - v)^{-1} = \sum_{k=0}^{\infty} \dfrac{v^k}{2^{k+1}}$ and $\delta\left[(2e - v)^{-1}\right] \leq \dfrac{1}{2 - \delta(v)}$.

Hence, from (6), we have get

$$\rho(z_i, z_{i+1}) \preceq (2e - v)^{-1}(2v_1 + v)\rho(z_{i-1}, z_i) = \tau\rho(z_{i-1}, z_i), \quad (7)$$

where $\tau = (2e - v)^{-1}(2v_1 + v)$.

Since v_1 commutes with $v = v_2 + v_3$, it follows that

$$(2e - v)^{-1}(2v_1 + v) = \left(\sum_{k=0}^{\infty} \frac{v^k}{2^{k+1}}\right)(2v_1 + v)$$
$$= 2v_1\left(\sum_{k=0}^{\infty} \frac{v^k}{2^{k+1}}\right) + v\left(\sum_{k=0}^{\infty} \frac{v^k}{2^{k+1}}\right)$$
$$= (2v_1 + v)\left(\sum_{k=0}^{\infty} \frac{v^k}{2^{k+1}}\right) = (2v_1 + v)(2e - v)^{-1}.$$

Thus, $(2e - v)^{-1}$ commutes with $(2v_1 + v)$. Then by Lemma 2.9 and Lemma 2.11, we have that

$$\delta(\tau) = \delta\left[(2e - v)^{-1}(2v_1 + v)\right] \leq \delta\left[(2e - v)^{-1}\right]\delta(2v_1 + v)$$
$$\leq \frac{1}{2 - \delta(v)}\left[2\delta(v_1) + \delta(v)\right] < \frac{1}{s}.$$

Since $\delta(\tau) < \dfrac{1}{s}$, by Lemma 2.9 and Lemma 2.11, it follows that $e - s\tau$ is invertible. Moreover,

$$(e - s\tau)^{-1} = \sum_{k=0}^{\infty}(s\tau)^k \text{ and } \delta\left[(e - s\tau)^{-1}\right] \leq \frac{1}{2 - s\delta(\tau)} .$$

Since $\delta(\tau) < \dfrac{1}{s} < 1$, by Remark 2.10, we have that

$$\left\| \tau^i \right\| \to 0 \quad (i \to \infty). \tag{9}$$

From (7), we get

$$\begin{aligned}
\rho(z_i, z_{i+1}) &\preceq \tau \rho(z_{i-1}, z_i) \\
&\preceq \tau^2 \rho(z_{i-2}, z_{i-1}) \\
&\vdots \\
\rho(z_i, z_{i+1}) &\preceq \tau^i \rho(z_0, z_1)
\end{aligned} \tag{10}$$

for all $i \in \mathbb{N}$. Hence, for $i, j \in \mathbb{N}$ with $i < j$, using (8) and (10), we obtain

$$\begin{aligned}
\rho(z_i, z_j) &\preceq s\left[\rho(z_i, z_{i+1}) + \rho(z_{i+1}, z_j)\right] \\
&\preceq s\rho(z_i, z_{i+1}) + s^2\left[\rho(z_{i+1}, z_{i+2}) + \rho(z_{i+1}, z_j)\right] \\
&\vdots \\
&\preceq s\rho(z_i, z_{i+1}) + s^2\rho(z_{i+1}, z_{i+2}) + s^3\rho(z_{i+1}, z_{i+2}) \\
&\quad + \ldots + s^{j-i-1}\rho(z_{j-2}, z_{j-1}) + s^{j-i-1}\rho(z_{j-1}, z_j) \\
&\preceq s\tau^i \rho(z_0, z_1) + s^2\tau^{i+1}\rho(z_0, z_1) + s^3\tau^{i+2}\rho(z_0, z_1) \\
&\quad + \ldots + s^{j-i-1}\tau^{j-2}\rho(z_0, z_1) + s^{j-i-1}\tau^{j-1}\rho(z_0, z_1) \\
&\preceq s\tau^i\left(e + s\tau + (s\tau)^2 + \ldots + (s\tau)^{j-i-2} + (s\tau)^{j-i-1}\right)\rho(z_0, z_1) \\
&\preceq s\tau^i\left(\sum_{k=0}^{\infty}(s\tau)^k\right)\rho(z_0, z_1) = s\tau^i(e - s\tau)^{-1}\rho(z_0, z_1).
\end{aligned}$$

Obviously, from (9) it follows that

$$\left\| s\tau^i(e - s\tau)^{-1}\rho(z_0, z_1) \right\| \to 0 \quad (i \to \infty)$$

and by Lemma 2.6 there exists $N \in \mathbb{N}$ such that for any $c \in \mathcal{B}$, with $c \gg \theta$ is

$$\rho(z_i, z_j) \preceq s\tau^i(e - s\tau)^{-1}\rho(z_0, z_1) \ll c,$$

for all $j > i > N$.

This implies that $\{z_i\}$ is Cauchy sequence. Since $(\mathcal{Z}, \rho)$ is complete, there exists $z_* \in \mathcal{Z}$ such that $z_i \to z_*$ $(i \to \infty)$.

Supposse that $\mathcal{F}$ is continuous. It follows that $z_{i+1} = \mathcal{F}z_i \to \mathcal{F}z_*$ $(i \to \infty)$. By uniqueness of the limit of sequence in $(\mathcal{Z}, \rho)$, we have that $\mathcal{F}z_* = z_*$. Thus z_* in $\mathcal{Z}$ is a fixed point of $\mathcal{F}$.

On the other hand, if $(\mathcal{Z}, \rho)$ is α-regular, by using (3), we have

$$\alpha(z_i, z_*) \succeq s, \text{ for all } i \in \mathbb{N}. \tag{11}$$

Now we show that z_* is a fixed point of $\mathcal{F}$, i.e. $\mathcal{F}z_* = z_*$. From (1) and (11), we obtain

$$\begin{aligned}
\rho(z_*, \mathcal{F}z_*) &\preceq s\left[\rho(z_*, \mathcal{F}z_i) + \rho(\mathcal{F}z_i, \mathcal{F}z_*)\right] \\
&\preceq s\rho(z_*, \mathcal{F}z_i) + s\left[v_1\rho(z_i, z_*) + v_2\rho(z_i, \mathcal{F}z_i) + v_3\rho(z_*, \mathcal{F}z_*)\right] \\
&\preceq s\rho(z_*, z_{i+1}) + sv_1\rho(z_i, z_*) \\
&\quad + s^2v_2\left[\rho(z_i, z_*) + \rho(z_*, z_{i+1})\right] + sv_3\rho(z_*, \mathcal{F}z_*) \\
&= s(e + sv_2)\rho(z_{i+1}, z_*) + s(v_1 + sv_2)\rho(z_i, z_*) + sv_3\rho(z_*, \mathcal{F}z_*), \text{ i.e.}
\end{aligned}$$
$$(e + sv_3)\rho(z_*, \mathcal{F}z_*) \preceq .$$
$$\preceq s(e + sv_2)\rho(z_{i+1}, z_*) + s(v_1 + sv_2)\rho(z_i, z_*). \tag{12}$$

Similarly,

$$\begin{aligned}
\rho(\mathcal{F}z_*, z_*) &\preceq s\left[\rho(\mathcal{F}z_*, \mathcal{F}z_i) + \rho(\mathcal{F}z_i, z_*)\right] \\
&\preceq s\left[v_1\rho(z_*, z_i) + v_2\rho(z_*, \mathcal{F}z_*) + v_3\rho(z_i, \mathcal{F}z_i)\right] + \rho(\mathcal{F}z_i, \mathcal{F}z_*) \\
&\preceq sv_1\rho(z_*, z_i) + sv_2\rho(z_*, \mathcal{F}z_*) + \\
&\quad + s^2v_3\left[\rho(z_i, z_*) + \rho(z_*, z_{i+1})\right] + s\rho(z_{i+1}, z_*) \\
&= sv_2\rho(z_*, \mathcal{F}z_*) + s(e + sv_3)\rho(z_{i+1}, z_*) + s(v_1 + sv_3)\rho(z_i, z_*), \text{ i.e.}
\end{aligned}$$
$$(e - sv_2)\rho(z_*, \mathcal{F}z_*) \preceq$$
$$\preceq s(e + sv_3)\rho(z_{i+1}, z_*) + s(v_1 + sv_3)\rho(z_i, z_*). \tag{13}$$

Hence, by combining (12) and (13), we obtain

$$\begin{aligned}
(2e - sv_2 - sv_3)\rho(z_*, \mathcal{F}z_*) &\preceq s(2e + sv_2 + sv_3)\rho(z_{i+1}, z_*) + \\
&\quad + s(2v_1 + sv_2 + sv_3)\rho(z_i, z_*), \text{ i.e.}
\end{aligned}$$
$$(2e - sv)\rho(z_*, \mathcal{F}z_*) \preceq$$
$$\preceq s(2e + sv)\rho(z_{i+1}, z_*) + s(2v_1 + sv)\rho(z_i, z_*). \tag{14}$$

Note, that

$$\delta(sv) = s\delta(v) \le (s+1)\delta(v) \le 2s\delta(v_1) + (s+1)\delta(v) < 2.$$

Since by Lemma 2.9, $2e - sv$ is invertible, it follows from (14) that

$$\begin{aligned}
\rho(z_*, \mathcal{F}z_*) &\preceq \\
&\preceq (2e - sv)^{-1}\left[(2se + s^2v)\rho(z_{i+1}, z_*) + (2sv_1 + s^2v)\rho(z_i, z_*)\right].
\end{aligned}$$

Therefore, by Lemma 2.7 and Lemma 2.8, $\{\rho(z_i, z_*)\}$, $\{\rho(z_{i+1}, z_*)\}$ and $\{\tau_1\rho(z_{i+1}, z_*) + \tau_2\rho(z_i, z_*)\}$ are c-sequences (we mark τ_1 and τ_2 respectively by $(2e - sv)^{-1}(2se + s^2v)$, $(2e - sv)^{-1}(2sv_1 + s^2v)$).

Hence, for any $c \in \mathcal{B}$ with $c \gg \theta$, there exists $N \in \mathbb{N}$ such that

$$\rho(z_*, \mathcal{F}z_*) \preceq \tau_1\rho(z_{i+1}, z_*) + \tau_2\rho(z_i, z_*) \ll c.$$

This implies, based on Lemma 2.12, that $\rho(z_*, \mathcal{F}z_*) = \theta$. Therefore, $\mathcal{F}z_* = z_*$. This completes the proof. □

Next example illustrates the above result.

Example 3.4. Consider the algebra $\mathcal{B} = C^1_{\mathbb{R}}[0,1]$ with the norm

$$\|z\| = \|z\|_\infty + \|z'\|_\infty .$$

Define on $\mathcal{B}$ a multiplication in the usual way. Then, $\mathcal{B}$ is a Banach algebra with unite $e = 1$. If

$$\mathcal{K} = \{z \in \mathcal{B} : z(x) \geq 0, x \in [0,1]\},$$

then $\mathcal{K}$ is a solid cone which is not normal.

Suppose that $\mathcal{Z} = [0,1)$ and define a mapping $\rho : \mathcal{Z} \times \mathcal{Z} \to \mathcal{B}$ by

$$\rho(z,y)(x) = |z-y|^2 e^x , \text{ for all } z, y \in \mathcal{Z} .$$

Then $(\mathcal{Z}, \rho)$ is a complete cone b-metric space over Banach algebra $\mathcal{B}$. Let $\mathcal{F} : \mathcal{Z} \to \mathcal{Z}$ and $\alpha : \mathcal{Z} \times \mathcal{Z} \to \mathcal{B}$ be defined as follows:

$$\mathcal{F}z = \begin{cases} \dfrac{\sqrt{5}}{3}z, & \text{if } z \in [0,1]; \\ z+1, & \text{if } z > 1, \end{cases} \text{ and } \alpha(z,y) = \begin{cases} s, & \text{if } z,y \in [0,1]; \\ \theta, & \text{elsewhere.} \end{cases}$$

Then, the mapping $\mathcal{F}$ is α-admissible. In fact, let $z,y \in \mathcal{Z}$ such that $\alpha(z,y) \succeq s$. By definition of the mapping α, it implies that $z,y \in [0,1]$. Therefore,

$$\alpha(\mathcal{F}z, \mathcal{F}y) = \alpha\left(\frac{\sqrt{5}}{3}z, \frac{\sqrt{5}}{3}y\right) = s .$$

Also, there exists z_0 in $\mathcal{Z}$ such that $\alpha(z_0, \mathcal{F}z_0) \succeq s$. Indeed, for $z_0 = 1$, we have

$$\alpha(z_0, \mathcal{F}z_0) = \alpha(1, \mathcal{F}1) = \alpha\left(1, \frac{\sqrt{5}}{3}\right) = e .$$

Since $[0,1]$ is complete, then $(\mathcal{Z}, \rho)$ is α-regular. Indeed, let $\{z_i\}$ be a sequence in $\mathcal{Z}$ such that $\alpha(z_i, z_{i+1}) \succeq s$ for all $i \in \mathbb{N}$ and let $z_i \to z \in \mathcal{Z} (i \to \infty)$. Then $\{z_i\} \subset [0,1]$ and $z_i + z \to 2z$ $(i \to \infty)$. Therefore, $z_i \to z$ $(i \to \infty)$ in $(\mathcal{Z}, \rho)$. This implies that $z \in [0,1]$ and that $\alpha(z_i, z) = s$, for all $i \in \mathbb{N}$. Furthemore, by choosing $v_1 = \dfrac{1}{9} + \dfrac{1}{9}x$, $v_2 = \dfrac{1}{18} + \dfrac{1}{18}x$ and $v_3 = \dfrac{1}{24} + \dfrac{1}{24}x$ in $\mathcal{K}$, simple calculations show that all the conditions of Theorem 3.3 are satisfied so there exists a fixed point $z = \theta$ of the mapping $\mathcal{F}$. □

Now we state a theorem in which we shall establish the uniqueness of fixed point of a generalized Reich type contraction as follows:

Theorem 3.5. *Let $(\mathcal{Z}, \rho)$ be a complete cone b-metric spaces over Banach algebra $\mathcal{B}$ with coefficient $s \geq 1$, $\mathcal{K}$ be the underlying solid cone and $\alpha : \mathcal{Z} \times \mathcal{Z} \to \mathcal{B}$ be a function. Suppose the mapping $\mathcal{F} : \mathcal{Z} \to \mathcal{Z}$ is a generalized Reich type contraction with vectors $v_k \in \mathcal{K}(k=1,2,3)$ such that v_1 commutes with $v_2 + v_3$. Suppose that:*

1) *$\mathcal{F}$ is α-admissible mapping;*
2) *there exists z_0 in $\mathcal{Z}$ such that $\alpha(z_0, \mathcal{F}z_0) \succeq s$;*
3) *either $\mathcal{F}$ is continuous or $(\mathcal{Z}, \rho)$ is α-regular;*
4) *for any $z,y \in Fix(\mathcal{F})$, there exists $x \in \mathcal{Z}$ such that $\alpha(z,x) \succeq s$ and $\alpha(y,x) \succeq s$, where $Fix(\mathcal{F})$ denotes the set of all fixed points of $\mathcal{F}$,*

then $\mathcal{F}$ has a unique fixed point z_* in $\mathcal{Z}$.

PROOF. Following the same arguments to those in the proof of Theorem 3.3, we obtain the existence of fixed point.

To show that fixed point is unique, we take $z_*, y_* \in Fix(\mathcal{F})$ such that $z_* \neq y_*$. Hence, by hypothesis 4), there exists $x \in \mathcal{Z}$ such that

$$\alpha(z_*, x) \succeq s \text{ and } \alpha(y_*, x) \succeq s . \tag{15}$$

Since $\mathcal{F}$ is α-admissible mapping and $z_*, y_* \in Fix(\mathcal{F})$, from (15) we obtain

$$\alpha(z_*, \mathcal{F}^i x) \succeq s \text{ and } \alpha(y_*, \mathcal{F}^i x) \succeq s, \text{ for all } i \in \mathbb{N} . \tag{16}$$

Now, from (1) and (16), we get

$$\rho(z_*, \mathcal{F}^i x) = \rho(\mathcal{F}z_*, \mathcal{F}(\mathcal{F}^i x))$$
$$\preceq v_1 \rho(z_*, \mathcal{F}^{i-1}x) + v_2 \rho(z_*, \mathcal{F}z_*) + v_3 \rho(\mathcal{F}^{i-1}x, \mathcal{F}(\mathcal{F}^{i-1}x))$$
$$\preceq v_1 \rho(z_*, \mathcal{F}^{i-1}x) + sv_3 \left[\rho(\mathcal{F}^{i-1}x, z_*) + \rho(z_*, \mathcal{F}^i x)\right], \text{ i.e.}$$
$$(e - sv_3)\rho(z_*, \mathcal{F}^i x) \preceq (v_1 + sv_3)\rho(z_*, \mathcal{F}^{i-1}x) . \tag{17}$$

Similarly,

$$\rho(\mathcal{F}^i x, z_*) = \rho(\mathcal{F}(\mathcal{F}^i x), \mathcal{F}z_*)$$
$$\preceq v_1 \rho(\mathcal{F}^{i-1}x, z_*) + v_3 \rho(z_*, \mathcal{F}z_*) + v_2 \rho(\mathcal{F}^{i-1}x, \mathcal{F}(\mathcal{F}^{i-1}x))$$
$$\preceq v_1 \rho(\mathcal{F}^{i-1}x, z_*) + sv_2 \left[\rho(\mathcal{F}^{i-1}x, z_*) + \rho(z_*, \mathcal{F}^i x)\right], \text{ i.e.}$$
$$(e - sv_2)\rho(\mathcal{F}^i x, z_*) \preceq (v_1 + sv_2)\rho(\mathcal{F}^{i-1}x, z_*) . \tag{18}$$

Adding up (17) and (18), we have

$$(2e - sv_2 - sv_3)\rho(z_*, \mathcal{F}^i z_*) \preceq (2v_1 + sv_2 + sv_3)\rho(z_*, \mathcal{F}^{i-1}x)$$
$$(2e - sv)\rho(z_*, \mathcal{F}^i x) \preceq (2v_1 + sv)\rho(z_*, \mathcal{F}^{i-1}x)$$
$$\rho(z_*, \mathcal{F}^i x) \preceq (2e - sv)^{-1}(2v_1 + sv)\rho(z_*, \mathcal{F}^{i-1}x), \text{ i.e.}$$

$$\rho\left(z_*, \mathcal{F}^i x\right) \preceq \tau \rho\left(z_*, \mathcal{F}^{i-1} x\right), \qquad (19)$$

where $\tau = \left(2e - sv\right)^{-1}\left(2v_1 + sv\right)$. Hence,

$$\rho\left(z_*, \mathcal{F}^i x\right) \preceq \tau \rho\left(z_*, \mathcal{F}^{i-1} x\right)$$
$$\preceq \tau^2 \rho\left(z_*, \mathcal{F}^{i-2} x\right)$$
$$\vdots$$
$$\rho\left(z_*, \mathcal{F}^i x\right) \preceq \tau^i \rho\left(z_*, x\right), \text{ for all } i \in \mathbb{N}.$$

Since $\delta(\tau) < 1$, by Remark 2.10, it follows that $\left\|\tau^i\right\| \to 0 \left(i \to \infty\right)$ and so

$$\left\|\tau^i \rho\left(z_*, x\right)\right\| \le \left\|\tau^i\right\| \left\|\rho\left(z_*, x\right)\right\| \to 0 \ \left(i \to \infty\right).$$

Therefore, based on Lemma 2.6, we conclude that for any $c \in \mathcal{B}$ with $c \gg \theta$, there exists $N \in \mathbb{N}$ such that

$$\rho\left(z_*, \mathcal{F}^i x\right) \preceq \tau^i \rho\left(z_*, x\right) \ll c \text{ for all } i \in \mathbb{N}.$$

Hence, $\mathcal{F}^i x \to z_* \left(i \to \infty\right)$. Similarly, we get that $\mathcal{F}^i x \to y_*$ $\left(i \to \infty\right)$.

Then, by uniquieness of the limit, we have $z_* = y_*$. The theorem is thus proved. □

The next theorem is an ordered version of generalized Riech type contraction on cone b-metric space with Banach algebra.

Theorem 3.6. *Let $\left(\mathcal{Z}, \sqsubseteq\right)$ be a partially ordered set, let $\left(\mathcal{Z}, \rho\right)$ be a complete cone b-metric spaces over Banach algebra $\mathcal{B}$ with coefficient $s \ge 1$ and $\mathcal{K}$ be the underlying solid cone. Let $\mathcal{F} : \mathcal{Z} \to \mathcal{Z}$ be continuous non-decreasing mapping with respect to $\sqsubseteq$. Assume that the following conditions are valid:*

1) *there exists vectors $v_k \in \mathcal{K}$ $\left(k = 1, 2, 3\right)$ such*
$$2s\delta(v_1) + (s+1)\delta(v_2 + v_3) < 2 \text{ and}$$
$$\rho\left(\mathcal{F}z, \mathcal{F}y\right) \preceq v_1 \rho\left(z, y\right) + v_2 \rho\left(z, \mathcal{F}z\right) + v_2 \rho\left(y, \mathcal{F}y\right),$$
for all $z, y \in \mathcal{Z}$ with $z \sqsubseteq y$;

2) *there exists $z_0 \in \mathcal{Z}$ such that $z_0 \sqsubseteq \mathcal{F}z_0$,*

then $\mathcal{F}$ has a unique fixed point z_* in $\mathcal{Z}$.

PROOF. Let $\alpha_j : \mathcal{Z} \times \mathcal{Z} \to \mathcal{B}$ be function defined by

$$\alpha_j\left(z, y\right) = \begin{cases} s, & \text{if } z \sqsubseteq y ; \\ \theta, & \text{elsewhere.} \end{cases}$$

Note that condition 1) implies that the mapping $\mathcal{F}$ is a generalized Reich contraction. Since $\mathcal{F}$ is non-decreasing mapping it follows that it is also α_j-admissible mapping. The condition 2) implies that there exists $z_0 \in \mathcal{Z}$ such that $\alpha_j\left(z_0, \mathcal{F}z_0\right) = s$. Therefore, since $\mathcal{F}$ is continuous, all the conditions of Theorem 3.3 are satisfied, we conclude that the mapping $\mathcal{F}$ has a fixed point in $\mathcal{Z}$. This completes the proof. □

Now we deduce many existing results in the mention literature for metric, cone metric and cone b-matric spaces, as follows:

Let $\alpha : \mathcal{Z} \times \mathcal{Z} \to \mathcal{B}$ be the function defined by $\alpha(x, y) \ge 1$, for all $z, y \in \mathcal{Z}$. Then

- Theorems 3.1, 3.2 and 3.4 in Hussain at al. (2017) are special cases of our Theorems 3.3 and 3.5, respectively, with $v_2 = v_3 = \theta$.
- Theorems 3.1, 3.2 and 3.5 in Malhotra et al. (2015) are special cases of our Theorems 3.3 and 3.5, respectively, with $v_1 = 1$, $v_2 = v_3 = \theta$.
- Theorems 3.1, 3.2 and 3.3 in Malhotra et al. (2017) are special cases of our Theorems 3.3 and 3.5, respectively, with $s = 1$, $v_1 = \theta$, $v_2 = v_3$.

Let $\alpha : \mathcal{Z} \times \mathcal{Z} \to \mathcal{B}$ be function defined by $\alpha(x, y) = 1$ for all $z, y \in \mathcal{Z}$. Then,

- Theorems 3.1 and 3.2 in Xu and Radenović (2015) are special case of our Theorem 3.5, with $s = 1$, $v_2 = v_3 = \theta$ and $v_1 = \theta$, $v_2 = v_3$, respectively.
- Theorems 2.1 and 2.2 in Liu and Xu (2013) are special cases of our Theorem 3.5 with normal cone $\mathcal{K}$, with $s = 1$, $v_2 = v_3 = \theta$ and $v_1 = \theta$, $v_2 = v_3$, respectively.
- Theorems 1 and 2 in Riech (1971) are special case of our Theorem 3.5 with a metric space $\left(\mathcal{Z}, \rho\right)$ where $\delta(v_1) = v_1$ for all $v_1 \in \mathbb{R}^+$.

Let the function $\alpha_j : \mathcal{Z} \times \mathcal{Z} \to \mathcal{B}$ be define by $\alpha_j(z, y) = 1$ for all $z, y \in \mathcal{Z}$.

- Theorems 2.1 and 2.2 in Nieto and Rodríguez-López (2005) are special cases of our Theorems 3.6 with a metric space $\left(\mathcal{Z}, \rho\right)$, where $\delta(v_1) = v_1$ for $v_1 \in \mathbb{R}^+$, $s = 1$ and $v_2 = v_3 = \theta$.

CONCLUSION

In this paper we introduced the notion of generalized Riech type α-admissible mappings on cone metric space over Banach algebra and we prove three fixed point theorems for those contractions. We notice that our results are actual generalization of the recent results of Liu and Xu (2013), Xu and Radenović (2015), Malhotra et al. (2015), Hussain et al. (2017), Riech (1971), Nieto and Rodríguez-López (2005) and many known results in the literature.

REFERENCES

Du, W. 2010. A note on cone metric fixed point theory and its equivalence. Nonlinear Analysis: Theory, Methods and Applications, 72(5), pp. 2259-2261. doi:10.1016/j.na.2009.10.026

Huang, L., & Zhang, X. 2007. Cone metric spaces and fixed point theorems of contractive mappings. Journal of Mathematical Analysis and Applications, 332(2), pp. 1468-1476. doi:10.1016/j.jmaa.2005.03.087

Huang, H., & Radenović, S. 2016. Some fixed point results of generalized Lipschitz mappings on cone b-metric spaces over Banach algebras. J. Computational Analysis and Applications, 20(3), pp. 566-583.

Huang, H., & Radenović, S. 2015. Common fixed point theorems of generalized Lipschitz mappings in cone b-metric spaces over Banach algebras and applications. Journal of Nonlinear Sciences and Applications, 8(5), pp. 787-799. doi:10.22436/jnsa.008.05.29

Huang, H., & Radenović, S. 2015. Common fixed point theorems of generalized Lipschitz mappings in cone metric spaces over Banach algebras. Appl. Math. Inf. Sci., 9(6). pmid:2990

Huang, H., & Xu, S. 2013. Fixed point theorems of contractive mappings in cone b-metric spaces and applications. Fixed Point Theory and Applications, 2013(1), p. 112. doi:10.1186/1687-1812-2013-112

Huang, H., Radenovic, S., & Deng, G. 2017. A sharp generalization on cone b-metric space over Banach algebra. The Journal of Nonlinear Sciences and Applications, 10(02), pp. 429-435. doi:10.22436/jnsa.010.02.09

Hussain, N., Al-solami, A. M., & Kutbi, M. A. 2017. Fixed points of α-admissible mappings in cone b-metric spaces with Banach algebra. Journal of Mathematical Analysis, 8(2), pp. 89-97.

Kadelburg, Z., Radenović, S., & Rakočević, V. 2011. A note on the equivalence of some metric and cone metric fixed point results. Applied Mathematics Letters, 24(3), pp. 370-374. doi:10.1016/j.aml.2010.10.030

Kadelburg, Z., & Radenović, S. 2013. A note on various types of cones and fixed point results in cone metric spaces. Asian Journal of Mathematics and Applications, Article ID amma0104, 7 pages.

Liu, H., & Xu, S. 2013. Cone metric spaces with Banach algebras and fixed point theorems of generalized Lipschitz mappings. Fixed Point Theory and Applications, 2013(1), p. 320. doi:10.1186/1687-1812-2013-320

Malhotra, S. K., Sharma, J. B., & Shukla, S. 2015. Fixed points of α-admissible mappings in cone metric spaces with Banach algebra. International Journal of Analysis and Applications, 9(1), pp. 9-18.

Malhotra, S. K., Sharma, J. B., & Shukla, S. 2017. Fixed points of generalized Kannan type α-admissible mappings in cone metric spaces with Banach algebra. Theory and Applications of Mathematics and Computer Science, 7(1), pp. 1-13.

Nieto, J. J., & Rodríguez-López, R. 2005. Contractive Mapping Theorems in Partially Ordered Sets and Applications to Ordinary Differential Equations. Order, 22(3), pp. 223-239. doi:10.1007/s11083-005-9018-5

Reich, S. 1971. Some remarks concerning contraction mappings. Canadian Mathematical Bulletin, 14, pp. 121-124. doi:10.4153/cmb-1971-024-9

Rudin, W. 1991. Functional Analysis.New York: McGraw-Hill. 2nd edition.

Samet, B., Vetro, C., & Vetro, P. 2012. Fixed point theorems for -contractive type mappings. Nonlinear Analysis: Theory, Methods and Applications, 75(4), pp. 2154-2165. doi:10.1016/j.na.2011.10.014

Xu, S., & Radenović, S. 2015. Fixed point theorems of generalized Lipschitz mappings on cone metric spaces over Banach algebras without assumption of normality. Fixed Point Theory and Applications, 2014(1), p. 102. doi:10.1186/1687-1812-2014-102

ANALYSIS OF SHANNON CAPACITY FOR SC AND MRC DIVERSITY SYSTEMS IN $\alpha - \kappa - \mu$ FADING CHANNEL

MILAN SAVIĆ[1,*]**, MARKO SMILIĆ**[1]**, BRANIMIR JAKŠIĆ**[2]

[1]Faculty of Natural Sciences and Mathematics, University of Priština, Kosovska Mitrovica, Serbia
[2]Faculty of Technical Sciences, University of Priština, Kosovska Mitrovica, Serbia

ABSTRACT

In this paper, the analysis of Shannon capacity for selection combining (SC) and maximal ratio combining (MRC) diversity systems in the generalized $\alpha - \kappa - \mu$ fading channel is presented. Closed-form expressions for probability density function (PDF) at the output of SC and MRC diversity systems are given. Also, closed-form expressions for Shannon capacity for cases of SC diversity with independent and identically distributed branches, MRC diversity with independent and identically distributed branches and for case of no diversity are derived. The obtained results are numerically calculated and graphically presented for different combinations of fading parameters α, κ and μ.

Keywords: $\alpha - \kappa - \mu$ distribution, Selection Combiner (SC), Maximal Ratio Combiner (MRC), Shannon capacity, Diversity system.

INTRODUCTION

During transmission, the signal transmitted between the transmitter and the receiver is exposed to various effects. These effects such as shadowing and multipath, adversely affect the signal being transmitted and diminish the performance of the system (Simon & Alouini, 2005a). There are several ways to reduce the impact of the presented effects on system performance. One of the most commonly used ways to reduce the impact of multipath fading is to use the diversity concept such as space diversity (Freeman, 2005). This diversity concept effectively reduce the impact of multipath fading and increase the performance of the system by using multiple transmit or receiver antennas (Stüber, 2002). These antennas are spaced sufficiently far apart so as to obtain signals that fade independently (Ibnkahla, 2005). Diversity combining techniques that are often used are selection combining technique (SC), equal gain combining technique (EGC), maximal ratio combining technique (MRC).

Performance analysis over different channel fading model are considered in many paper. Probability density function (PDF) and cumulative distribution function (CDF) over Rayleigh fading channel for EGC diversity system are given in (Talha et al., 2010). Bit error rate under $\alpha - \mu$, $\kappa - \mu$ and $\eta - \mu$ fading channel for SC diversity system is presented in (Mitrović et al., 2009; Subadar et al., 2010). Also, bit error rate under $\kappa - \mu$ and $\eta - \mu$ fading channel for MRC diversity system is presented in (Dixit & Sahu, 2012). System performances such as probability output (P_{out}) and symbol error rate (SER) over Weibull and $\alpha - \mu$ fading channel for SC diversity are shown in (Katiyar, 2015; Sagias et al., 2003). Same system performances in $\alpha - \mu$, $\kappa - \mu$ and $\eta - \mu$ fading channel for MRC diversity are given in (Aldalgamouni et al., 2013; Subadar et al., 2012; Milišić et al., 2009). Shannon capacity over

κ and Gamma fading channel for MRC and SC diversity systems is analyzed in (Yilmaz, 2012; Subadar & Das, 2017). Diversity techniques are not the only method to reduce the impact of fading and improve the characteristics of the system. A widely used technique is the technique of adaptive transmission. By combining adaptive transmission techniques and diversity techniques, better performance of the system is achieved. Analysis of the capacities of such systems by using adaptive transmission algorithms and diversity techniques over $\alpha - \mu$, $\kappa - \mu$, Nakagami-m, Weibull and Rayleigh fading channels are investigated in (Mohamed et al., 2013; Subadar & Sahu, 2010; Panić et al., 2013; Subadar et al., 2010; Bessate & El, 2017; Simon & Alouini, 2005b).

In this paper, we investigate Shannon capacity over generalized $\alpha - \kappa - \mu$ fading channel. We consider cases for the proposed fading model when the system does not have a diversity, but also when the system has SC diversity and MRC diversity. Closed-form expressions of PDF and Shannon capacity for these systems will be presented.

SYSTEM AND CHANNEL MODEL

No diversity

In this case, the system we are discussing consists of a transmitter and receiver without a diversity combiner. Also, transmission through the slowly changing $\alpha - \kappa - \mu$ fading channel is considered. For this system, probability density function for received signal-to-noise ratio is given in (Huang & Yuan, 2018) as:

---

* Corresponding author: milan.savic1@pr.ac.rs

$$
\begin{aligned}
f_g(g) \;=\;& \frac{\alpha\mu\,(1+\kappa)^{\frac{1+\mu}{2}}\,g^{\frac{\alpha(\mu+1)}{4}-1}}{2\kappa^{\frac{\mu-1}{2}}e^{\kappa\mu}\tilde{g}^{\frac{\alpha(\mu+1)}{4}}} \\
\times\;& e^{-\mu(1+\kappa)\frac{g^{\frac{\alpha}{2}}}{\tilde{g}^{\frac{\alpha}{2}}}}\,I_{\mu-1}\!\left(2\mu\sqrt{\kappa\,(1+\kappa)\,\frac{g^{\frac{\alpha}{2}}}{\tilde{g}^{\frac{\alpha}{2}}}}\right)
\end{aligned}
\tag{1}
$$

where parameter α represents nonlinearity of propagation environment, parameter κ is Rice factor, parameter μ represents number of clusters in propagation environment, $\tilde{g}$ represents average SNR and $I_v\,(\cdot)$ denotes modified Bessel function (Huang & Yuan, 2018).

By transforming Bessel function using equation (8.445) from (Gradshteyn & Ryzhik, 2000) and replacing in equation (1) we obtain:

$$
\begin{aligned}
f_g(g) \;=\;& \frac{\alpha\mu\,(1+\kappa)^{\frac{1+\mu}{2}}}{2\kappa^{\frac{\mu-1}{2}}e^{\kappa\mu}}e^{-\mu(1+\kappa)\frac{g^{\frac{\alpha}{2}}}{\tilde{g}^{\frac{\alpha}{2}}}} \\
\times\;& \sum_{j=0}^{\infty}\frac{\left(\mu\sqrt{\kappa\,(1+\kappa)}\right)^{\mu+2j-1}g^{\frac{\alpha(\mu+j)}{2}-1}}{j!\,\Gamma\,(\mu+j)\,\tilde{g}^{\frac{\alpha(\mu+j)}{2}}}
\end{aligned}
\tag{2}
$$

SC diversity with L branches

In this case, we consider a SC diversity receiver with L branches, operating over $\alpha-\kappa-\mu$ fading channel. All branches are identically and independently distributed. Selective combining (SC) is combining technique where the strongest signal is chosen among L branches of diversity system. PDF of the SNR at the output of the SC receiver with L branches can be calculated by using expression (4) from (Mitrović et al., 2009):

$$
f_g^{SC}\,(g) = Lf_g(g)\left(F_g\,(g)\right)^{L-1}
\tag{3}
$$

where $F_g\,(g)$ represents a cumulative distribution function and $f_g\,(g)$ represent a probability density function for $\alpha-\kappa-\mu$ fading given in equation (2). Cumulative distribution function can be calculated as:

$$
F_g\,(g) = \int_0^g f_g\,(g)\,\mathrm{d}g
\tag{4}
$$

Substituting equation (2) in equation (4) and applying equation (3.381/1) from (Gradshteyn & Ryzhik, 2000), cumulative distribution function becomes:

$$
\begin{aligned}
F_g(g) \;=\;& \frac{\mu\,(1+\kappa)^{\frac{1+\mu}{2}}}{\kappa^{\frac{\mu-1}{2}}e^{\kappa\mu}}\sum_{j=0}^{\infty}\frac{\left(\mu\sqrt{\kappa\,(1+\kappa)}\right)^{\mu+2j-1}}{j!\,\Gamma\,(\mu+j)} \\
\times\;& \left(\frac{1}{\mu\,(1+\kappa)}\right)^{\mu+j}\gamma\!\left(\mu+j,\frac{\mu\,(1+\kappa)}{\tilde{g}^{\frac{\alpha}{2}}}g^{\frac{\alpha}{2}}\right)
\end{aligned}
\tag{5}
$$

where $\gamma\,(n,x)$ represents lower incomplete Gamma function defined as (8.350/1) from (Gradshteyn & Ryzhik, 2000). Transforming lower incomplete Gamma function from equation (5) by using relation $\gamma\,(n,x)=\sum_{p=0}^{\infty}\frac{x^{n+p}\Gamma(n)e^{-x}}{\Gamma(n+p+1)}$ and replacing in equation (5),

after some mathematical manipulation, we obtain cumulative distribution function for $\alpha-\kappa-\mu$ fading model:

$$
\begin{aligned}
F_g(g) \;=\;& \frac{\mu\,(1+\kappa)^{\frac{1+\mu}{2}}}{\kappa^{\frac{\mu-1}{2}}e^{\kappa\mu}}\sum_{j=0}^{\infty}\frac{\left(\mu\sqrt{\kappa\,(1+\kappa)}\right)^{\mu+2j-1}}{j!\,\Gamma\,(\mu+j)\,(\mu\,(1+\kappa))^{\mu+j}} \\
\times\;& \sum_{p=0}^{\infty}\frac{\Gamma\,(\mu+j)}{\Gamma\,(\mu+j+p+1)}\left(\frac{\mu\,(1+\kappa)}{\tilde{g}^{\frac{\alpha}{2}}}g^{\frac{\alpha}{2}}\right)^{\mu+j+p}e^{-\frac{\mu(1+\kappa)}{\tilde{g}^{\frac{\alpha}{2}}}g^{\frac{\alpha}{2}}}
\end{aligned}
\tag{6}
$$

Substituting equations (2) and (6) in equation (3) we obtain expression for probability density function of the SNR at the output of the SC receiver with L branches:

$$
f_g^{SC}\,(g) = LK_{pdf}\,g^{\frac{\alpha(\mu+j)}{2}}e^{-\frac{\mu(1+\kappa)}{\tilde{g}^{\frac{\alpha}{2}}}g^{\frac{\alpha}{2}}}\left(K_{cdf}\,g^{\frac{\alpha(\mu+j+p)}{2}}e^{-\frac{\mu(1+\kappa)}{\tilde{g}^{\frac{\alpha}{2}}}g^{\frac{\alpha}{2}}}\right)^{L-1}
\tag{7}
$$

where

$$
K_{pdf} = \frac{\alpha\mu\,(1+\kappa)^{\frac{1+\mu}{2}}}{2\kappa^{\frac{\mu-1}{2}}e^{\kappa\mu}}\sum_{j=0}^{\infty}\frac{\left(\mu\sqrt{\kappa\,(1+\kappa)}\right)^{\mu+2j-1}}{j!\,\Gamma\,(\mu+j)\,\tilde{g}^{\frac{\alpha(\mu+j)}{2}}}
\tag{8}
$$

and

$$
K_{cdf} = \frac{\mu\,(1+\kappa)^{\frac{1+\mu}{2}}}{\kappa^{\frac{\mu-1}{2}}e^{\kappa\mu}}\sum_{j=0}^{\infty}\sum_{p=0}^{\infty}\frac{\left(\mu\sqrt{\kappa\,(1+\kappa)}\right)^{\mu+2j-1}(\mu\,(1+\kappa))^{p}}{j!\,\Gamma\,(\mu+j+p+1)\,\tilde{g}^{\frac{\alpha(\mu+j+p)}{2}}}
\tag{9}
$$

MRC diversity with L branches

In this case, we consider a MRC diversity receiver with L branches, operating over $\alpha-\kappa-\mu$ fading channel. All branches are identically and independently distributed. Maximal Ratio Combining (MRC) is combining technique where received signals from all diversity branches are co-phased, proportionally weighted, and combined to maximize the output SNR (Subadar et al., 2010). PDF of the SNR at the output of the MRC receiver with L branches can be calculated by using relation (12) from (Milišić et al., 2009) where is $\alpha_{MRC}=\alpha; \kappa_{MRC}=\kappa; \mu_{MRC}=L\mu; \tilde{g}_{MRC}=L\tilde{g}$. Applying this relation in equation (2), PDF of the SNR at the output of the MRC receiver with L branches becomes:

$$
\begin{aligned}
f_g^{MRC}\,(g) \;=\;& \frac{\alpha L\mu\,(1+\kappa)^{\frac{1+L\mu}{2}}}{2\kappa^{\frac{L\mu-1}{2}}e^{L\kappa\mu}}e^{-L\mu(1+\kappa)\frac{g^{\frac{\alpha}{2}}}{(L\tilde{g})^{\frac{\alpha}{2}}}} \\
\times\;& \sum_{j=0}^{\infty}\frac{\left(L\mu\sqrt{\kappa\,(1+\kappa)}\right)^{L\mu+2j-1}g^{\frac{\alpha(L\mu+j)}{2}-1}}{j!\,\Gamma\,(L\mu+j)\,(L\tilde{g})^{\frac{\alpha(L\mu+j)}{2}}}
\end{aligned}
\tag{10}
$$

SHANNON CAPACITY ANALYSIS

Channel capacity is one of the most important performance measures of the system. The Shannon capacity of a channel defines its theoretical upper bound for the maximum rate of data transmission at an arbitrarily small bit error probability, without any delay or complexity constraints (Ibnkahla, 2005). It can be expressed as:

$$
C = B\int_0^{\infty}\log_2\,(1+g)\,f_g\,(g)\,\mathrm{d}g
\tag{11}
$$

where C represents Shannon capacity given in $bits/s$, B denotes denotes transmission bandwidth given in Hz and $f_g(g)$ represent probability density function. Using relation $\log_2(1+g) = \ln(1+g)/\ln(2)$, expression (11) can be rewritten as:

$$\frac{C}{B} = \frac{1}{\ln(2)} \int_0^\infty \ln(1+g) f_g(g)\, dg \qquad (12)$$

Shannon capacity - no diversity

Shannon capacity for system without diversity over $\alpha-\kappa-\mu$ fading channel can be calculated by replacing equation (2) in equation (12). After replacing equation (2) in equation (12) and after some mathematical manipulation, we obtain:

$$\frac{C_{ND}}{B} = K_{ND} \int_0^\infty g^{\frac{\alpha(\mu+j)}{2}-1} e^{-\frac{\mu(1+\kappa)g^{\frac{\alpha}{2}}}{\tilde{g}^{\frac{\alpha}{2}}}} \ln(1+g)\, dg \qquad (13)$$

where

$$K_{ND} = \frac{\alpha\mu(1+\kappa)^{\frac{1+\mu}{2}}}{2\ln(2)\kappa^{\frac{\mu-1}{2}} e^{\kappa\mu}} \sum_{j=0}^\infty \frac{\left(\mu\sqrt{\kappa(1+\kappa)}\right)^{\mu+2j-1}}{j!\,\Gamma(\mu+j)\,\tilde{g}^{\frac{\alpha(\mu+j)}{2}}} \qquad (14)$$

By using equations (8.4.6/5) where is $\ln(1+x) = G_{2,2}^{1,2}\left(x\left|\begin{matrix}1,1\\1,0\end{matrix}\right.\right)$ and (8.4.3/1) where is $e^{-x} = G_{0,1}^{1,0}\left(x\left|\begin{matrix}-\\0\end{matrix}\right.\right)$ from (Prudnikov & Brychkov, 2003), equation (13) becomes:

$$\begin{aligned}\frac{C_{ND}}{B} &= K_{ND} \int_0^\infty g^{\frac{\alpha(\mu+j)}{2}-1} \\ &\times\ G_{2,2}^{1,2}\left(g\left|\begin{matrix}1,1\\1,0\end{matrix}\right.\right) G_{0,1}^{1,0}\left(\frac{\mu(1+\kappa)g^{\frac{\alpha}{2}}}{\tilde{g}^{\frac{\alpha}{2}}}\left|\begin{matrix}-\\0\end{matrix}\right.\right) dg \end{aligned} \qquad (15)$$

where $G_{p,q}^{m,n}\left(x\left|\begin{matrix}a_1...a_n,a_{n+1}...a_p\\b_1...b_m,b_{m+1}...b_q\end{matrix}\right.\right)$ represents MeijerG function. Integral from equation (15) can be solved by using equation (2.24.1/1) from (Prudnikov & Brychkov, 2003). Applying this equation, Shannon capacity for system without diversity is:

$$\frac{C_{ND}}{B} = K_{ND}\frac{\sqrt{2}}{\alpha(2\pi)^{\frac{2\alpha-1}{2}}} G_{2\alpha,2+2\alpha}^{2+2\alpha,\alpha}\left(\frac{(\mu(1+\kappa))^2}{4\tilde{g}^\alpha}\left|\begin{matrix}\Lambda_{ND}\\\Psi_{ND}\end{matrix}\right.\right) \qquad (16)$$

where

$$\Lambda_{ND} = \left(\Delta\alpha, -\left(\frac{\alpha(\mu+j)}{2}\right)\right), \left(\Delta\alpha, 1-\frac{\alpha(\mu+j)}{2}\right) \qquad (17)$$

and

$$\Psi_{ND} = (\Delta k, b_1), \left(\Delta\alpha, -\left(\frac{\alpha(\mu+j)}{2}\right)\right), \left(\Delta\alpha, -\left(\frac{\alpha(\mu+j)}{2}\right)\right) \qquad (18)$$

Equation (16) represent closed-form expression of Shannon capacity for system without diversity over $\alpha-\kappa-\mu$ fading channel. This expression is valid only for integer values of fading parameter α. Also, this expression is general, and Shannon capacity for system without diversity over other fading models such as $\alpha-\mu$, $\kappa-\mu$, Nakagami - m and Rayleigh models can be obatined from it.

Shannon capacity - SC diversity with L branches

Shannon capacity at the output of SC diversity receiver with L branches can be calculated by replacing equation (7) in equation (12). Substituting equation (7) in equation (12), applying relation for transforming logarithm and exponential functions over MeijerG function what is explained in previous section and using equation (2.24.1/1) from (Prudnikov & Brychkov, 2003) we obtain Shannon capacity:

$$\frac{C_{SC}}{B} = LK_{pdf}^{SC}\left(K_{cdf}^{SC}\right)^{L-1} G_{2\alpha,2+2\alpha}^{2+2\alpha,\alpha}\left(\frac{(L\mu(1+\kappa))^2}{4\tilde{g}^\alpha}\left|\begin{matrix}\Lambda_{SC}\\\Psi_{SC}\end{matrix}\right.\right) \qquad (19)$$

where

$$K_{pdf}^{SC} = \frac{\mu(1+\kappa)^{\frac{1+\mu}{2}}}{\sqrt{2}\ln(2)\kappa^{\frac{\mu-1}{2}} e^{\kappa\mu}(2\pi)^{\frac{2\alpha-1}{2}}} \sum_{j=0}^\infty \frac{\left(\mu\sqrt{\kappa(1+\kappa)}\right)^{\mu+2j-1}}{j!\,\Gamma(\mu+j)\,\tilde{g}^{\frac{\alpha(\mu+j)}{2}}} \qquad (20)$$

$$\begin{aligned}K_{cdf}^{SC} =&\ \frac{\mu(1+\kappa)^{\frac{1+\mu}{2}}}{\kappa^{\frac{\mu-1}{2}} e^{\kappa\mu}} \sum_{j=0}^\infty \sum_{p=0}^\infty \\ &\frac{\left(\mu\sqrt{\kappa(1+\kappa)}\right)^{\mu+2j-1}(\mu(1+\kappa))^p}{j!\,\Gamma(\mu+j+p+1)\,\tilde{g}^{\frac{\alpha(\mu+j+p)}{2}}}\end{aligned} \qquad (21)$$

$$\begin{aligned}\Lambda_{SC} =&\ \left(\Delta\alpha, -\left(\frac{\alpha L(\mu+j+p)-\alpha p}{2}\right)\right), \\ &\left(\Delta\alpha, 1-\frac{\alpha L(\mu+j+p)-\alpha p}{2}\right)\end{aligned} \qquad (22)$$

$$\begin{aligned}\Psi_{SC} =&\ (\Delta k, b_1), \left(\Delta\alpha, -\left(\frac{\alpha L(\mu+j+p)-\alpha p}{2}\right)\right), \\ &\left(\Delta\alpha, -\left(\frac{\alpha L(\mu+j+p)-\alpha p}{2}\right)\right)\end{aligned} \qquad (23)$$

Shannon capacity - MRC diversity with L branches

Shannon capacity at the output of SC diversity receiver with L branches can be calculated by replacing equation (10) in equation (12). Substituting equation (10) in equation (12), applying relation for transforming logarithm and exponential functions over MeijerG function what is explained in previous section and using equation (2.24.1/1) from (Prudnikov & Brychkov, 2003) we obtain Shannon capacity:

$$\frac{C_{MRC}}{B} = K_{MRC} G_{2\alpha,2+2\alpha}^{2+2\alpha,\alpha}\left(\frac{(L\mu(1+\kappa))^2}{4(L\tilde{g})^\alpha}\left|\begin{matrix}\Lambda_{MRC}\\\Psi_{MRC}\end{matrix}\right.\right) \qquad (24)$$

where

$$\begin{aligned}K_{MRC} =&\ \frac{L\mu(1+\kappa)^{\frac{1+L\mu}{2}}}{\sqrt{2}\ln(2)\kappa^{\frac{L\mu-1}{2}} e^{L\kappa\mu}(2\pi)^{\frac{2\alpha-1}{2}}} \\ &\times \sum_{j=0}^\infty \frac{\left(\mu\sqrt{\kappa(1+\kappa)}\right)^{L\mu+2j-1}}{j!\,\Gamma(L\mu+j)(L\tilde{g})^{\frac{\alpha(L\mu+j)}{2}}}\end{aligned} \qquad (25)$$

$$\Lambda_{MRC} = \left(\Delta\alpha, -\left(\frac{\alpha(L\mu+j)}{2}\right)\right), \left(\Delta\alpha, 1-\left(\frac{\alpha(L\mu+j)}{2}\right)\right) \qquad (26)$$

$$\Psi_{MRC} = (\Delta k, b_1), \left(\Delta\alpha, -\left(\frac{\alpha(L\mu+j)}{2}\right)\right),$$
$$\left(\Delta\alpha, -\left(\frac{\alpha(L\mu+j)}{2}\right)\right) \qquad (27)$$

NUMERICAL RESULTS

In this section, the analytically obtained results will be numerically calculated and graphically presented.

Figure 1 depicts Shannon capacity over $\alpha - \kappa - \mu$ fading channel for system without diversity. The results are shown for different combinations of parameters κ and μ while the value of the fading parameter α is fixed. From Figure 1 it can be seen that increasing the value of these parameters increases the capacity of the channel. Also, from the Figure 1 it can be seen that parameter μ more influence on the channel capacity than parameter κ.
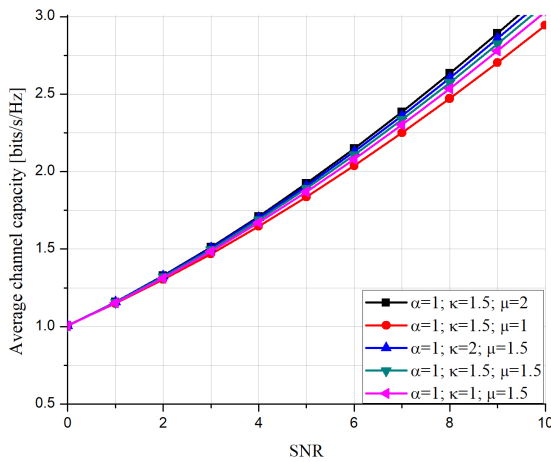

Figure 2. Shannon capacity for $\alpha - \kappa - \mu$ and other fading models obtained from it.

Figure 1. Influence of fading parameters κ and μ on channel capacity.

Figure 2 depicts Shannon capacity over $\alpha - \kappa - \mu$ fading channel and other fading models obtained from it for system without diversity. Results of channel capacity are shown for $\alpha - \kappa - \mu$, $\alpha - \mu$, $\kappa - \mu$, Nakagami-*m* and Rayleigh fading models. Figure 2 is obtained by using values from Table 1 and by using equation (16). Also, Table 1 represents a generality of $\alpha - \kappa - \mu$ fading model.

Figure 3 depicts Shannon capacity over $\alpha - \kappa - \mu$ fading channel for SC diversity receiver with L branches. Results are shown for values given in Table 1 and by using equation (19). The Figure 3 shows that the higher capacity is obtained for SC diversity receiver. Also, by increasing the number of the branches, channel capacity is increased.

Figure 4 depicts Shannon capacity over $\alpha - \kappa - \mu$ fading channel for MRC diversity receiver with L branches. Results are shown for values given in Table 1 and by using equation (24). The Figure 4 shows that the higher capacity is obtained for MRC diversity receiver. Also, by increasing the number of the branches, channel capacity is increased.

Figure 3. Shannon capacity for SC diversity system with L branches.

Table 1. Generality of $\alpha - \kappa - \mu$ fading model

Other fading models obtained from $\alpha - \kappa - \mu$ fading model				
	$\alpha - \kappa - \mu$	$\alpha - \mu$	$\kappa - \mu$	Nakagami-*m*	Rayleigh
α	1	1	2	2	2
κ	1.5	$\kappa \to 0$	1.5	$\kappa \to 0$	$\kappa \to 0$
μ	1.5	1.5	1.5	1.5	1

Figure 5 shows the difference in the achieved capacity when we use the system without diversity, SC diversity with L branches and MRC diversity with L branches. The comparison was made in relation to the number of branches that use diversity systems. Thus, it can be seen from the Figure 5 that the maximum capacity is reached when the number of branches is $L = 3$. When we perform the comparison for the same number of branches but dif-

ferent diversity systems, we see that the MRC diversity system gives a better capacity than the SC diversity system. When we observe a system for $L = 2$ branches, we see that it gives a smaller capacity in relation to a system with $L = 3$ branches, but, more capacity than a system that does not have diversity. For $L = 2$ branches, MRC diversity gives better capacity than SC diversity. Results shown in Figure 5 are obtained from equations (16), (19) and (24) and parameter values given in Table 1.
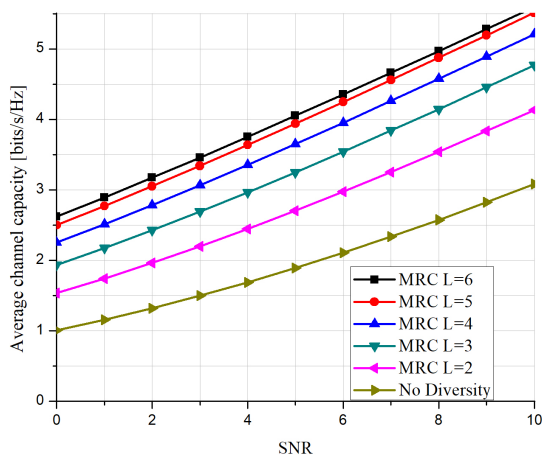
Figure 4. Shannon capacity for MRC diversity system with L branches.
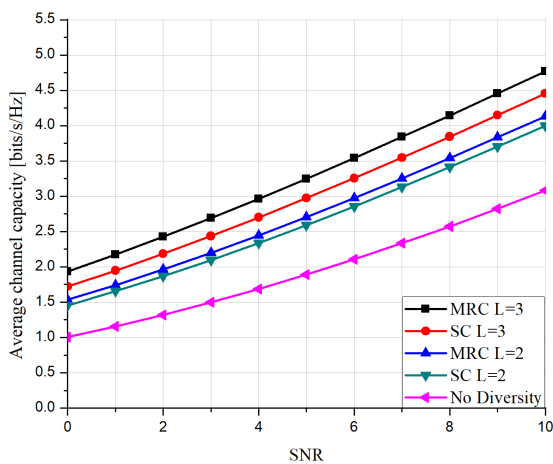
Figure 5. Comparison of Shannon capacity for SC and MRC diversity systems with L branches.

With the increase in SNR, capacity of the channel is also increased. In this paper, Shennon capacity for lower SNR values on the receiver (from $0 - 10$dB) in order to represent the influence of parameters and used diversity techniques on channel capacity is considered.

CONCLUSION

In this paper, Shannon capacity analysis for $\alpha - \kappa - \mu$ fading channel by using different system models is presented. Closed-form expression for probability density function and Shannon capacity of system without diversity, SC diversity system with L branches and MRC diversity system with L branches are given.

Numerical results obtained from analytical closed-form expression are calculated and graphically presented for different combination of fading parameters and different system models. At the end, comparison of proposed system models are made.

The higher channel capacity are achieved by using MRC diversity system with L branches. The least channel capacity are achieved for system without diversity. Although it provides less capacity compared to the MRC diversity, SC diversity is often used in practice realization for simpler implementation. Also, diversity systems with more than $L = 3$ branches are not implemented in the practical applications because of complexity. Complexity is reflected in increasing the computational complexity of receiving and transmitting algorithms, as well as the power required to process the signals. A larger number of antennas will also affect the price of the receiver.

ACKNOWLEDGMENTS

REFERENCES

Aldalgamouni, T., Magableh, A. M., & Al-Hubaishi, A. 2013. Performance of selected diversity techniques over the alfa-mi fading channels. WSEAS Transactions on Communications, 12(2), pp. 41–51.

Bessate, A. & El, B. F. 2017. A tight approximate analytical framework for performance analysis of equal gain combining receiver over independent Weibull fading channels. EURASIP Journal on Wireless Communications and Networking, 2017(1). doi:10.1186/s13638-016-0790-2.

Dixit, D. & Sahu, P. R. 2012. Performance of L-Branch MRC Receiver in - and - Fading Channels for QAM Signals. IEEE Wireless Communications Letters, 1(4), pp. 316-319. doi:10.1109/wcl.2012.042512.120240.

Freeman, R. L. 2005. Fundamentals of Telecommunications. Hoboken, NJ, USA: Wiley. doi:10.1002/0471720941.

Gradshteyn, I. & Ryzhik, I. 2000. Table of Integrals, Series, and Products.San Diego: Academic Press. 5th edn.

Huang, H. & Yuan, C. 2018. Cooperative spectrum sensing over generalized fading channels based on energy detection. China Communications, 15(5), pp. 128-137. doi:10.1109/cc.2018.8387992.

Ibnkahla, M. 2005. Signal Processing for Mobile Communications Handbook. 872.

Katiyar, H. 2015. Performance Analysis of Space Diversity in Alfa-Mi Fading Channel. International Jouranl of Electrical and Electronics Engineers, 7(2), pp. 38-46.

Milišić, M., Hamza, M., & Hadžialić, M. 2009. BEP/SEP and Outage Performance Analysis of -Branch Maximal-Ratio Combiner for Fading. International Journal of Digital Multimedia Broadcasting, , pp. 1-8. doi:10.1155/2009/573404.

Mitrović, Z. J., Nikolić, B. Z., Đorđević, G. T., & Stefanović, M. 2009. Influence of Imperfect Carrier Signal Recovery on Performance of SC Receiver of BPSK Signals Transmitted over alfa-mi Fading Channel. Electronics, 13(1), pp. 58-62.

Mohamed, R., Ismail, M. H., Newagy, F., & Mourad, H. M. 2013. Closed-form Capacity Expressions for the $\alpha-\mu$ Fading Channel with SC Diversity under Different Adaptive Transmission Strategies. Frequenz, 67(3-4). doi:10.1515/freq-2012-0708.

Panić, S., Stefanović, M., Anastasov, J., & Spalević, P. 2013. Fading and interference mitigation in wireless communications. New York: CRC Press.

Prudnikov, A. & Brychkov, J. 2003. Integrals and series.Moscow: Fizmatlit. 2nd edn.

Sagias, N. C., Mathiopoulos, P. T., & Tombras, G. S. 2003. Selection diversity receivers in Weibull fading: outage probability and average signal-to-noise ratio. Electronics Letters, 39(25), p. 1859. doi:10.1049/el:20031189.

Simon, M. K. & Alouini, M. 2005a. Digital Communication over Fading Channels. Hoboken, NJ, USA: Wiley. doi:10.1002/0471715220.

Simon, M. K. & Alouini, M. 2005b. Digital Communication over Fading Channels. Hoboken, NJ, USA: Wiley. doi:10.1002/0471715220.

Stüber, G. L. 2002. Principles of mobile communication. Kluwer Academic Publishers. 2nd edn., 752.

Subadar, R. & Das, P. 2017. Performance of L-SC receiver over K-fading channels. In 2017 8th International Conference on Computing, Communication and Networking Technologies (ICC-CNT).Institute of Electrical and Electronics Engineers (IEEE)., pp. 1-4. doi:10.1109/icccnt.2017.8203908.

Subadar, R., Reddy, T. S. B., & Sahu, P. R. 2010. Capacity analysis of dual -SC and -MRC systems over correlated Nakagami-m fading channels with non-identical and arbitrary fading parameters, pp. 1–5.

Subadar, R., Reddy, T. S. B., & Sahu, P. R. 2012. Big Data analytics. In 2012 International Conference on Communication, Information and Computing Technology (ICCICT).Institute of Electrical and Electronics Engineers (IEEE)., pp. 1-4. doi:10.1109/iccict.2012.6398180.

Subadar, R. & Sahu, P. R. 2010. Performance of L-MRC receiver over independent Hoyt fading channels. In 2010 National Conference On Communications (NCC).Institute of Electrical and Electronics Engineers (IEEE)., pp. 1-5. doi:10.1109/ncc.2010.5430232.

Talha, B., Primak, S., & Patzold, M. 2010. On the Statistical Properties of Equal Gain Combining over Mobile-to-Mobile Fading Channels in Cooperative Networks. In 2010 IEEE International Conference on Communications.Institute of Electrical and Electronics Engineers (IEEE)., pp. 1-6. doi:10.1109/icc.2010.5501898.

Yilmaz, F.and Alouini, M. 2012. A Novel Unified Expression for the Capacity and Bit Error Probability of Wireless Communication Systems over Generalized Fading Channels. IEEE Transactions on Communications, 60(7), pp. 1862-1876. doi:10.1109/tcomm.2012.062512.110846.

A COMPARATIVE ANALYSIS OF ELECTRONIC AND TRADITIONAL LEARNING

NEBOJŠA DENIĆ[1], MERDAN ZEJNELAGIĆ[2], NATAŠA KONTREC[1*]

[1]Faculty of Sciences and Mathematics, University of Priština, Kosovska Mitrovica, Serbia
[2]Faculty of information technology, Alfa BK University, Belgrade, Serbia

ABSTRACT

Modern way of living and functioning of human society requires a new principle of decision making and adjusting to contemporary living needs. In times when humans have perfected the contemporary living needs with their technological achievements yet another disadvantage among those needs has appeared. Studying possibilities and adjusting to educational requirements have hardly made any progress in years. Traditional learning methods are implemented by means of book, pencil and paper, as was the case thousands of years ago, supporting functioning of human society. This paper, based on researches founded on implementation of educational software and researches founded on postulates of implementation of frontal education and summarizing related specialized literature from this area, will set forth possibilities for implementation of information and communications technologies (ICT) and educational software in teaching. The results of this research indicate that the students who were using electronic methods of learning in combination with traditional learning had become more motivated, skilled and interested in a new way of thinking that activates all senses in order to form their intellectual personality.

Keywords: Teaching, Education, Electronic learning.

INTRODUCTION

Today, one of the most challenging tasks is the improvement of methods of traditional learning. A need to improve these methods originates from this fact that traditional learning represents an improper bond between knowing and recognizing for both the individual and the society. The majority of modern society frowns upon learning for personal gains. On those bases, an idea to improve traditional learning methods occurred, in order to develop a literate and technologically functional society with the use of modern technologies (Denić & Petković, 2018). Distance learning represents an educational process with no limitations, obstacles and interferences, and as such, it is available to everyone and at all times, by means of modern technologies and mass media with the aim of supporting the process of education and gaining new knowledge, and offers a two-way possibility for communication as a social and interactive tool, which is one of the most important reasons for improving the traditional methods of education. Distance education has been extensively researched in (Moor et al., 2011; Anderson, 2008; Moore & Kearsley, 2005; Keegan, 2005; Simonson, 2001; Simonson & Schlosser, 2004; Keegan, 1996). As agreed by most authors, the description and scope of learning has been regenerated and improved over the years (Chawinga & Zozie, 2016), so we can state with certainty that the modern learning method is founded upon understanding the fact that students and teachers need not be present in the same premises but their interaction can be established from a distance with the

assistance offered by ICT (Denić et al., 2017b; Chawinga & Zozie, 2016; Moore & Kearsley, 2004). However, the most widely accepted definition of electronic learning, on which this paper is founded upon, describes the electronic lesson as an interactive possibility for transfer of teacher's knowledge so that he can, based on his personal devotion and syllabus' design, provide prompt, anticipated and motivated effort for adoption of the aforementioned knowledge (Moor et al., 2011). E-learning continuum is presented in Figure 1.

| Classical Teaching F2F | The use of ICT in teaching | Hybrid teaching | Online education |

E-Learning

Distance learning
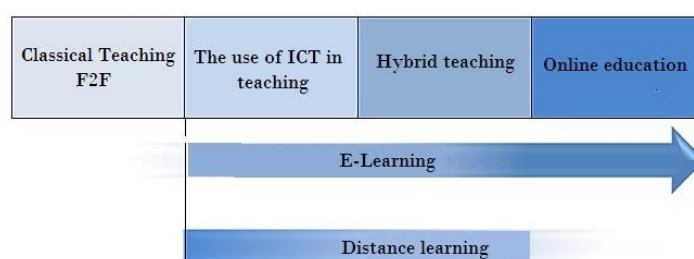
Figure 1. E-learning continuum.

QUALITY IN TEACHING BASED ON ICT

High quality ICS (Information Communication System) is comprised of institutions that commonly belong to another subsystem (educational institution, Ministry of Education, state), and connectivity channels that provide an unobstructed flow of information within the system (exchange of data, mail on teacher-student relation, notices) and communicators that proficiently and regularly update the materials within the system (teachers) (Hassanzadeh et al., 2012). Education based on ICT is for the most part more meaningful, interesting and of higher

quality (Denić et al., 2014). Each student can practically and actively take part in lecturing and in this manner achieve required level of recognition by teachers. The quality of design directly affects the quality of lecturing and is one of the most important factors for high quality educational content. The content comprises entire material included in educational process, as well as additional materials designed by students and teachers together and by doing so, enrich the educational content. These entities and their interaction can be illustrated in a didactic triangle (Figure 2).
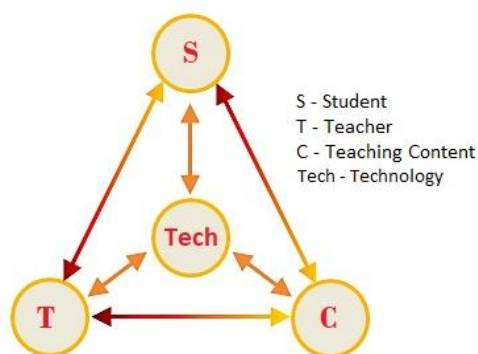
Figure 2. Didactic triangle.

Elementary and high school education, besides aiming at gaining of knowledge, is founded upon developing of students' intellectual capabilities, individual decision making as well as developing their abilities for additional improvements (Denić et al., 2014). In academic education and post-academic studies, e-learning provides immeasurable contributions to all spheres of education and directly affects improvement of quality of teaching and quality of education. Professors, lecturers and teachers contribute significantly to quality of education with their extracurricular activities and directly affect the society's general education. High quality extracurricular content contains good graphic quality and understandable multimedia content (text, sound, image, video, animation). Extracurricular content must be connected and adjusted with the content of the educational institution. ICT unify concepts of education and technologies into one. However, the concept of electronic learning is repeatedly misunderstood. Electronic learning has the goal to improve the meaningfulness of education, add up missed knowledge and enable enhancing of the traditional knowledge with practical part of education, but not to take over the leading role in education. In a narrower sense, electronic learning is more comprising, practical and broader than traditional method of learning, but electronic learning without traditional method of learning (required explanation and interpretation by teachers) almost has no major advantage in science. In many occasions we have witnessed that pupils of elementary and high schools that posses high quality and comprising ICS manage to achieve remarkable success at national and international level competitions and knowledge Olympics. In comparison, the difference in educational content is minor. Teachers who pass the knowledge stick to the same or similar teaching educational system. Pupils of same age often have similar intellectual capabilities. The advantage of success is in additional material that can easily be transferred in a high quality ICS (Denić et al., 2017a). Therefore, once solved task is being kept and updated in electronic classroom, where every next generation of students has the opportunity to enhance this solved task and use it as an example in practice, and each reprocessed task is preserved and with the teacher's meticulousness gets re-updated in the database, leaving high quality content for new success in the related area for generations to come. E-learning surroundings is comprised of a Learning Management System (LMS), a Content Management System (CMS) and a Knowledge Management System (KMS) and some of the tools for content authorization (Gavrilović et al., 2018; Babu, 2005; Moore et al., 2011; Wilen-Daugenti, 2009). E-learning surrounding is an informational system (IS) based on World Wide Web (Lee & Lee, 2008).

RESEARCH DESCRIPTION

Improving of living needs for both individual human beings and society in general is one of the hot topics in modern times. 21st Centuries advanced achievements have made impact on improvement of all aspects of life. Modern medicine, industry, economy, technology, in one word everything that surrounds us is related to information technologies and computers. ICT with the use of computer systems and IT equipment have improved all needs of human society. Whether it concerns military equipment, medical lasers, industrial machines, means of transport, satellites (everything that surrounds us) is controlled by a computer today. Computers have used their endless possibilities to a limited extent in education. Improvement of modern education as well as creating an interactive educational content represents an endless treasury for education of modern people. Today, there is a large number of elementary and high schools in our surroundings, that still base their lectures on traditional methods of education. Also, there is not a single student who has not met with or has not used a modern computer. IT generation of people is represented by people who have been in contact with computers from the day they were born. Computers are both the need and the object of interest by people.

Testing is a possibility to check the students' knowledge on all levels. It is conducted with the use of previously designed questions in written or electronic form. Testing represents a way to assess the students' abilities and knowledge. The use of modern technologies also resulted in a possibility to learn through testing. Testing with the use of computers presents an educational experience and a better educational possibility. The possibility to learn on students' mistakes brings additional stimulus and will for further improvement. Electronic testing has the greatest social contribution in modern psychology. Electronic testing represents a method of modern assessment of human abilities. By means of electronic testing and learning, the wrong

answer no longer represents an obstacle for decision making, but instead it encourages the user to learn from own mistakes. The wrong answers will provide the user with the dual experience in education. He will learn what the correct answer to a question is but also what the wrong answer to a question is. The related researches have shown that humans are capable of remembering 20% of information he/she had heard, 40% of information he/she had both seen and heard, and 75% of information he/she had seen, heard and actively implemented in practice.

For the needs of this paper, the pupils of 5th, 6th, 7th and 8th grade of an elementary school in Kosovo and Metohija have been tested. The questions were designed with the goal to improve intellectual and sensory capability of pupils. Intellectual capabilities are: analysis, synthesis, abstract opinion, ability to reach a conclusion, dealing with terminology, use of symbols and terms, recognizing similarities as well as prompt thinking etc. Sensory abilities include hearing, seeing, rapid response and replying etc. The questions are grouped into different areas, as follows:

- Knowledge of hardware, software and computers;
- Educational issues;
- Operating system and its components;
- Structural issues;
- Windows applications;
- Computer networks;
- General issues.

Based on books used in elementary schools, a database with questions was created, and pupils who have successfully finished the 5th grade were tested with ten randomly selected questions. The answers were divided into five groups, as follows:

+ the pupil recalls the teaching content satisfactorily;
0 the pupil recalls the teaching content superficially;
- the pupil needs to be reminded of the teaching content;
/ the pupil has difficulties recalling the teaching content.

After testing of pupils who had successfully completed the 5th grade of elementary school, the pupils of the 6th, 7th and 8th grade of elementary school were tested.

RESEARCH RESULTS

The research conducted on ten pupils who had completed the fifth grade in different elementary schools, provided the results presented in Table 1 and Figure 3.

The research indicated that the pupils who have been using the traditional method of learning have forgotten a significant part of content and needed to be reminded of this content. The content that they have been learning in elementary schools was to some extent interesting and less creative. When asked what their biggest incentive in learning was, most of them pointed out knowledge of computers and computer equipment.

Table 1. Test results of pupils who had completed the 5th grade in 2016/17 school year.

List of pupils	Class	Answer
Pupil 1	5.	0
Pupil 2	5.	-
Pupil 3	5.	+
Pupil 4	5.	0
Pupil 5	5.	0
Pupil 6	5.	/
Pupil 7	5.	0
Pupil 8	5.	-
Pupil 9	5.	+
Pupil 10	5.	0

Table 2. Test results of pupils who had completed the 7th, 8th and 9th grade in 2016/17 school year.

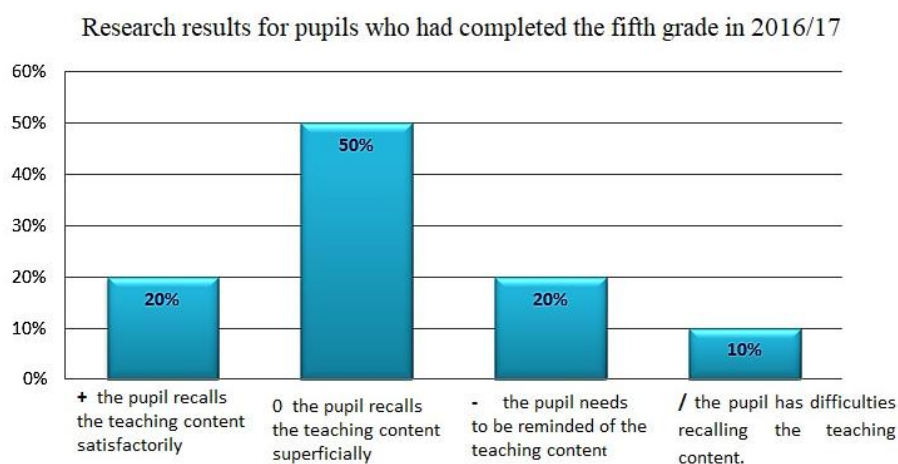| List of pupils	Class	Answer
Pupil 1	7.	0
Pupil 2	6.	-
Pupil 3	7.	0
Pupil 4	8.	0
Pupil 5	8.	+
Pupil 6	8.	-
Pupil 7	6.	/
Pupil 8	7.	/
Pupil 9	7.	-
Pupil 10	6.	-

Figure 3. Research results for 5th grade students in 2016/17.

The second research, conducted on ten pupils who had completed the fifth grade of elementary school and attended the 6th, 7th and 8th grade, indicated the results presented in Table 2 and Figure 4.

The survey has shown that the pupils have no permanent memory of the knowledge gained in this manner but need a shorter time period to recall the tasked area. The content they had studied in elementary schools was interesting but not creative enough. When asked what was their biggest incentive in learning most of them agreed the reason was the overall possibilities of computers and internet. Based on the conducted survey we can easily reach a conclusion that the method for designing educational content is outdated, flawed and non-interactive. During the entire course of the lectures, a pupil is only offered dry material with necessary typical exercises which only activate recognizing of practical knowledge to a certain extent.
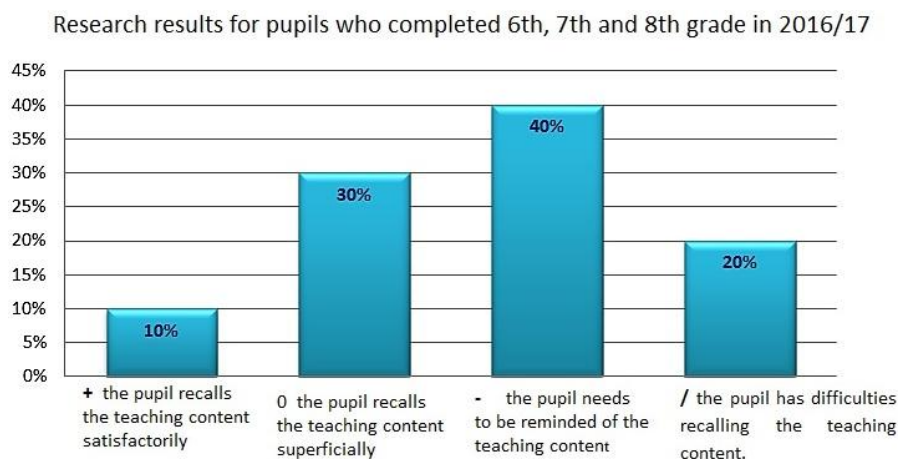
Figure 4. Research results for 6th, 7th, 8th grade students in 2016/17.

INTRODUCING STUDENTS WITH SOFTWARE FOR ELECTRONIC LEARNING AND THEIR SURVEY RESULTS

After completing the survey, each student had a possibility to solve the interactive test with the help of *SmartNotebook 17.0* application. All students were divided into pairs and were solving the same test. The test was consisted of 10 new questions. Each student understood the rules of the competition in prompt and simple way and afterwards completed the final survey (Table 3). With its audio and video effects, the application awoke attention of all surveyed pupils and enticed them to think creatively. After successful completion of the quiz, the students had a possibility to get acquainted with other questions from the offered database. The acquainting had the purpose to have the pupils assess the application subjectively.

The pupils completed the survey with the following offered responses:

- 0 – I think that the offered application is useless for my studying;
- 1 – I think that the offered application is inapplicable for my studying;
- 2 – I think that the offered application is a solid base for my studying;
- 3 – I think that the offered application is creative for my studying;
- 4 – I think that the offered application is useful for my studying;
- 5 – I think that the offered application is ideal for my studying.

Table 3. Final survey on content quality of Smart Notebook application and its implementation in practice.

List of pupils	Class	Mark
Pupil 1	6.	3
Pupil 2	6.	4
Pupil 3	6.	4
Pupil 4	6.	5
Pupil 5	6.	5
Pupil 6	6.	4
Pupil 7	6.	3
Pupil 8	6.	5
Pupil 9	6.	4
Pupil 10	6.	4
Pupil 11	7.	5
Pupil 12	6.	5
Pupil 13	7.	4
Pupil 14	8.	5
Pupil 15	8.	3
Pupil 16	8.	2
Pupil 17	6.	3
Pupil 18	7.	5
Pupil 19	7.	5
Pupil 20	8.	5
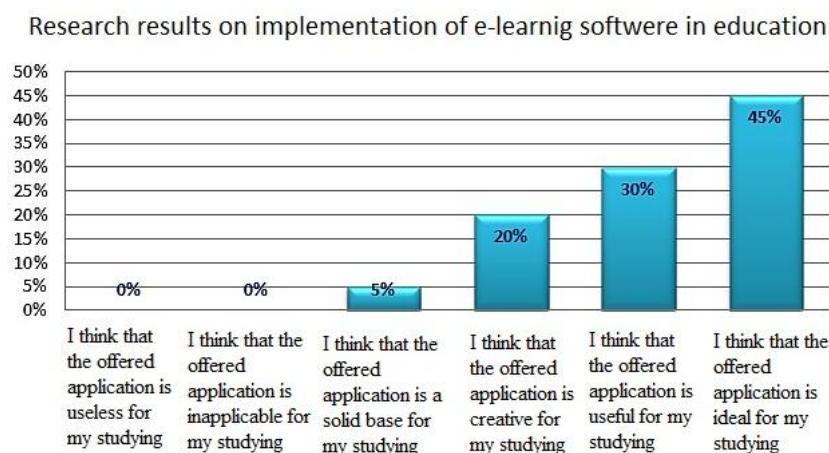
Figure 5. Research results on implementation of e-learning in education.

Based on the conducted research we have received the following results on implementation of *Smart Notebook* application in contemporary education of pupils, as in Figure 5.

Based on the overall research and interest from the pupils for modern technologies and possibilities for achieving adequate goals in contemporary education of pupils we can safely say that software for electronic learning have positive effect on the pupils' creative thinking. They proved useful in surmounting the tasked content at hand and with adequate implementation along with the traditional method of learning assist in overall pupils' education. A pupil can overcome the tasked areas through fun and play, make a subjective ruling on accuracy of the asked question and in that manner complete his/her own knowledge or enhance creative learning by learning from the wrong answer. The knowledge gained like this is more permanent than traditional learning. A pupil is given a possibility to select one of the offered answers and in this way his thinking can be adequately evaluated and guided to proper and mature thinking.

CONCLUSION

Modern education represents a vital precondition for continued existence and developing of a modern society. The ICT with its importance and connections to other sciences represents one of the most important factors for progress and enhancement of the human community needs. Today, information technologies represent one of more important subjects at all faculty departments. Whether we are talking about medicine, mathematics, physics, construction or other social sciences, the informatics has the leading role in their education and enhancement. Various software packages, with the assistance of computers, have found their use in implementation of very important and precise jobs for decades. The importance of IT education is in proportion with the importance of technological development of a modern society. Contemporary methods of learning and educating, such as electronic learning and distance learning, have provided access to the required knowledge to all people in need. With help of electronic

learning, education can no longer be placed under the field of a traditional classroom. Global trends in education place electronic learning at one of the leading positions of modern education. A proper use of electronic learning can have immeasurable effects in education and teaching. However, we must be aware that internet and computers also have their downsides. Without adequate assistance by a competent lecturer some negative effects and hazards can also be experienced when information technologies are used in education. A well planned content of electronic learning is adjustable and applicable for the needs of each individual student. Whether it concerns hard working students, students less able to remember or handicapped persons, the electronic learning offers additional support in improving gaining of required knowledge. Beside its contribution to memorizing and adopting new information, the electronic learning also enables children to develop emotional and social skills. The education assisted by the electronic learning directly affects the students' behavior. Software used during lectures can be designed in various colors. Based on such display of information, both brain hemispheres are triggered and a student can remember and accept new information in an easier way. Practical lectures have shown that children who follow lectures designed on basis of multimedia content accept new information in an easier and faster way in comparison to children who learn by means of a traditional method of learning with books. The electronic learning has positive influence on manifold aspects of children's development. In a physical context, a hand-eye-hearing relationship is developed, while in an intellectual context children have a possibility for better memorizing and enhancing team spirit skills, as well as developing their own memorizing skills. In the future, the electronic learning will represent a foundation in education, in both educational institutions and each individual child in particular.

REFERENCES

Anderson, T. 2008. The theory and practice of online learning. Canada: Athabasca University Press.

Babu, N. S. C. 2005. Quality Assurance Framework for e-Learning. India: ELEL Tech.

Chawinga, W. D., & Zozie, P. A. 2016. Increasing Access to Higher Education Through Open and Distance Learning: Empirical Findings From Mzuzu University, Malawi. The International Review of Research in Open and Distributed Learning, 17(4). doi:10.19173/irrodl.v17i4.2409

Denić, N., Živić, N., & Spasić, B. 2014. Application Of Information And Communication Techologies In School Education. Annals Of The Oradea University. Fascicle Of Management And Technological Engineering., XXIII (XIII)(3). doi:10.15660/auofmte.2014-3.3062

Denić, N., Nešić, Z., Radojičić, M., Petković, D., & Stevanović, M. 2017a. Contribution to the research of children protection in use of interent. Tehnički vjesnik, 24, pp. 525-533.

Denić, N., Gavrilović, S., & Kontrec, N. 2017b. Information and communications technologies in function of teaching process. The University Thought - Publication in Natural Sciences, 7(2), pp. 58-63. doi:10.5937/univtho7-15472

Denić, N., & Petković, D. 2018. Obrazovni softver. Kosovska Mitrovica: Prirodno matematički fakultet. ISBN 978-86-80795-36-2.

Gavrilović, S., Denić, N., Petković, D., Živić, N. V., & Vujičić, S. 2018. Statistical evaluation of mathematics lecture performances by soft computing approach. Computer Applications in Engineering Education, 26(4), pp. 902-905. doi:10.1002/cae.21931

Hassanzadeh, A., Kanaani, F., & Elahi, S. 2012. A model for measuring e-learning systems success in universities. Expert Systems with Applications, 39(12), pp. 10959-10966. doi:10.1016/j.eswa.2012.03.028

Keegan, D. 1996. Foundations of distance education. London: Croom Helm.

Keegan, D., (Eds). 2005. Theoretical Principles of Distance Education.Informa UK Limited. doi:10.4324/9780203983065

Lee, J., & Lee, W. 2008. The relationship of e-Learner's self-regulatory efficacy and perception of e-Learning environmental quality. Computers in Human Behavior, 24(1), pp. 32-47. doi:10.1016/j.chb.2006.12.001

Moore, M., & Kearsley, G. 2011. Distance Education: A Systems View of Online Cengage Learning.

Moore, J. L., Dickson-Deane, C., & Galyen, K. 2011. e-Learning, online learning, and distance learning environments: Are they the same. The Internet and Higher Education, 14(2), pp. 129-135. doi:10.1016/j.iheduc.2010.10.001

Moore, M. G., & Kearsley, G. 2005. Distance education: A systems view. Belmont, CA: Thomson Wadsworth.

Simonson, M. 2001. Distance education and online instruction: Profession or Field. The Quarterly Review of Distance Education, 2(4); 301-302.

Simonson, M., & Schlosser, C. 2004. We Need A Plan, An Instructional Design Approach for Distance Education Courses. Fischler College of Education: Faculty Articles.

Wilen-Daugenti, T. 2009. Edu: Technology and Learning Environments in Higher Education. Peter Lang, International Academic Publishers. doi:10.3726/b11473

INTERPOLATION LOGISTIC FUNCTION IN THE SURFACE POTENTIAL BASED MOSFET MODELING

TIJANA KEVKIĆ[1,★]**, VLADICA STOJANOVIĆ**[1]

[1]Faculty of Natural Sciences and Mathematics, University of Priština, Kosovska Mitrovica, Serbia

ABSTRACT

Introduction of the Interpolation Logistic (IL) function in an approximate Surface-Potential-Based MOSFET model has been proposed in this paper. This function can be precisely determined in accordance with different MOSFET device characteristics. The IL function also provides continual behavior of the surface potential in entire useful region of MOSFET operation. Unlike the approximate analytical models which can meet in literature, continual and smooth transition of the surface potential between weak and strong inversion region here is achieved without using of any empirical parameter. Furthermore, thanks to the IL function, speed and manner of that transition are controlled. The values obtained for the surface potential are verified extensively with the numerical data, and a great agreement is found for the MOSFET devices from different technology generations.

Keywords: MOSFET modeling, Interpolation Logistic function, Surface potential, Parameters estimation.

INTRODUCTION

Since the choice of a suitable MOSFET model is crucial to the efficiency in the design of both analog and digital integrated circuits, the used model must satisfy some important conditions. First of all, it should reflect the correct physical behavior in order to achieve acceptable accuracy over the required bias conditions. Further, the model must accurately represent device operation over a wide variety of process parameters, geometries and regions of operation. Apart from accuracy, the model used should be as simple as possible in order to limit circuit simulation time.

Among the most accurate physically based MOSFET models are so-called surface potential- based models (henceforth referred to as the SPBM). SPBM fulfill mentioned conditions by the combination of the accuracy of the implicit single-piece models and the short calculation time of regional models (Arora, 1993; Araújo et al., 1995; Prégaldiny et al., 2004). On the other hand, a major difficulty related to these models is an implicit relation between the surface potential ψ_s and the MOSFET terminal voltages, which needs numerically solutions (Eftimie & Rusu, 2007). Unfortunately, numerical iterative procedures require long computation times what is not desirable from the physical and design point of view (Enz et al., 1995; Chen & Gildenblat, 2001). An attempt to overcome this difficulty is proposed in van Langevelde & Klaassen (2000) as the closed-form approximation for the surface potential. However, that approximation uses for ψ_s an empirical smoothing function with a smoothing parameter with no physical meaning. Hence, the accuracy of the approximation introduced in van Langevelde & Klaassen (2000) is about 2-3mV which is not always adequate for an accurate modeling of MOSFET characteristics (Hossain & Chowdhury, 2016).

Instead of the empirical smoothing function for ψ_s, here is proposed a new one that is computationally efficient, well behaved and extremely accurate. This new function is based on the so-called interpolation logistic function which depends on MOSFET devices characteristics. The modified SPBM with proposed new function gives an accurate and continual description of the surface potential in entire inversion region, without any empirical determinations. Finally, the simulated ψ_s values are compared extensively with numerically obtained results of the mentioned implicit relation and a great agreement was found for MOSFET devices which belong to the different technology generations.

DEFINITION OF PROBLEM

In the useful range of the n-type MOSFET transistor operation, under the gradual channel and charge sheet approximations, for electrostatic surface potential is obtained the following implicit relation:

$$V_G = V_{FB} + \psi_s + \gamma \sqrt{\psi_s + u_T \exp\left(\frac{\psi_s - 2\phi_F - V_{ch}}{u_T}\right)}. \quad (1)$$

Here V_G, V_{FB} and u_T are gate voltage, flat-band voltage and thermal voltage, respectively. ϕ_F is bulk potential, while V_{ch} is the channel potential. N_A is channel doping concentration, t_{ox} is thickness of oxide, and γ is body effect coefficient. Numerical solution of Eq.(1) can be obtained by using Newton-Raphson algorithm (Osrecki, 2015). On the other side, the explicit approximate solution of the Eq. (1) developed in van Langevelde & Klaassen (2000)

★ Corresponding author: tijana.kevkic@pr.ac.rs

PHYSICS

has following form:

$$\psi_s^*(V_G) = f + u_T \ln \left\{ \gamma^{-2} u_T^{-1} \left[V_G - V_{FB} - f - \frac{\psi_{s_{wi}} - f}{\sqrt{1 + \left(\frac{\psi_{s_{wi}} - f}{4u_T}\right)^2}} \right]^2 \right.$$
$$\left. - u_T^{-1} f + 1 \right\},$$
(2)

where

$$\psi_{s_{wi}} = \left(\sqrt{V_G - V_{FB} + \frac{\gamma^2}{4}} - \frac{\gamma}{2} \right)^2$$
(3)

is the surface potential in the weak inversion region and f is empirical function given by:

$$f(V_G) = \frac{2\phi_F + V_{ch} + \psi_{s_{wi}}(V_G)}{2} - \frac{1}{2}\sqrt{\left(\psi_{s_{wi}}(V_G) - 2\phi_F - V_{ch}\right)^2 + 4^2}.$$
(4)

The value of function f should changes smoothly from $\psi_{s_{wi}}$ in the weak inversion region to $2\phi_F + V_{ch}$ on the onset of the strong inversion region. Smoothness of that transition is controlled by the smoothing parameter which value was firstly fixed at a convenient value of 0.02V (van Langevelde & Klaassen, 2000). Later, it has been replaced with different classes of functions which vary from a value close to zero in depletion and weak inversion region to a value close to 0.02V (Basu & Dutta, 2006; Kevkić et al., 2016, 2017).

However, several simulations have shown that results of Eq. (2) deviate significantly from numerical results of the implicit equation (1). The observed deviations are greater for values of applied gate voltages near and below threshold (i.e., in the weak inversion regime) as well as for scaled MOSFET devices i.e. for devices with thinner gate oxides and higher substrate doping. This is consequence of purely empirical nature of function f, what means that f does not take into account changes in specific technology characteristics of the MOSFET devices. Additionally, smoothing parameter does not have physical meaning or role, except to prevent the interruption of the function f at threshold.

MODEL FORMULATION

The simple empirical function f, given by Eq. (4), unifies the weak and strong inversion approximations without inclusion of changes in the technological characteristics of MOSFET devices. In order to take into account mentioned changes and improve description of device behavior, here we suggest *the Interpolation Logistic (IL)* functional form for f:

$$f_{IL}(V_G) = \psi_{s_{wi}}(V_G) - \frac{u_T}{a} \ln \left[1 + b \exp\left(\frac{a}{u_T}\left(\psi_{s_{wi}}(V_G)\right.\right.\right.$$
$$\left.\left.\left. - 2\phi_F - V_{ch}\right)\right)\right].$$
(5)

Here, $a, b > 0$ are the fitting parameters which can be obtained by using a specific fitting procedure, described in detail in

the following. Notice that in the weak inversion region (i.e., when $\psi_s < 2\phi_F + V_{ch}$), the exponential term in Eq. (5) becomes negligible, so $f_{IL} \approx \psi_{s_{wi}}$. On the other side, in the strong inversion region (i.e., when $\psi_s > 2\phi_F + V_{ch}$), the exponential term in Eq. (5) becomes dominant and approximation $f_{IL} \approx 2\phi_F + V_{ch} + \ln b$ holds. Obviously, term $\ln b$ can be used to clarify some practically observed deviations from the value $2\phi_F + V_{ch}$. It can be easily proven that from the inequalities $f_{IL}(V_G) \geq 2\phi_F + V_{ch}$ and $\psi_s > 2\phi_F + V_{ch}$ follows

$$b \leq 1 - \exp\left(-\frac{a}{u_T}\left(\psi_{s_{wi}}(V_G) - 2\phi_F - V_{ch}\right)\right) < 1,$$

and vice versa. Therefore, the values of the fitting parameter b can indicate the changes of the reference f-values from $2\phi_F + V_{ch}$. In particular, if no deviation, i.e., if in the strong inversion region $f_{IL}(V_G) \approx 2\phi_F + V_{ch}$ holds, it will be $b \approx 1$.

The estimation of the fitting parameters $a, b > 0$ can be done by using the standard fitting procedure based on the following algorithm:

- Step 1. For given gate voltage values $V_G^{(1)}, \ldots, V_G^{(n)}$, numerically solve Eq. (1) with respect to ψ_s, i.e., compute the values of $\psi_s^{(1)}, \ldots, \psi_s^{(n)}$ such that:

$$V_G^{(k)} - V_{FB} - \psi_s^{(k)} = \gamma\left[\psi_s^{(k)} + u_T \exp\left(\frac{\psi_s^{(k)} - 2\phi_F - V_{ch}}{u_T}\right)\right]^{1/2}.$$

- Step 2. Find values $f_1, \ldots, f_n$ as the solutions of equations $\psi_s^{(k)} = \psi_s^*(V_G^{(k)})$, $k = 1, \ldots, n$.

- Step 3. Minimize the objective function:

$$F(a, b) := \sum_{k=1}^{n} \left(f_{IL}(V_G^{(k)}) - f_k\right)^2$$

with respect to $a, b > 0$.

- Step 4. For obtained values $a^*, b^* > 0$ which satisfies $F(a^*, b^*) = \min F(a, b)$ form the IL-function $f_{IL}(V_G)$, as it is given in Eq. (5).

Table 1. Estimated values of the f_{IL}-fitted parameters, according to the MOSFETs technological characteristics.

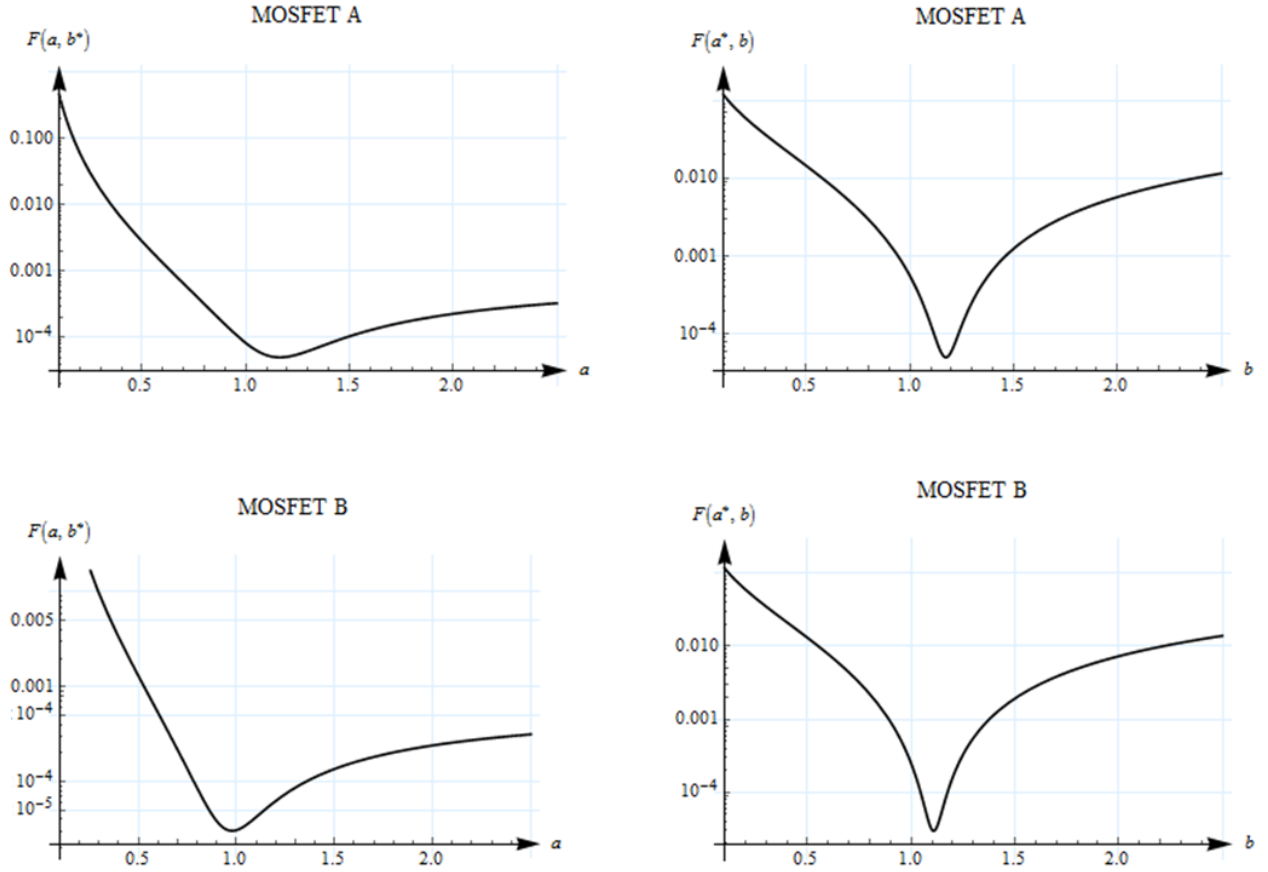| Items	MOSFET A	MOSFET B
t_{ox} (nm)	2.5	1.2
N_A (cm^{-3})	5×10^{17}	5×10^{18}
γ (V$^{1/2}$)	0.2891	0.4494
$2\phi_F$ (V)	0.9100	1.0416
V_{FB} (V)	-0.8000	-1.0000
a^*	1.1638	0.9887
b^*	1.1737	1.1019

Figure 1. Graphs of the objective function $F(a, b^*)$ (left diagrams) and $F(a^*, b)$ (right diagrams). Device parameters are: MOSFET A (diagrams above) and MOSFET B (diagrams bellow).

Notice that minimization of the objective function $F(a, b)$ in the Step 4 of previous algorithm is performed by using the non-linear last squared approximate method, i.e., by solving the coupled equations $\partial F(a, b)/\partial a = \partial F(a, b)/\partial b = 0$. Estimates of the f_{IL} parameters $(a, b) = (a^*, b^*)$ obtained from described algorithm are shown in Table 1, for two MOSFETs with significantly different technological characteristics. All estimates have been obtained based on the series of $n = 50$ equidistant values of gate voltage V_G, and the whole algorithm has been implemented in the software package `MATHEMATICA 11.0`.

Graphs of the functions $a \mapsto F(a, b^*)$ and $b \mapsto F(a^*, b)$, for both of the considered MOSFETs devices are shown in Fig 1. As it can easily be seen, in both cases the function $F(a, b)$ attains a unique minimum at the point $(a, b) = (a^*, b^*)$.

MODEL VALIDATION

The functions $f(V_G)$ and $f_{IL}(V_G)$ are plotted in the above diagrams in Fig. 2 along with the real-based values $f_1, \ldots, f_n$ which were obtained in the Step 2 of previously developed algorithm, and taken as reference values. Diagrams bellow show approximations of the surface potential $\psi_s^*(V_G)$, obtained from Eq. (2), by using both of the functions f and f_{IL}, respectively.

The improvement of the original explicit SPB model (van Langevelde & Klaassen, 2000) by introducing the Interpolation Logistic function can be clearly seen from Tables 2 and 3. They show the mean values of the absolute errors (AE), fractional errors (FE) and squared errors (SE) for functions $f(V_G)$ and $f_{IL}(V_G)$, as the approximate surface potential $\psi_s^*(V_G)$. As reference values have been used ones obtained by the previous developed algorithm. For both of considered devices the errors were computed separately in weak and strong inversion region, as well as in the whole approximation region.

As we can see, all the estimated errors are smaller in the case of function $f_{IL}(V_G)$, for both of the MOSFETs. This is particularly pronounced in the case of MOSFET A, where for instance, fractional errors which occur in the strong and whole approximation regions are more than six times smaller than corresponding FE value where function f was used. In the case of MOSFET B, these errors are smaller five times, approximately.

These facts also confirms the Fig. 3 where the absolute errors $AE = \psi_s^* - \psi_s$ are shown in the logarithmic scales, for both of the mentioned approximations, in the weak and strong inversion, separately. The values of $\psi_s^*(V_G)$ have been obtained from Eq. (2) by using fitting functions $f(V_G)$ and $f_{IL}(V_G)$, respectively. It is easy to observe that, in all cases, the values of the $\psi_s^*(V_G)$ with interpolation function $f_{IL}(V_G)$ show the slightest deviation from reference values.
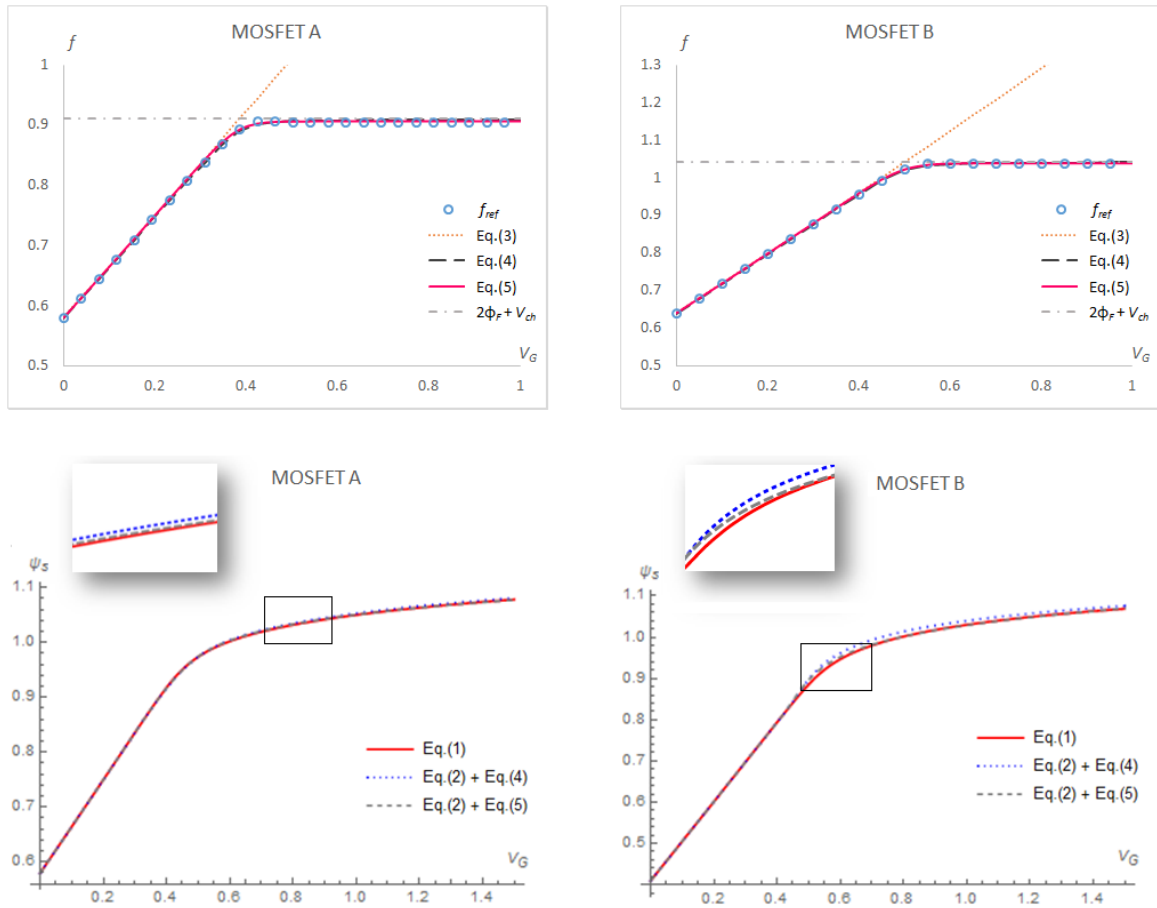
Figure 2. Diagrams above: Empirical function $f(V_G)$ (dashed lines) and interpolation function $f_{IL}(V_G)$ (solid lines), compared with reference values (dots). Diagrams bellow: Approximation of the SP using the Eq. (2) with $f(V_G)$ and $f_{IL}(V_G)$. Device parameters are the same as in the MOSFET A (left diagrams) and MOSFET B (right diagrams).
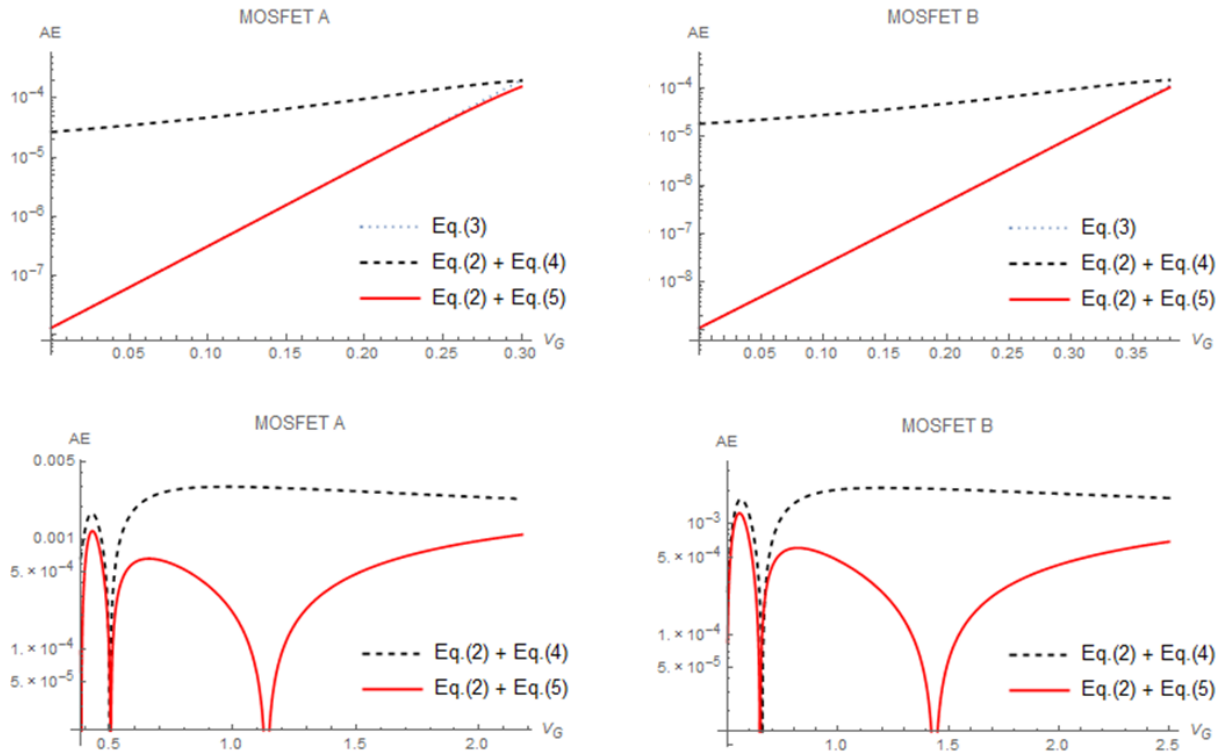
Figure 3. Log-diagrams of the absolute errors of the surface potential approximations $\psi_s^*(V_G)$, fitted with functions $f(V_G)$ and $f_{IL}(V_G)$, in the the weak inversion (diagrams above), and the strong inversion region (diagrams bellow).

Table 2. Estimated errors obtained by various types of the f-fitting (MOSFET A).

Errors	Regions	f-fitting		ψ_s^*-approximation	
		Eq.(4)	Eq.(5)	Eq.(4)	Eq.(5)
AE	Weak inversion	1.53E-03	9.73E-04	1.07E-04	8.53E-05
	Strong inversion	2.97E-03	5.59E-04	2.47E-03	3.76E-04
	Whole region	2.62E-03	6.55E-04	1.90E-03	3.05E-04
FE (%)	Weak inversion	2.12E-01	1.19E-01	1.37E-02	9.97E-03
	Strong inversion	3.28E-01	6.17E-02	2.37E-01	3.68E-02
	Whole region	3.00E-01	7.52E-02	1.83E-01	3.03E-02
SE	Weak inversion	2.39E-06	2.11E-06	1.19E-08	7.03E-09
	Strong inversion	9.50E-06	8.22E-07	6.71E-06	2.06E-07
	Whole region	7.76E-06	1.12E-06	5.08E-06	1.64E-07

Table 3. Estimated errors obtained by various types of the f-fitting (MOSFET B).

Errors	Regions	f-fitting		ψ_s^*-approximation	
		Eq.(4)	Eq.(5)	Eq.(4)	Eq.(5)
AE	Weak inversion	1.23E-03	7.39E-04	6.54E-05	2.63E-05
	Strong inversion	2.08E-03	4.46E-04	1.78E-03	3.32E-04
	Whole region	1.84E-03	5.14E-04	1.36E-03	2.68E-04
FE (%)	Weak inversion	1.54E-01	7.87E-02	7.64E-03	2.79E-03
	Strong inversion	2.00E-01	4.03E-02	1.52E-01	2.89E-02
	Whole region	1.86E-01	5.13E-02	1.16E-01	2.36E-02
SE	Weak inversion	1.71E-06	1.40E-06	6.26E-09	3.80E-09
	Strong inversion	4.66E-06	5.20E-07	3.43E-06	1.73E-07
	Whole region	7.76E-06	1.12E-06	2.60E-06	1.38E-07

CONCLUSIONS

Implementation of the Interpolation Logistic function in explicit surface potential based MOSFET model is described. This function provides continual transition of the surface potential between two distinct regions of MOSFET operation and simultaneously controls speed and manner of that transition. Except the need for usage of any empirical functions or parameters with no physical meaning is eliminated, by introducing the proposed function is achieved significantly higher degree of accuracy for the surface potential over a wide range of the device parameters. Moreover, the complexity of the calculations increases only marginally over the original model which contains pure empirical function for surface potential.

REFERENCES

Araújo, C. A. I., Schneider, M. C., & Galup-Montoro, C. 1995. An explicit physical model for the long-channel MOS transistor including small-signal parameters. Solid-State Electronics, 38(11), pp. 1945-1952. doi:10.1016/0038-1101(95)00023-m.

Arora, N. 1993. MOSFET Models for VLSI Circuit Simulation. Vienna: Springer-Verlag. doi:10.1007/978-3-7091-9247-4.

Basu, D. & Dutta, A. 2006. An explicit surface-potential-based MOSFET model incorporating the quantum mechanical effects. Solid-State Electron., 50, pp. 1299–1309.

Chen, T. L. & Gildenblat, G. 2001. Analytical approximation for the MOSFET surface potential. Solid-State Electronics, 45(2), pp. 335-339. doi:10.1016/s0038-1101(00)00283-5.

Eftimie, S. & Rusu, A. 2007. MOSFET model with simple extraction procedures suitable for sensitive analog simulations. Rom. J. Inf. Sci. Tech., 10, pp. 189-197.

Enz, C., Krummenacher, F., & Vittoz, E. 1995. An analytical MOS transistor model valid in all regions of operation and dedicated to low-voltage and low-current applications. Analog Integrated Circuits and Signal Processing, 8(1), pp. 83-114. doi:10.1007/bf01239381.

Hossain, M. & Chowdhury, M. 2016. Comprehensive doping scheme for MOSFETs in ultra-low-power subthreshold circuits design. Microelectronics Journal, 52, pp. 73-79. doi:10.1016/j.mejo.2016.03.007.

Kevkić, T., Stojanović, V., & Joksimović, D. 2017. Application of generalized logistic functions in surface-potential-based MOSFET modeling. Journal of Computational Electronics, 16(1), pp. 90-97. doi:10.1007/s10825-016-0935-x.

Kevkić, T., Stojanović, V., & Petković, D. 2016. Modification of transition's factor in the compact surface-potential-based MOSFET model. The University Thought - Publication in Natural Sciences, 6(2), pp. 55-60. doi:10.5937/univtho6-11360.

Osrečki, Z. 2015. Compact MOSFET model.University of Zagreb. Thesis.

Prégaldiny, F., Lallement, C., van Langevelde, R., & Mathiot, D. 2004. An advanced explicit surface potential model physically accounting for the quantization effects in deep-submicron MOSFETs. Solid-State Electronics, 48(3), pp. 427-435. doi:10.1016/j.sse.2003.09.005.

van Langevelde, R. & Klaassen, F. 2000. An explicit surface-potential-based MOSFET model for circuit simulation. Solid-State Electronics, 44(3), pp. 409-418. doi:10.1016/s0038-1101(99)00219-1.

ON THE STARK BROADENING OF K III AND Ca IV SPECTRAL LINES

MILAN S. DIMITRIJEVIĆ[1, 2, ⋆]

[1]Astronomical Observatory, Belgrade, Serbia
[2]Sorbonne Université, Observatoire de Paris, Université PSL, CNRS, LERMA, F-92190, Meudon, France

ABSTRACT

Stark full widths at half maximum (FWHM) for ten multiplets of doubly charged potassium ion (K III), and 35 multiplets of triply charged calcium ion (Ca IV) have been calculated for electron density of 10^{17} cm^{-3} by using the symplified modified semiempirical (SMSE) method. The calculations were performed for temperatures from 5 000 K to 80 000 K, for K III and for temperatures from 10 000 K to 160 000 K for Ca IV, for broadening by collisions with electrons. The results obtained here will be implemented in the STARK-B database which is a memeber of Virtual atomic and molecular data center (VAMDC).

Keywords: Stark broadening, Spectral lines, Line profiles, K III, Ca IV.

INTRODUCTION

Data on Stark broadening, or broadening of spectral lines by collisions with charged particles due to Stark effect in a fluctuating electric microfield are needed in many research fields in astrophysics, for laboratory plasma diagnostics, for design of lasers and investigations of laser produced plasma, in inertial fusion research as well as for different technologies which use plasmas, like light industry, and cutting, welding and melting metals using lasers.

Line broadening data for as much as possible larger number of spectral lines is needed because we do not know *a priori* the chemical composition of a stellar atmosphere. Stark broadening research of the lines of trace elements is also needed because with the development of space astronomy, instruments like Goddhard High Resolution Spectrograph (GHRS) on Hubble Space Telescope, produce spectral line profiles with unpreceded resolution and accuracy and with modern computers all calculations become more and more easier.

K III and Ca IV lnes are the two successive members of the Chlorine isoelectronic sequence. Fritzsche et al. (2006) underline the importance of atomic data for them in fusion research as well as for estimating the energy loss through impurity ions. Stark broadening data for their spectral lines are needed for laboratory plasma diagnostics, in astophysics, for fusion plasma research and in plasma physics.

Since there is no neither experimental nor theoetical data for Stark broadening of K III and Ca IV spectral lines, here are calculated Stark full widths at half maximum (FWHM) for 10 multiplets of K III, and 35 of Ca IV by using the simplified modified semiempirical method (Dimitrijević & Konjević, 1987), since a sufficiently complete set of atomic data, needed for a more sophysticated calculation does not exist.

The obtained results will be included in the STARK-B (Sahal-Bréchot et al., 2015, 2018), a database for Stark widths and shifts of spectral lines broadened by collisions with charged particles.

SYMPLIFIED MSE FORMULA

When there is no data for more sophysticated theoretical methods, or when data for a lot of spectral lines are needed, what is the case especially in astrophysics e.g. for model atmosphere or radiative transfer calculations, might be very useful the simplified modified semiempirical formula (Dimitrijević & Konjević, 1987) for Stark widths of isolated, singly, and multiply charged ion lines. This formula may be used in the case when the nearest atomic energy level ($j' = i'$ or f'), having an allowed dipol transition from or to the initial (i) or final (f) energy level of the considered spectral line, is far enough, so that the condition $x_{jj'} = E/|E_{j'} - E_j| \leq 2$ is satisfied. Than, full width at half maximum is given as (Dimitrijević & Konjević, 1987):

$$W(\text{Å}) = 2.2151 \times 10^{-8} \frac{\lambda^2(\text{cm})N(\text{cm}^{-3})}{T^{1/2}(\text{K})}(0.9 - \frac{1.1}{Z})\times$$

$$\times \sum_{j=i,f}(\frac{3n_j^*}{2Z})^2(n_j^{*2} - \ell_j^2 - \ell - 1). \quad (1)$$

In the upper equation, N and T are the electron density and temperature, $E = 3kT/2$ is the energy of perturbing electron, $Z - 1$ is the ionic charge, n the effective principal quantum number and λ is the transition wavelength.

RESULTS AND DISCUSSION

By using the symplified modified semiempirical (SMSE) method (Dimitrijević & Konjević, 1987), Stark full widths at half

---

⋆ Corresponding author: mdimitrijevic@aob.rs

Table 1. This table gives electron-impact broadening (Stark broadening) Full Widths at Half Intensity Maximum (W) for K III spectral lines, for a perturber density of 10^{17} cm^{-3} and temperatures from 5 000 to 80 000 K. The configuration is $3s^23p^4(^3P)n\ell$. Also is given quantity $3kT/2\Delta E$ for $T = 20\,000$ K, where ΔE is the energy difference between closest perturbing level and the closer of initial and final levels.

Transition	T(K)	W[Å]	3kT/2ΔE
K III $3d^2$F-$4p^2$D^o	5000.	0.732E-01	2.98
$\lambda = 2366.6$ Å	10000.	0.518E-01	5.95
	20000.	0.366E-01	11.9
	40000.	0.259E-01	23.8
	80000.	0.183E-01	47.6
K III $4s^2$P-$4p^2$D^o	5000.	0.328	2.98
$\lambda = 3312.2$ Å	10000.	0.232	5.95
	20000.	0.164	11.9
	40000.	0.116	23.8
	80000.	0.820E-01	47.6
K III $4s^2$P-$4p^2$P^o	5000.	0.311	1.89
$\lambda = 3205.3$ Å	10000.	0.220	3.78
	20000.	0.155	7.56
	40000.	0.110	15.1
	80000.	0.777E-01	30.2
K III $4p^2$D^o-$5s^2$P	5000.	1.23	2.98
$\lambda = 5070.3$ Å	10000.	0.873	5.95
	20000.	0.617	11.9
	40000.	0.436	23.8
	80000.	0.309	47.6
K III $4p^2$P^o-$5s^2$P	5000.	1.38	1.89
$\lambda = 5342.9$ Å	10000.	0.976	3.78
	20000.	0.690	7.56
	40000.	0.488	15.1
	80000.	0.345	30.2
K III $4p^2$D^o-$3d^2$D	5000.	0.182	2.98
$\lambda = 1678.3$ Å	10000.	0.129	5.95
	20000.	0.911E-01	11.9
	40000.	0.644E-01	23.8
	80000.	0.456E-01	47.6
K III $4p^2$P^o-$3d^2$D	5000.	0.190	1.89
$\lambda = 1707.1$ Å	10000.	0.134	3.78
	20000.	0.948E-01	7.56
	40000.	0.670E-01	15.1
	80000.	0.474E-01	30.2
K III $4s^4$P-$4p^4$P^o	5000.	0.310	0.176
$\lambda = 3376.2$ Å	10000.	0.219	0.352
	20000.	0.155	0.704
	40000.	0.110	1.41
	80000.	0.776E-01	2.82
K III $4s^4$P-$4p^4$D^o	5000.	0.256	0.176
$\lambda = 3006.0$ Å	10000.	0.181	0.352
	20000.	0.128	0.704
	40000.	0.905E-01	1.41
	80000.	0.640E-01	2.82
K III $4s^4$P-$4p^4$S^o	5000.	0.203	0.176
$\lambda = 2601.3$ Å	10000.	0.144	0.352
	20000.	0.102	0.704
	40000.	0.719E-01	1.41
	80000.	0.508E-01	2.82

Table 2. This table gives electron-impact broadening (Stark broadening) Full Widths at Half Intensity Maximum (W) for Ca IV spectral lines, for a perturber density of 10^{17} cm^{-3} and temperatures from 10 000 to 160 000 K. Also is given quantity $3kT/2\Delta E$, where ΔE is the energy difference between closest perturbing level and the closer of initial and final levels.

Transition	T(K)	W[Å]	$3kT/2\Delta E$
Ca IV (^{3}P)3d^{4}D-(^{3}P)4p^{4}P^o	10000.	0.401E-02	0.270
$\lambda = 773.3$ Å	20000.	0.284E-02	0.539
	40000.	0.201E-02	1.08
	80000.	0.142E-02	2.16
	160000.	0.100E-02	4.31
Ca IV (^{3}P)3d^{4}D-(^{3}P)4p^{4}D^o	10000.	0.402E-02	0.239
$\lambda = 745.2$ Å	20000.	0.284E-02	0.479
	40000.	0.201E-02	0.958
	80000.	0.142E-02	1.92
	160000.	0.100E-02	3.83
Ca IV (^{3}P)3d^{4}F-(^{3}P)4p^{4}D^o	10000.	0.548E-02	0.239
$\lambda = 858.2$ Å	20000.	0.387E-02	0.479
	40000.	0.274E-02	0.958
	80000.	0.194E-02	1.92
	160000.	0.137E-02	3.83
Ca IV (^{3}P)3d^{4}P-(^{3}P)4p^{4}P^o	10000.	0.663E-02	0.270
$\lambda = 971.7$ Å	20000.	0.469E-02	0.539
	40000.	0.332E-02	1.08
	80000.	0.235E-02	2.16
	160000.	0.166E-02	4.31
Ca IV (^{3}P)3d^{4}P-(^{3}P)4p^{4}D^o	10000.	0.650E-02	0.239
$\lambda = 927.7$ Å	20000.	0.460E-02	0.479
	40000.	0.325E-02	0.958
	80000.	0.230E-02	1.92
	160000.	0.163E-02	3.83
Ca IV (^{3}P)3d^{4}P-(^{3}P)4p^{4}S^o	10000.	0.636E-02	0.206
$\lambda = 871.4$ Å	20000.	0.450E-02	0.413
	40000.	0.318E-02	0.826
	80000.	0.225E-02	1.65
	160000.	0.159E-02	3.30
Ca IV (^{3}P)4s^{4}P-(^{3}P)4p^{4}P^o	10000.	0.112	0.270
$\lambda = 2586.1$ Å	20000.	0.794E-01	0.539
	40000.	0.561E-01	1.08
	80000.	0.397E-01	2.16
	160000.	0.281E-01	4.31
Ca IV (^{3}P)4s^{4}P-(^{3}P)4p^{4}D^o	10000.	0.913E-01	0.270
$\lambda = 2295.8$ Å	20000.	0.645E-01	0.539
	40000.	0.456E-01	1.08
	80000.	0.323E-01	2.16
	160000.	0.228E-01	4.31
Ca IV (^{3}P)4s^{4}P-(^{3}P)4p^{4}S^o	10000.	0.711E-01	0.270
$\lambda = 1979.5$ Å	20000.	0.503E-01	0.539
	40000.	0.355E-01	1.08
	80000.	0.251E-01	2.16
	160000.	0.178E-01	4.31
Ca IV (^{3}P)3d^{2}F-(^{3}P)4p^{2}D^o	10000.	0.701E-02	0.284
$\lambda = 937.1$ Å	20000.	0.495E-02	0.567
	40000.	0.350E-02	1.13
	80000.	0.248E-02	2.27
	160000.	0.175E-02	4.54

Transition	T(K)	W[Å]	3kT/2ΔE
Ca IV (^{3}P)3d^{2}P-(^{3}P)4p^{2}D^o	10000.	0.476E-01	0.284
$\lambda = 2231.7$ Å	20000.	0.336E-01	0.567
	40000.	0.238E-01	1.13
	80000.	0.168E-01	2.27
	160000.	0.119E-01	4.54
Ca IV(^{3}P)3d^{2}P-(^{3}P)4p^{2}P^o	10000.	0.486E-01	0.289
$\lambda = 2264.9$ Å	20000.	0.344E-01	0.578
	40000.	0.243E-01	1.16
	80000.	0.172E-01	2.31
	160000.	0.122E-01	4.62
Ca IV (^{3}P)3d^{2}P-(^{3}P)4p^{2}S^o	10000.	0.428E-01	0.259
$\lambda = 2071.5$ Å	20000.	0.303E-01	0.518
	40000.	0.214E-01	1.04
	80000.	0.151E-01	2.07
	160000.	0.107E-01	4.15
Ca IV (^{3}P)3d^{2}P-(^{3}P)4p^{2}D^o	10000.	0.729E-01	0.284
$\lambda = 2715.7$ Å	20000.	0.516E-01	0.567
	40000.	0.365E-01	1.13
	80000.	0.258E-01	2.27
	160000.	0.182E-01	4.54
Ca IV (^{3}P)3d^{2}P-(^{3}P)4p^{2}P^o	10000.	0.750E-01	0.289
$\lambda = 2765.1$ Å	20000.	0.531E-01	0.578
	40000.	0.375E-01	1.16
	80000.	0.265E-01	2.31
	160000.	0.188E-01	4.62
Ca IV (^{3}P)4s^{2}P-(^{3}P)4p^{2}D^o	10000.	0.136	0.284
$\lambda = 2720.8$ Å	20000.	0.965E-01	0.567
	40000.	0.682E-01	1.13
	80000.	0.482E-01	2.27
	160000.	0.341E-01	4.54
Ca IV (^{3}P)4s^{2}P-(^{3}P)4p^{2}P^o	10000.	0.141	0.289
$\lambda = 2770.3$ Å	20000.	0.996E-01	0.578
	40000.	0.704E-01	1.16
	80000.	0.498E-01	2.31
	160000.	0.352E-01	4.62
Ca IV (^{3}P)4s^{2}P-(^{3}P)4p^{2}S^o	10000.	0.117	0.284
$\lambda = 2486.3$ Å	20000.	0.824E-01	0.567
	40000.	0.583E-01	1.13
	80000.	0.412E-01	2.27
	160000.	0.291E-01	4.54
Ca IV (^{1}D)3d^{2}P-(^{1}D)4p^{2}D^o	10000.	0.729E-02	0.229
$\lambda = 730.6$ Å	20000.	0.516E-02	0.457
	40000.	0.365E-02	0.915
	80000.	0.258E-02	1.83
	160000.	0.182E-02	3.66
Ca IV (^{1}D)3d^{2}P-(^{1}D)4p^{2}P^o	10000.	0.721E-02	0.219
$\lambda = 720.4$ Å	20000.	0.510E-02	0.439
	40000.	0.361E-02	0.877
	80000.	0.255E-02	1.75
	160000.	0.180E-02	3.51

Transition	T(K)	W[Å]	3kT/2ΔE
Ca IV (^{1}D)3d^{2}D-(^{1}D)4p^{2}D^o	10000.	0.876E-02	0.262
$\lambda = 813.2$ Å	20000.	0.620E-02	0.523
	40000.	0.438E-02	1.05
	80000.	0.310E-02	2.09
	160000.	0.219E-02	4.19
Ca IV (^{1}D)3d^{2}P-(^{1}D)4p^{2}D^o	10000.	0.839E-02	0.229
$\lambda = 776.9$ Å	20000.	0.593E-02	0.457
	40000.	0.419E-02	0.915
	80000.	0.297E-02	1.83
	160000.	0.210E-03	3.66
Ca IV (^{1}D)3d^{2}P-(^{1}D)4p^{2}P^o	10000.	0.828E-02	0.219
$\lambda = 765.3$ Å	20000.	0.585E-02	0.439
	40000.	0.414E-02	0.877
	80000.	0.293E-02	1.75
	160000.	0.207E-02	3.51
Ca IV (^{1}D)3d^{2}G-(^{1}D)4p^{2}F^o	10000.	0.965E-02	0.262
$\lambda = 848.5$ Å	20000.	0.682E-02	0.523
	40000.	0.483E-02	1.05
	80000.	0.341E-02	2.09
	160000.	0.241E-02	4.19
Ca IV (^{1}D)3d^{2}F-(^{1}D)4p^{2}F^o	10000.	0.141E-01	0.262
$\lambda = 1002.2$ Å	20000.	0.996E-02	0.523
	40000.	0.704E-02	1.05
	80000.	0.498E-02	2.09
	160000.	0.352E-02	4.19
Ca IV (^{1}D)3d^{2}F-(^{1}D)4p^{2}D^o	10000.	0.132E-01	0.229
$\lambda = 947.7$ Å	20000.	0.932E-02	0.457
	40000.	0.659E-02	0.915
	80000.	0.466E-02	1.83
	160000.	0.329E-02	3.66
Ca IV (^{1}D)3d^{2}S-(^{1}D)4p^{2}P^o	10000.	0.373E-01	0.219
$\lambda = 1490.4$ Å	20000.	0.263E-01	0.439
	40000.	0.186E-01	0.877
	80000.	0.132E-01	1.75
	160000.	0.931E-02	3.51
Ca IV (^{1}D)4s^{2}D-(^{1}D)4p^{2}F^o	10000.	0.108	0.262
$\lambda = 2509.5$ Å	20000.	0.764E-01	0.523
	40000.	0.540E-01	1.05
	80000.	0.382E-01	2.09
	160000.	0.270E-01	4.19
Ca IV (^{1}D)4s^{2}D-(^{1}D)4p^{2}D^o	10000.	0.856E-01	0.262
$\lambda = 2193.5$ Å	20000.	0.606E-01	0.523
	40000.	0.428E-01	1.05
	80000.	0.303E-01	2.09
	160000.	0.214E-01	4.19
Ca IV (^{1}D)4s^{2}D-(^{1}D)4p^{2}P^o	10000.	0.798E-01	0.262
$\lambda = 2103.6$ Å	20000.	0.564E-01	0.523
	40000.	0.399E-01	1.05
	80000.	0.282E-01	2.09
	160000.	0.200E-01	4.19

Transition	T(K)	W[Å]	3kT/2ΔE
Ca IV (^{1}D)4p^{2}F^o-(^{1}D)5s^{2}D	10000.	0.126	0.262
λ = 2091.3 Å	20000.	0.892E-01	0.523
	40000.	0.631E-01	1.05
	80000.	0.446E-01	2.09
	160000.	0.315E-01	4.19
Ca IV (^{1}D)4p^{2}D^o-(^{1}D)5s^{2}D	10000.	0.167	0.260
λ = 2376.7 Å	20000.	0.118	0.520
	40000.	0.836E-01	1.04
	80000.	0.591E-01	2.08
	160000.	0.418E-01	4.16
Ca IV (^{1}D)4p^{2}P^o-(^{1}D)5s^{2}D	10000.	0.185	0.260
λ = 2492.0 Å	20000.	0.131	0.520
	40000.	0.927E-01	1.04
	80000.	0.655E-01	2.08
	160000.	0.463E-01	4.16
Ca IV (^{1}S)3d^{2}D-(^{1}S)4p^{2}P^o	10000.	0.628E-02	0.244
λ = 912.0 Å	20000.	0.444E-02	0.488
	40000.	0.314E-02	0.976
	80000.	0.222E-02	1.95
	160000.	0.157E-02	3.90
Ca IV (^{1}S)4s^{2}S-(^{1}S)4p^{2}P^o	10000.	0.953E-01	0.244
λ = 2339.8 Å	20000.	0.674E-01	0.488
	40000.	0.476E-01	0.976
	80000.	0.337E-01	1.95
	160000.	0.238E-01	3.9

maximum (FWHM) for 10 multiplets of K III and 35 multiplets of Ca IV have been calculated for electron density of 10^{17} cm^{-3} and for temperatures from 5 000 K to 80 000 K in the case of K III while for Ca IV the chosen temperature range was from 10 000 K to 160 000 K. Calculations were performed for broadening of spectral lines by collisions with electrons. Energy levels and ionization energies needed for the corresponding calculations have been taken from Sugar & Corlis (1985); Sansonetti (2008); Kramida et al. (2018) in the case of K III and from Sugar & Corlis (1985); Kramida et al. (2018) in the case of Ca IV. The data for energy levels are incomplete for any more sophysticated calculation but using them, SMSE method, who needs less atomic data, can be applied.

The results of our calculations of Stark widths for K III spectral lines are shown in Table 1 and for Ca IV in Table 2. The extrapolation to lower perturber densities is linear while for higher extrapolation is linear to densities where the influence of Debye screening is negligible or reasonably small. The wavelengths presented in Tables 1 and 2 are the calculated ones from the averaged energy levels for multiplet so that they differ from the observed ones. In the last column is shown the quantity $3kT/2\Delta E$, which represents the ratio of the average energy of free electrons, $E = 3kT/2$, and the energy difference between the initial or final and the closest perturbing level,and is taken the larger of such values for initialand final level.

Table 3. This table gives electron-impact broadening (Stark broadening) Full Widths at Half Intensity Maximum (W) for K III $4s^{(2S+1)}$P-$4p^{2S+1}$L^o (L=S, P, D) supermultiplet, for a perturber density of 10^{17} cm^{-3} and temperature of 10 000 K, in [Å] and in $[10^{12}$s$^{-1}]$ units.

Transition	T(K)	W[Å]	W[10^{12} s^{-1}]
K III 4s^{2}P-4p^{2}D^o	10000.	0.232	0.398
λ = 3312.2 Å			
K III 4s^{2}P-4p^{2}P^o	10000.	0.220	0.403
λ = 3205.3 Å			
K III 4s^{4}P-4p^{4}P^o	10000.	0.219	0.362
λ = 3376.2 Å			
K III 4s^{4}P-4p^{4}D^o	10000.	0.181	0.377
λ = 3006.0 Å			
K III 4s^{4}P-4p^{4}S^o	10000.	0.144	0.401
λ = 2601.3 Å			

$$\Delta E = \text{Max}[E/\Delta E_{i,i'}, E/\Delta E_{f,f'}] \qquad (2)$$

This ratio is the validity condition for the used method. If $3kT/2\Delta E = 1$, it is the threshold for the corresponding inelastic transition. If it is lower than one, elastic collisions are dominant and it is so called low temperature limit, and the applied method is completely convenient and valid. If it is larger than one the inelas-

tic collisions start to play more and more important role with its increase and the method underestimates the real value. However, since the Stark width decrease monotonically with the increase of temperature, if we look at the value of Stark width at lower temperatures, where the condition given by Eq. (2) is satisfied, and the obtained value for the needed temperature, the right value is between these limits, so that we have a rough estimate for it.

The Stark widths obtained here, enable to check the similarities of these line broadning parameters within a supermultiplet and transition array. If such similarities exist, they could be used for derrivation of missing values, on the basis of the known ones. Namely, Wiese & Konjević (1982) found that Stark line widths in angular frequency units in a supermultiplet usually agree within about 30 per cent and within a transition array within about 40 per cent. We will check this for K III, belonging to the chlorine isoelectronic sequence, for the supermltiplet $4s^{(2S+1)}P-4p^{2S+1}L^o$ (L=S, P, D). In order to do so we should transform the Stark widths expressed in Å-units to the widths in angular frequency units, what can be done by the following formula:

$$W(Å) = \frac{\lambda^2}{2\pi c} W(s^{-1}), \tag{3}$$

where c is the speed of light.

The values in Å and in s^{-1} are presented in Table 3. We can see that for values in Å the highest value in supermultiplet is 52% higher from the lowest and in transition array 61%, but this is because of the influence of wavelength. In s^{-1} units, when the width is liberated from this influence, the maximal value in both supermultiplet and transition array is only 11% larger from the smaller one what is well within the limits found by Wiese & Konjević (1982).

The Stark widths obtained here for K III and Ca IV spectral lines will be included in the STARK-B database (Sahal-Bréchot et al., 2015, 2018), one of the databases which enter also in the european Virtual Atomic and Molecular Data Center - VAMDC (Dubernet et al., 2010; Rixon et al., 2011; Dubernet et al., 2016), which can be found on the web site http://portal.vamdc.org/.

CONCLUSION

By using the SMSE method we have calculated Stark widths for 10 K III and 35 Ca IV multiplets as a function of temperature. The presented widths are also used to check how similar they are within a supermultiplet and transition array. These data will be implemented in STARK-B database. Since other experimental or theoretical data for these ions do not exist it is not possible to make a comparison with other results. The data obtained in this work may be of interest for stellar physics, plasma diagnostics and inertial fusion reearch.

REFERENCES

Dimitrijević, M. S. & Konjević, N. 1987. Simple estimates for Stark broadening of ion lines in stellar plasma. Astronomy and Astrophysics, 172, pp. 345-349.

Dubernet, M. L., Antony, B. K., Ba, Y. A., et al. 2016. The virtual atomic and molecular data centre (VAMDC) consortium. Journal of Physics B: Atomic, Molecular and Optical Physics, 49(7), 074003.

Dubernet, M. L., Boudon, V., Culhane, J. L., et al. 2010. Virtual atomic and molecular data centre. Journal of Quantitative Spectroscopy and Radiative Transfer, 111(15), pp. 2151-2159. doi:10.1016/j.jqsrt.2010.05.004.

Fritzsche, S., Finkbeiner, M., Fricke, B., & Sepp, W. 2006. Level energies and lifetimes in the 3p4 3d configuration of chlorine-like ions. Physica Scripta, 52(3), pp. 258-266. doi:10.1088/0031-8949/52/3/006.

Kramida, A., Ralchenko, Y., & Reader, J. 2018. NIST ASD Team, NIST Atomic Spectra Database. Gaithersburg, MD: National Institute of Standards and Technology. (ver. 5.5.1), Retrived from https://physics.nist.gov/asd, 2018, December 9.

Rixon, G., Dubernet, M. L., Piskunov, N., et al. 2011. VAMDC-The Virtual Atomic and Molecular Data Centre-A New Way to Disseminate Atomic and Molecular Data-VAMDC Level 1 Release. AIP Publishing., pp. 107-115. doi:10.1063/1.3585810.

Sahal-Bréchot, S., Dimitrijević, M. S., & Moreau, N. 2018. STARK-B database. Observatory of Paris / LERMA.Astronomical Observatory of Belgrade. Retrieved from http://stark-b.obspm.fr, 2018 December 9.

Sahal-Bréchot, S., Dimitrijević, M. S., Moreau, N., & Nessib, N. B. 2015. The STARK-B database VAMDC node: a repository for spectral line broadening and shifts due to collisions with charged particles. Physica Scripta, 90(5), p. 54008. doi:10.1088/0031-8949/90/5/054008.

Sansonetti, J. E. 2008. Wavelengths, Transition Probabilities, and Energy Levels for the Spectra of Potassium (K I through K XIX). J. Phys. Chem. Ref. Data, 37, pp. 7-96; DOI: 10.1063/1.2789451.

Sugar, J. & Corlis, C. 1985. Atomic Energy Levels of the Iron-Period Elements: Potassium through Nickel. J . Phys. Chem. Ref. Data, 14, Suppl. 2, pp. 1–664.

Wiese, W. L. & Konjević, N. 1982. Regularities and similarities in plasma broadened spectral line widths (Stark widths). Journal of Quantitative Spectroscopy and Radiative Transfer, 28(3), pp. 185-198. doi:10.1016/0022-4073(82)90022-x.

Available Online

This journal is available online. Please visit http://www.utnsjournal.pr.ac.rs or http://www.utnsjournal.com to
search and download published articles.